NASA CR-132379

INITIAL DEVELOPMENT OF AN ABLATIVE LEADING EDGE FOR THE SPACE SHUTTLE ORBITER

GRUMMAN

Errata (NASA CR 132379)

Page	Paragraph, line	Instead of	Read
332	2 , 4	if the l.e. area is comparable to the current carbon-carbon areas.	if the number of flights were to slip, in the years covered by the traffic model, from 445 to 300.
337	3 , 1	Total program cost for 445 flights is estimated $43M (for 600 ft^2 of l.e. area) and $38M (for 280 ft^2 area as in the current carbon-carbon wing l.e.);	Total program cost is estimated $43M and $38M for 445 and 300 flights respectively (for 280 ft^2 area as in the current carbon-carbon wing l.e.);
338	4 , 9	Appendix 6	Data Package
339	0 , 5	Appendix 5	Data Package
339	2 , 10	Appendix 3	Data Package
345	1 , 3	Δcu_β	Δc_{n_β}
345	1 , 3	reunion	recession

INITIAL DEVELOPMENT OF AN ABLATIVE LEADING EDGE FOR THE SPACE SHUTTLE ORBITER

by

G. DaForno and L. Rose, Grumman Aerospace Corporation

and

J. Graham and P. Roy, AVCO Systems Division

Prepared under Contract NAS 1-11416

March 1974

Grumman Aerospace Corporation
Bethpage, New York 11714

1. Report No.	2 Government Accession No.	3 Recipient's Catalog No
NASA CR-132379		

4. Title and Subtitle	5 Report Date
INITIAL DEVELOPMENT OF AN ABLATIVE LEADING EDGE FOR THE SPACE SHUTTLE ORBITER	December 1973
	6. Performing Organization Code: NONE
7. Author(s): G. DaForno, J. Graham, P. Roy, L. Rose	8. Performing Organization Report No.: NONE
	10. Work Unit No.
9. Performing Organization Name and Address: Grumman Aerospace Corporation, Bethpage, N.Y. / AVCO Systems Division, Wilmington, Mass.	11 Contract or Grant No: NAS1 - 11416
	13 Type of Report and Period Covered: Final
12. Sponsoring Agency Name and Address: National Aeronautics and Space Administration, Langley Research Center, Hampton, Virginia 23365	14. Sponsoring Agency Code

15. Supplementary Notes

16. Abstract

A state-of-the-art preliminary design for typical wing areas is developed. Seven medium-density ablators (with/without honeycomb, flown on Apollo, Prime, X15A2) are evaluated. The screening tests include: 1) leading-edge models sequentially subjected to ascent heating, cold soak, entry heating, post-entry pressure fluctuations, and touchdown shock and, 2) virgin/charred models subjected to bondline strains. Two honeycomb reinforced 30 pcf elastomeric ablators were selected. Roughness/recession degradation of low speed aerodynamics appears acceptable. The design, including attachments, substructure and joints, is presented.

17. Key Words (Suggested by Author(s))	18. Distribution Statement
Charring Ablators Shuttle Orbiter Leading Edges Thermal Protection System Leading Edge Roughness	Unclassified – Unlimited Cat. 28

19. Security Classif. (of this report)	20 Security Classif. (of this page)	21. No. of Pages	22. Price*
Unclassified	Unclassified		

* For sale by the National Technical Information Service, Springfield, Virginia 22151

PRECEDING PAGE BLANK NOT FILMED

TABLE OF CONTENTS

CONTENTS

OF

DATA PACKAGE*

*Detailed information on the leading edge design, supporting data from tests, etc., on file at NASA, LRC.

ILLUSTRATIONS

TABLES

INITIAL DEVELOPMENT OF AN ABLATIVE LEADING EDGE FOR THE SPACE SHUTTLE ORBITER

G. DaForno and L. Rose, Grumman Aerospace Corp.

J. Graham and P. Roy, AVCO Systems Division

SUMMARY

The work described in this report includes design, testing and related efforts required to determine the feasibility of utilizing ablators on the leading edges of the space shuttle orbiter. The specific tasks involved are: 1) the definition of a representative leading edge environment, 2) evaluation of seven candidate ablators under sequential test conditions using leading edge configurations, 3) analysis of the effects of surface roughness on subsonic aerodynamics, 4) trade-off studies to determine the most efficient structural design and ablator to wing attachment scheme, 5) a preliminary design of the leading edge defining selected attachment and seal concepts and, 6) a cost analysis outlining the expenditures required. An additional effort was involved in the fabrication of eight ablator leading edge models which were submitted to NASA for testing in a reentry heating environment at the Johnson Spacecraft Center.

Significant findings are: 1) ablators are feasible TPS for the leading edge areas and are reasonably cost competitive relative to the carbon/carbon system, 2) of available ablators, it appears that only those which use honeycomb reinforcement are acceptable; and, 3) none of the ablators produce surface roughness which will significantly degrade subsonic aerodynamic performance.

Of the seven ablators evaluated, two 30 pcf elastomers appear to be most promising (i.e. Avco Mod 7 Hc and Martin ESA 3560 HF). These materials, both reinforced with honeycomb, are in the state of development where only minimal work would be required to apply them with confidence to the orbiter leading edges.

FOREWORD

This report describes the body of the work, while a separate Data Package contains supporting data of specialized interest such as the detailed test results and the design of models that have been produced but not used. The Data Package (of some 550 pages) can be consulted at, or obtained on loan from the Thermal Protection Branch, Material Division, NASA Langley Research Center.

Part of the work presented in this report was conducted under NASA Contract NAS1-11416 (March 1972, December 1973), and part under independent development efforts at Grumman and AVCO. Contract NAS1-11416 to the Grumman Aerospace Corporation included a subcontract to AVCO for design studies and material testing. Proprietary ablators were procured from the Martin-Marietta Corporation, Denver Division and the AVCO Corporation, AVCO Systems Division.

The NASA Langley technical monitor was Mr. S. Tompkins, Thermal Protection Branch, Material Division, while D. Curry, JSC was the contact at JSC.

The work described is the result of a team effort. Other people closely involved were: (at Grumman) F. Peinemann, C. Osonitsch, J. Valentine; (at AVCO) H. Loercher, D. Mosher, R. Brown; (at NASA Langley Research Center) R. Levine and R. Brown. Many tests were conducted in the facilities of the Thermal Protection Branch, NASA Langley. Moreover, for the vibration tests, the NASA Langley Thermoacoustic Facility was used with the cooperation of C. Rucker, Load Division, Acoustic Dynamics Section. All these tests are described in this report, including one test conducted by the Thermal Protection Branch with one extra model produced under this program.

As questions arose, this study had the ready cooperation of the Martin Marietta Corporation, Denver Division in the persons of P. Plank, A. Norton, B. Maccalous and C. Miller. In particular, the Martin Corporation in the persons of A. Norton and B. Maccalous agreed to the purchase of the Prime and X15A2 ablators under the demanding schedule of the study.

When, as a result of the screening tests, it became advisable to select two, rather than one, ablators, both ablator houses, AVCO and Martin, displayed exceptional cooperation in fabricating, in a very cost effective fashion, the models for the evaluation of the l.e. design at NASA, JSC.

A short version of this report can be found in the following paper: G. DaForno, J. Graham, S. Tompkins, Initial Development of an ablative leading edge for the Space Shuttle orbiter, AIAA Paper No. 73-739, presented at the AIAA 8th Thermophysics Conference, Palm Springs, Ca., July 16-18, 1973. Minor refinements in the design were made after that paper was presented and the data in this report are to be regarded as definitive.

All the models, both those used in the program and those not used (in particular the three rain erosion samples) are with the Thermo Protection Branch, NASA Langley, with the exception of eight l.e. models that are with the Thermal Technology Branch, Structures and Mechanics Division, NASA JSC.

0. SUBJECT

The subject of the work presented here is the use of a charring ablator heat shield as a thermal protection system (TPS) for the wing and fin leading edges (l.e.) of the space shuttle orbiter. More specifically, our theme comprises neither a justification for the use of an ablative l.e. nor a comparison with other TPSs envisioned for the orbiter l.e. Rather, we are dealing with the development of detailed and comprehensive information on an ablative l.e.

The general expectation during Phase B of the Shuttle program has been that an ablative l.e. for the orbiter is feasible, but development studies had not been carried out. In particular, no experimental data were available on the performance of ablators under a sequence of environments representative of this application. Such a sequence includes a novel aspect, namely, a charring phase during ascent followed by an extended period in cold soak and only finally by the primary charring during entry. Moreover, characteristics such as weight, cost, etc., had not been based on a systematic effort at a minimum weight and cost design. But of course, estimates for such characteristics were used in trade-off studies during Phase B. Basically the only information available at the start of this study were some (non-sequential) ablator test data (Ref. 1), the design studies on Graham et al. (Ref. 2) and some initial studies on aerodynamic characteristics degradation due to l.e. roughness on delta wing orbiters (Refs. 3 and 4).

The ablative l.e. can be considered either as a permanent TPS for the entire traffic of the Shuttle or as a mere temporary TPS to reduce risks in the initial orbiter flights and to insure against delays in the availability of a reusable TPS. Emphasis in this study is on the first alternative even though most of the effort is also applicable to the other.

1. PROBLEM

The problem we have attacked is that of the initial development of an ablative l.e. for the orbiter, using state-of-the-art technology. 'State-of-the-art' means, among other things, that the ablator is an off-the-shelf well-developed material, requiring at most, a modest effort in the area of low-cost fabrication. 'Initial development' means that the end result of this effort is to be a preliminary design for the wing midspan, the design being untested as a whole. However, all the key issues are to be examined at least in a 'first-cut' fashion, key selections (e.g., the ablator) are to be tested and an overall picture is to be formed rapidly of the entire problem. The preliminary design produced should be such that the next step is large scale fabrication and testing.

The steps obviously necessary for this goal are: (i) establish the design ground rules and the requirements, such as the environment to be withstood, the roughness that can be tolerated, etc; (ii) select an ablator; (iii) evolve the refurbishment procedure and the attachment scheme; (iv) design substructures ablator and joints; (v) draw up a preliminary design and determine its characteristics, its cost and the time needed to transform it into qualified hardware. These five steps are discussed in this report with supporting data relegated to a separate Data Package. In addition, the following is also presented: (a) how the wing l.e. design can be adapted to the fin l.e.; (b) comments on what prospectives there are for cost and weight improvement; (c) recommendations for the next step following this initial development of an ablative l.e.; and finally (d) a description of certain models that have been fabricated but not tested under this study (these models will evaluate, in small scale, the design).

No special attention is devoted to the fin l.e. The justification for such an attitude is the fact that RSI is being considered adequate as a fin l.e. TPS and that we expect the fin l.e. thermal protection to be a much simpler problem than the wing l.e. The essential elements of the design can be applied to the fin by just scaling ablator thickness to the reduced heating.

2. DESIGN GROUND RULES AND REQUIREMENTS

Apart from the obvious ground rule of striking for minimum cost -- the theme of the Shuttle program -- NASA set out important ground rules for this effort. One ground rule is quite predictable. It requires that:

a) the wing main structure is of aluminum, not of titanium. This means that this study has few points of contact with another detailed study of an ablative l.e., Ref. 5. Obviously in the bookkeeping of weight and costs, if the l.e. substructure is of titanium, the l.e. design must be charged with the penalties of reducing the structural temperature 350°F at the interface with the wing main structure.

Other ground rules are less predictable. They require:

b) to consider typical delta wing orbiters, maintaining flexibility with respect to the prevailing configurations. In other words this is a technology study not tied to a specific orbiter design. Since it is necessary to be more specific, e.g. to obtain the design environment, typical end-of-Phase-B/beginning-of-Phase-C orbiters were considered. They were the NASA 040A, the Grumman 473 and the Rockwell ATP, 000089B and 000033 (or 7D) orbiters. For the external geometry, an ad hoc configuration was used with lines that are a compromise between the Grumman 473 and the Rockwell 000033. This compromise is given in figure 1 (planform and cross section at wing midspan) and 2 (distribution of wing l.e. radii). The l.e. shape is almost identical to that of the 473 orbiter except for the characteristic hook at the nose of the 473.

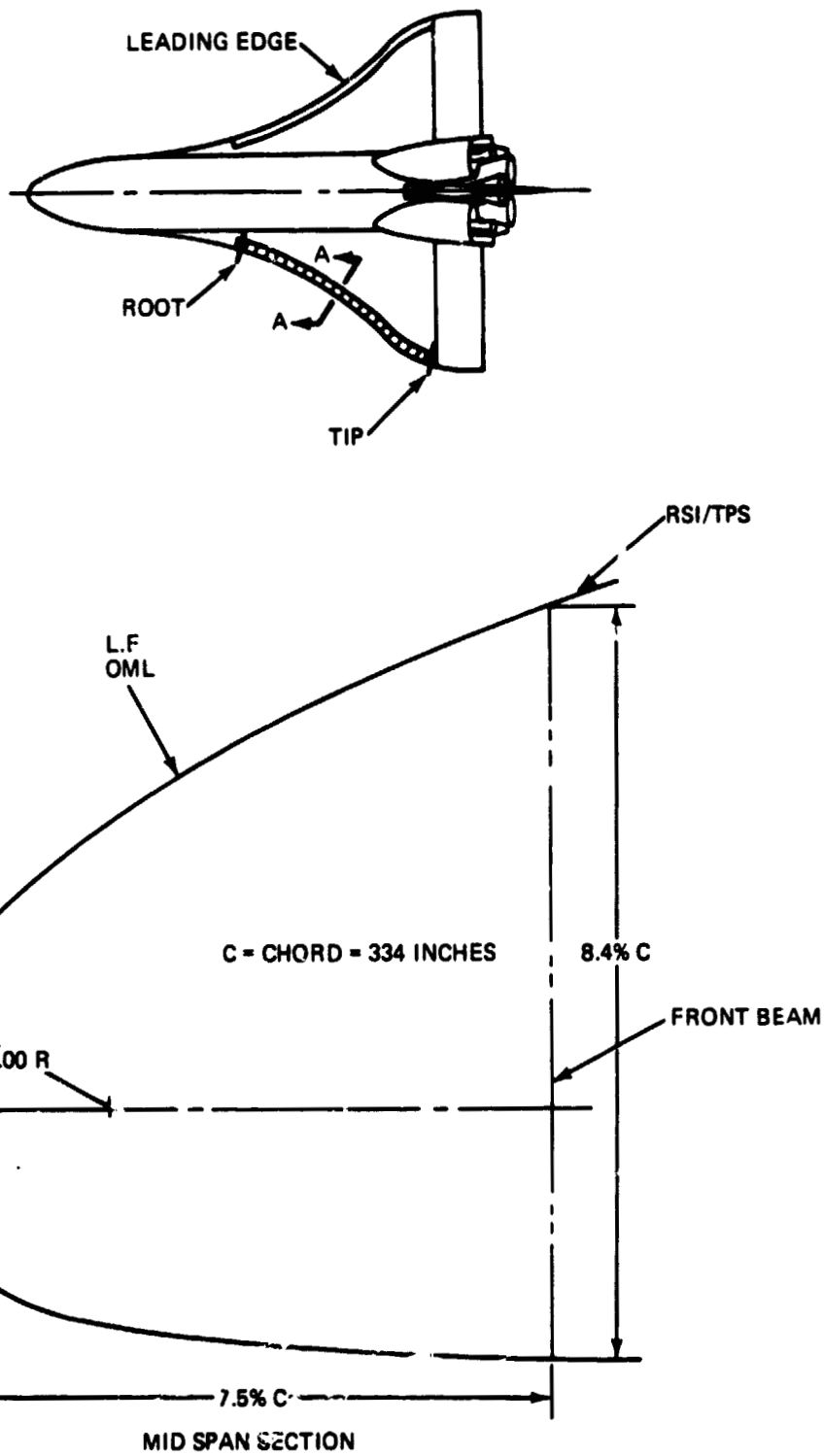

Figure 1 Configuration Used in the Study

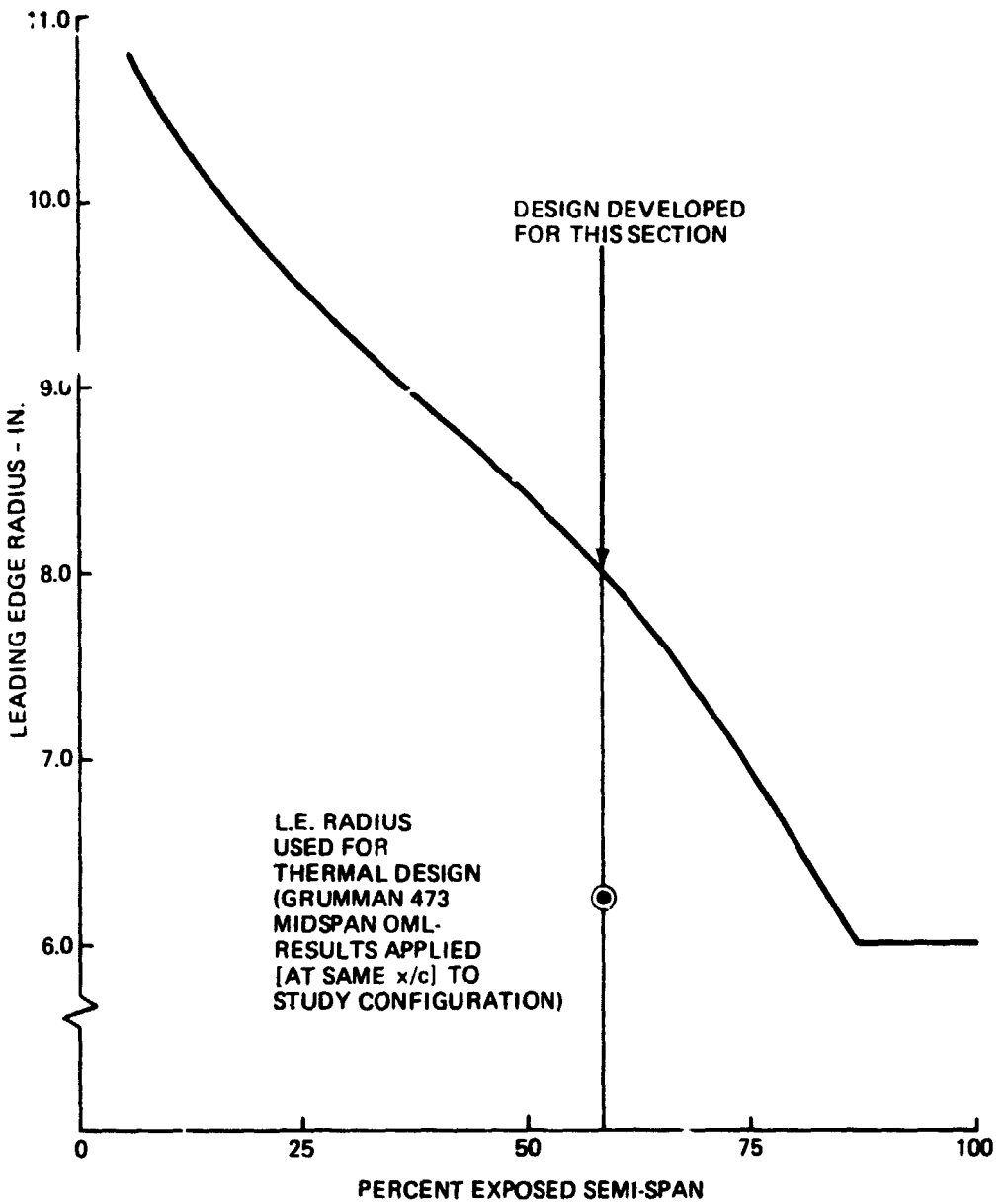

Figure 2. Wing Leading Edge Radius Definition for Configuration Used

c) to design a typical wing midspan section and neglect the special areas, such as fillets, the shock impingement area (if the bow shock is reasonably stationary during entry) or the kink area in double delta designs.

d) to forgo interchangeability or compatibility with the carbon-carbon (CC) system, but strive for an absolute optimum ablative l.e.

e) to interface with the reusable surface insulation (RSI) and the acreage TPS and not with a metallic TPS.

f) to protect with ablator the entire region ahead of the wing front beam, even though RSI can be used ahead of the front beam (usually at some 8 or 10% of the chord) at least on the leeward side.

g) to plan for the entire NASA traffic model (Ref. 6) (a total of 447 flights on an appropriate schedule and a fleet of five orbiters). A slightly different traffic model was prescribed for costing the ablative l.e.

h) to take the Shuttle system 'frozen' rather than 'rubber' for trade-offs of components weight versus cost. A 'rubber' system is appropriate for Phase A and B type studies, while the 'frozen' rule should reflect the relevance of this study to a system already in preliminary design.

On the whole these ground rules represent a reasonable compromise between the many constraints. Perhaps the biggest problem is rule (f) that imposes a larger l.e. area ($\simeq$ 600 ft^2 per orbiter) compared to the area that is not

covered by RSI in current configurations (e.g., some 300 ft^2). Ablator costs and weights may have to be at least adjusted for these areas if rule (f) is rejected. This rule, however, was dictated by the fact that by custom, the structural interface between wing and l.e. is at the front beam, while the thermal interface between l.e. TPS and acreage TPS is ahead of the l.e., at the maximum surface temperature tolerated by the RSI (the entire l.e. substructure is designed and bookkept under the l.e., see e.g., Ref. 7). Therefore, admitting RSI on the l.e. would have meant designing the substructure for the special requirements of the RSI, which was outside the scope of this study. The only way to allow in this study RSI ahead of the front beam would have been to start out from a given nose spar as interface.

There is also some measure of inconsistency between requiring a frozen shuttle system and forgoing interchangeability with the CC system, since a natural application for the ablative l.e. could be as back-up TPS for the CC system. Moreover comparisons with the CC system are of course considerably more difficult if compatibility is not required. However, one possible advantage is the exploration of the absolute optimum ablative l.e., unconstrained in any way. Unfortunately, the optimizations weight-versus-cost are done with values of a pound that are considerably different than those for a rubber system used in Phase B of the Shuttle program (see, for example Refs. 8 and 9).

Rule (h) requires the estimation of the value of a pound for a 'frozen' shuttle system. Such value does not appear in the literature. Naturally it should be larger than the value of a pound for the 'rubber' Shuttle system which during Phase B and beginning of Phase C ranged from 25,000 to 30,000 $/lbs. In estimating the 'frozen' value of a pound, the same point of view should be taken as in the case of the frozen system, namely (1) the payload is rubberized, (2) each flight has a full payload, and (3) the same performance, i.e. payload

carried, is desired no matter whether the shuttle system suffers a weight growth or shrinkage. Of course, a critical review of this point of view is not relevant here. It follows that if the orbiter undergoes a weight increase (decrease), flight(s) need to be added (eliminated) to carry the same total payload over the entire traffic. From the costs of these flights, one can easily calculate the cost of a weight change. We will make the reasonable assumption that number of vehicles, shuttle program DDT&T costs, schedule, turn-around times, etc. will remain the same. Then, when ΔWp is the payload that cannot be carried in each flight because of an increase in weight ΔWp of the orbiter, the cost of the extra flights needed is $\Delta Wp.Nc_2/Wp$ where N is the number of flights in the traffic model, Wp the payload of the orbiter and c_2 the (recurrent) cost of an operational flight. The value of weight savings is then Nc_2/Wp. For the NASA traffic model, the current payload of 65 K lbs, and the currently projected cost per flight of 10.5M$ (Ref. 10), the value of a pound is 72,000 $/lb. We tried as much as possible not to use ground rule (h) and the extremely high value of a pound it imposes upon this study.

Turning now to the requirements for the ablative i.e., these are:

(a) First of all, to withstand the environments, aerothermal, structural and natural. The data needed to characterize these environments are examined in Section 3.

(b) Roughness and shape change should produce acceptable degradation of the low speed aerodynamic characteristics of the orbiter. Ultimately, one would like to know the maximum 'acceptable' value for roughness levels below the maximum. This question is taken up in a preliminary fashion in Section 4.

(c) Roughness should produce a shift in boundary layer transition that causes 'acceptable' heating increases in the RSI area; probably much more important than the roughness effect, the ablator should cause 'acceptable' contamination of the RSI. But no information is available on what is 'acceptable,' nor could the detailed study needed be fitted into our study.

(d) The refurbishment of the orbiter l.e. should fit into the vehicle turnaround time which is currently (June 1973) required to be between 150 and 250 elapsed hours. (Ref. 11).

3. ORBITER L.E. ENVIRONMENT

This section covers the effort involved in determining the environmental factors that characterize the environment encountered over a typical set of missions. From such data came the design environments used in this study. Full details are collected in the Data Package.

3.1 Thermal

The aerothermal environment (pressure, shear stress and cold wall heat flux) for two shuttle orbiters configurations (GAC 473 and NASA 040A) and several trajectories (nominal, dispersed, and abort ascent/reentry) were first determined for wing LE, fin LE and nose. A matrix of aerothermal environmental factors was generated. Similar data available of the NAR, MDAC, & LMSC Phase B orbiters were included in this matrix.

A brief outline of the methods used in the calculations of heat flux, shear stress and pressure follows.

Stagnation line/point pressures were calculated using the hypersonic relation:

$$P_{SL} = 1.35\ P_\infty\ M^2_{\Lambda,EFF} \qquad M_{\Lambda,EFF} = M_\infty \cos \Lambda_{EFF}$$

$$\Lambda_{EFF} = \sin^{-1}\left\{ \sin \Lambda \cos \phi + \cos \Lambda \sin \alpha \sin \phi \right\}$$

ϕ dihedral

Λ l.e. sweep

Pressure distributions normal to the leading edge were calculated using modified Newtonian theory on the windward and Prandtl-Meyer expansion on the leeside.

Heat flux values were calculated by modifying the Fay-Riddell one foot reference sphere values calculated for each trajectory for radius difference at the nose and by swept cylinder theory on the leading edges,

$$\dot{q}_{SL} = 0.707 \; \dot{q}_{REF}\sqrt{\frac{R_{REF}}{R_\Lambda}} \qquad (\cos \Lambda_{EFF})^{1.2}$$

$\dot{q}_{REF}$ is the stagnation point heating on the sphere with radius R_{REF}, R_Λ is the stagnation point l.e. radius evaluated in a plane normal to the l.e. (subscript Λ means in the plane normal to the l.e.). Distributions normal to the leading edge were calculated using a Lees distribution normalized by the stagnation value,

$$\frac{\dot{q}}{\dot{q}_{SL}} = \frac{\left(\frac{\rho}{\rho_{SL}}\right)_\Lambda \left(\frac{U_e}{U_\infty}\right)_\Lambda}{\left\{\frac{2}{U_{\infty,\Lambda}} \cdot \frac{dU_e}{ds} \int_0^s \left(\frac{\rho}{\rho_{SL}}\right)_\Lambda \cdot \left(\frac{U_e}{U_\infty}\right)_\Lambda \cdot ds\right\}^{1/2}}$$

All heat flux are for a cold wall ($H_w/H_e \to o$). The temperature distributions are at radiation equilibrium conditions. U_e is the boundary edge velocity, U_∞ the free stream velocity, s is the arc length (from the stagnation point) measured in a plane normal to the l.e. Shear stress was calculated using a Reynolds analogy with the analogy factor of 1.24,

$$\tau = \frac{\dot{q}\, V_e}{1.24\, g(H_r - H_w)} \qquad H_r >> H_w$$

V_e = boundary layer edge velocity
g = acceleration of gravity
H_r = recovery enthalpy

Shear stress distributions on the leading edges are normalized by the stagnation line value. On the nose, they are normalized by the maximum value.

Heat flux and pressure amplification on the wing leading edge due to bow shock impingement has been included. The shock envelope was determined through a combination of blast wave, shock expansion theories and experimental Schlieren data along the nominal trajectory.

Viscid/inviscid interaction corrections at low Reynolds number were applied to heating in regions of attached boundary layers, and found to be dominant

near peak entry heating where increases of up to 20% were incorporated. No data exist on low-Reynolds-number effects on heating amplification due to shock impingement. Applying a correction such as that for attached boundary layers would be overly conservative and therefore has not been done.

From the detailed data generated (nearly 250 curves, see Data Package), a matrix of aerothermal environments was extracted. Actually, it was schematized in two matrixes, one of 'dominant' heating rates, etc. and one of maximum heating rates. For the stagnation region, figures 3 and 4 give heat flux and pressure gradient respectively; the parameters of the mid points in these matrixes are given in tables 1 and 2. For the GAC 473 the maximum environment is experienced only on some 2.5% of the leading edge area. Tables 3 and 4 give the dominant and maximum aerothermal environment for the typical windward region where the windward spanwise joint is located.

The ascent trajectories evaluated were nominal and abort to orbit. Nominal ascent precedes a normal seven day orbital mission, whereas abort to orbit is succeeded by one revolution and entry. The difference in the two ascent environments is minimal.

The entry environment deserves closer scrutiny. As seen in figure 3, it depends closely on trajectory and configuration. Some data points should be discounted on the basis of unrealistic leading edge geometry in configurations that have not been scrutinized from all points of view. The remainder can be grouped into two categories based on whether or not the leading edge is sometimes, during entry, impinged upon by the bow shock of the vehicle. The categories are designated dominant (no impingement) and maximum (impingement) and exist for ascent as well. The categories are outlined in figures 3 and 4 and presented in tables 1 and 2.

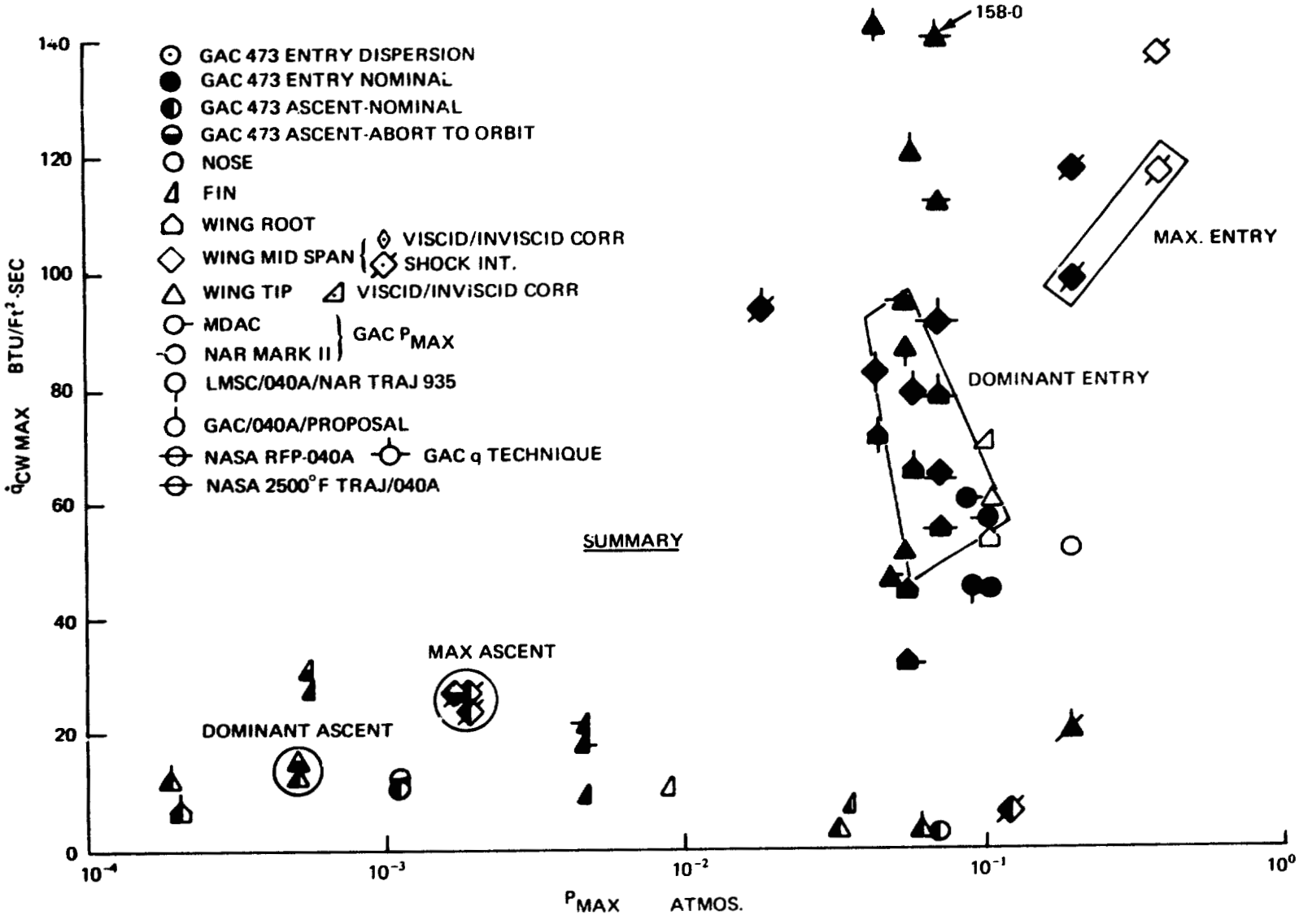

Figure 3. Matrix of Heating Environments of Orbiter Nose and Leading Edges

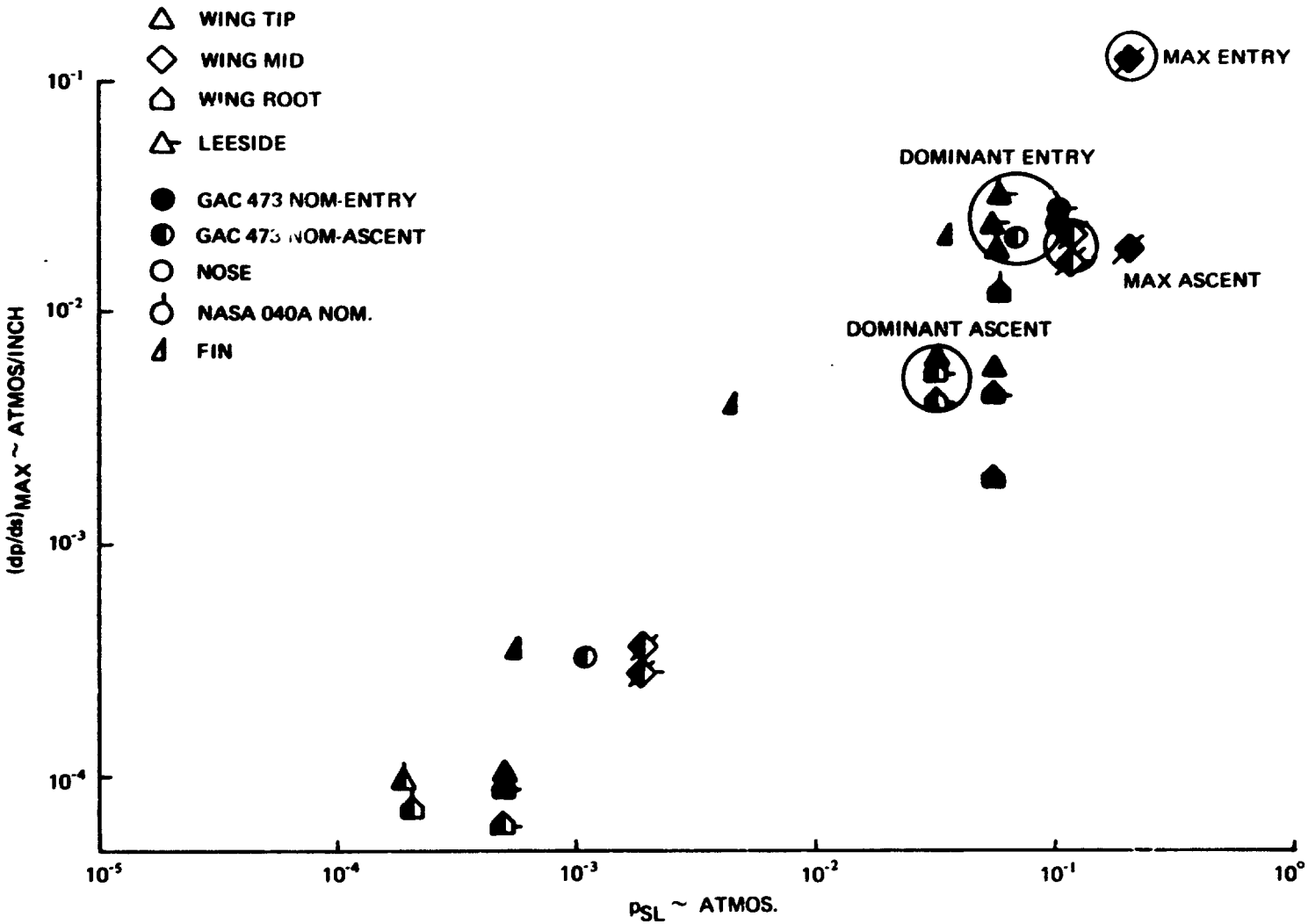

Figure 4 Matrix of Pressure Environments of Orbiter Nose and Leading Edges

Table 1 Typical Ascent Environments for L.E. Stagnation Region

		Dominant	Maximum
$\dot{q}_{cw}$	$Btu/ft^2 \cdot sec$	14	25
P_{Max} at $\dot{q}_{cw}$	atmos	5×10^{-4}	1.8×10^{-3}
H at $\dot{q}$	Btu/#m	10,200	10,200
$P_{t\infty}$ at P_{Max}	atmos	48.5	48.5
$T_{t\infty}$ at $\dot{q}_{cw}$	^oR	8700	8700
M_∞ at P_{max}	–	28	28
Altitude at $\dot{q}_{cw}$	ft	300,000	300,000
ρ_s at $\dot{q}_{cw}$	$\#m/ft^3$	1.3×10^{-6}	4.9×10^{-6}
Re_∞ at $\dot{q}_{cw}$	1/ft	–	–
$\left(\frac{dP}{ds}\right)_{Max}$	atmos/inch	5×10^{-3}	2×10^{-2}
τ_{Max}	$\#f/ft^2$	1.5	1.5
Q	Btu/ft^2	6,700	12,000
Time at $\dot{q}_{cw}$	sec	250	250

Symbols

P	Pressure
P_t	Total pressure
T_t	Total Temperature
ρ_s	Density at stagnation point
$Re_\infty = \frac{U_\infty \rho_\infty}{\mu_\infty}$	
τ	Shear stress
$\left(\frac{dP}{ds}\right)_{Max}$	Max pressure gradient on the L.E. (in a plane normal to the L.E.)

Subscripts

∞	Free stream
Max	Along trajectory or on L.E.

Table 2 Typical Entry Environments for L.E. Stagnation Region

		Dominant	Maximum
$\dot{q}_{cw}$	Btu/ft^2-sec	70	110
P_{Max} (at $\dot{q}_{cw}$)	atmos	7×10^{-2}	.3
H at $\dot{q}_{cw}$	Btu/#m	11,400	11,400
P_{t_∞} at P_{Max}	atmos	320	320
T_{t_∞} at $\dot{q}_{cw}$	^oR	10,75	10,750
M_∞ at P_{Max}	–	14	14
Altitude at $\dot{q}_{cw}$	ft	220,000	220,000
f_s at $\dot{q}_{cw}$	#m/ft^3	$.8 \times 10^{-4}$	3×10^{-4}
Re at $\dot{q}_{cw}$	1/ft	1.9×10^4	1.9×10^4
$\frac{dP}{ds}$	atmos/inch	2.8×10^{-2}	1.3×10^{-1}
τ_{Max}	#f/ft^2	2.4	2.4
Q.	Btu/ft^2	64,200	124,800
Time at $\dot{q}_{cw}$	sec	800	800

Symbols: See Table 1.

Table 3 Typical Ascent Environments for Windward Joint Region

		Dominant	Maximum
$\dot{q}_{cw}$	$Btu/ft^2\text{-}sec$	1.4	2.5
P_{Max}	atmos	0.3×10^{-4}	0.11×10^{-3}
H at $\dot{q}_{cw}$	Btu/#m	same as for stagn. line	same as for stagn. line
$\rho_{t\infty}$ at P_{Max}	atmos	↓	↓
$T_{t\infty}$ at $\dot{q}_{cw}$	^oR	↓	↓
M_∞ at P_{Max}	–	↓	↓
Altitude at $\dot{q}_{cw}$	ft	↓	↓
ρ_s at $\dot{q}_{cw}$	$\#m/ft^3$	↓	↓
Re at $\dot{q}_{cw}$	1/ft	↓	↓
$\frac{dP}{ds}$	atm/inch	negligible	negligible
τ_{Max}	$\#f/ft^2$	0.15	0.15
Q	Btu/ft^2	670	1200
Time at $\dot{q}_{cw}$	sec	250	250

Symbols: See Table 1

Table 4 Typical Entry Environments for Windward Joint Region

		Dominant	Maximum
$\dot{q}_{cw}$	Btu/ft^2-sec	27	42
P_{Max}	atmos	4.1×10^{-2}	0.21
H at $\dot{q}_{cw}$	Btu/#m	same as for stagn. line	same as for stagn. line
$P_{t\infty}$ at P_{Max}	atmos	↓	↓
$T_{t\infty}$ at $\dot{q}_{cw}$	^oR	↓	↓
M_∞ at P_{Max}	–	↓	↓
Altitude at $\dot{q}_{cw}$	ft	↓	↓
ρ_s at $\dot{q}_{cw}$	$\#m/ft^3$	↓	↓
Re at $\dot{q}_{cw}$	1/ft	↓	↓
$\frac{dP}{dS}$	atm/inch	negligible	negligible
τ_{Max}	$\#f/ft^2$	0.72	0.72
Q	Btu/ft^2	18,300	34,700
Time at $\dot{q}_{cw}$	sec	800	800

Symbols: See Table 1

In estimating the surface area affected by maximum heating, the information generated on the Grumman 473 represent easily a worst case, since the bow shock is estimated to be stationary on a fixed span position. Figure 5 indicates a maximum no-shock heating of 50.8 Btu/ft^2-sec to occur at the wing tip. Figure 6 presents the midspan shock-impingement heat flux. Comparison of these figures and application for the distribution given in figure 7 indicates that heat fluxes greater than 50.8 will be experienced over only 2-1/2% chord on the leading edge. Spanwise one can take for safety that there is amplification over 10% of the exposed span, which is reasonable since the shock traverses only about 5% exposed span. This leads to the conclusion that only about 2-1/2% of the total wing leading edge surface* receives greater than the dominant (50.8) heat flux. The figures also indicate that this condition persists for only 2/3 of the total entry time. If shock impingement is eliminated, the midspan environment of the 473 orbiter becomes the same as for the wing tip, figure 6.

The same sort of considerations are applied to the windward region where the spanwise joint is located (8% chord).

3.2 Structural

3.2.1 Static Structural Environment

The structural environment was obtained from a separate study of three critical flight conditions made for the Grumman 473 and NASA 040A shuttle orbiters. These critical flight conditions are listed in tables 5a and 5b identified as Max $q\alpha$ (+), Max $q\alpha$ (-) and 2-1/2g pullout. Data generated for these conditions are as follows:

---

* Wing L.E. defined as 10% of the chord.

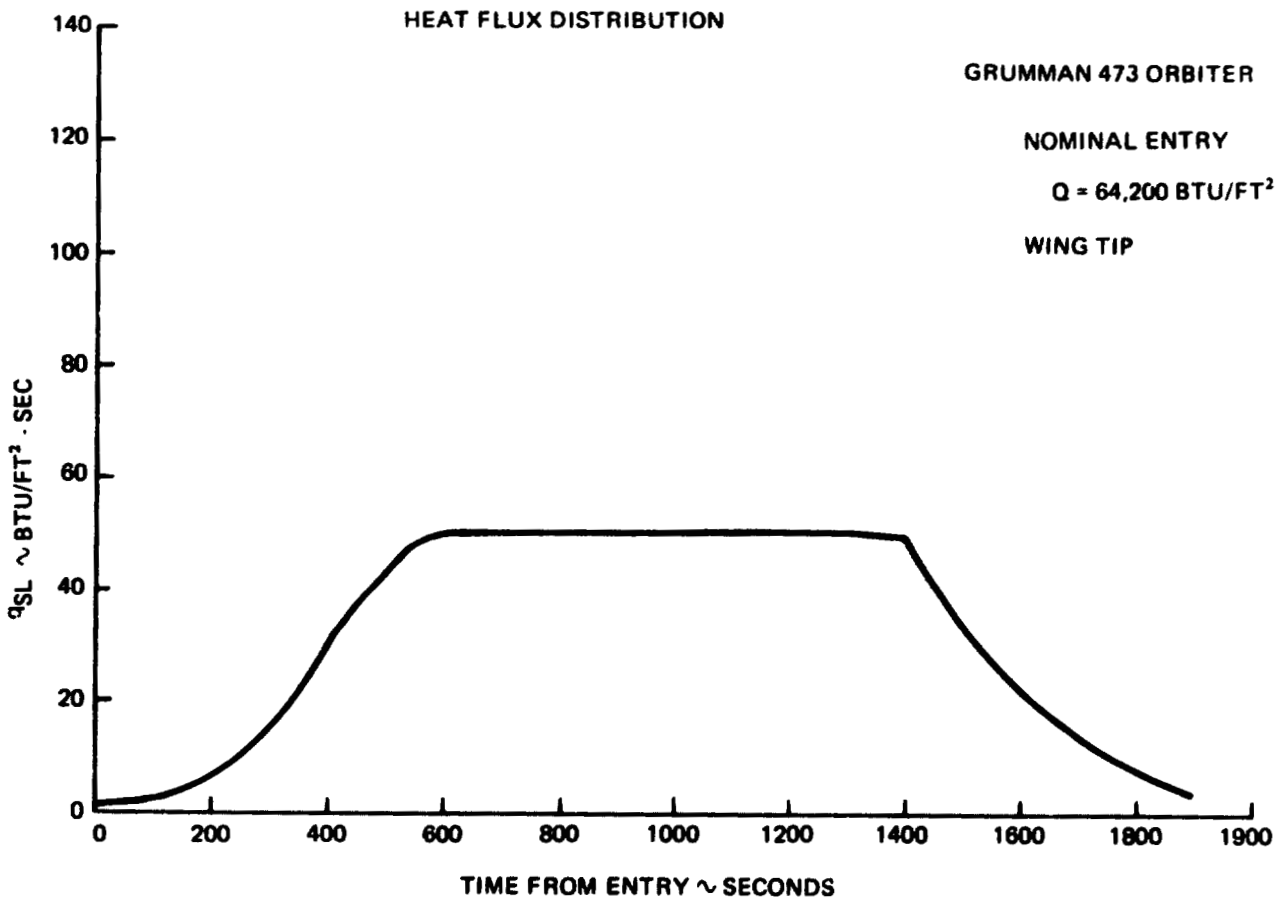

Figure 5 Heat Flux Time History During Entry Without Shock Impingement

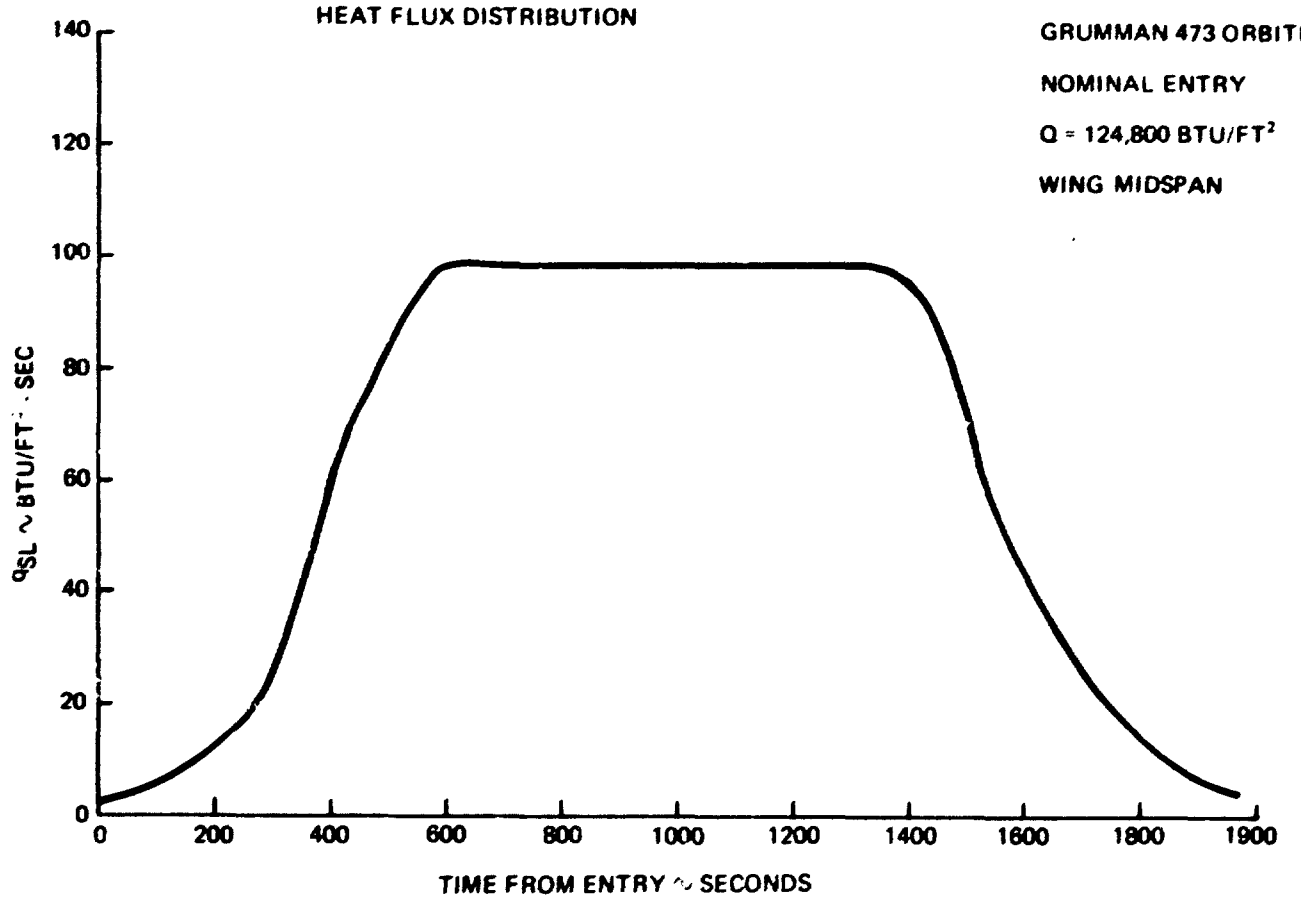

Figure 6 Heat Flux Time History During Entry with Shock Impingement

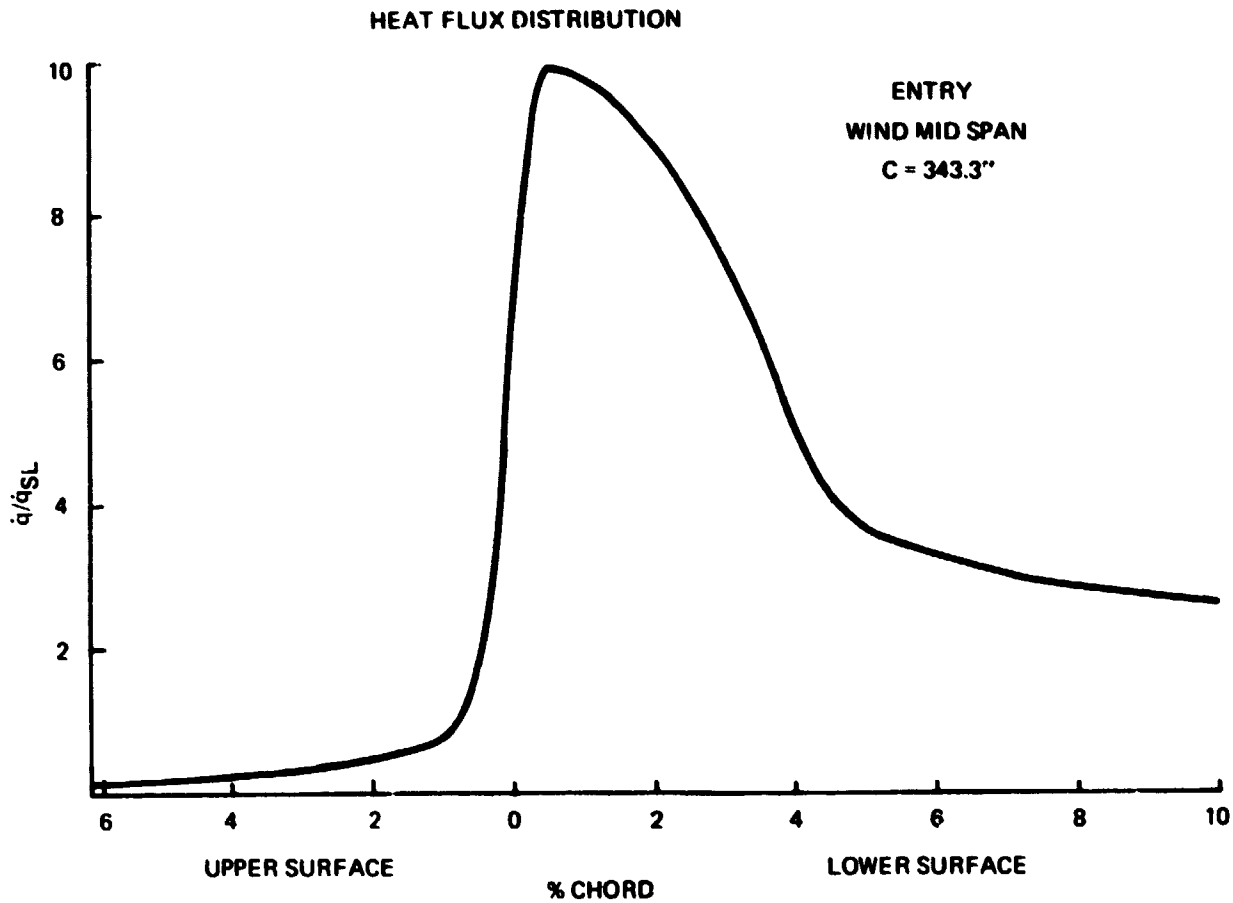

Figure 7 Heat Flux L.E. Distribution During Entry Without Shock Impingement

Table 5 Critical Conditions for Structural Environment

(a) 040A Orbiter

	Critical Conditions*			Other Conditions		
	Max $q\alpha(+)$	Max $q\alpha(-)$	2½g Pullout	Landing (Touch-Down)	Entry*	Abort on Ascent
Ascent/Entry/Post Entry	Ascent	Ascent	Post Entry	Post Entry	Entry	Ascent
Altitude (ft)	33,000	33,000	15,000	0	160,000	130,000
Velocity (ft/sec)	972	972	634	223	8,400	7,100
Mach Number	1.0	1.0	0.60	0.20	5.63	7.2
Angle of Attack (degrees)	3.0	3.0	13.2	20.7	27	29
Wing Structure Temperature [Based on Ablative TPS & Alum]	Room Temp	Room Temp	200°F	Hot Condition	100°F	Room Temp

(b) 473 Orbiter

	Critical Conditions*			Other Conditions		
	Max $q\alpha(+)$	Max $q\alpha(-)$	2½g Pullout	Landing (Touch-Down)	Entry*	Abort on Ascent
Ascent/Entry/Post Entry	Ascent	Ascent	Post Entry	Post Entry	Entry	Ascent
Altitude (ft)	28,000	28,000	14,000	0	160,000	130,000
Velocity (ft/sec)	1320	1320	734	313	10,000	7,100
Mach Number	1.28	1.28	0.69	0.28	9.1	7.2
Angle of Attack (degrees)	3.2	3.2	7.4	20.7	30	29
Wing Structure Temperature [Base on Ablative TPS & Alum]	Room Temp	Room Temp	200°F	Hot Condition	100°F	Room Temp

*Nominal trajectory.

1. External pressure distribution along the chordwise contour (up to the front beam of the leading edge) were obtained at root, midspan, and tip (as shown typically in figures 8 and 9 for the 040A & 473 orbiters respectively). Complete data for all flight conditions are given in the Data Package. Figures 10 and 11 define the root, midspan and top locations. Total shear and moment with respect to the front beam for these locations are also available (references in the Data Package).
2. Internal pressure distribution as shown in figures 8 and 9.
3. Spanwise deflections of the front beam are given in figures 12 and 13 and spanwise curvatures in figures 14 and 15.
4. The spanwise strains in the caps of the front beam and therefore also in the aluminum l.e. substructure if and where the substructure follows the beam deflections is shown in figures 16 and 17.

These data were condensed into one matrix showing the relation of strain versus curvature in the L.E. upper and lower skin just forward of the front beam (if the skin follows the front beam) for all three flight conditions, figure 18.

Figure 18 data are used to establish the spanwise stress/strain environment for the design of the substructure.

3.2.2 Dynamic Structural Environment

The wing leading edge vibration environments were investigated for five conditions--lift off, max q on ascent, entry, max q on post entry, and touchdown--

040A ORBITER

MAX q α (+) & q α (−)

NOTE:
- CONTOURS ARE CROSS SECTIONS NORMAL TO THE L.E.
- PRESSURES ARE PLOTTED ALONG NORMALS TO THE OML

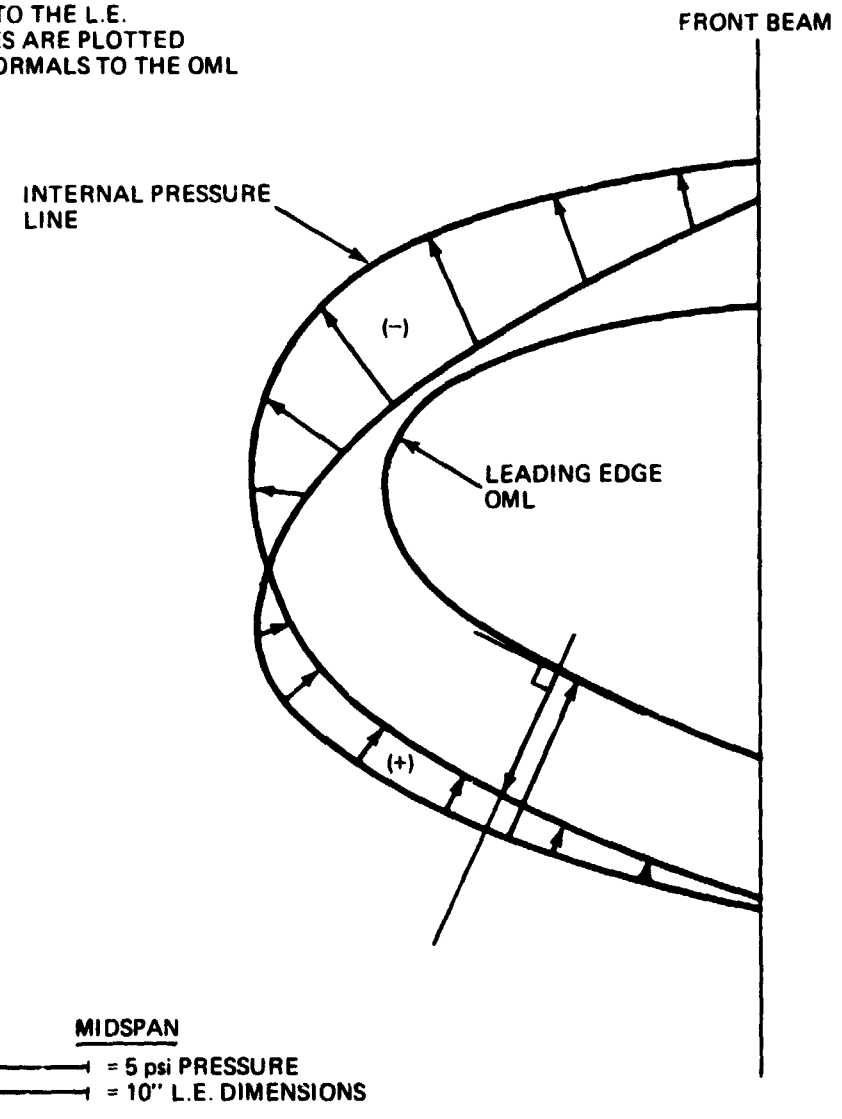

Figure 8 Aerodynamic Loads at One Critical Condition - 040A Orbiter

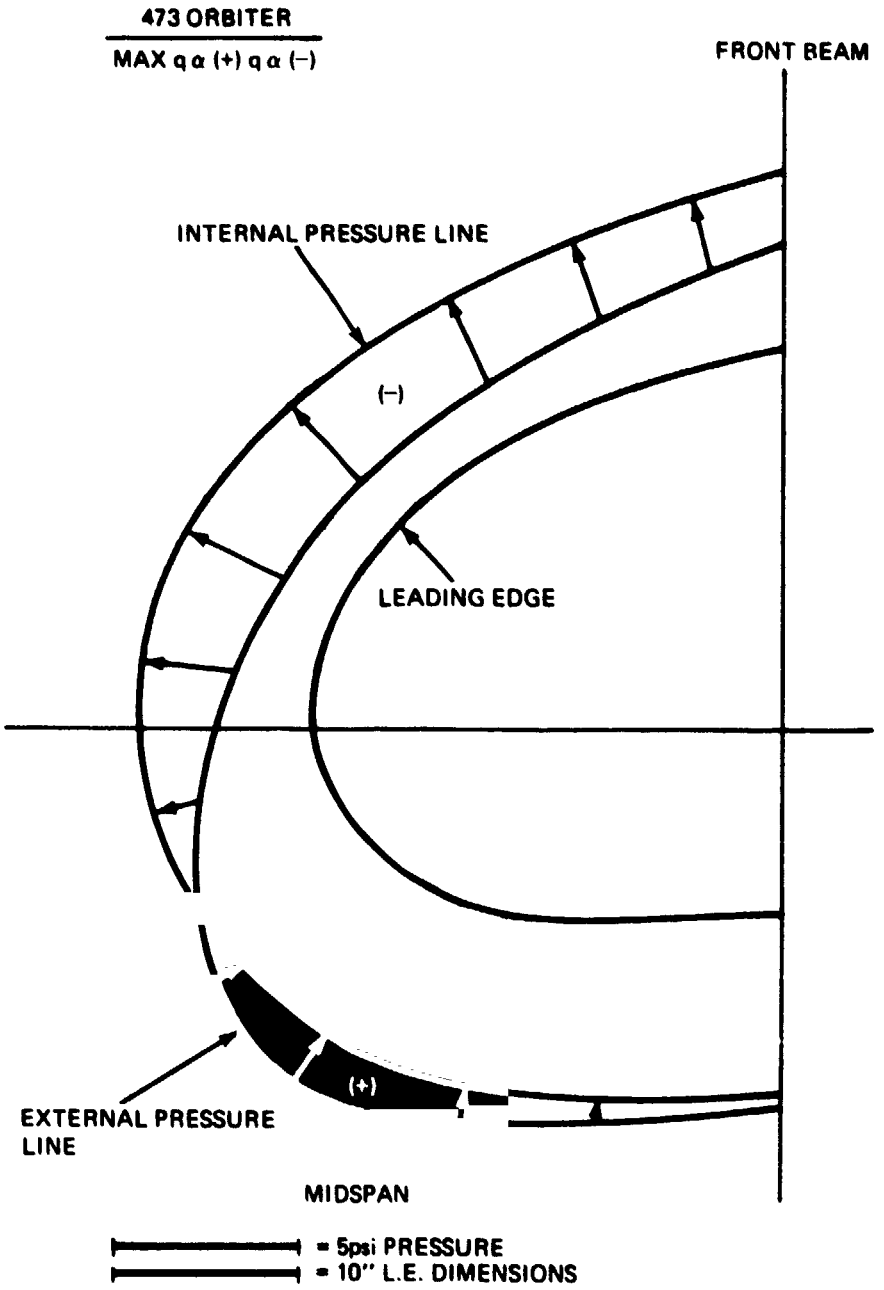

Figure 9 Aerodynamic Loads at One Critical Condition - 473 Orbiter

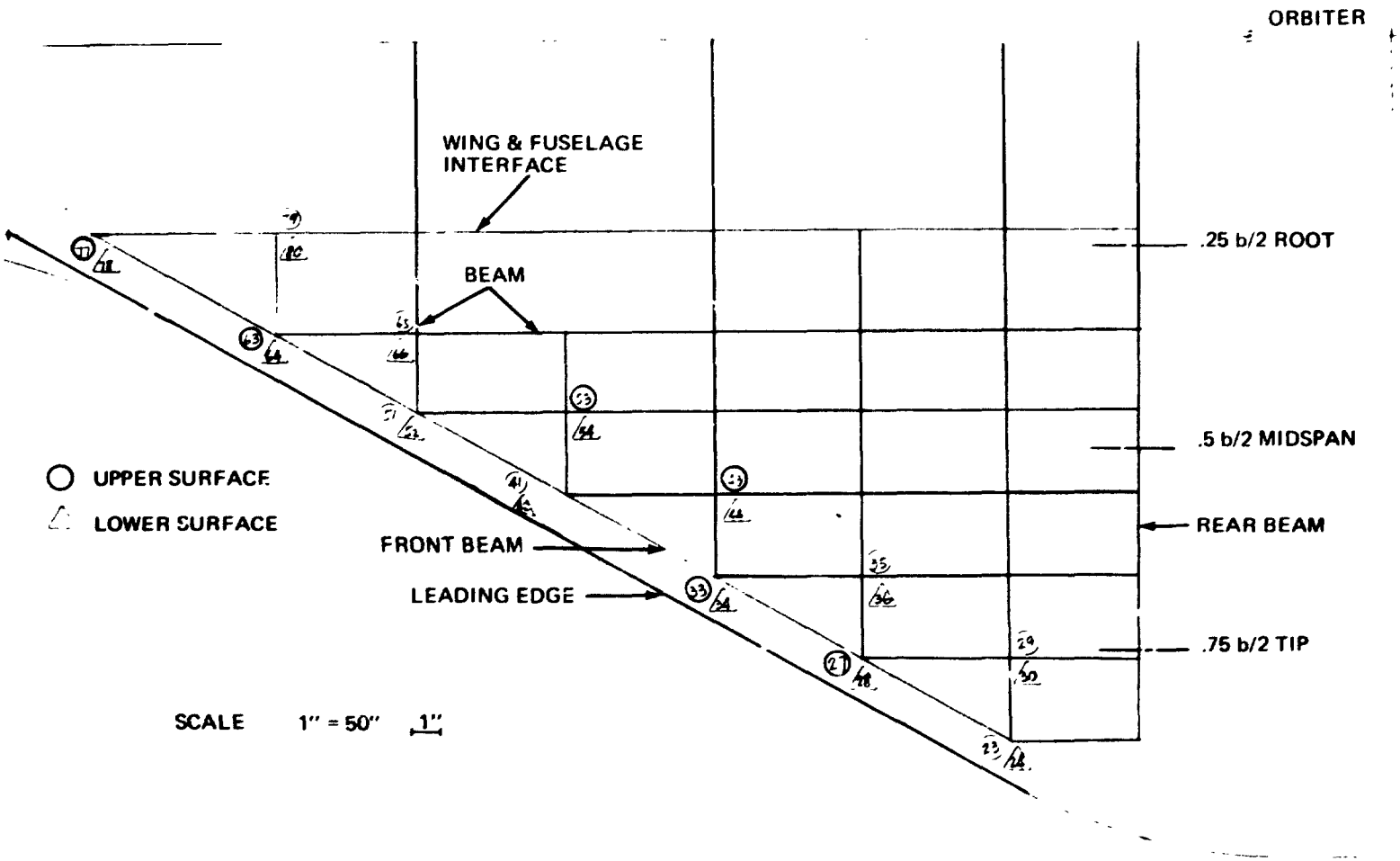

Figure 10 040A Orbiter: Typical Wing Structure

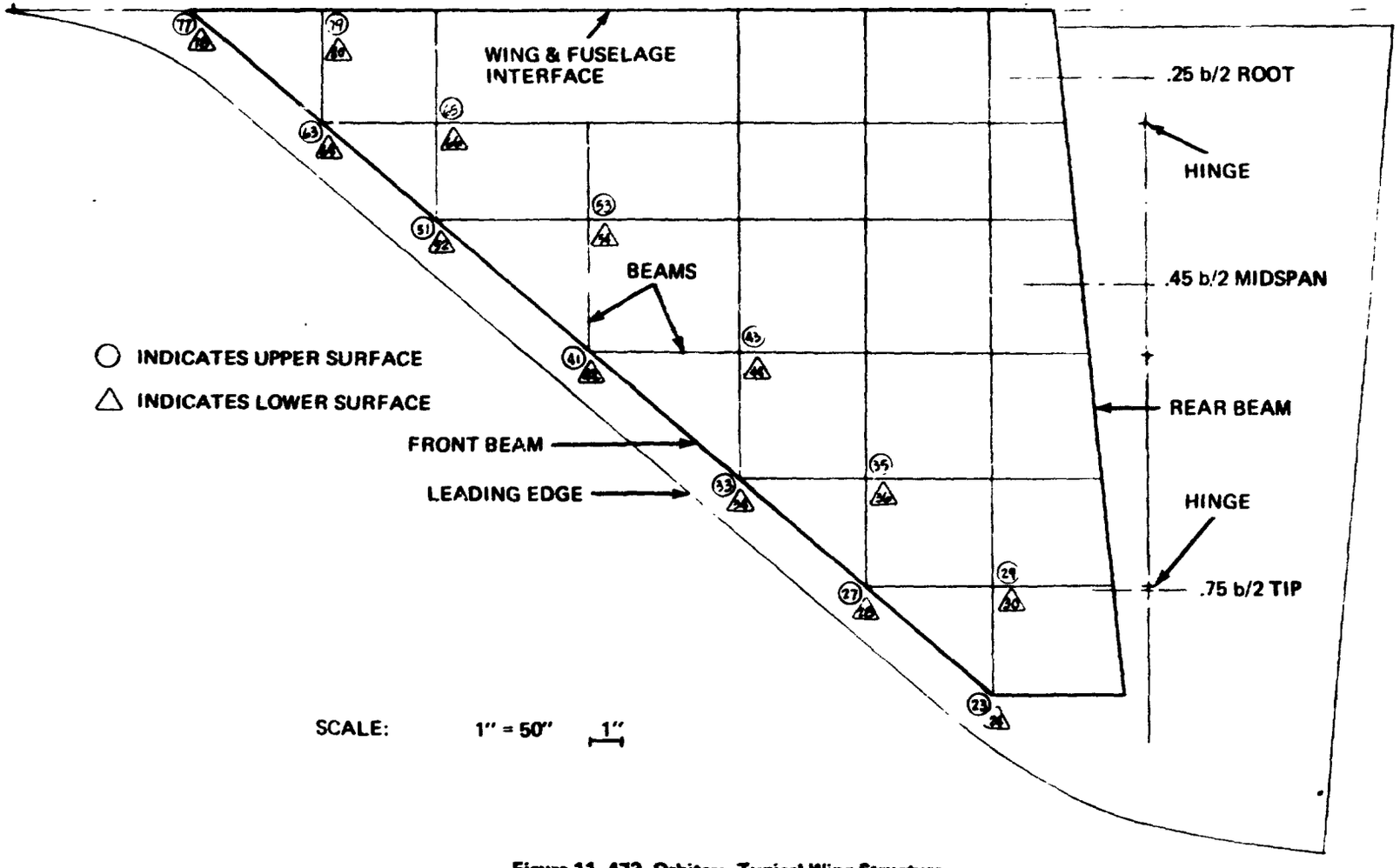

Figure 11 473 Orbiter: Typical Wing Structure

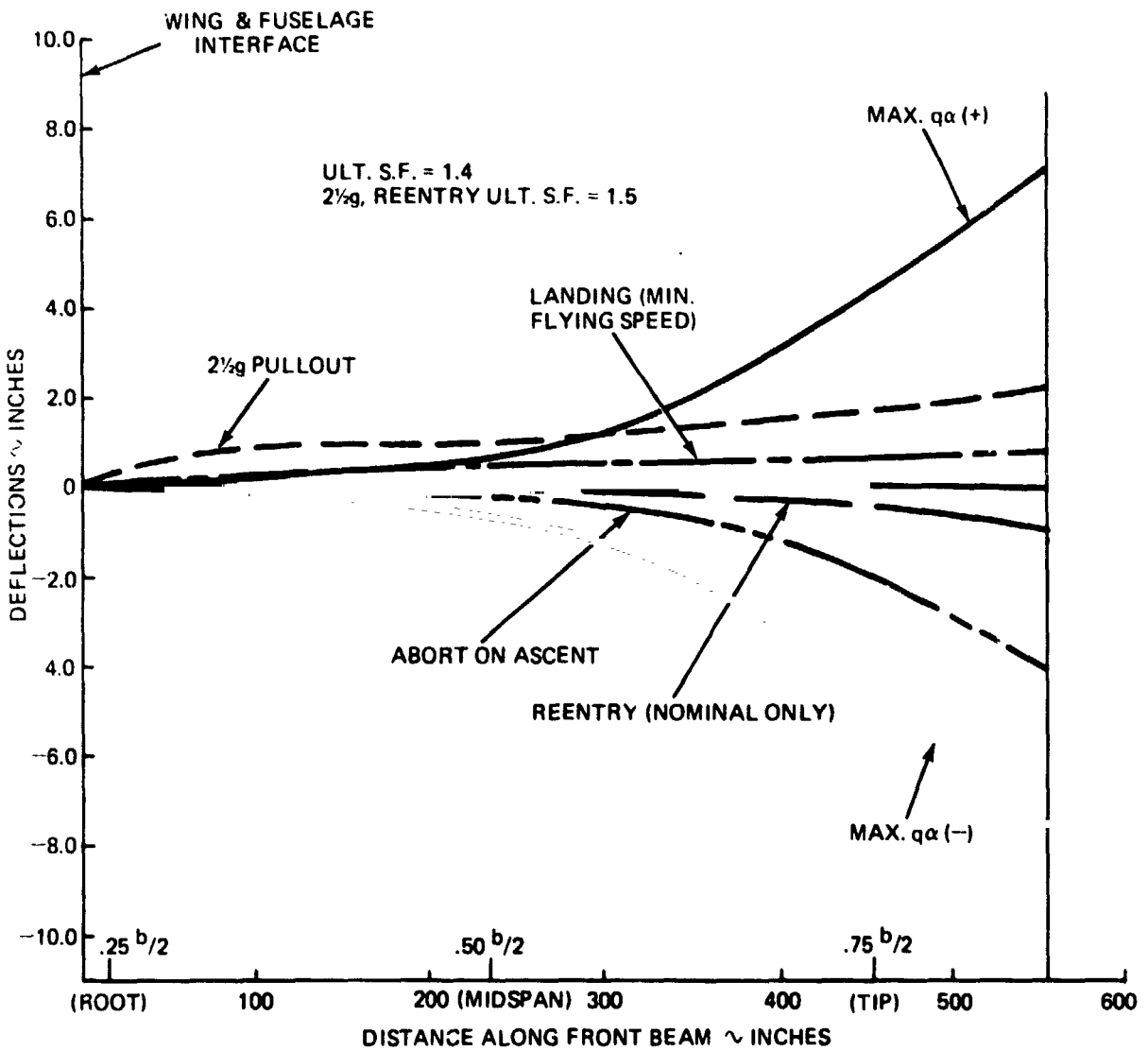

Figure 12. Wing Front Beam Deflections For 040A Orbiter Configuration

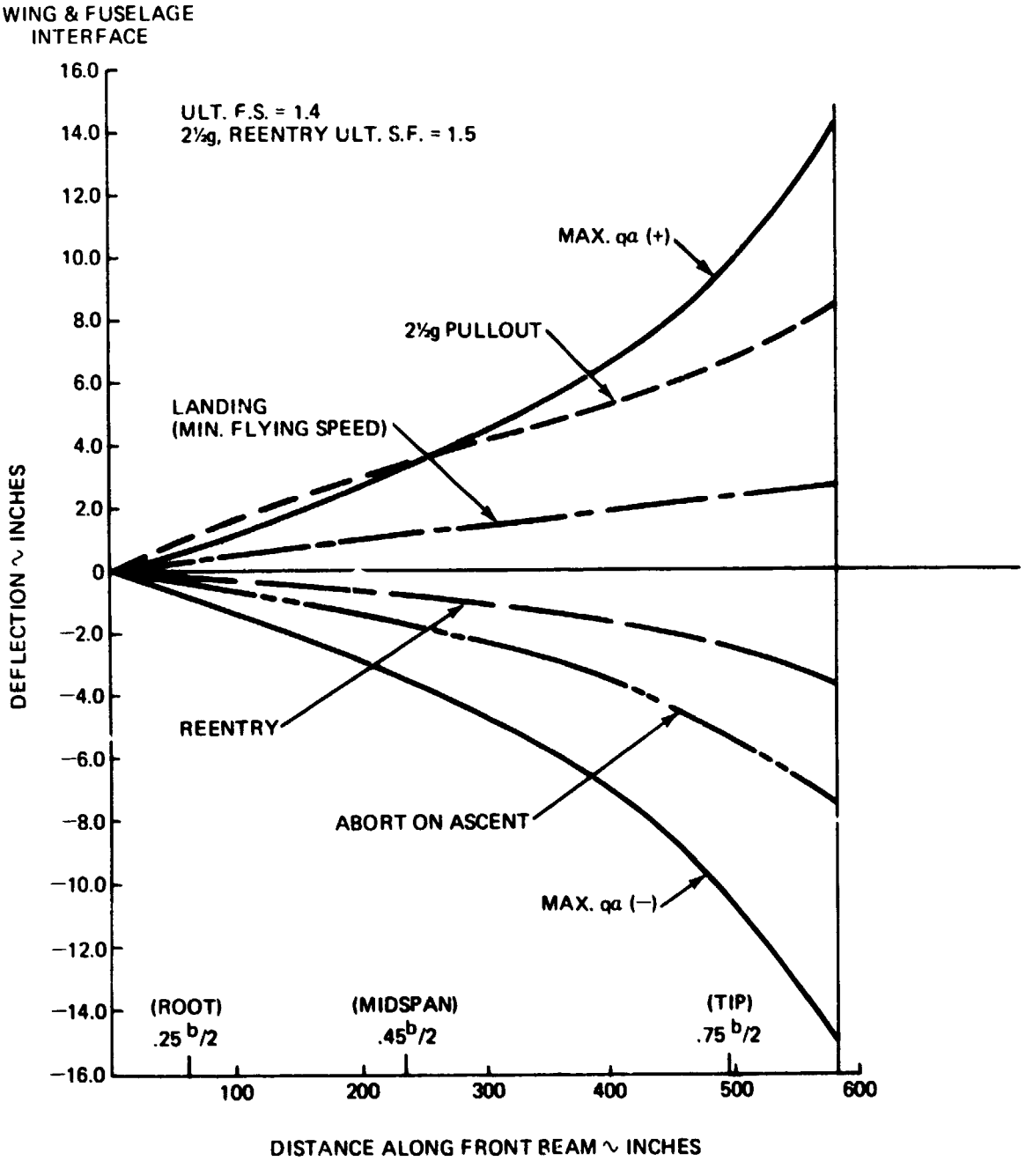

Figure 13. Wing Front Beam Deflections For 473 Orbiter Configuration

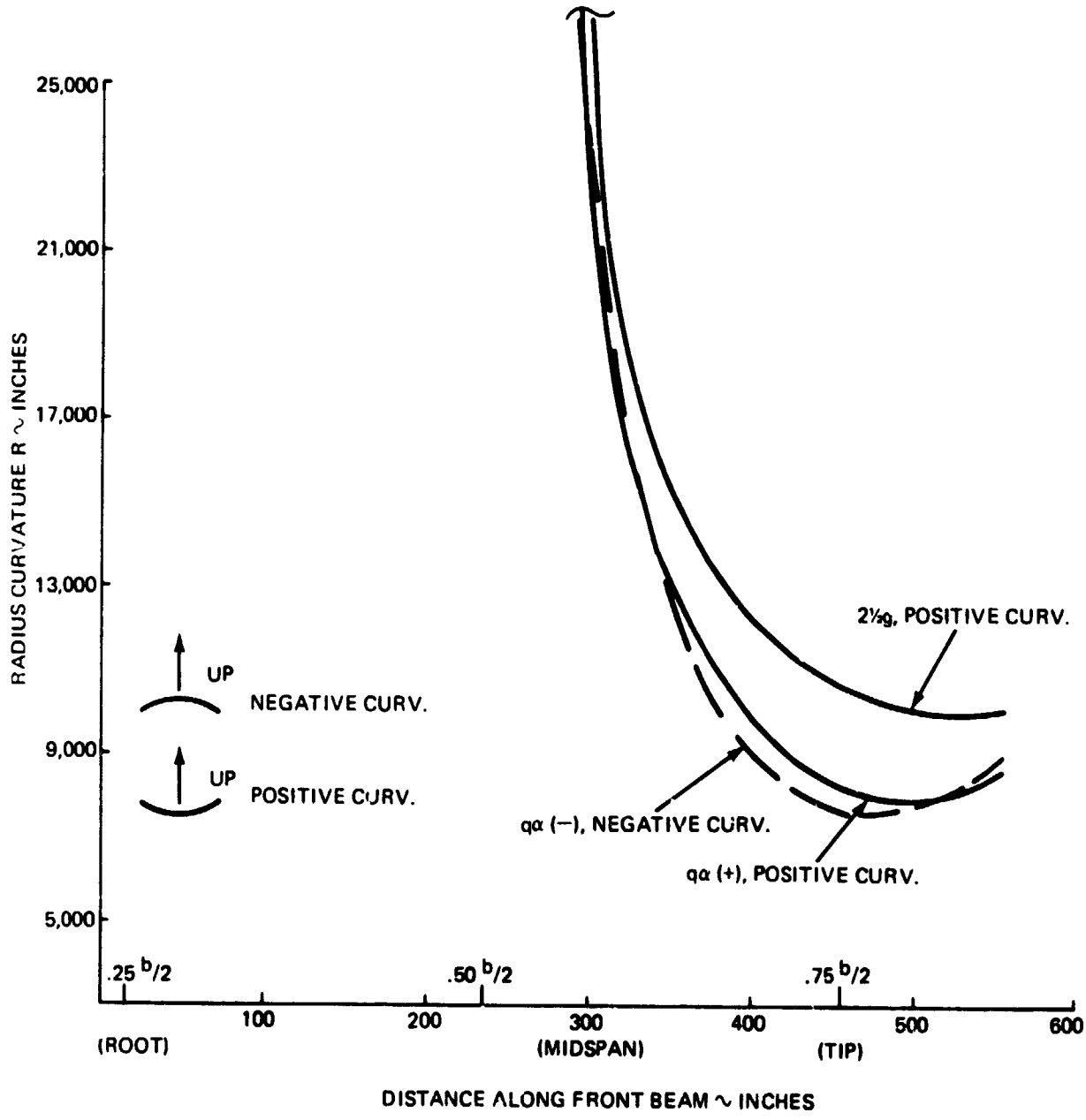

Figure 14. 040A Orbiter – Spanwise Curvature of Front Beam (at Midweb)

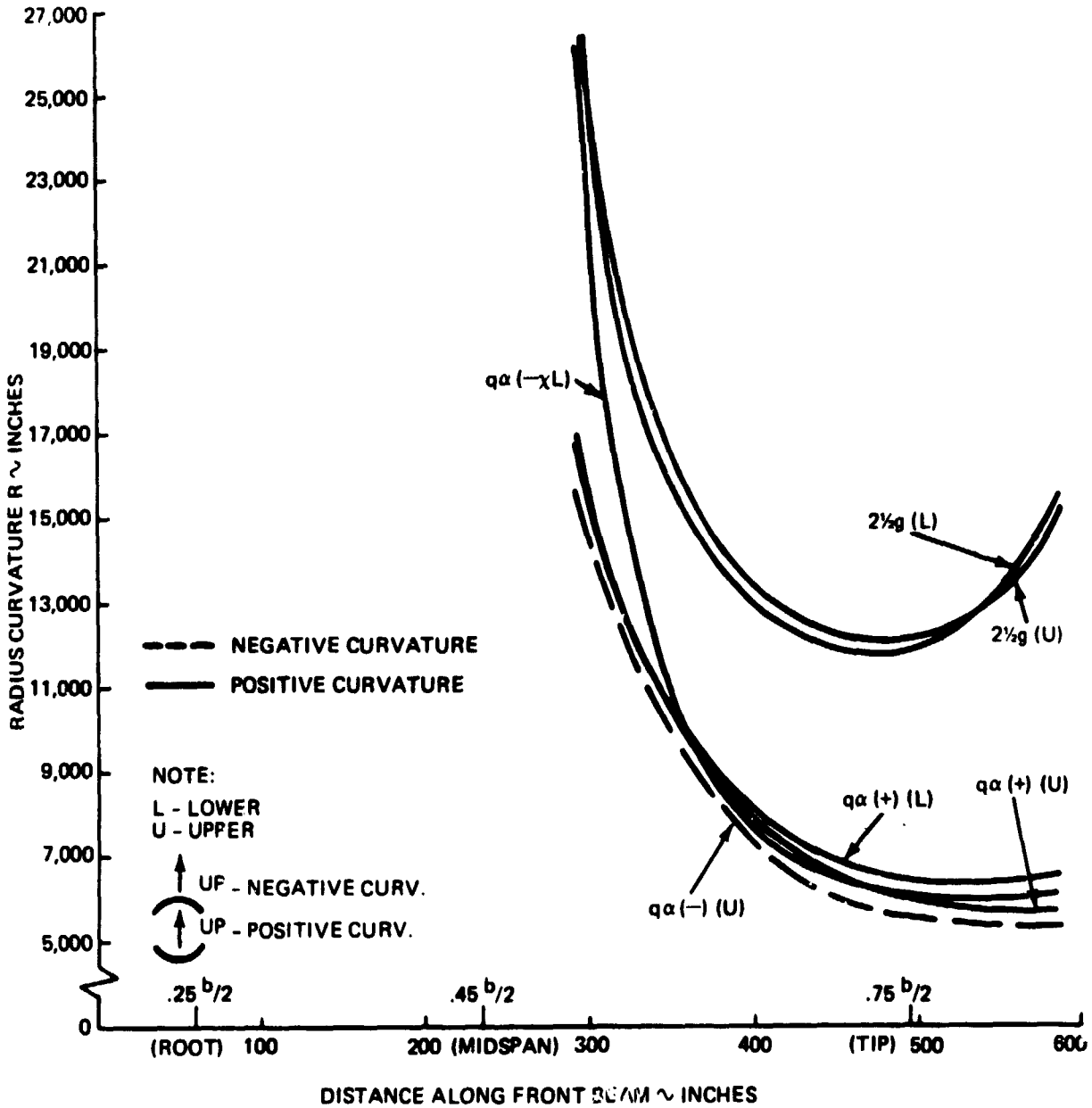

Figure 15 473 Orbiter – Spanwise Curvature of Front Beam Caps

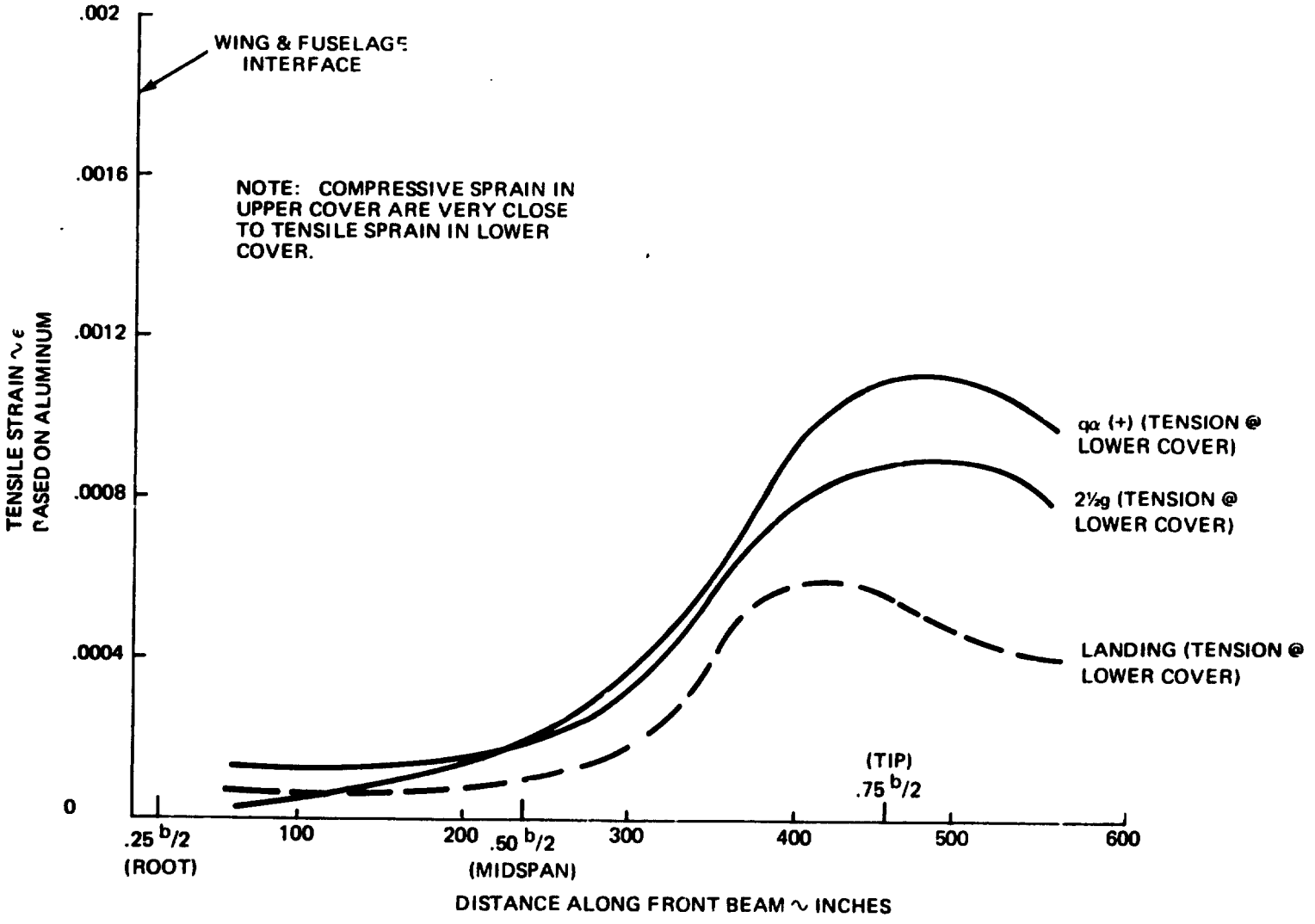

Figure 16. 040A Orbiter – Tensile Strain Along Front Beam

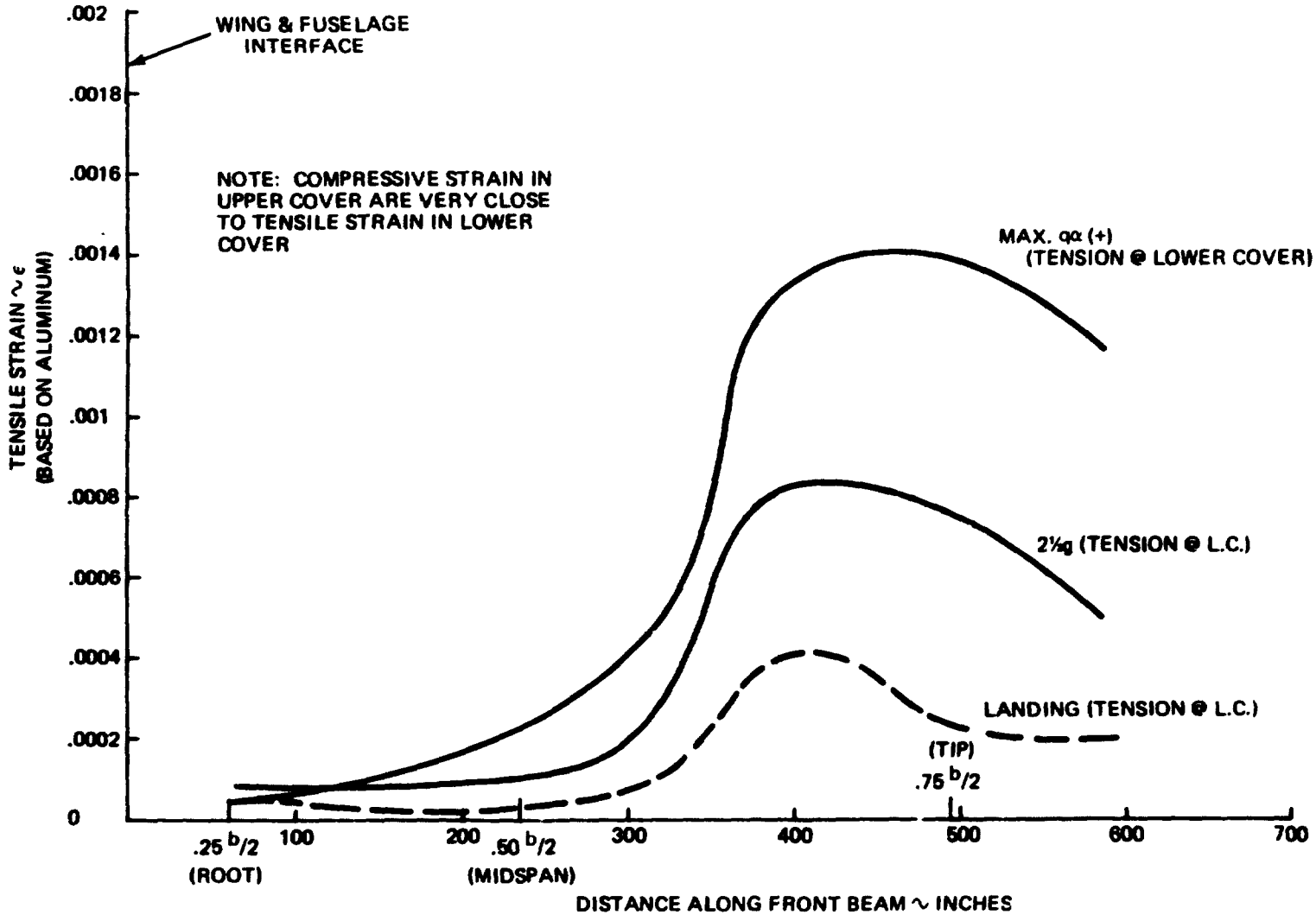

Figure 17. 473 Orbiter -- Tensile Strain Along Front Beam

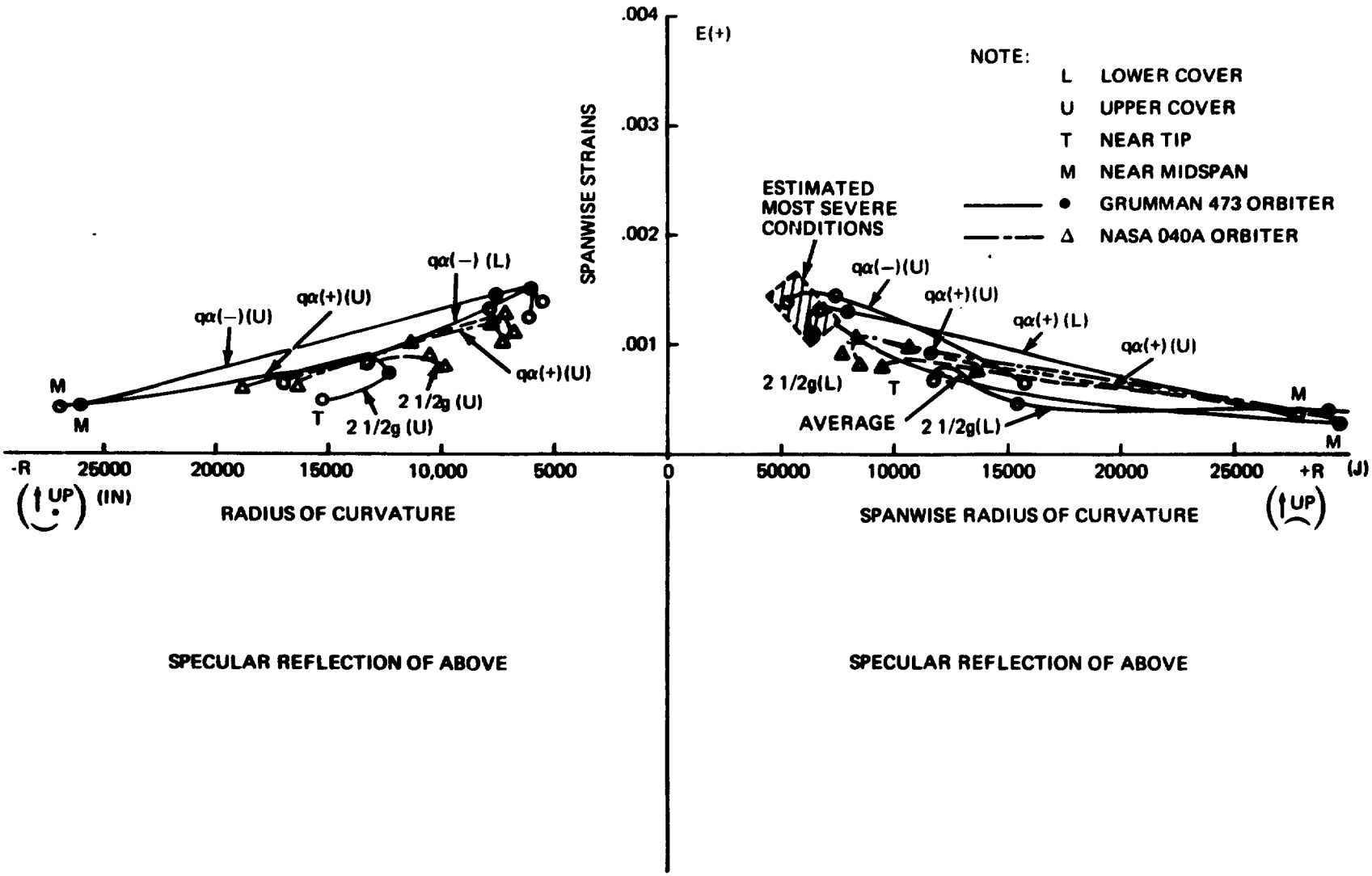

Figure 18 Matrix of °F Substructure Strains Near Front Beam

for the Grumman 473 and NASA 040A shuttle orbiters. The vibration source and duration are shown in table 6.

From the sound pressure levels for each condition figure 19 was prepared which shows the most severe sound pressure levels and durations which an ablative L.E. would be exposed to in the virgin and the charred state.

In addition, touchdown generates the most severe acceleration condition on the charred ablator, 11 g at 15 Hz for two seconds. This may occur twice, once after regular flight and once after ferry to a depot.

3.3 Natural

The natural environments for the L.E. include rain, hail, cold soak, humidity and blowing sand and dust. Not only the values of the environmental factors, but also the conditions on the trajectory must be determined.

The critical natural environments for rain, hail, humidity and blowing sand and dust are given in table 7.

The trajectory conditions for the most severe rain encounter are given in table 8.

The orbiter undergoes a cold soak period of from one orbit to seven days. During that time the external surfaces, including the ablative leading edges are maintained at temperatures of between -150 and 200° F and experience pressures of less than 10^{-6} atmospheres.

A more complex problem is to determine the thermal environment during the initial phase of entry which occurs in the upper atmosphere (> 400,000). Calculations indicate the flow may be considered to be free molecular and therefore there is little heat flux or pressure dependence on geometry. This

Table 6 Vibration Environments for the Wing L.E.

Condition	Source	Condition Definition*			Environment Definition			Source of Data
		Altitude Ft.	Mach Number	Surface Temperature For Abl. TPS	Pressure Fluctuation Spectrum	Associated Acceleration Spectrum	Exposure Time Per Flight	
Lift Off	Sound Due to Engine Firing	00.000	0.00	R.T.	Fig. 3-17 Virgin	–	10 Sec	Est. from SAT V Spec-MFSC IN-AS i N-AD 70-1 July 1970 Prelim Limit loads for GIII Orb. HO Tank & SRM - #B36-123MO-72007 6/9/72
Max Q (Ascent)	Pressure fluctuations in Shock-Induced Separated regions	28,000 (GAC 473) 30,000 (NASA 040A)	1.3 (GAC 473) .95 (NASA 040A)	R.T.	↓	–	70 Sec	Est. from NASA TMX-2274 Vol III Paper 10 & NASA SP-SSPD-16, 1971; Ames Wind Tunnel Data – J. Dods #TMX 2570
Entry	Pressure fluctuations in separated regions due to shock impingement	206,000 to 116,000	18 to 3	950°F	Fig. 3-17 Charred	–	700 Sec	Report BBN on "Unsteady Aerodynamic Loads During Reentry of the Straight Wing Orbiter Config" – by: H.H. Heller D.G. Holmes
Max Q Post Entry	Pressure fluctuations in shock-induced separated regions	56,000 to 21,000	1.9 to 0.54	490°F	↓	–	250 Sec	GAC F-14 Report #LD303-141-2/A51-338R-16-6
Touchdown	Vibratory response to landing impact	0	0.28	180°F	–	11G at 15 Hz	2 sec	GAC Preliminary Dynamic Analysis

*Nominal trajectory typical for orbiter configurations. Conditions given are those for which the spectra are given.

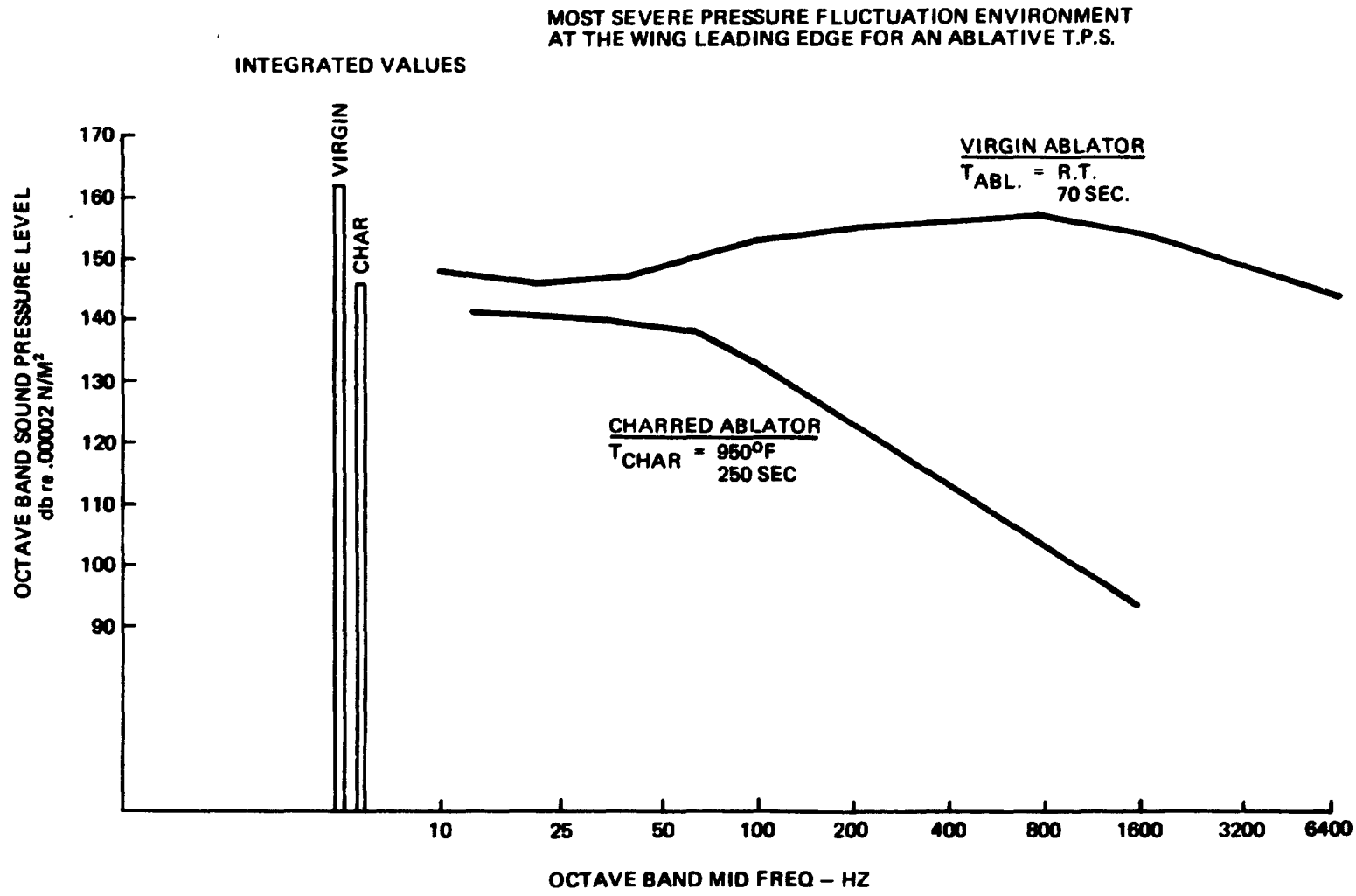

Figure 19. Design Pressure Fluctuation Environment for the Wing L.E.

Table 7 Critical Natural Environments for 040A and 473 Orbiter Leading Edge

Condition	Source	Environmental Definition
Launch Pad, Ascent, Flyback	Rain and Hail Accumulated damage or erosion	• Rainfall distribution: NASA TMX 64589 Tables 4.1, 4.3, 4.4 and 4.5 • Hail: NASA SP 8057, para 6.4 single exposure
In orbit	Cold Soak	2×10^{-7} mm Hg at -200°F for 7 days
Ground Operations	Humidity	Humidity cycle specified in NASA TMX 64589, para 3.2.1
Launch Pad, Ground operations	Blowing sand and dust	As specified in NASA TMX 64589, para 6.2

Table 8 Conditions Typical for Most Severe Rain Environment for GAC 473 and 040A Orbiters

Mach no.	– 0.38	Altitude	– 1000 ft
Velocity	– 420 fps.	Flt. Path Angle	– -15°
Dynamic Pressure	– 206 psf.	Rain fall rate	– 1.52 lb/min. ft^2
Reynolds no/ft	– 2.64×10^6/ft.	Rain Exposure Time	– 250 sec.
Angle of Attack	– 5.5°	Average Drop Dia.	– 3.8 min.

permits the calculated environment of one vehicle (namely the GAC 473) to be applied to all. The small difference in wing sweep between vehicles causes a variance of 15% and 7% in heat flux and pressure respectively, between the orbiter configurations. The free molecular heat flux and pressure is independent of leading edge radius.

Since this free molecular heat flux is low ($\dot{q} < 1$ Btu/ft^2-sec) and the initial starting temperature is assumed to be -175^o F (610,000 ft), the wall during the initial phase of entry may not be assumed to be in radiation equilibrium. Rather, the ablator must first absorb most of the heat to raise the temperature to a point where radiation dominates. The task of evaluating the ablator temperature rise involves having a knowledge of its properties. However, for the typical class of ablators to be considered later, general statements can be made. The wing leading edge pressure history is given in figure 20. Surface temperature records of two typical ablators are given in figure 21 and reflect a realistic balance of heat in the initial entry phase blending into radiation equilibium. Figure 22 was derived from figure 21 and is an indication of the temperature-time gradient experienced by typical leading edge ablators.

3.4 Aerodynamic

The flight range in which the ablative leading edge might most affect orbiter aerodynamic performance occurs during the post entry, subsonic portion of the trajectory. It is here that a vehicle designed for hypersonic flight has little margin for change in the critical aerodynamic parameters.

The significant aerodynamic environment parameters (Reynolds number, dynamic pressure, etc) during post entry, subsonic flight are presented in figure 23 for a typical orbiter.

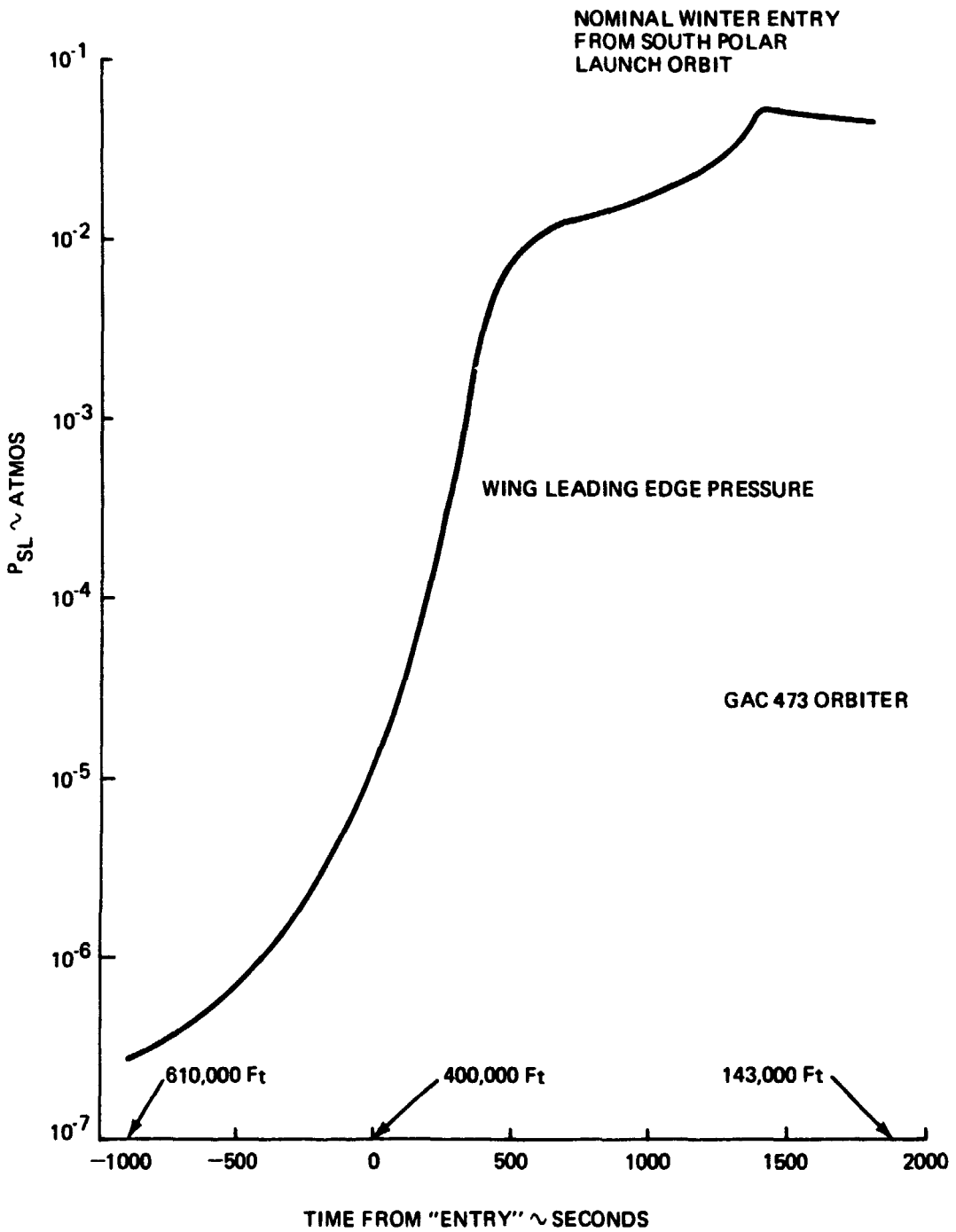

Figure 20. L.E. Pressure Environment at the Beginning of Entry

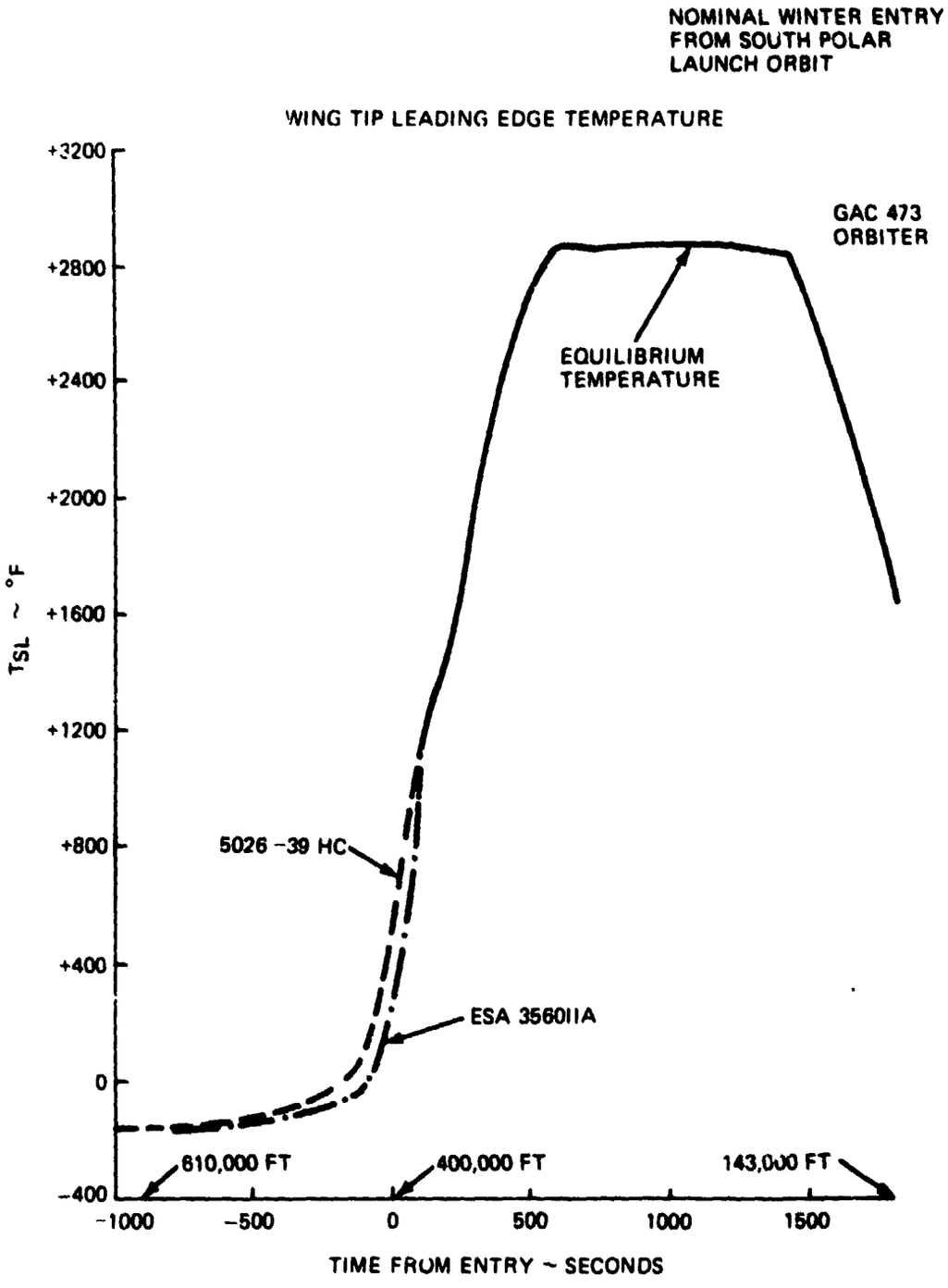

Figure 21 L.E. Surface Temperature Environment at the Beginning of Entry

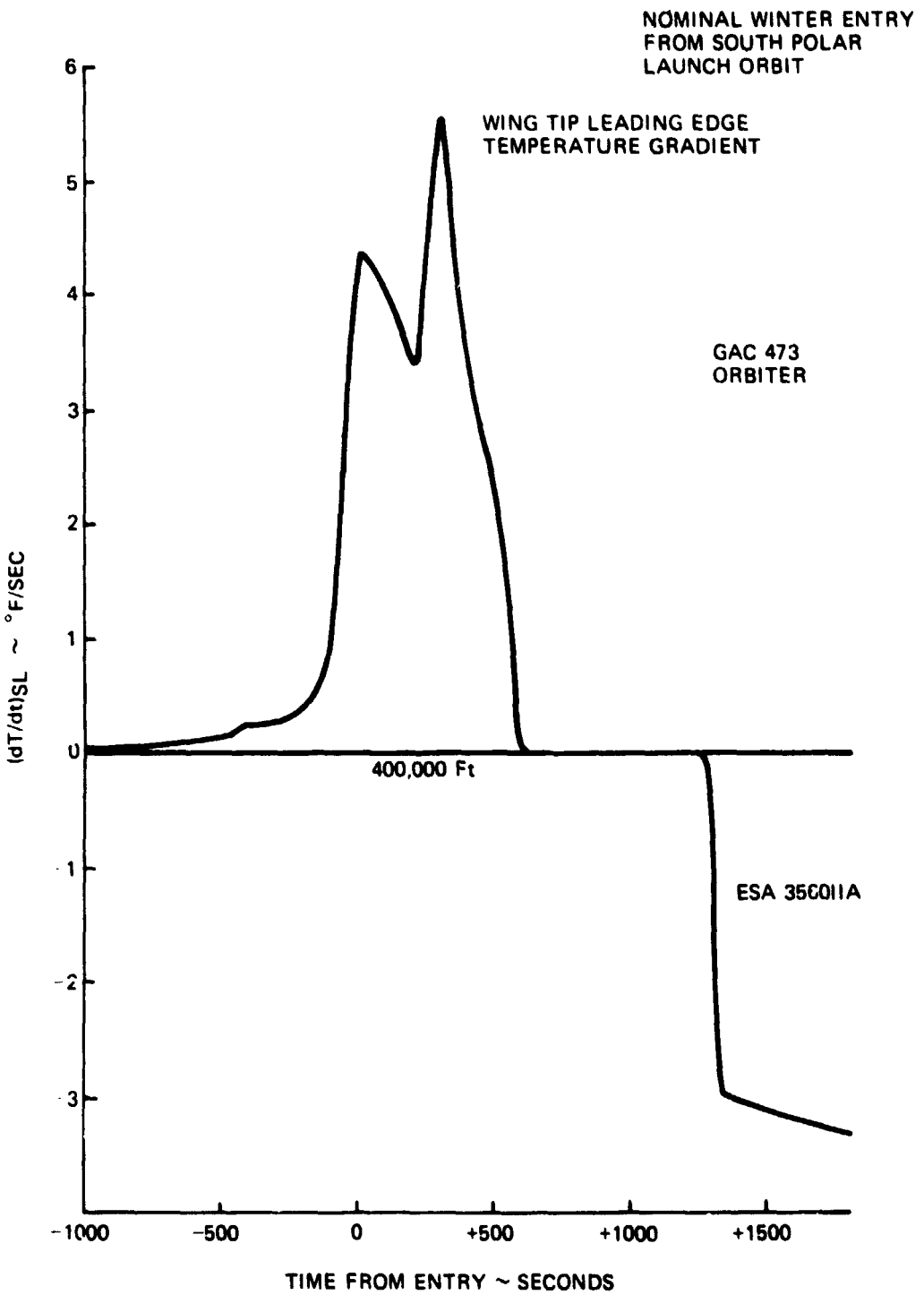

Figure 22 L.E. Surface Temperature Gradient Environment at the Beginning of Entry

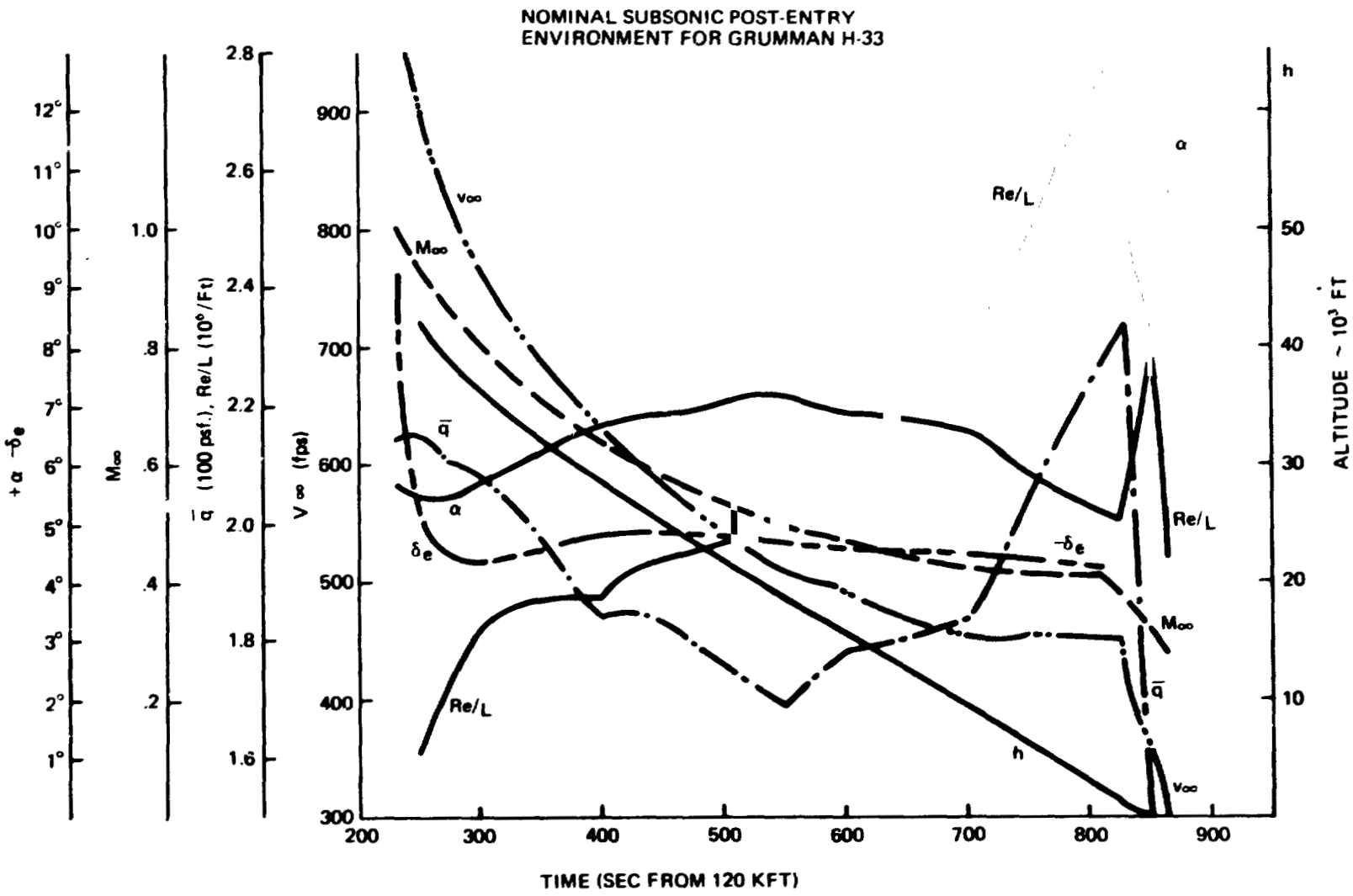

Figure 23 Trajectory and Aerodynamic Environment During Orbiter Subsonic Flight

3.5 Selection of Design Environment

The design environment selected for this study represents typical data of end-of-Phase-B/beginning-of-Phase-C orbiters. It consists of:

a) Aerothermal environment: dominant environment; for the stagnation region, tables 1 and 2; for the distribution on the l.e., the Grumman 473 orbiter, figure 7; for the history along the trajectory, the Grumman 473 orbiter; for typical values for the windward joint region; tables 3 and 4.

b) Structural environment--static: the Grumman 473 orbiter, table 5, figures 9, 11, 13, 15, 16, and 18.

c) Structural environment--dynamic, figure 19.

d) Natural environment--tables 7 and 8.

e) Aerodynamic environment at low speed--figure 23.

4. AERODYNAMIC CHARACTERISTICS DEGRADATION DUE TO ROUGHNESS AND RECESSION (PRELIMINARY STUDY)

The ablative i.e. roughness and recession should produce 'acceptable' degradation of the low speed aerodynamic characteristics of the orbiter. More precisely one needs to know the maximum 'acceptable' value for roughness and recession and what is the cost penalty of any given roughness/recession below the maximum and within the ranges that the candidate ablators may produce.

Since little effort has been devoted to this area, roughness and recession are continually identified as an area of uncertainty. We attempt to provide - within the limit of a brief and preliminary study - a quantitative assessement of the degradation involved, at least in some typical orbiter designs at a specific time during the evaluation of the design.

The point of view we take is of providing the degradation assessment ('go/no-go' and cost penalties) under the orbiter requirements as they are now formulated (e.g., landing speed 150 kt; minimum float time, 10 sec; max retrieved payload, 45,000 lbs) and also within the safety margins that one would like to set (e.g., in the case of the Grumman orbiters, 4 sec of safety on minimum float time). However it must be borne in mind that, even if none of the ablators were to pass all the 'go/no-go' criteria, one has still the option of reexamining the broader policy question of relaxed requirements. For example, the landing speed could be increased; retrieved payload can be reduced, in fact advantage could be taken of the fact that such a large number of flights for orbit are empty in the current traffic models; a harder look can be taken at the safety factors with possible lower requirements; even such expensive propositions as wing resizing in a frozen environment can be considered. Therefore, we are examining not absolute 'go/no-go' limits but rather limits that do not upset current requirements.

Since this is only a brief preliminary study, a plan for a detailed study is presented in Section 11.

4.1 Review of State-of-the-Art

4.1.1 Aerodynamic Characteristics Affected

With a typical delta-wing orbiter at subsonic speed, the aerodynamic situations to be considered for roughness/recession are usefully schematized (Ref. 12) as follows:

- Subsonic cruise/cruise to depot, etc — low-to-moderate α; main aerodynamic characteristics involved: c_D, c_L, L/D. Typical situation: $\alpha \sim 10^o$; typical aerodynamic characteristic: (L/D) max.
- Landing/approach to landing/handling qualities affected — high α; main aerodynamic characteristics involved: c_L, lateral stability, side force, pitching moments. Typical situation: $\alpha \sim 20^o$; typical aerodynamic characteristics: $c_{L_{max}}$, $c_{n\beta}$, $c_{l\beta}$.

The critical aerodynamic phenomenon is, of course, l.e. separation on the wing and loss of l.e. suction. Roughness/recession may affect the angle-of-attack (suitably defined) at which l.e. separation appears and especially the rate at which l.e. separation spreads inboard as α is increased.

4.1.2 Importance of Effects

Much initial concern was generated by studies/flights of the PRIME and X24 vehicles (Refs. 13, 14, 15 and 16). These results, especially the performance of the X24 fins were misinterpreted by many. These vehicles are lifting bodies. Flow patterns similar to those presented for example by Pyle and Montoya for the X24 (Ref. 13) do not occur on a delta wing orbiter. Moreover, at least some of the effects on drag are due to acreage roughness — we are here concerned only with l.e. roughness. Therefore, the lifting bodies results are not applicable here. This is not to say that useful information cannot be extracted

from references 13, 14, and 15 (q.v. in following sections).

Initial work at Grumman is the basis for initial conclusions that roughness may cause some 5 to 10% decrease in (L/D) max and that recession has no serious consequences (Ref. 12). NASA/Langley data are the basis for NASA's initial assessment of l.e. roughness (Ref. 17) as an important but low criticality area.

No strong recommendations — from the aerodynamic point of view — have been offered as far as the ablator selection for the l.e. (Ref. 12).

It seems that only the Grumman end-of-Phase-B configurations incorporated an aerodynamic "safety feature" - forward camber (Grumman H33 and 473 designs) - against the detrimental effects of l.e. roughness/recession.

4.1.3 Roughness

4.1.3.1 Roughness Levels

Experimental data on roughness on the candidate ablators or for that matter on other charring ablators are extremely scarce, even without precharring. No data are available with precharring. As far as measurements on a flight article, such measurements were made on PRIME (Ref. 13), but were directed to acreage roughness. Only an area-weight average is presented in reference 14. No measurements appear to have been made specifically around the l.e. of the fins. No measurements on the X15 A2 l.e. have been uncovered. On the Apollo, near the rims of the shield, crack depths between 0.35" and 0.6" (maximum) have been measured (Ref. 18).

As far as measurements on flat samples tested in ground facilities, there appear to be some old data on some Martin materials (Ref. 19). Cursory maeaurements at Avco on 5026/39 M and Hc flat samples, have given the following results (Ref. 20):

5026-39 M - 500 μ-inches plus cracks

5026-39 Hc
- roughness of filler, 500 μ-inches
- honeycomb protrusions above filler, 0.020"

As far as roughness measurements on l.e. samples tested in ground facilities, no data appear to exist.

A tentative picture of the roughness levels at least on a charring ablator (epoxy, elastomer but not carbon-phenolic) seems to be (Ref. 19):

- There are three types of roughness: (1) char roughness (between honeycomb cells); (2) honeycomb-caused roughness; and (3) cracks.
- Typical values of char roughness seem to be 500 μ-inches (Ref. 19; also a graphite value between 100 μ-inches and 300 μ-inches reported in Ref. 21).
- Working value for honeycomb protrusions ~ 0.020" for an epoxy (Ref. 20). Elastomers at intermediate heating rates swell and therefore give rise to different levels.
- On a molded ablator, apparently (Ref. 20) there is no honeycomb-caused roughness; however, one would expect more crack roughness because of lower char stability. No data on this tradeoff are available.

One would expect that for a given ablator, roughness be correlated with:

- Heating rate (and also total heat load)
- Mechanical stress (dp/ds, τ, pressure fluctuation, and thermal stresses) during and after the heat loading time.

Therefore, the previously quoted roughness measurements should be carefully associated with an environment. Unfortunately, nothing is precisely known in this area.

Information on roughness patterns can be obtained from inspection of Apollo and PRIME, as in Ref. 13. However, this is not essential at this point of development of the subject. Perhaps a question of some importance is to identify a density or a spacial frequency of cracks on molded and honeycomb ablators. A density for honeycomb-caused roughness follows from cell dimensions. Together, one gets an overall measure of the roughness density. In Refs. 3 and 4, a 40% grit density was used.

Figure 24 gives an idea of how the roughness levels previously identified compare with the roughness levels that are significant for some of the fluid mechanical phenomena on the l.e. of the orbiter. Note, though, that figure 24 is derived from rough-wall flat plate calculations applied locally around the l.e. This appears to be reasonable at low angles of attack, up to say α_{cruise}. One key phenomenon is missing, i.e. formation of l.e. separation bubbles/vortex sheets, since it cannot be easily quantified. One conclusion follows from figure 24: Char roughness cannot possibly have any effect on aerodynamic characteristics.

A question that falls outside our scope is how to estimate flight roughness from arc jet tests.

4.1.3.2 Testing in Aerodynamic Facilities

Inexpensive testing for aerodynamic effects is done neither if flight nor in tunnels with actually ablated surfaces. Therefor - the simulation in tunnel of TPS roughness there are the following three questions looked at during the PRIME studies (Refs. 13, 14 and 15):

a. Can we use 'reproduced and roughness' in place of actual roughness?

b. Can we use carborundum grit in place of 'reproduced roughness' on large-scale models?

c. Can we use small models instead of large ones (with carborundum grit)?

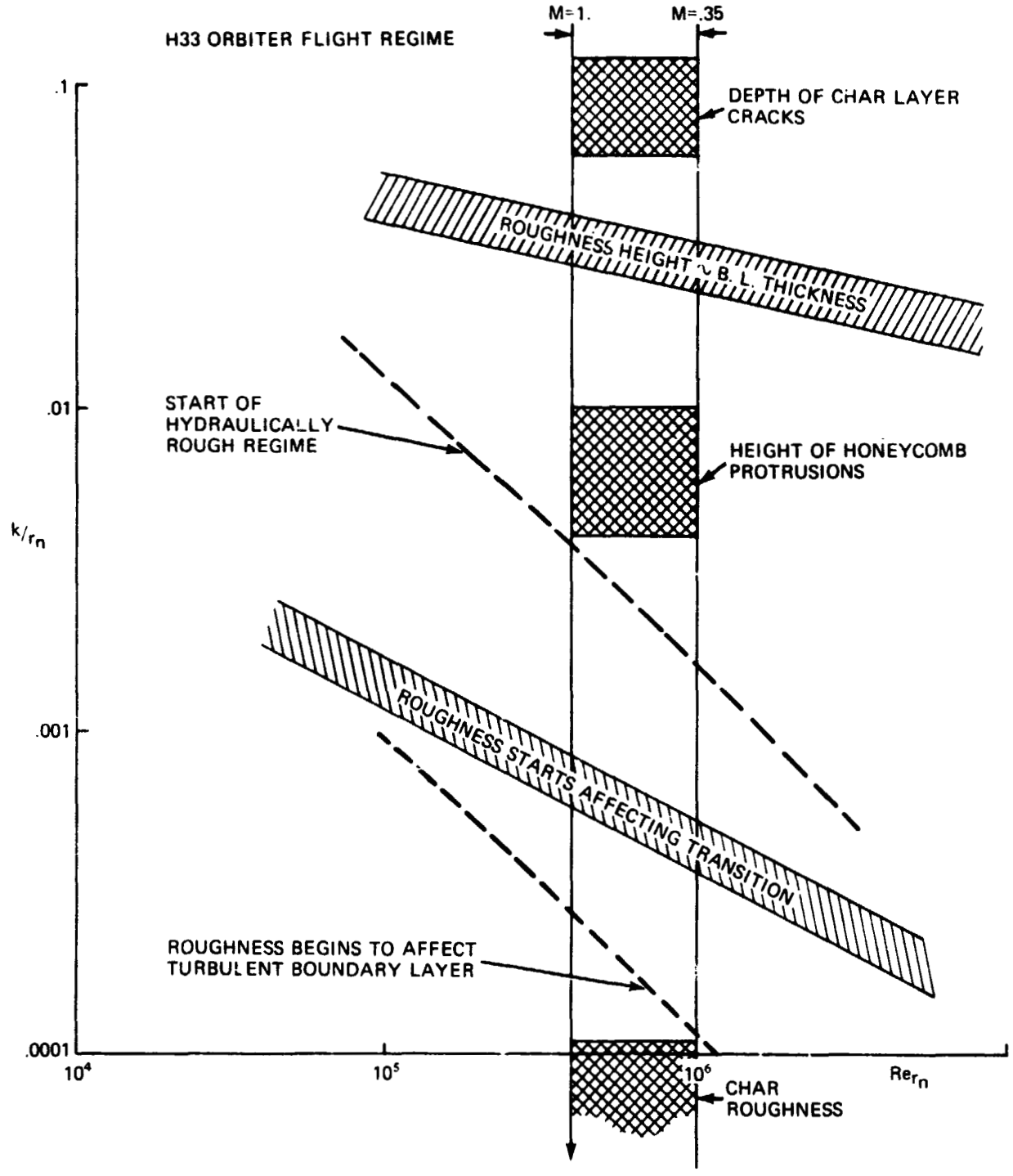

Figure 24. Roughness Levels

Answers to questions b) and c) are available including a tentative explanation of the lateral directional stability question of Ref. 14.

Roughness levels, peak-to-valley, are usually taken to be equal to the grit size, which seems adequate in this context.

In testing, one should try to maintain a constant grit density if one wants to be able to compare different grit sizes. A 40% density — appropriately measured — was held in references 3 and 4.

A quick method for applying grit while carefully controlling its density has been developed at Grumman (Ref. 3).

Unfortunately, roughness simulation for aerodynamic facilities is made very difficult by the mismatch in Reynolds number flight/tunnel (see fig. 25, for flight and two tunnels: the NASA/Langley LTPT and the Grumman LSWT).

A method for extrapolation tunnel-to-flight is needed. This is a crucial topic. The problem has two aspects: (i) How to reduce an estimated (flight) roughness level, to a k_{tunnel}; and (ii) How to extrapolate to flight the aerodynamic characteristics measured in the tunnel at the tunnel roughness level.

The first question has not been looked at.

For the second question, one procedure is used at Grumman for drag at moderate α -- find a drag plateau in Re_k and interpret that as transition shifting that would occur in flight because of high Re rather than because of roughness. This interpretation is in agreement with actual transition observation in reference 22. Figure 26 shows a typical variation of drag with roughness size, showing the regions with and without boundary layer transition shifting to be separated by a small constant C_D plateau region. These data are typical of results in refs. 22 and 23; however, in Decker's tests (ref. 23) the plateau shrinks to a point, and sometimes there is more than one plateau. These discrepancies have not yet been explained. We do not know what fluid mechanical

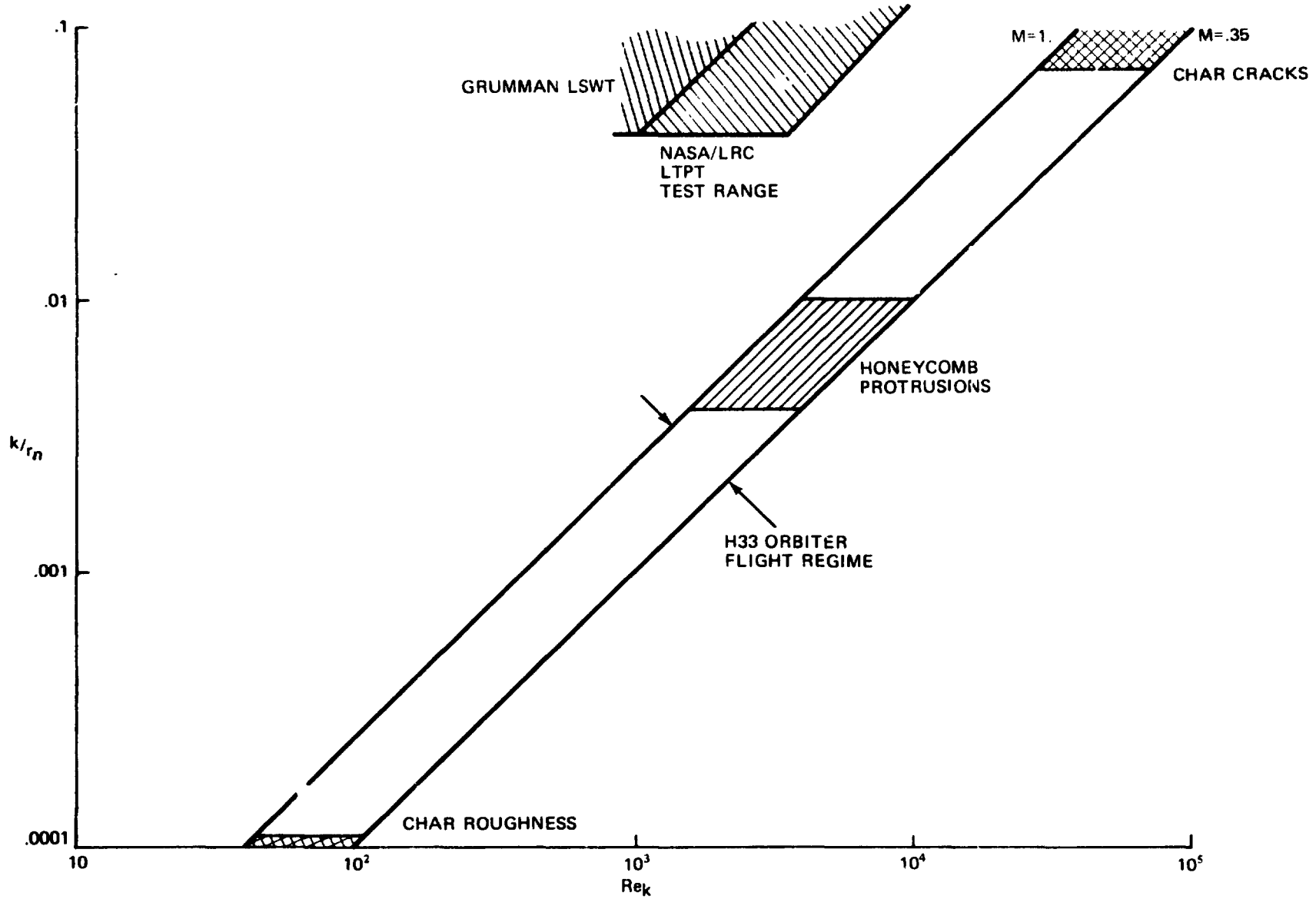

Figure 25. Roughness Levels - Flight/Tunnel

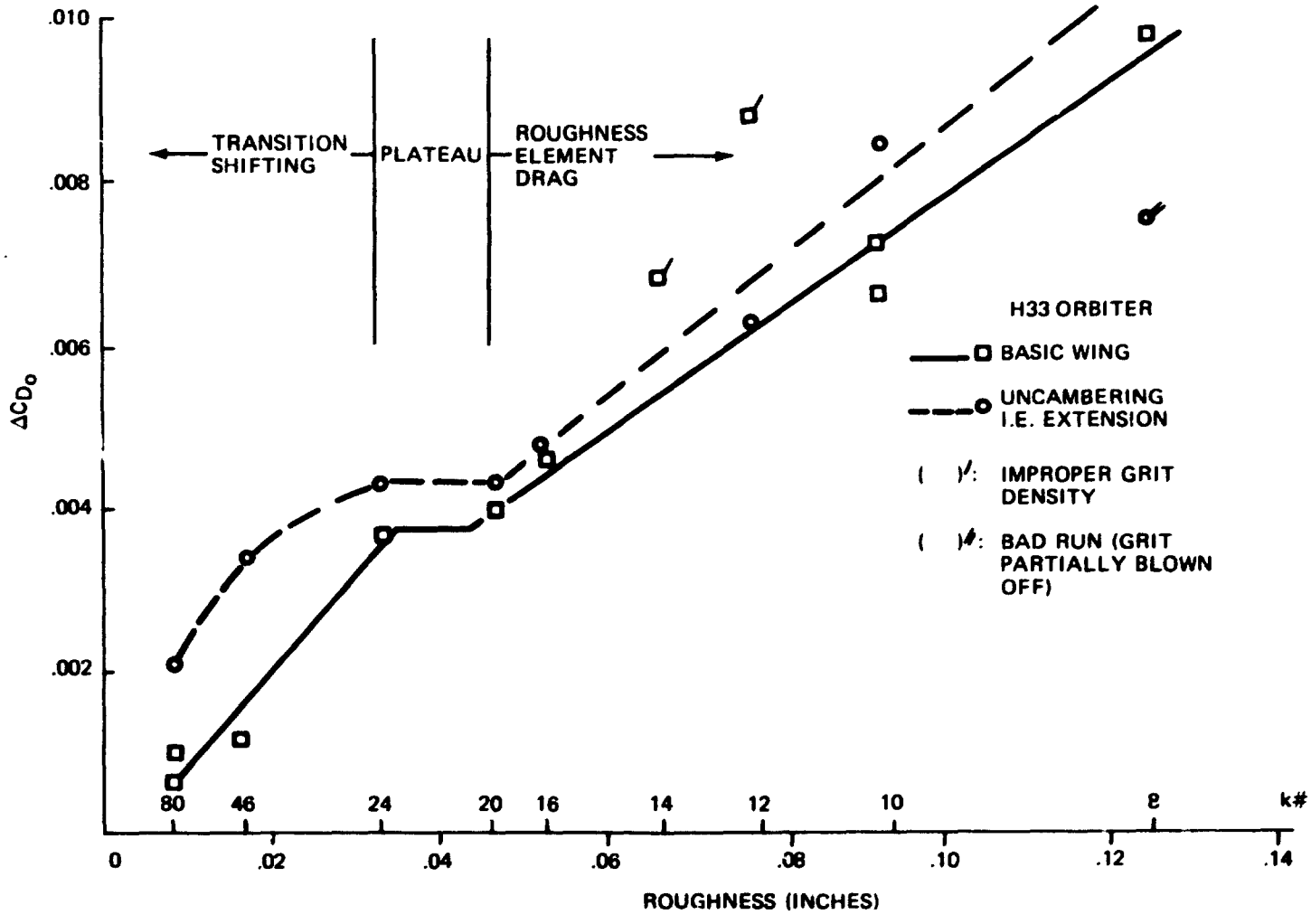

Figure 26(a) Zero Lift Drag Increase Due to LER Effects

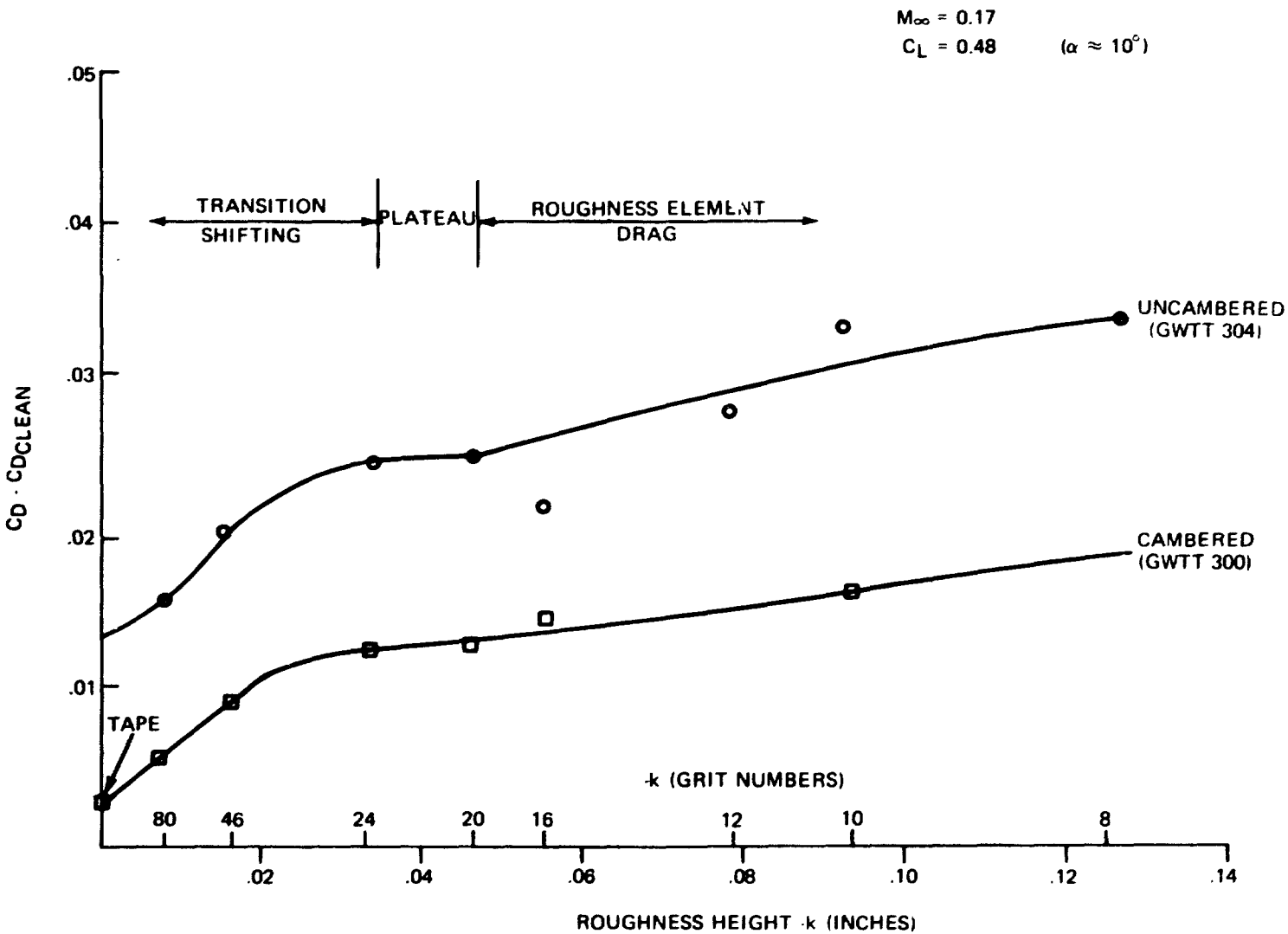

Figure 26 (b) Drag Plateaus for Cambered and Uncambered Wing on H33 at Moderate Lift.

phenomena cause the plateaus in NASA/LRC data and therefore cannot judge whether these phenomena would disappear in flight. One suspects that the one-plateau behavior — transition shifting — is characteristic of low Reynolds number. Therefore, the plateau procedure should be useful also for roughness studies at transonic speeds.

Interpretation of other quantities c_{Lmax}, $c_{n\beta}$ and $c_{l\beta}$ with transition shifting is not obvious. $c_{n\beta}$ and $c_{l\beta}$ versus Re_k have characteristic behaviors and flatten out on high-Reynolds values (see Fig. 27). This holds promise for subsonic and transonic speeds extrapolations.

Another scaling method is the use of Re_k as the parameter to maintain constant, flight vs tunnel, while neglecting k/r_n. This method seems to hold promise.

4.1.3.3 Theory

We are not hoping for a predictive theory, but for a guide to identify the various roughness regime and interpret the experimental data.

The key issue in the only known effort (at Grumman) is the feasibility of a theory for predicting roughness-induced drag increase and l.e. separation conditions. This would give a handle on flight, as well as tunnel, Reynolds number effects. Of course, we are looking only for relative effects with/without roughness. There exists the capability of predicting low-speed pressure distributions on wing, tail etc; 2-D boundary layer methods for rough surfaces are also available (Ref. 24). Identification of l.e. separation with 2-D boundary layer theory also seems possible (Ref. 25). Extension to sweep may be necessary, as yet there is no final answer on whether the entire theory is feasible. Of course this would be applicable to moderate α.

For high α with l.e. separation, the dominant fluid mechanical mechanisims are insufficiently mapped out to start speaking of theories. There are at least some tunnel data with surface flow visualization (Ref. 26).

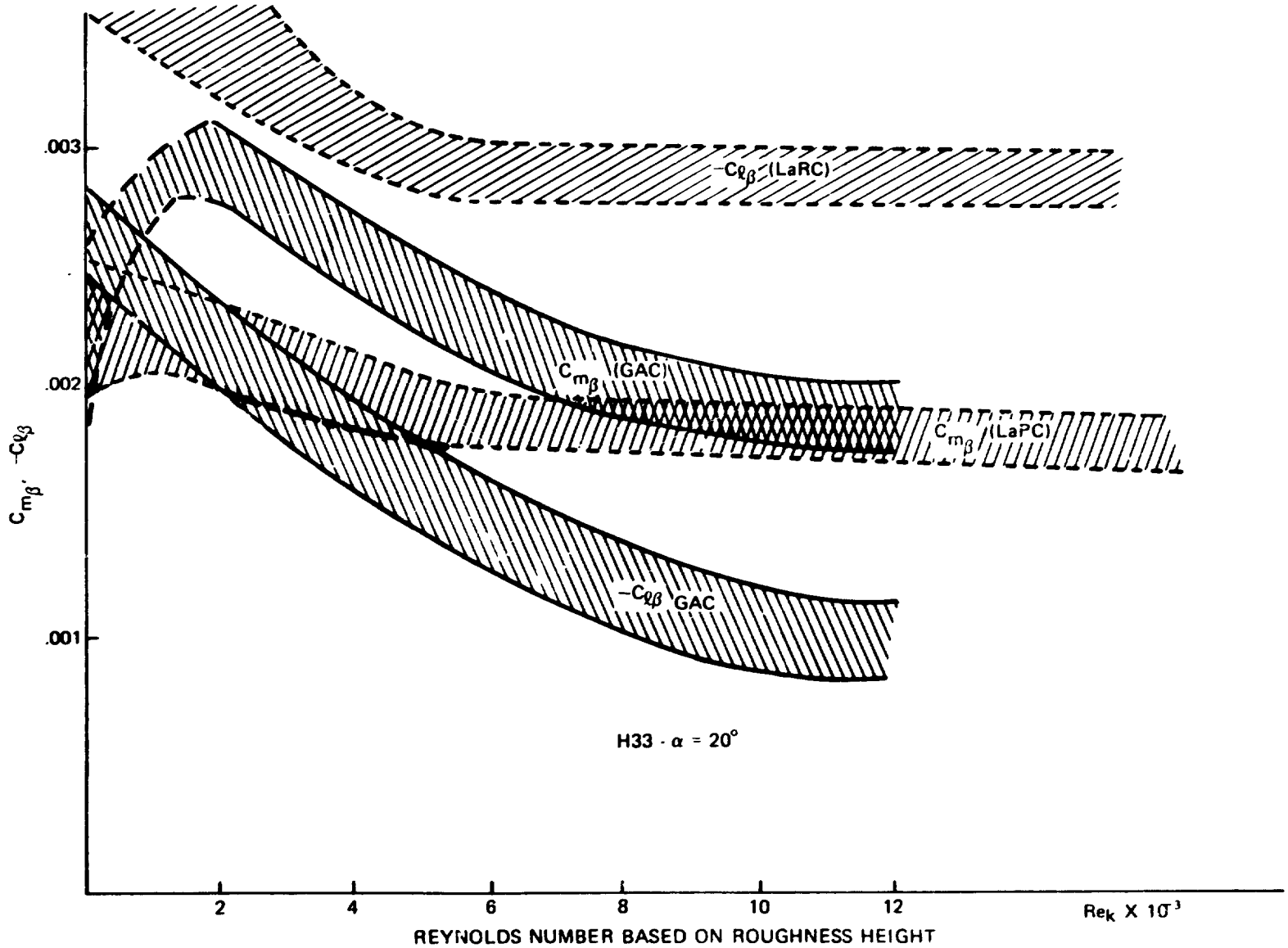

Figure 27 Effect of LER on Lateral Stability Derivatives

4.1.3.4 Aerodynamic Data with Roughness Effects

A literature search revealed that the only useful data available on (entire) l.e. roughness at low speed are for:

a. Grumman H33 orbiter - Grumman low-speed wind-tunnel tests on 1/25 model scale (Refs. 3 and 4).

b. Same orbiter - NASA/LRC LTPT tests on a 1/67.5 model scale (Ref. 23).

c. Same orbiter but with uncambered wing (Ref. 4).

d. A 22% thick airfoil section - some old NASA tests (Ref. 27).

There are also two l.e. roughness studies in the transonic regime:

e. C5A aircraft models - tests in 3 facilities at M = 0.7-0.79, moderate to low α (Ref. 28).

f. Cropped uncambered delta-wing half-model (Ref. 22) - extensive roughness program, M = 0.8 - 1.15, α = 0.

4.1.3.5 Results

The experimental results are currently examined parametrically vs roughness levels — some eight grit levels were tested in reference 4 and some six in reference 23. The Grumman data are also tentatively interpreted correcting for Reynolds number effects as indicated above in Section 4.1.3.2. General observations from an examination of the data (Refs. 3, 4, and 23) are:

a. As reported previously (Ref. 12) L/D degradation at moderate α is small, typically a 10% reduction at the largest grit No. 8, or a Δ L/D of 0.5.

b. 10% reduction in L/D max in Grumman's data or Δ L/D max of about 0.6 compare with NASA/LRC 14% reduction from plateau level.

c. Wing l.e. produces essentially the entire effect — tail and nose cap contributions were negligible. Found both in Grumman's (low Re) and

NASA/LRC (high Re) data. Faint effects of tail seen in NASA/LRC data.

d. Effects on lateral stability derivatives at moderate α were on the level of data scatter. Same results from NASA/LRC data.

e. A high α, Grumman data show sizable changes in lateral stability derivatives (Fig. 37). However, when the low Re Grumman $c_{n\beta}$ is compared to the high Re NASA/LRC value,* one is drawn to the conclusion that Grumman $c_{n\beta}$ picks up Reynolds number effects (transition shifting?) and that the good agreement NASA/Grumman data indicate no roughness effects on $c_{n\beta}$. Why doesn't $c_{l\beta}$ follow the same trend with agreement NASA/Grumman on the same level above $Re_k > 10 \times 10^4$?*

f. 10% reduction in $c_{L_{max}}$ at largest (No. 8) grit, no change of α for $c_{L_{max}}$ (Grumman data).

g. Forward camber effects from Grumman data -- Δc_D on the H33 model with a leading edge extension designed to remove the camber was twice that of the basic cambered configuration - due mainly to transition shifting differences. $\Delta(L/D)/(L/D)$ plateau was roughly twice as large for the uncambered as for the cambered wing for $\alpha \leq 7^\circ$, but of course as α increased the difference between the two wings vanished.

4.1.3.6 Assessment/Recommendation for Ablator Selection

The assessment of roughness effects reported in preceding Sections 3.1.2 and 4.1.3.5, is derived by examining aerodynamic characteristics parametrically

---

* One has to keep in mind that the Langley tests have been performed with a -5° elevon deflection, whereas the Grumman tests had no control deflections except for one point (Ref. 4), which indicated that LER affected the drag but not lift increment due to the contol deflection. (LER = leading edge roughness).

versus roughness. What has not yet been done is to determine a roughness level and obtain its associated value of aerodynamic characteristics degradation. No recommendation has yet emerged for the roughness input to (i) ablator selection, (ii) Hc vs molded question.

The questions that need to be looked at at the present time in this area are:

(i) 'go/no-go' criterion for what to label 'excessive roughness' from an aerodynamic viewpoint. Some such criterion is among the primary criteria for the ablators screening.

(ii) A way to convert in dollar value the aerodynamic penalties, e.g., Δ L/D and stability loss. This is a difficult problem.

(iii) Leading edge roughness data are needed of the type obtained in the l.e. tests of this study.

4.1.3.7 Fixes

The most obvious fixes for the l.e. roughness problem are:

(i) Ablator selection: assure char stability; select Hc or molded depending upon whether Hc improves or degrades smoothness — at typical orbiter heating loads for elastomer or epoxies.

(ii) Aerodynamic device (forward camber) as in the Grumman H33 orbiter. Penalties of this device have not been specifically investigated.

4.1.4 Leading Edge Shape Change

4.1.4.1 Recession/Swelling Levels

Work on defining these levels has been carried out at Grumman. Preliminary (locally one dimensional without precharring effects) recession estimates on H33 and 04OA orbiter wings with the Avcoat 5026/39 M have shown very small (Fig. 28) l.e. shape changes over most of the wing span. This implies that

---

* See previous footnote.

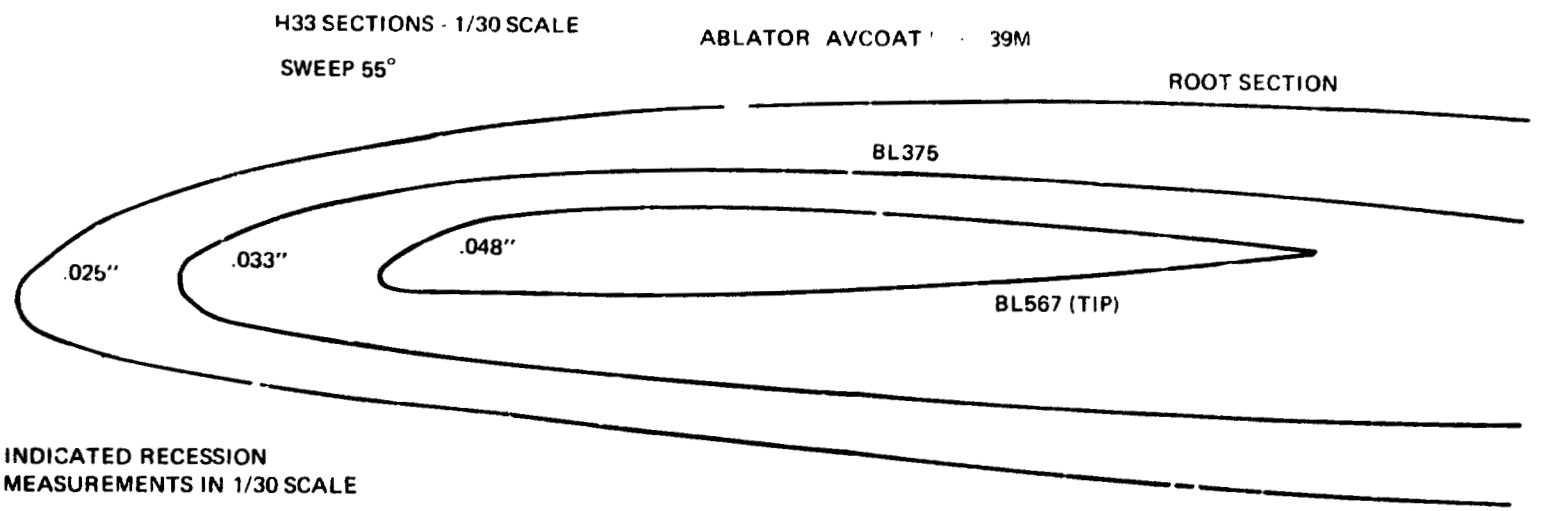

Figure 28 Recession on H33 Wing Leading Edge

the l.e. shape changes significantly only near the wing and that overall aerodynamic characteristics remain essentially unchanged. For the other materials of this study, the same conclusion holds, as for most elastomers. At these heating rates, the material swelling partially balances the recession. Remarkable local swelling resulting in a pronounced shape discontinuity has been measured (Ref. 1) near the joint of two different ablators, such as an elastomer and an epoxy. However in this study we consider only a single ablator l.e. (see Section 5).

4.1.4.2 Data

For an orbiter the only exploratory data on recessed l.e. without roughness are those of reference 29 (Grumman H33 orbiter).

Data for airfoils/wings give qualitative clues as to the aerodynamic effects of l.e. shape change, except that there is no precise comparison with/without shape change near the l.e. with the rest of the geometry unchanged. The data of reference 29 indicate negligible change of aerodynamic characteristics with and without recession. The recession simulated was several times larger than that estimated for the case in question.

The currently estimated recession, figure 28, is too small to make more experimental effort worthwhile on a configuration whose l.e. radii are reasonably large. The estimate does not account for the preconditioning effect of ascent heating.

4.1.4.3 Assessment/Recommendations for Material Selection

Initial assessment of l.e. recession is that this is not an area of serious aerodynamic penalties (Ref. 29). Possibly this assessment must be tempered for configurations whose tip l.e. (chordwise) radii are of the order of a

couple of inches, but it is doubtful that such configurations will be seriously proposed.

No recommendations have yet been advanced for ablator selection from this point of view.

Current needs in this area are (as for roughness): (i) Go/No-Go criterion; and (ii) dollar value of degradation.

4.1.4.4 Fixes

A simple fix has been proposed to prevent l.e. recession to unacceptable shapes which is much simpler than trying to design a stable l.e. shape. This scheme, (shown in figure 29), consists of predicting the recession on a given desired final l.e. shape and adding this amount of ablator to this l.e. This guarantees an acceptable l.e. shape for post-entry flight. Refinement of this initial shape synthesis by iteration is straightforward.

Weight penalties, if any (e.g. thicker ablator near the stagnation point) have not been studied. This scheme depends, of course upon the ability to predict recession for l.e. shapes (q.v. in following section). If the wing l.e. radius is very small only at the outboard sections, this fix could be restricted to that region.

4.1.4.5 Recession Predictability on the L.E.

One dimensional recession predictions for single heating pulses and neglecting mechanical removal are common practice. One question is whether they are adequate for aerodynamic assessment purposes.

Experimental data on recession/swelling rates on flat samples are available for the materials under consideration in this program (see Figs. 30 and 31).*

Some experimental data on recession/swelling of l.e. models are available for the Avcoat 5026/39 HC and the DC 325 HC (Ref. 1). None of these data include ascent heating.

---

* See footnote next page.

-040A-

ABLATOR = AVCO 5026/39M

FIRST 10% OF WING SECTION
AT B.L. 300 (MIDSPAN)

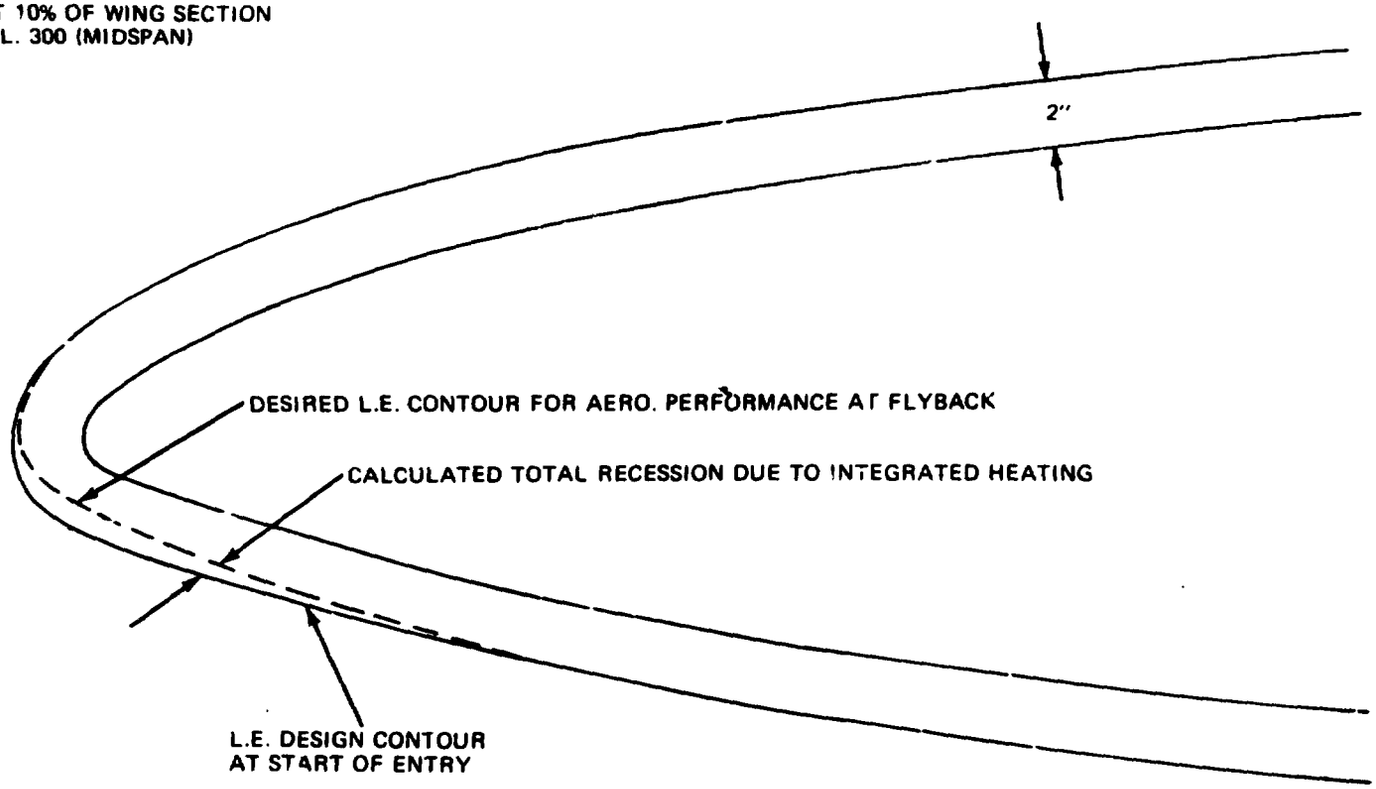

Figure 29 Concept for Leading Edge Shape Optimization

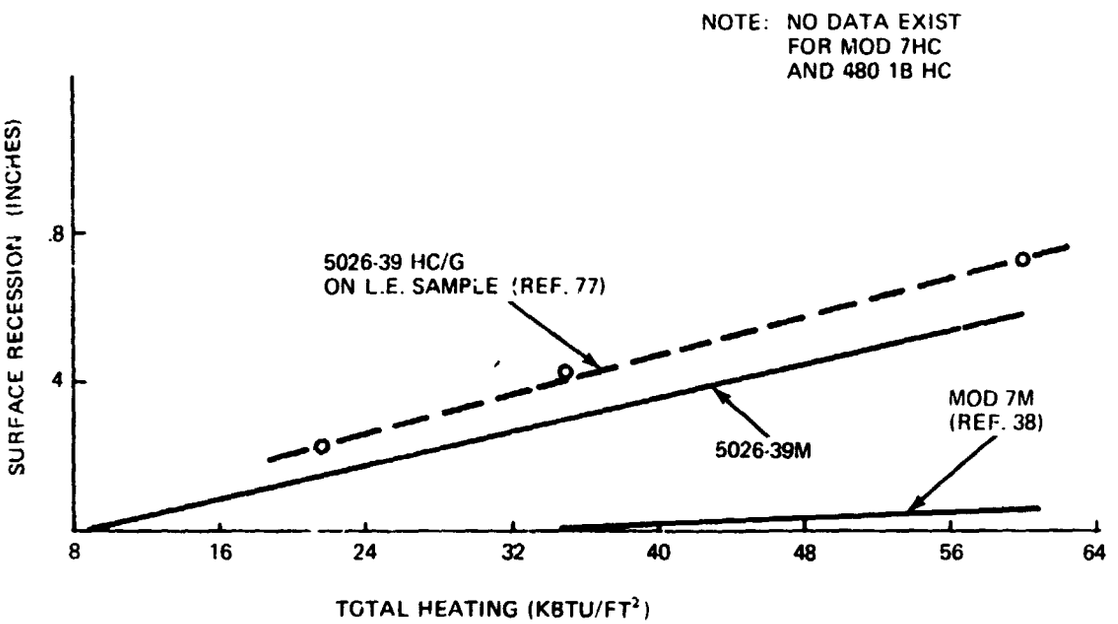

Figure 30 Total Recession of some Candidate Ablators

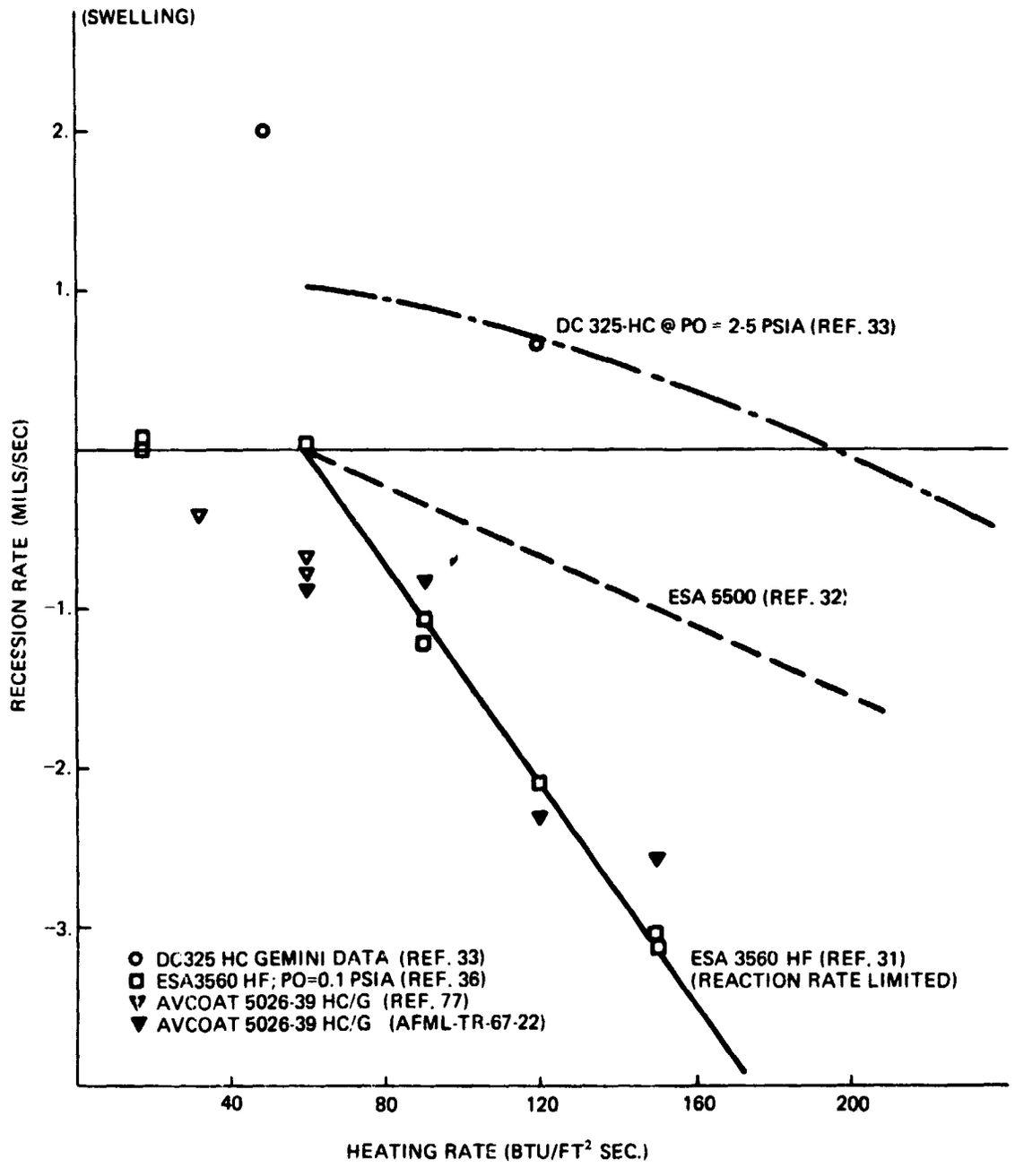

Figure 31 Recession Rates of some Candidate Ablators

A point that has been looked at whether or not locally one dimensional recession calculations are adequate for the leading edge in absence of ascent heating. The answer seems to be yes, since splash experimental data on recession agree with l.e. data (Fig. 32) at least at the moderate heating rates anticipated for the orbiter wing.

4.2 Methods for Determining Cost Penalties for Aerodynamic Degradation Due to Effects of L.E. Roughness/Recession at Subsonic Speeds

Three Steps in the Problem

Determination of dollar costs of l.e. roughness/recession-induced aerodynamic degradation can be broken down into three tasks:

1. Taking tunnel data of the relevant aerodynamic characteristics obtained with various roughnesses; relating tunnel/flight aerodynamic and roughness values; obtaining leading edge roughness (LER) increments ΔC_L, ΔC_D, etc for flight.
2. Relating the flight aerodynamic performance degradation to dollar costs. (Still parametrically vs roughness/recession)
3. Determination of ablator roughness/recession.

---

* Data are from references 1 and 30 to 37. Data on ESA 3560 H has been included since it is very similar in recession rate to ESA 3560 HF (see Fig. 31). A few flight data points for the recession of DC 325 on the Gemini vehicle (Ref. 33) are also incorporated in figure 31. There are also a few flight data on the recession of ESA 3560 HF and ESA 5500 on PRIME (Ref. 36), but these are classified and not included in this memo.

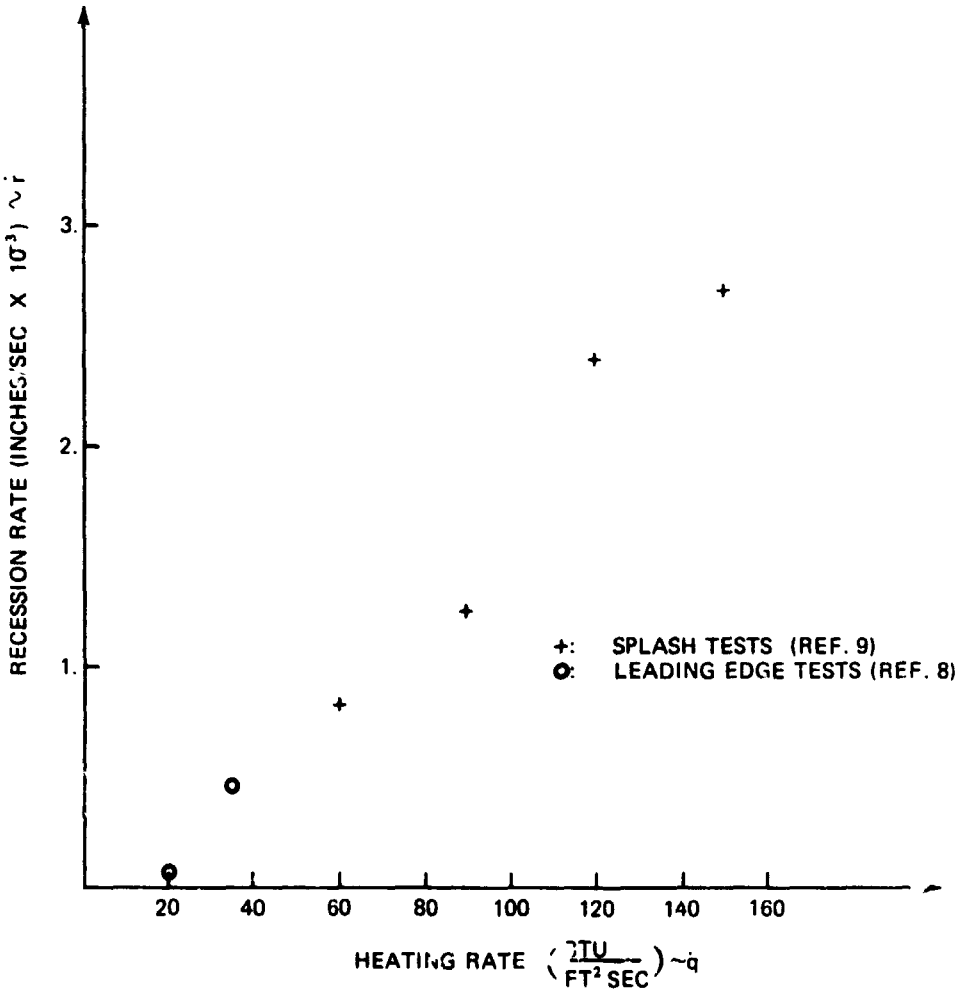

Figure 32 Recession Rate Data for Avcoat 5026-39 HC/G

Aerodynamic Quantities Affected

The moderate α subsonic regime encompasses the nominal conditions during:

- Subsonic post-entry cruise
- Landing -- approach/flare/deceleration to touchdown
- Ferry to depot

In this regime, stability is not noticeably degraded by LER effects (Refs. 3 and 4). The most significant LER sensitive aerodynamic characteristic here is L/D max, which governs two quantities of fundamental interest: (1) range of the post-entry flight phase; and (2) 'float time' -- the time taken to decelerate from the end of flare to touchdown velocity.

A minimum subsonic range - therefore a minimum L/D max is set by tolerances on the inertial navigation equipment during entry. Existing surplus capability and additional buffer potential from aerodynamic clean-up mentioned below indicate that this will not be critical. LER range degradation for ferry-to-depot is not a problem, since l.e. replacement away from depot is quite feasible. Indeed, air-transportable, aluminum leading edges will be available, at no extra cost, since they are needed in the subsonic flight tests.

'Float time' is of paramount importance to the case of landing the orbiter -- a 10-second minimum has been established.

At high α, the critical condition is landing. The significant LER-affected parameters at this condition are:

$C_{L_{trimmed}}$ -- governing the landing speed

$C_{l\beta}$, $C_{n\beta}$ -- governing the lateral-directional stability of the vehicle

Typically we can evaluate these characteristics at α = 19 deg which is representative of orbiter tailscrape angle.

Method for Relating 'Float Time' to L/D Degradation

The procedure is indicated schematically in figure 33. From reference 39, we can relate 'float time' to $(L/D)_{max}$. Since there is a minimum of 10 seconds 'float time', there is a minimum for $(L/D)_{max}$. Having selected a desirable safety margin for t_{float}, there follows a minimum desirable $(L/D)_{max}$. Then from steps 1 and 3 above, one gets a $\Delta(L/D)_{max}$ representing LER degradation of the orbiter configuration from a smooth, i.e., nonablative, l.e. condition. Now this degradation reduces the configuration $(L/D)_{max}$ below the minimum desirable.

To restore minimum t_{float} one looks first for aerodynamic clean-ups of negligible cost; beyond such 'cheap fixes' that involve localized redesign, one gets to the point of vehicle resizing, i.e., the photographic scaling of major components without changing the baseline design as assumed in the typical $24K value of a pound added to, or saved from, the orbiter. Therefore, to arrive at the dollar value of the degradation one needs to:

- Enumerate the 'cheap fixes' that can be brought to bear. Of course, one assumes that the benefits accruing from the nonablative-related fixes have not already been absorbed by some other degradation mechanism not considered here;
- Estimate the costs of introducing these fixes;
- Define the potential clean-up of the configuration, i.e., to estimate the total L/D improvement that all the cheap fixes can provide; and finally,
- Determine the LER L/D degradation that has to be taken care by 'expensive' fixes.

Naturally, in the process one has to work with a reference configuration (available $(L/D)_{max}$ with smooth l.e.) and make a few policy decisions (desirable t_{float}).

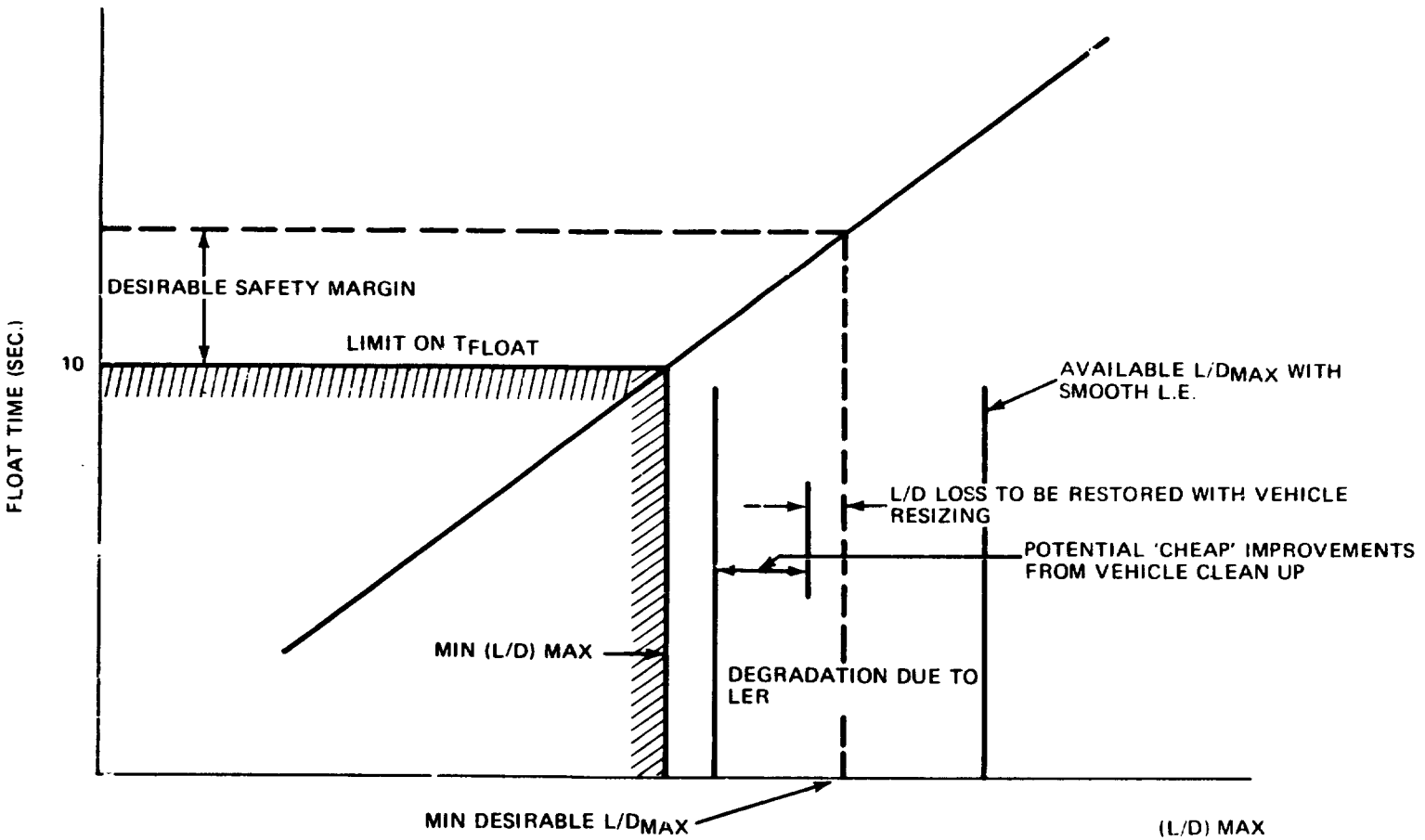

Figure 33 Relation Between Float Time and $(L/D)_{MAX}$

Levels of Design Rigidity and Fixes

We consider three levels of design 'rigidity':

a. Frozen-only l.e. design-free.

b. Partially rubber-aerodynamic component clean-up (if a permissible but only through local shape changes, e.g., cleaning the lines of the OMS pods.

c. Totally rubber-freedom to redesign and resize major components of the orbiter, with the corresponding impact on the entire system.

The first level represents the ground rule of this study, but the other two will also be considered briefly.

For each level we have the following potential aerodynamic design changes to improve the aerodynamic characteristics:

a. Frozen vehicle: (1) introduce l.e. camber — in the Grumman 473 orbiter, further increase l.e. camber, provided no prohibitive changes in trim drag occur in other speed regimes; (2) reduction of retrieved payload, an extreme measure that implies added flights.

b. Partially rubber, in addition to the preceding options: aerodynamic clean-up for $(L/D)_{max}$ improvements, depending upon the configuration and also its stage of developement. For example, in the case of the 473 orbiter in mid-1972, the following clean-ups were attractive: OMS pods lines, ACPS pods lines, boat-tailing.

c. Rubber, in addition to the preceding options: for $(L/D)_{max}$ improvements, wing resizing; for c_{n_β} tail resizing.

If instead of the full traffic model, we consider only the test flights, we should account for the absence of retrieved payload, i.e. some 45,000 lb of lower landing weight.

Costs of Payload Reduction or Resizing

For a frozen vehicle and the full NASA traffic model, if payload reduction is required, the cost penalties are extremely high. The same occurs if resizing of wing and tail is necessary.

This is brought out by simple estimates of such costs as follows.

Payload Reduction Due to LER (L/D) Reduction and Related Costs

Assume that an ablative l.e. is used for the entire program; the payload is not quantized; and that all (445) flights planned involved entry with a full 45,000-lb payload (very conservative). For equilibrium glide at a minimum $(L/D)_{max}$ (determined by a minimum allowable t_{float}), the payload reduction for an L/D degradation $\Delta(L/D)$ beyond the maximum permissible value is $\Delta W = D\ \Delta(L/D)$.

Using a cost/flight value of \$10.5M, (which is equal to \$230/lb of retrieved payload); a drag of 32,800 lb; total program payload of $45{,}000 \times 445 = 2 \times 10^7$ lb, the total increase in program cost of additional flights required to return this full program payload from orbit for a frozen or partially rubber vehicle is:

$$\text{Cost} = \$3.4 \times 10^9 \times \Delta(L/D) \qquad \text{(based on 1971 dollars)}$$

For any measurable value of the L/D loss, this cost is clearly extremely high.

Wing Resizing Due to LER L/D Reduction and Related Costs

Assume: an enlarged wing of same plan-form and characteristics with LER; no change in wing-body interference and equilibrium glide; using the following values of the basic Grumman 473 orbiter:

$$\Omega = \frac{\text{wing weight}}{\text{total weight}} \times \text{iteration factor} = 0.156$$

$$A = \text{reference area} = 3760 \text{ ft}^2$$

$$\frac{C_{D_W}}{C_D} = \frac{\text{wing drag}}{\text{total drag}}_{L/D_{max}} = 0.47$$

$$\frac{C_{Do}}{C_{D_i}} = 1.14 \qquad \frac{C_{L_W}}{C_L} = \frac{\text{wing lift}}{\text{total lift}} = 0.8$$

and the first order formula for wing area increase required to restore L/D:

$$\frac{\Delta A}{A} = \frac{\Delta C_{D_{LER}}/C_D}{\Omega - \frac{C_{D_W}}{C_D} - \frac{2}{\frac{C_{D_o}}{C_{D_i}} + 1}\left[\Omega - \frac{C_{I_W}}{C_L}\right]}$$

we get $$\frac{\Delta A}{A} = 3.36 \frac{\Delta C_{D_{LER}}}{C_D}$$

where $\frac{\Delta C_{D_{LER}}}{C_D}$ = fractional increase in drag due to LER effects.

Now, using the dollar value of a pound weight increase based on a traffic model of 445 flights in 1971 dollars, (Ref. 8) with a wing density of 5.31 lb/ft^2 of reference area, we have a cost figure:

$$\text{Cost} = \$ 1.6 \times 10^9 \frac{\Delta C_{D_{LER}}}{C_D}$$

This employs a value of \$24,000/lb weight increase for parallel burn vehicle, which is slightly high for the wing. This is, however, appropriate to a rubber system.

Again extremely high costs result from wing resizing.

Wing Resizing Due to LER $C_{L_{max}}$ Reduction and Related Costs

Taking those results in reference 4-14 where the largest roughness — corresponding in geometric scale to $k_{flight} = 1.57"$ — was used, as indicative of conditions in flight. Neglect the question of extrapolation to flight Reynolds number and take the tunnel data at face value. Reference 4-14 indicates an LER induced $\Delta C_L = -.065$ untrimmed and $\Delta C_m = -.0035$ at $\delta_e = 0$ deg and $\alpha = 19$ deg. Approximately one half of this lift loss is due to increased axial force due to LER. Net effect when trimmed at $\alpha = 19$ deg. is

$$\Delta C_{L_{trimmed}} = -.08 ,$$

which is 11% of C_L required to meet the 150 kt shuttle landing speed requirement. If the orbiter wing was simply scaled up 11% to compensate for this degradation, the cost increase for such a totally rubber vehicle can be determined by :

$$\frac{\Delta A}{A} = \frac{\Delta C_{L_{LER}}/C_L}{\Omega - C_{L_{wing}}/C_L} = -1.55 \frac{\Delta C_{L_{LER}}}{C_L} \quad \text{(Wing area change required)}$$

$$\text{cost} = \$1.25 \times 10^9(-\Delta C_L)$$

$$= \$10^8 (\text{for } \Delta C_L = -.08) \quad \text{(Resultant cost increase)}$$

This assumes a 1-g landing at 150 kt with a 25,000 lb payload.

Tail Resizing Due to LER-Induced Loss of c_{n_β} and Related Costs

For the H33, assuming a tail density of 5 lb/ft^2, and having determined experimentally that total contribution of the tail to $c_{n_\beta} = 40$ counts, in the same fashion as above, we have a cost penality for tail area increase required to restore c_{n_β} to be:

$$\text{Cost} = \$2.65 \times 10^6/\text{count of } c_{n_\beta}$$

Very large amounts are predicted for recovering even a few counts of c_{n_β}.

Interpretation of High Costs for Payload Reduction and Resizing

The costs just estimated cannot be taken literally, since the costs are extremely large (in an absolute sense) for degradation values well within the current and in fact even future uncertainties in the L/D, $c_{L_{max}}$, etc. What these costs bring out is that payload reduction and resizing are not viable solutions as fixes for LER or recession degradation. The degradation must be absorbed within the aerodynamic characteristics buffer or must be corrected pursuing further the aerodynamic optimization of the vehicle without weight increase.

If the induced degradation exceeds the buffer, the cost of wing resizing or flight schedule increase becomes prohibitive, thus providing a rational "go/no-go" limit on max (Δ L/D) $\Delta c_{L_{max}}$, etc for use in ablator selection -- provided of course that at least one ablator passes this test. The problem is reduced to establishing maximum levels on Δ L/D, $\Delta c_{L_{max}}$, etc within the 'cheap fixes,' such as l.e. camber, taking advantage of line improvements, etc. The cost of such fixes is negligible in the scale of costs considered here. The picture emerging is one of essentially cost-free fixes of limited effect and of standard fixes that are to be considered too expensive. Schematizing, this means that there is a 'go/no-go' limit for each degraded quantity and below this limit the degradation is cost free. If more than one ablator passes the 'go/no-go' criterion, the one generating the least L/D reduction is obviously the 'more acceptable' from the aerodynamic viewpoint. Since, however, the cost penalty is negligible in this range, we cannot rationally assign a non-zero dollar value rating for the Δ L/D, $\Delta c_{L_{max}}$ induced by recession and roughness.

Naturally one must also keep in mind that the costs estimated are dependent upon policy, for example upon the traffic model for the retrieved payload. In the traffic model most of the flights from orbit are empty and taking advantage of such available weight is excluded here.

4.3 Aerodynamic Degradation vs Roughness

In this section we give a crude estimate of the degradation of c_{l_β} c_{n_β} $(L/D)_{max}$ and tailscrape c_L for one typical end-of-Phase-B configuration, the Grumman 473 orbiter. This configuration had considerable potential of minor aerodynamic clean-ups.

Since the only roughness data available are for the Grumman H33 orbiter, we will use those data as typical.

The end result is to be an estimate of the roughness values that cause the maximum acceptable degradation of c_{l_β} c_{n_β} $(L/D)_{max}$ and tailscrape c_L. Such values will be considered typical of the end-of-Phase-B orbiters.

Effect on c_{l_β}

Figure 34 shows the effect of roughness on $c_{l_\beta}(\alpha)$. Note that any 'wandering' in the c_{l_β} variation with α is restricted to $\alpha > \alpha_{\text{drag break}} = \alpha_{\text{suction break}}$. Inspection of figures 35 and 36 indicates that detail design differences (Fig. 35) and basic longitudinal control effects (Fig. 36) exert a more profound effect on c_{l_β} at high α than the worst roughness investigated. Preliminary flying qualities investigation (Ref. 40) indicate that shuttle orbiter designs characteristically exhibit too much lateral stability at high α rather than too little. Any firm conclusion on this point, however, is configuration dependent and subject to verification by man-in-the-loop simulation.

The best general assessment at this time is that roughness effects on c_{l_β} need

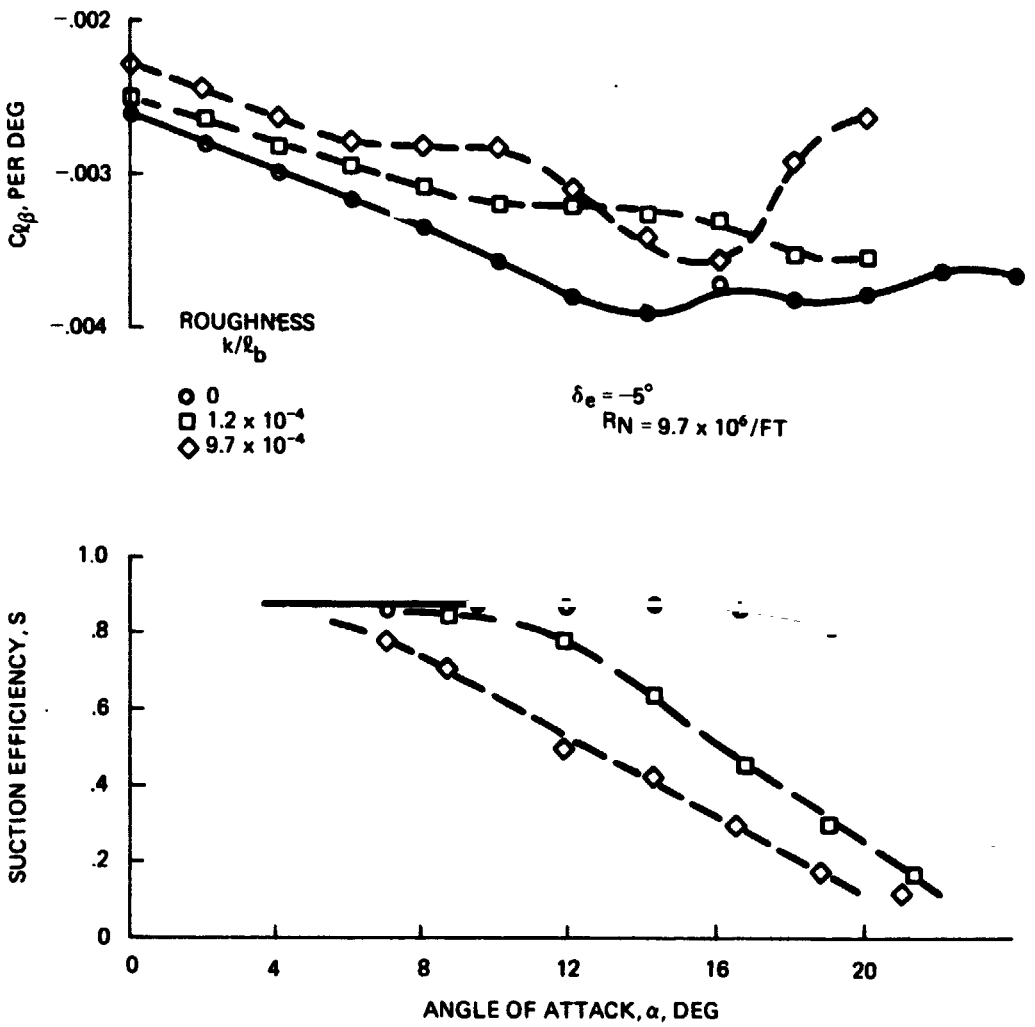

Figure 34. Effects of Roughness on H-33: Correlation Between C_{ℓ_β} & S

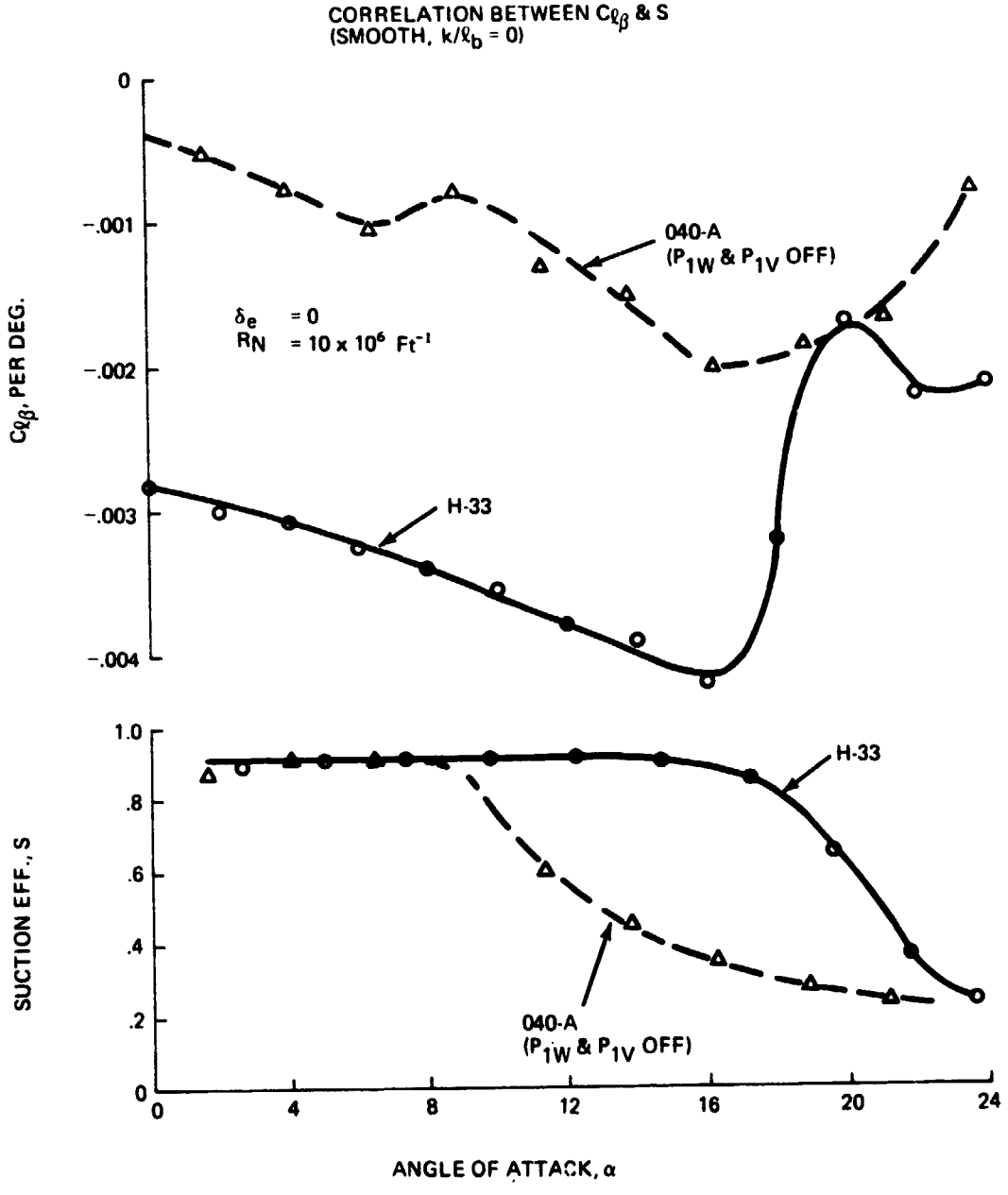

Figure 35 H-33 & 040-A Lateral Characteristics

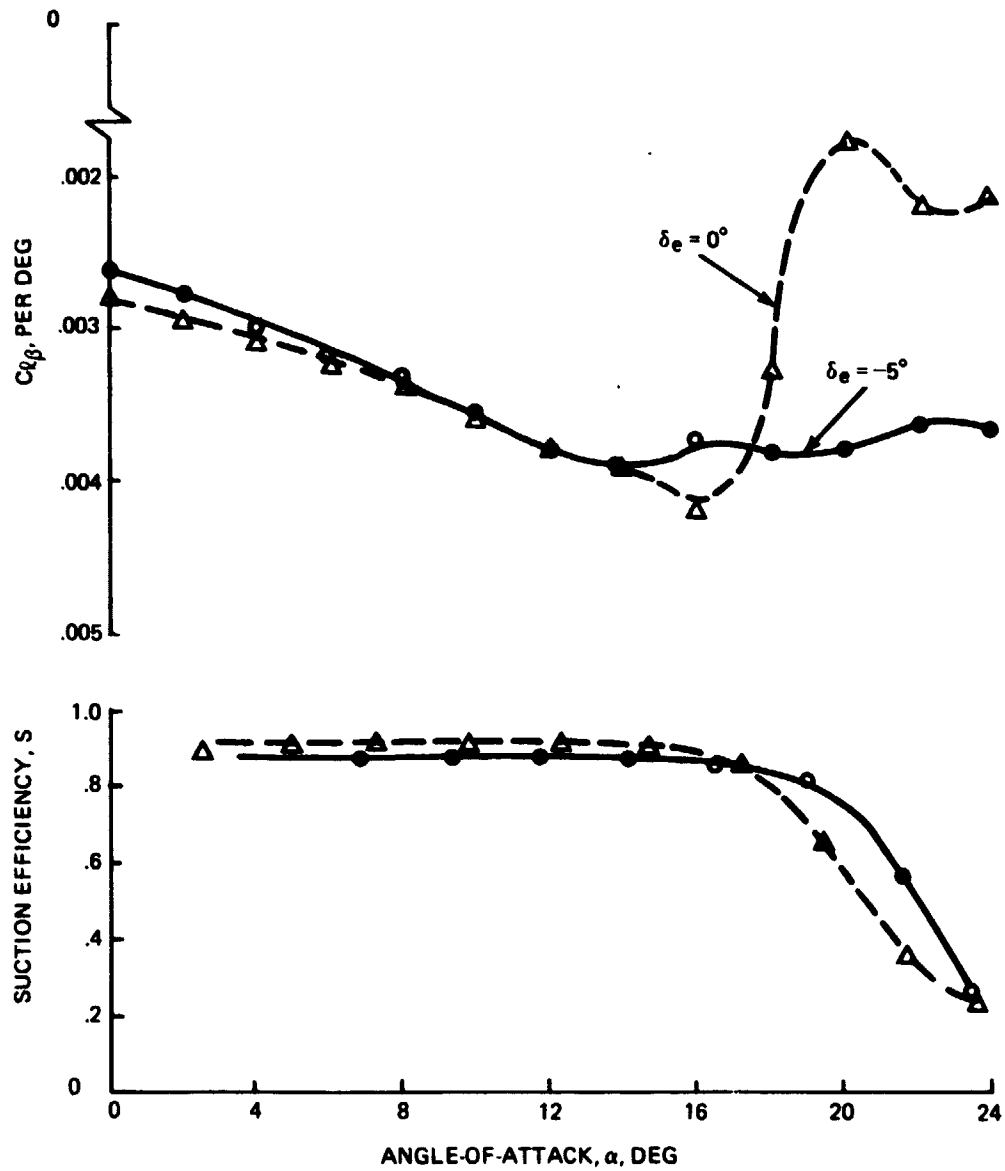

Figure 36 Effect of Elevator Deflection on H-33 Lateral Stability

not impact the design. Also, a preliminary gross statement is that roughness does not degrade significantly c_{l_β} up to roughness (peak-to-valley) values of one inch (the largest roughness used for figure 34 corresponds to 1.5 in. if scaled by k/r_n, to 1.3 in. if scaled by k/δ).

Effect on c_{n_β}

Figure 37 indicates that the tunnel data exhibit a four-count loss in c_{n_β} at low α with $k/l_b = 9.67 \times 10^{-4}$ roughness. The effective tail arm data in figure 37 indicate that the degradation at low α is due to a loss in vertical tail effectiveness. At $\alpha \geq 10$ deg and above, roughness effects on the wing apparently contribute to the degradation. Approximately 10% more vertical tail area would be required to overcome the low α c_{n_β} degradation due to $k/l_b = 9.67 \times 10^{-4}$ roughness.

At nigh α (α = 19 deg as reference), c_{n_β} is essentially unchanged in the tunnel data.

Considering the uncertainties in the extrapolation to flight Reynolds numbers, it is quite probable that the high α degradation in c_{n_β} is at most a couple of counts for the H33. Although this would not be serious for the H33, which exhibits a basic c_{n_β} level of $\sim$ 20 counts, the effects on the 040A, c_{n_β} clean $\sim$ 2 to 5 counts, would be substantial.

The preliminary conclusion is that, roughly peaking the effects of roughness up to the one-inch range, are not causing important degradation of c_{n_β}.

Effect on c_L at Tailscrape Angles

The H33 tunnel data (Ref. 37) showing the c_L degradation are presented in figure 38. Accounting for Reynolds number uncertainties, one obtains a maximum k for cost-free degradation of 0.8 in. (see Fig. 39), with increasing risks between 0.65 in. and 0.8 in.

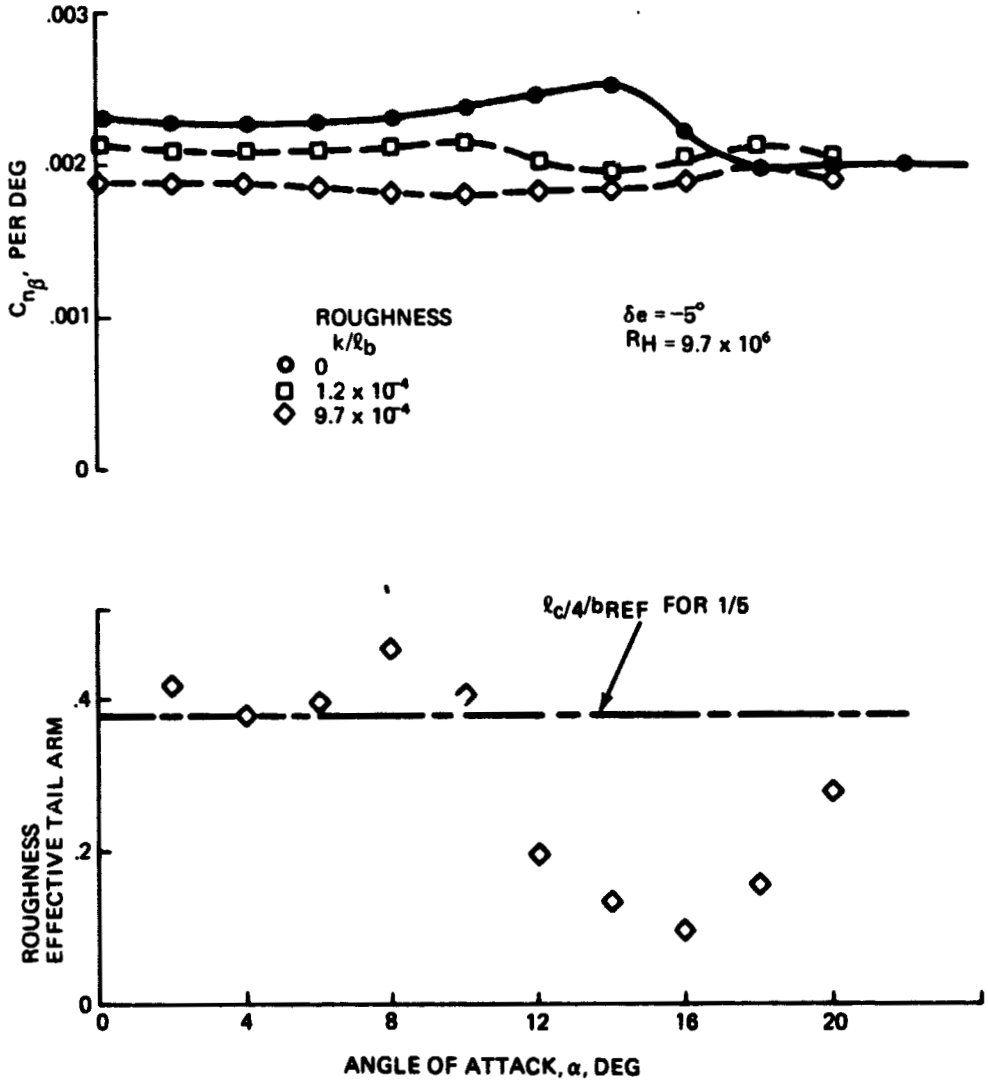

Figure 37 Effect of Roughness on H-33 Directional Stability

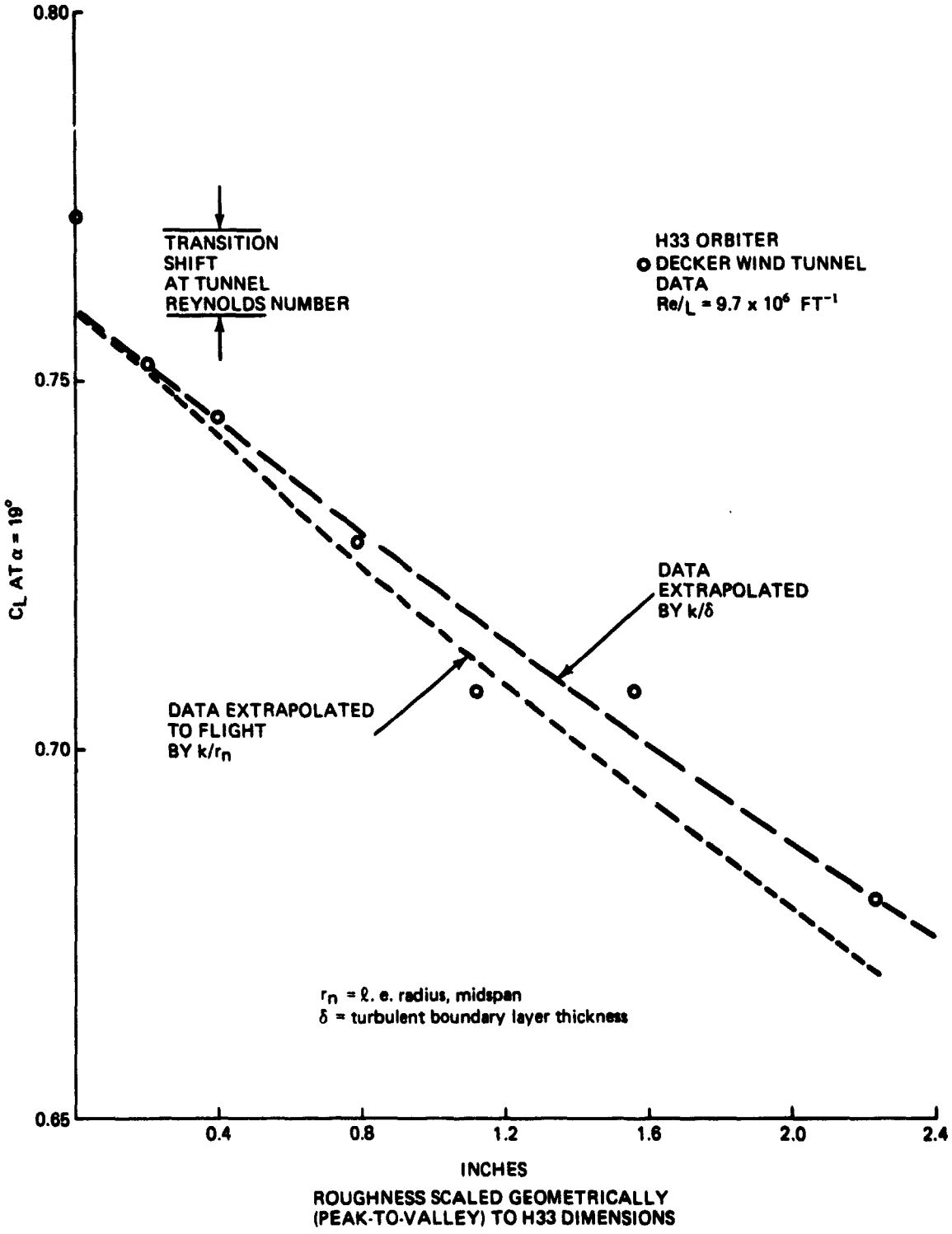

Figure 38 High α Lift Degradation Due To L.E. Roughness

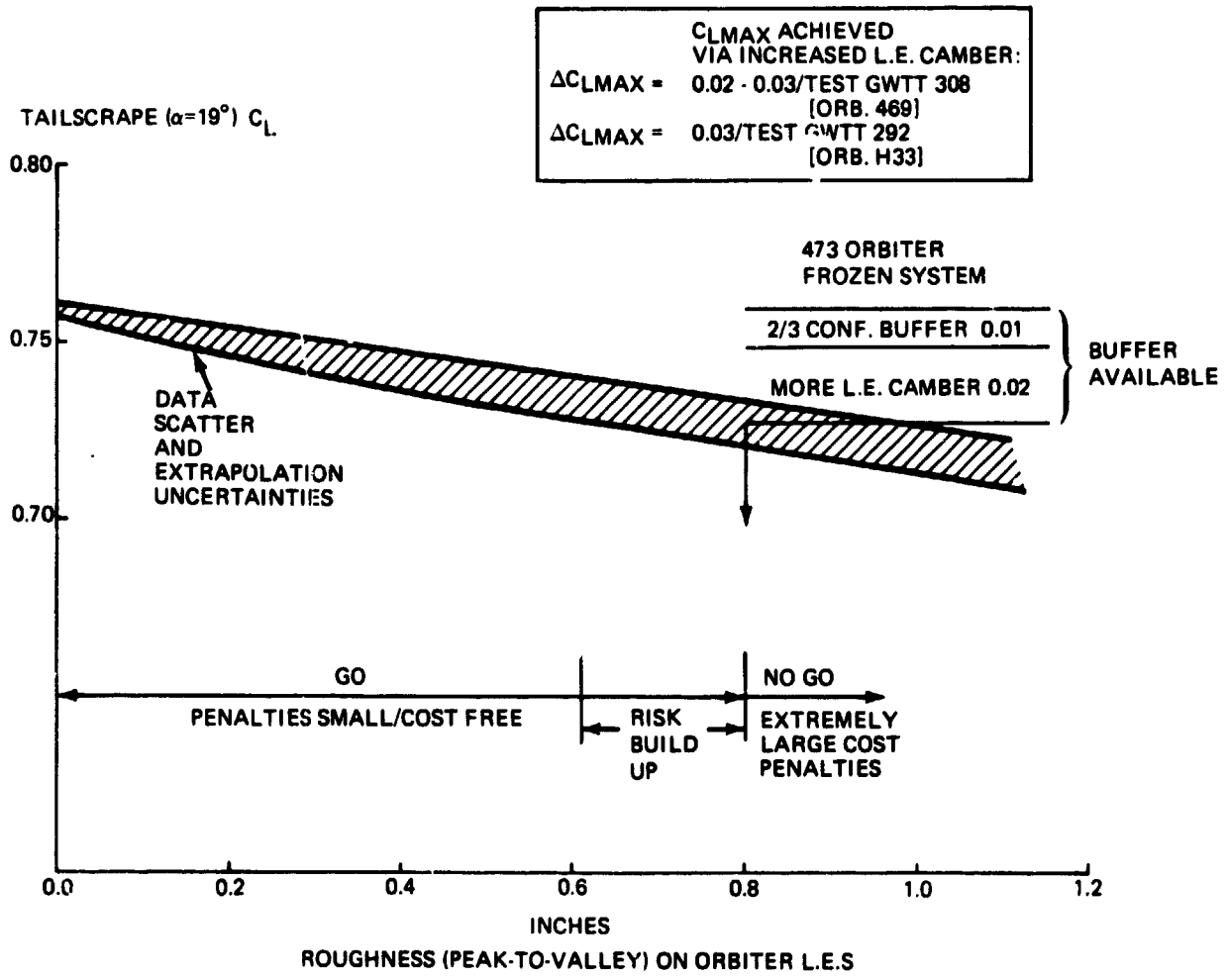

Figure 39 Maximum Acceptable Roughness Due to Landing Speed Requirements

If the orbiter wing were rubber, it would be possible to forestall roughness degradations on c_L to beyond α = 19 deg by further optimizing the wing twist, camber, nose form and tip shape. The feasibility of this is indicated by: (1) the fact that serious LER-generated c_L degradation is confined to α = 16 deg as shown in figure 34; and (2) the existence of a 6 deg shift in 'drag break' attributable to camber in the H33 design (see Fig. 35). Such a fix to give an added 3 deg in α (before LER induced lift deterioration becomes significant) would be essentially cost-free. At this time, it does not seem feasible to determine how much of an additional buffer can be built up with such fixes without further testing.

$(L/D)_{max}$ Degradation

The procedure given in Section 4.2 is quantized for the Grumman 473 orbiter (Refs. 41 to 43). The result is given in figure 40. For the frozen vehicle the basic buffer in $(L/D)_{max}$ is 1.25, so that even substantial portions of this (up to say 2/3 of it, i.e. of 0.8) could be allowed to be lost in the roughness degradation.

In general, l.e. camber on smooth l.e.'s can give relatively small improvements in $(L/D)_{max}$. In the case of a vehicle like the 473 orbiter, in which there is already l.e. camber, further increase of camber should probably give an extra Δ L/D of negligeable magnitude.

One therefore obtains as quantitative indication that the 473 should be able to accept a maximum of L/D loss of, say, 0.8.

The 473 orbiter in mid-1972 was at least partially rubber in the sense indicated above. It had also considerable clean-up potential that is conservatively estimated as follows:

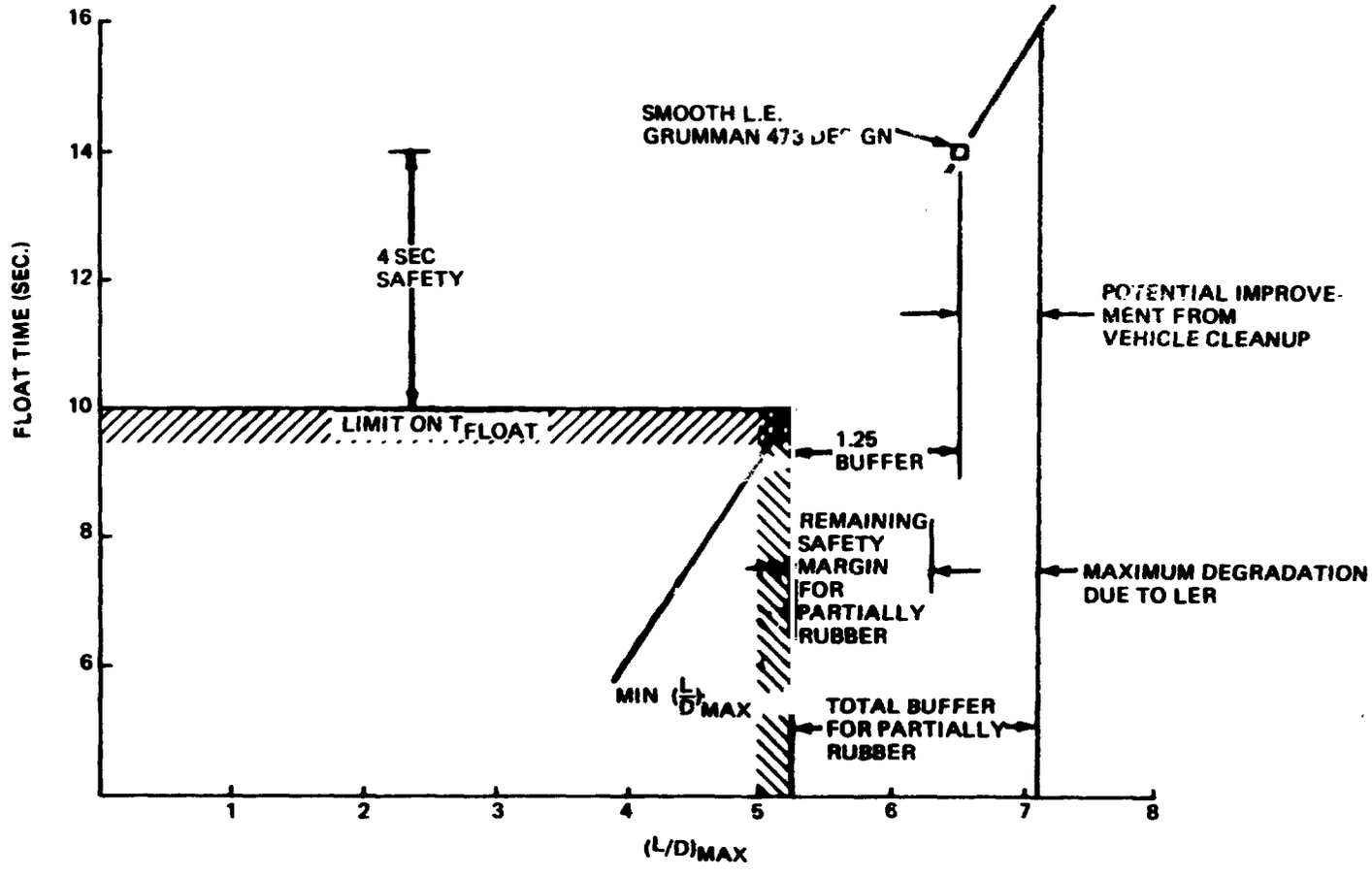

Figure 40 L/D Buffer for Grumman 473 Orbiter

Component	Current L/D Penalty (1972)	Conservative Improvement
OMS pods	0.7	0.25
ACPS pods	0.5	0.15
Shroud (boat-tailing)	0.35	0.2
		Total Δ (L/D) = 0.6

Costs: Negligible design and fabrication cost increments at this stage.

In summary then, for the Grumman 473 orbiter, the "go/no-go" limit is typically as tabulated:

Vehicle	$(L/D)_{max}$ Degradation Limit
Frozen	0.8
Partially Rubber	1.4
Rubber	1.4

Therefore we find that there exists an appreciable tolerance to L/D degradation before the 'float time' at landing is reduced beyond an acceptable minimum. This buffer can be increased by minor aerodynamics clean-up at negligible costs. On the other hand, tunnel data (extrapolated to flight as in figure 41) show that the L/D degradation due to roughness is quite visible.

In terms of roughness that can be tolerated within the limit $\Delta (L/D)_{max}$ of 0.8, figure 42 shows that k can be as high as 0.4 in. to 0.5 in. even taking a conservative attitude to the use of the available buffer.

Conclusions

Of the four quantities involved, $c_{l\beta}$, $c_{n\beta}$, c_L and $(L/D)_{max}$, we conclude that (on a typical flight scale, 6 in. of l.e. radius at midspan):

- $c_{l\beta}$, $c_{n\beta}$ unchanged up to peak-to-valley roughness of 1.0 in.
- c_L loss at tailscrape angles acceptable up to roughness of 0.65 to 0.8 in.
- $(L/D)_{max}$ loss acceptable up to 0.4 to 0.5 in.

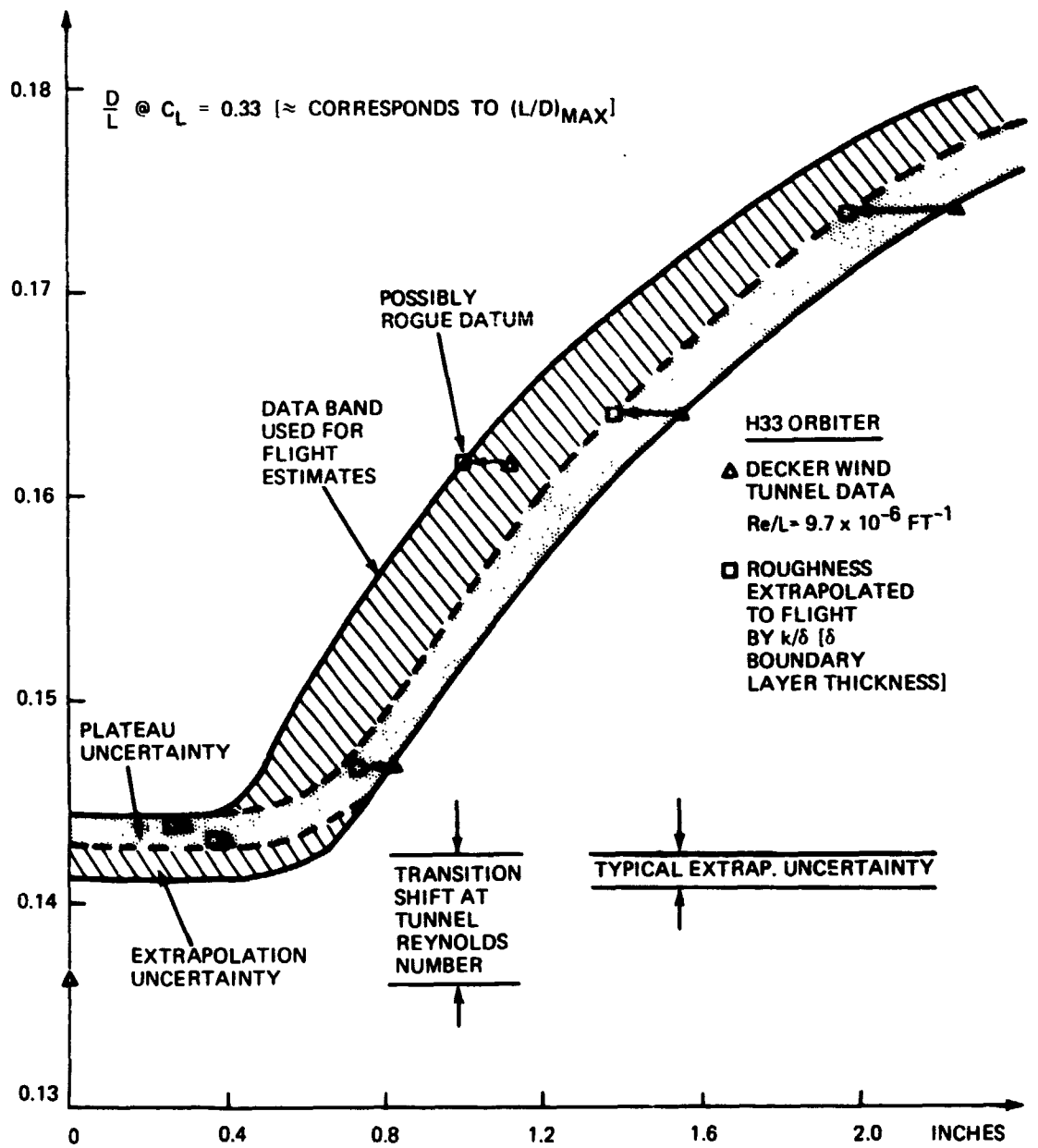

Figure 41. Extrapolated Tunnel Data Showing $(L/D)_{Max}$ Degradation Due to L.E. Roughness

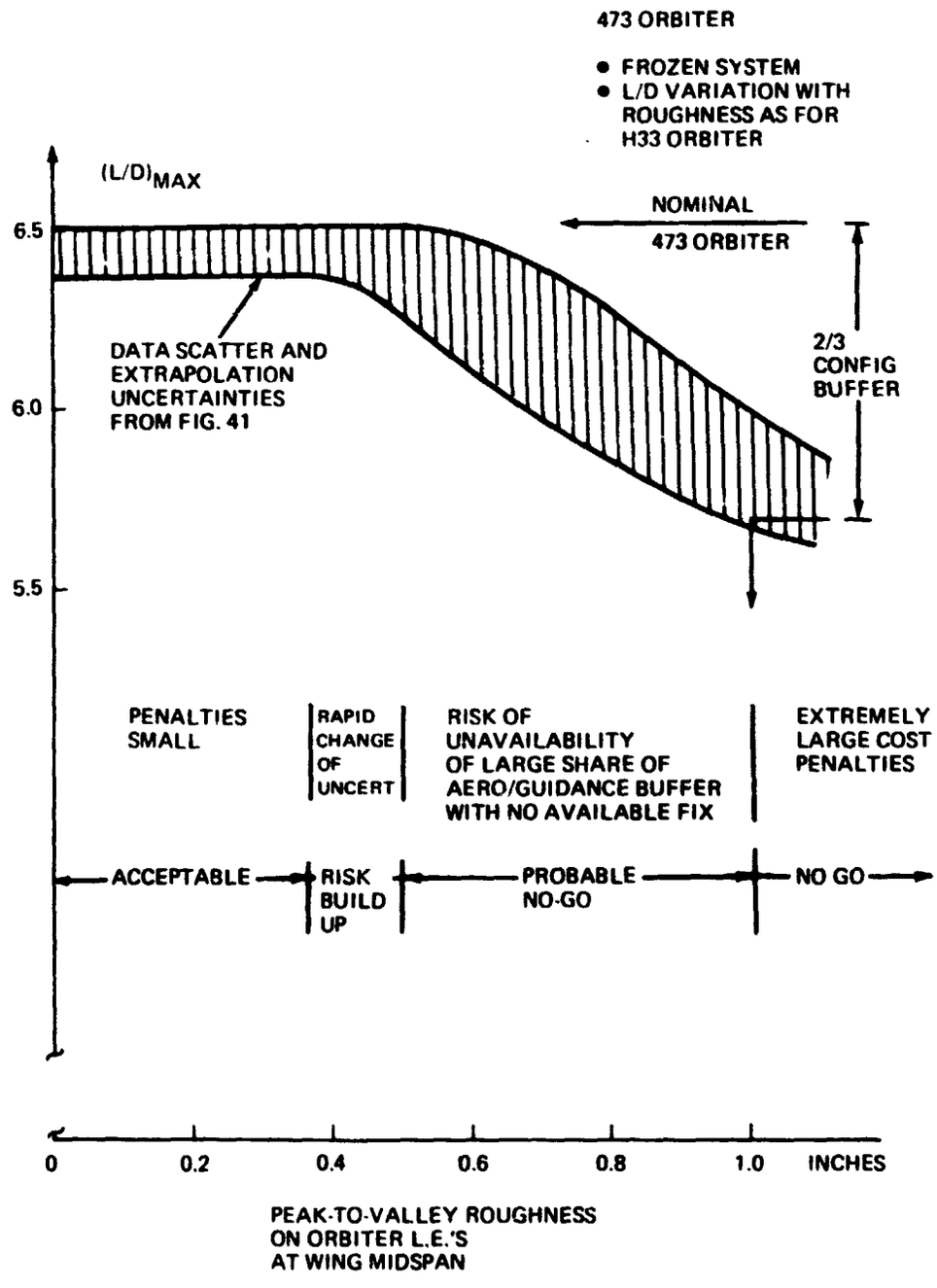

Figure 42. Maximum Acceptable Roughness Due to Float Time Requirements for a Typical Orbiter

These are the values for a typical single-delta orbiter like the 473, a frozen system and a large traffic of operational flights.

4.4 Minimizing Shape Change

We assume that one is willing to apply the concept presented in Section 4.1 to eliminate the major effects of shape change. Of course, one must be willing to do the work necessary to predict recession from ground experiments and theory; we believe that this is possible, but by no means do we imply that it can be done using information obtained from ablators flat models not subjected to the sequence of ascent heating, cold soak and entry heating at typical environmental conditions. In other words, the data for the prediction may have to be obtained.

Therefore, one has to contend only with the residual uncertainties in the predicted recession.

4.5 Aerodynamic Degradation vs Recession Uncertainties

We will now examine for a typical orbiter like the Grumman 473 the degradation of $c_{l\beta}$, $c_{n\beta}$, c_{Lmax}, $(L/D)_{max}$ due to recession uncertainties.

It turns out that wind tunnel tests (Ref. 44) have established that l.e. recession effects at moderate α can be neglected relative to roughness-produced effects. A l.e. shape change was simulated on a 1/25-scale H33 model, which corresponded to a recession more than three times that of the largest recession estimated* for any of the candidate ablators (see Section 5), and produced a $\Delta(L/D)_{max}$ of only -0.08. The major effect was a change in α stall resulting from a change in l.e. camber. Conclusion: $\Delta(L/D)$ from recession on delta wing orbiters for α below αstall will not exceed -.03 to -.04 — an order of magnitude less than LER effects. Note that this refers to the entire recession,

* Using, however, data from flat samples without ascent heating.

not just the residual prediction uncertainty.

The preliminary conclusion is that the degradation due to recession uncertainties is not a problem.

4.6 Conclusions

The preliminary assessment of the aerodynamic degradation is as follows:

- There are four aerodynamic characteristics we are concerned with $c_{l\beta}$, $c_{n\beta}$, c_{Lmax}, and $(L/D)_{max}$
- Roughness does not seem to affect $c_{l\beta}$ and $c_{n\beta}$
- c_L max and $(L/D)_{max}$ degradation due to roughness give the limits of go/no-go roughness as shown in figure 43. Below the 'go' limit the cost penalty is negligible
- Recession should be eliminated with the concept proposed; recession uncertainties have negligible effects

This preliminary assessment is based on a typical Phase-B single-delta orbiter such as the Grumman 473 with l.e. camber, a frozen vehicle and an operational traffic. For just the test flights at no payload, there is considerable buffer in the degradation acceptable, up to, perhaps, roughnesses of 1.0 in. (peak-to-valley) on the typical orbiter l.e.

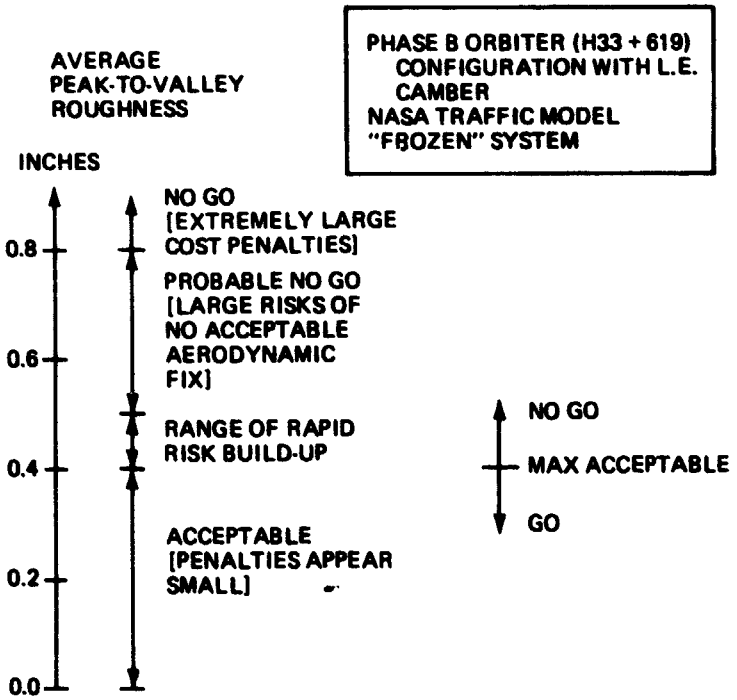

Figure 43. Estimated Maximum Acceptable L.E. Roughness for One Orbiter

5. ABLATOR SELECTION

5.1 Ground Rules and Criteria for Selection of Candidate Ablators

5.1.1 Ground Rules

Important ground rules were set out by NASA for the candidate ablators that could be considered in this study. These are:

a) To select developed materials (either off-the-shelf or requiring minor modifications for this application), especially flight tested.

b) To restrict the virgin density to the range 15 to 60 lbs/ft^2.

c) To consider a large number of candidates, in fact a minimum of six; this is consistent with the ground rules (Section 2) of a technology study and an absolute optimum i.e. for a large traffic model rather than a back-up system for a few initial flights.

d) To disregard improved formulations offered by the ablator manufacturers after the first test--a rule dictated by the need to conclude at some point the selection of the ablator.

Ground rules a) and b) are eminently reasonable when one considers the two key performance qualities desired in the ablators, i.e. thermal performance (i.e. insulation capability and char stability at low weight) and developed status (for low cost, low risks and short lead times). In fact, from these two points of view, charring ablators can essentially be grouped into three density ranges as shown in table 9. It becomes obvious that the ground rules codify the expectation that materials below 15 lbs/ft^3 will not work and that above 60 lbs/ft^3 the weight penalty is unacceptably high.

Table 9 Leading Edge Ablators Grouped by Density

Density Range	Advantages/Disadvantages
15 – 30 lb/ft^3	Low Weight Char Stability Problems Low Level of Flight Experience
30 – 60 lb/ft^3	Stable Char Flight Proven Candidates Inspection and Repair Procedures Defined
60 – 100 lb/ft^3	Weight Penalty Strong Chars Flight proven on Ballistic Missiles

It turned out that, because of the scope of the study, it became necessary to eliminate hybrids, i.e. multiple ablator l.e. designs. This would have required to study the compatibility problem between materials, since problems may arise from hybrids (Ref. 45). This would also have required to solve before hand the question of the joint between ablators. Of course, hybrid designs for the orbiter l.e. have been sketched (but not developed), see for example Refs. 46 and 47.

Another question in the nature of policy that had to be clarified is the difference between the following two material concepts, a developed 'material formulation' and developed 'material system'. 'Material formulation' is the basic material, 'material system' is that material fabricated in a H/S system, e.g. in a molded form, in a Hc form, etc. The question is: When for a certain material there is a developed formulation and a developed material system in the molded form, is the Hc form automatically a developed material system? The answer that we gave to this question is affirmative when the molded material system 'works' in the desired environment. Then the thermal behavior of the Hc system is expected to follow closely that of the molded system. The thermal properties should be very close and real variations should exist only for the structural properties. In this case we decided to consider the Hc system a marginally developed system.

It is almost obvious that when we speak of candidate materials or ablators we mean materials systems as defined above.

5.1.2 Criteria

The number of candidate ablative materials applicable to the shuttle leading edge is quite large. This is true even when it is noted that the requirement and the materials be in the density range $15 < \rho < 60$ lb/ft^3 excludes the higher

density carbon phenolic and silica phenolic (ρ =90 lb/ft^3) which have been well characterized and flight tested on numerous Air Force missile programs. Several lower density materials, some of which have undergone limited development testing are available and appear attractive for leading edge use. In fact it is clear from table 9 that trade-offs exist since insulation efficiency tends to decrease with increasing density, while char stability increases and the weight penality increases.

The choice of candidate materials for this study was based on the desire to investigate both epoxy and elastomeric systems in the density range of 15-60 lb/ft^3. An additional objective was to select materials which can be considered in the well developed category. In addition to the Dolan (Reference 48) and Price (Reference 49) sources, various other material studies (References 50 through 54) have been reviewed to insure a large degree of overall selection objectivity.

The following criteria guided the selection of the candidate materials:

1) Char Stability - The thermal nature of this material group is characterized by in-depth decomposition (charring). Extensive mass loss is possible, such as that associated with the NASA 602 material (Ref. 48).

Char stability, related to both extent of decomposition and char matrix constituents, is an important parameter since both surface recession and roughness must be "predictable" and char instability (spalling, erosion, etc) should be minimized to prevent degradation in subsonic aerodynamic performance. It should be noted that the char

layer will be subjected to vibration loads during low altitude maneuvers.

2) Thermal Efficiency - Materials will differ both in ablation and insulation performance. The objective is, of course, to select materials which have a high thermal efficiency (i.e., low weight) while also satisfying other system requirements.

3) Honeycomb or Molded - Factors such as cost, surface roughness, density, and char stability may be significantly influenced by whether a molded or honeycomb reinforcement version of a material is used.

4) Development (Characterization) Status - To meaningfully interpret the experimental data which are to be obtained from the screening tests only materials for which characterization (property) data are readily available should be chosen. A positive relationship exists between the amount of such property data and degree of development (process, fabrication techniques, etc.) and, hence, well-developed and characterized materials are desired.

5) Prior Flight Experience - As much as possible, the primary leading edge ablatives should be chosen from materials which have a listing of proven entry applications. Modifications based on shuttle application or basic process improvements should be considered for maximum program benefit.

6) Ease of Fabrication - Application of the material on a leading edge configuration gives rise to questions of fabrication both in respect to ease as well as to more fundamental concerns such as feasibility and cost. A significant factor here is the possibility of problems arising due to the use of a honeycomb material in a small radius leading edge.

7) Cost - This criterion (involving matters of material, processing, fabrication, development and refurbishment) is of primary concern and will strongly influence final selection.

5.2 Selection of Candidate Materials

5.2.1 Candidate Materials Selected

Based on the criteria just described the materials shown in table 10 are considered to best represent the group of candidates from which the ablative leading edge material may be chosen. This group represents also the best choice in terms of cost/time effectiveness for this program. The materials recommended for study cover a range of densities ($22 < \rho < 55$ lbs/ft^3) and include only systems which are either flight tested or are in an advanced state of development.

The following information describes the rationale used in choosing each material:

ESA 3560 IIA ($\rho = 56$ lbs/ft^3) This Martin elastomer was specifically developed to assure controlled contours and essentially

Table 10 Candidate Ablators Selected for the Orbiter Leading Edges

Commercial Designation	Matrix†	Virgin Density lbs/ft^3	Manufacturer	Flight Experience	Description
ESA 5500	Hc	55	Martin Marietta Co.	Prime (Fins Leading Edges and Chines)	Elastomeric silicone, higher-density carbon-enriched form of the ESA 3560 HF.
ESA 3560-IIA	M	56	Martin Marietta Co.	X-15A-2 (Wing Leading Edges)	Elastomeric silicome, fiber reinforced, premolded at low pressure and bonded at room temperature
5026/39	Hc	33	AVCO	Apollo (large areas)	Epoxy-Novolac resin with low density fillers and fiber reinforcement
5026/39	M	37	AVCO	Apollo (hatch and door areas)	
ESA 3560 HF	Hc	30	Martin Marietta Co.	Prime (large areas)	Elastomeric silicone, silica fiber reinforced, packed into a glass phenolic honeycomb core
Mod 7	M	35	AVCO	none	Elastomeric silicone, with silica accospheres, phenolic microballoons and quartz fibers
Mod 7	Hc	31	AVCO	none	
480-1B	Hc	22	AVCO	none	Elastomeric silicone, with silica microballoons and fiber reinforcement.

†M = Molded
Hc = Honeycomb reinforcement

zero recession to the l.e. of the X15-A2. It is premolded (to assure contour control) and is bonded at room temperature and low pressure (to simplify tooling). This material was chosen by MDAC for the Phase-B,l.e. design, because of 'easy fabrication and application for wide range of design thickness' and 'because of good rain erosion resistance' (Ref. 46, page B 3-25).

ESA 5500 (ρ = 55 lbs/ft^3) This alternate, high-density Martin elastomer has demonstrated performance in the high speed environment associated with entry vehicles (fin leading edges on PRIME vehicle). This material, which is used in a honeycomb, utilizes a filler which is principally carbon to minimize surface recession.

Avcoat 5026/39 (ρ = 33 lbs/ft^3) The basic Apollo heat shield material, this epoxy is one of the three materials selected to explore a medium value of density. The honeycomb version of this material was one of the three materials found superior in Ref. 9. This material was chosen by Grumman during the Space Shuttle Phase B studies (Ref. 55). The molded version of Avcoat 5026/39 is also flight tested -- it was used on the Apollo vehicle in hatch and door areas. The use of this molded configuration would be attractive, of course, due to the possibility of significant reduction in production costs.

MOD 7 (ρ = 35 lbs/ft^3) This material is considered representative of the elastomers at this density level. Avco recommends it for study in both molded and honeycomb configurations, as the resulting data should help assess the capability of elastomers in the medium density class to efficiently perform in the flight leading edge environment.

The material has been exposed to a significant amount of testing during development of Avco. It was developed originally for planetary-entry, thermal-protection applications and has been extensively evaluated at Avco and at various NASA facilities. In addition to being well characterized, the Mod 7 material has been subjected to a variety of processing and fabrication studies.

The material has been successfully exposed to -260° F on an aluminum substructure. As with the 5026-39, the need for honeycomb reinforcement in the Mod 7 will have to be established. Mod 7's advanced stage of development eliminates the need for any extensive activities relating to formulation, processing and fabrication.

In view of the large amount of development studies (Ref. 59), Mod 7 M is a developed material system.

Mod 7 Hc is a (marginally) developed system in the sense of Section 5.1.1, on the expectation that the thermal performance of Mod 7 M under entry heating is good, but there is the usual question of whether after the heating pulse the material possesses a char-virgin interface

strong enough to give the confidence a designer must have. A good reason to select Mod 7 Hc to include in the study at least one true comparison, molded versus honeycomb, for elastomers. One alternative would have been to select the molded counterpart of the 3560HF. This material, however, appears to be a research material*.

ESA 3560 HF (ρ = 30 lb/ft^3) This Martin material was utilized in the large areas of the PRIME vehicle. Because of the flight experience and background investigations (Reference 57) associated with this material, it appears to be a promising candidate. This is the material that has been considered in Lockheed's alternate Phase B studies (Ref. 58).

480-1B (ρ = 22 lbs/ft^3) This Avco elastomer, which utilizes silica microballoons rather than the less stable phenolic balloons of the 480-2 material series, is considered to be a representative of the low density candidate materials. As in the case of Mod 7, prior experience will allow more definitive data interpretation of the material group during this study. Use of alternate, non-Avco material candidates at this density level will make reliable data interpretation more difficult. While it might be possible to utilize this material in molded form Avco recommends that evaluation of this material be in a honeycomb configuration due to its low density.

The 480-1 series represents a class of Avco-developed, low density

*There is however a molded version or modification of the 3560 HF that was flown on PRIME in the fin fillet areas as a joint filler.

materials in the range of 15 to 22 lb/ft^3. These materials are lower density materials of Mod 7 and the same fabrication molding and bonding procedures are used. The particular version of 480-1 that is recommended for space shuttle L.E. evaluation is designated as 480-1B. This is a 22 lb/ft^3 material developed primarily for use as tactical missile thermal protection. This material has been tested under relatively high-shear conditions (~ 9 lb/ft^2) and exhibited a hard char with no cracks. However, a fiberglass honeycomb is recommended because of the material's low density and the uncertain strengths of the char-virgin material interface. As with the Mod 7, Avco has conducted extensive processing and fabrication studies with 480-1 materials.

As a whole, the group of ablators of table 10 covers quite well the key issues/criteria for the selection of a l.e. ablator. How the driving criteria/issues are covered is summarized in table 11.

Besides the ablators included, a point should be made about one outstanding ablator excluded, the DC 325 Hc (ρ = 55-57 lbs/ft^3) or S-3 material. The Gemini heat shield material, developed by Dow Corning for the NASA program and McDonnell-Douglas, is also a high density elastomer in a flexible honeycomb matrix. This material was one of the three that exhibited best thermal performance in a first test program aimed at verifying the feasibility of using state-of-the-art ablators for the orbiter leading edges (Ref. 45). Unfortunately, this material had to be excluded because it could not be procured.

Table 11 Driving Criteria for Selection of the Candidate Ablators

Driving Criteria for Selection	Materials Selected
Prior flight experience	AVCOAT 5026/39 Hc&M, ESA 5500, ESA 3560 IIA, ESA 3560 HF
Recession/contour control/char stability	ESA 3560 IIA, ESA 5500, AVCOAT 5026/39 HC
Honeycomb vs. molded question (especially at 30 lbs/ft^3)	AVCOAT 5026/39, Hc ⟷ M Mod 7 , Hc ⟷ M Also ESA 5500 and ESA 3560 IIA.
Good coverage of medium density (30 lbs/ft^3 materials)	AVCOAT 5026/39 Hc&M, ESA 3560 HF, Mod 7 Hc&M
Typical 30-to-20 lbs/ft^3 elastomers representing a wide class of materials such as the General Electric Co. and the NASA elastomers	Mod 7 Hc&M, 480 lb Hc
Ease of fabrication/low costs	AVCOAT 5026/39 M, ESA 3560 HA
20 lbs/ft^3 density range	480 1B Hc
Elastomers vs. epoxies	ESA 3560 HF, Mod 7 ⟷ AVCOAT 5026/39

5.2.2 Key Material Properties

Table 12 summarizes the more significant properties of the candidate materials. These properties have been determined not only be direct measurement but in some instances from interpretation of flight test data. A systematic effort at collecting property information for all candidate materials gave the detailed information found in the Data Package.

5.3 Screening Test Program

5.3.1 Rationale

The objectives of the screening test program were 1) to evaluate the candidate ablators under realistic leading edge environment conditions 2) to determine the critical factors which might affect the performance of an ablator on the leading edge and 3) to provide data which permit the selection of one ablator for the initial design. In order to define a meaningful test program consistent with these objectives the entire leading edge environment was reviewed. The leading edge must withstand moderately high ascent heating followed by cold soak in orbit and subsequent entry into the atmosphere. Combined with these thermal environments is the flexure experienced by the wing during ascent (peak q_α) and during maneuvering prior to landing.

Figure 44 shows schematically the sequence of environments encountered. Reviewing these environments it is clear that one of the primary requirements of the selected material is a strong char which will provide a stable contour for subsonic performance and also minimizes the chances of particles from the char impinging on the adjacent TPS. In order to properly assess this char realistically it is necessary that the material be tested 1) using a leading edge contour (where aerodynamic shear and pressure gradients exist) and 2) in a sequential environment where the gross effects of the total flight can be evaluated. Of particular interest is the effect of ascent heating on material

Table 12 Material Property Summary

Property	ESA5500	ESA3560IIAM	5026-39M	5026-39H/C		MOD7M	MOD7H/C		ESA3560HF		480-1B H/C
Density											
Virgin (Lb/Ft^3)	58.0	56.0	37.0	33.0		36.0	33.6		30.0		22.0
Char	30	21.3	18.5	16.5		20	18		12		16
Thermal											
Conductivity (BTU/ft-hr°F)											
Virgin	.13	.08	05	.05		.055	.064		.054		.056
Char	.20	.20	.14	.14		.24	.24		.64		
Specific Heat (BTU/lb °F)											
Virgin	.21	.26	0.33	0.33		0.38	0.38		.34		0.29
Char	.35	.26	0.27	0.27					.26		
				Rib. Direc.			Rib. Direc.		Rib. Direc.		
Structural				Par.	Per.		Par.	Per.	Par.	Per.	
Tensile Strength (psi)	140	240	1700	840	620	219	184.0	.0169	.0120	.090	
Modulus (psi x 10^{-6})	.006	6.2	0.13	.140	.100	.0078	.0075	.0074	.0053	.0048	
Ultimate Tensile Strain (%)	36	–	1.44	.80	1.00	3.4	3.1	2.8	4.5	4.5	
Thermal Expansion Coefficient (10^{-6} in/in.°F) (RT)			17.0	12.7	20.0	21.3					

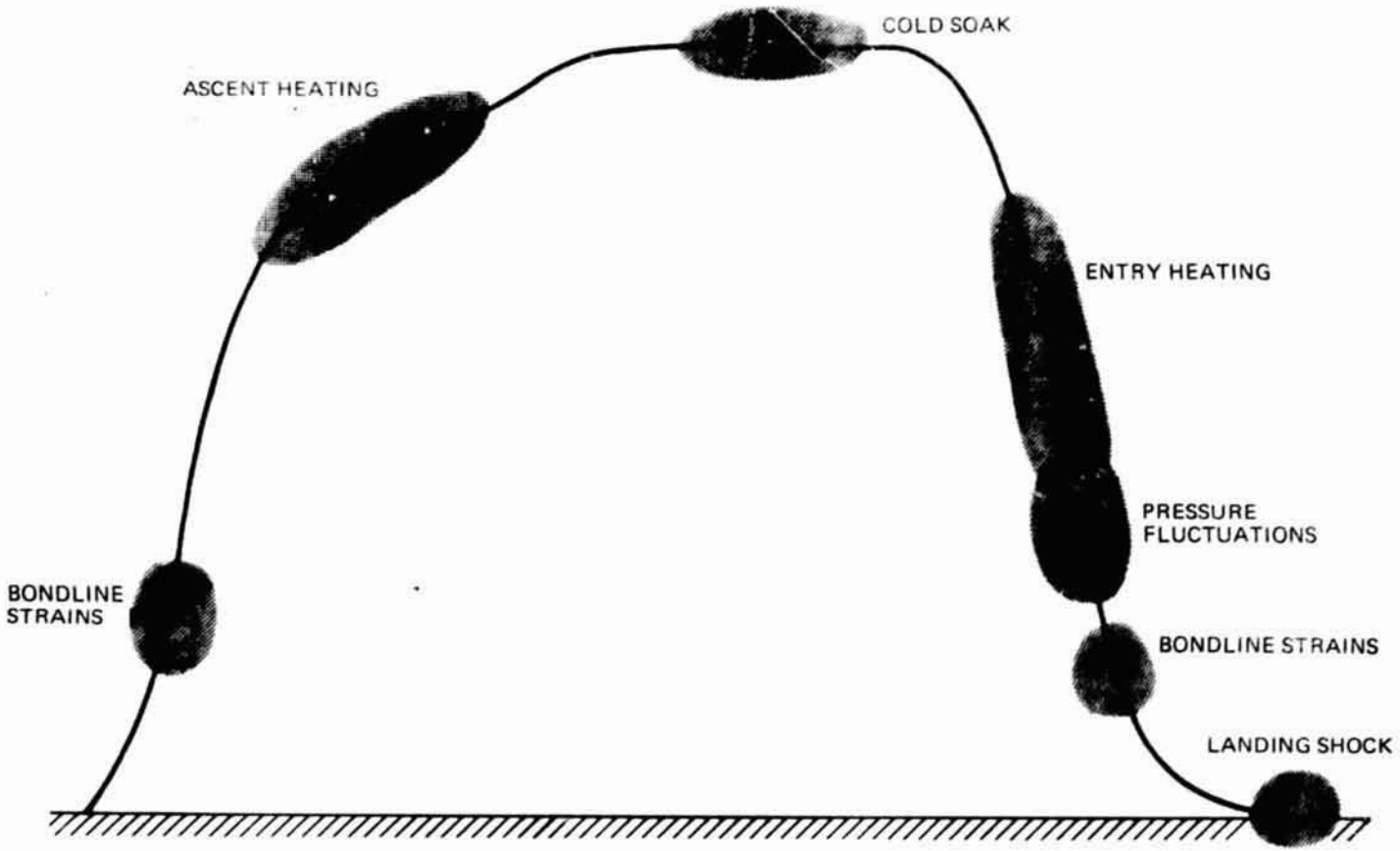

Figure 44 Key Environments For Screening Candidate Ablators

performance during reentry. In addition to the sequential environmental tests described above it was also desirable to determine the thermal efficiency and structural characteristics of the various materials so that they could be ranked according to weight and reliability considerations. The thermal efficiency could be best determined by instrumenting the leading edge models while the structural characteristics (flexure strength) of the materials were determined using beams of both the virgin and char material. The virgin tests allowed comparison with existing material property data while the charred beams would simulate the state of the ablator on the leading edge during maneuvering prior to landing.

5.3.2 Overview of Tests

The description of the ablator screening test program is shown in figure 45 and table 13. As can be seen two basic configurations were used 1) a leading edge specimen which was subjected to the sequence of environments shown and 2) a flexure beam which was used to determine the characteristics of the virgin and charred material. Samples were also procured for rain erosion tests which however were not carried out.

One model, the Mod 7 M, was used by NASA LaRc for other purposes. A replacement model was fabricated by Avco, however it was instrumented differently and was not cold-soaked. The results obtained with it are occasionally used here.

The key environments selected (table 13) are those that represent the most severe conditions for the four performance qualities just mentioned.

The policy we followed for the aerothermal environment tests was to fabricate a single specimen per material, in a relatively sophisticated model for an elaborate test sequence. The model was a l.e. configuration (figure 46), complete of substructure, tested sequentially under simulated ascent heating,

1. AEROTHERMAL TEST

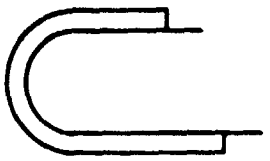

SEQUENTIAL
- ASCENT HEATING
- COLD SOAK IN ORBIT
- REENTRY HEATING
- VIBRATION
- LANDING SHOCK

2. FLEXURE TESTS

- VIRGIN MATERIAL
- CHARRED SURFACE

Figure 45 Screening Tests

Table 13 Overview of Screening Program and Results

		FLIGHT ENVIRONMENT TO BE SIMULATED	FLIGHT CONDITIONS TO BE SIMULATED	FACILITY	TEST CONDITIONS	MAIN RESULTS
Leading Edge Models		Sequence: 1. Heating During Ascent	$\dot{q}_{cw}$ = 9.5 Btu/ft²–sec Total enthalpy ≃10,200 Btu/lb$_f$ Total Q = 5390 Btu/ft²	AVCO Rovers Arc-Jet	$\dot{q}_{cw}$ = 9.5 Btu/ft²–sec ('cold wall') Total enthalpy = 10,000 Btu/lb Time of test = 560 sec	In stag. region, epoxies char, elastomers discolor only; Minor mass losses, dimensional changes
		2. Cold Soak in Orbit	Temperature = –200° F Pressure = 1 x 10^{-7} atm Time of flight = max 7 days	Grumman 4'x8' N_2 chamber	Temperature ≅ –200° F Pressure ≅ 1→10 x 10^{-7} atm Time of test = 2 hrs	No visible effects
		3. Heating During Entry	$\dot{q}_{cw}$ = 60 Btu/ft² – sec Total enthalpy ≃11,400 Btu/lb$_f$ Total Q ≃ 55,000 Btu/ft²	NASA/LaRC Arparatus A	$\dot{q}_{hw}$ = 60 Btu/ft² · sec ('hot wall') Total enthalpy = 3,700 Btu/lb Time of test = to 200° F backface temperature	Char stability problems with 3 molded materials; 4801B fails. Effectiveness and soak-out temperatures, Fig. 50 Ablation history, Fig. 51 Shape change, Fig. 52
		4. Pressure Fluctuations After Entry	SPL ≃ 146 at 60 Hz SPL ≃ 88 at 500 Hz Average surface temperature 950°F Flight time ≃ 900 sec	NASA/LaRC Thermoacoustic Facility	SPL ≃ 117 db at 60 Hz; SPL = 108 at 500 Hz Max surface temperature = 500° F Time of testing = 900 sec	All models appear unaffected; Later, the ESA 3560 IIA loses nose cap
		5. Shock at Touchdown	Acceleration = 11 g Frequency = 15 Hz Duration = 2 sec (twice ?) 1 axis, leeward → windward	Grumman MB C-10 Force Shaker	Acceleration (max) = 11g Sinusoidal, with frequency = 17 Hz Time of testing = 2 sec, twice 3 orthogonal axes	No visible effects
Flexure Models	Set # 1	Bondline Strains During Ascent	Temperature & pressure below 20,000 ft altitude Max bondline strain on l.e. = 0.0020	Grumman T. Olsen Tensile Test Machine	Room temperature and pressure Bondline strains up to 0.0028	No visible effects
	Set # 2	Sequence: 1. Charring During Entry	$\dot{q}_{cw}$ ≃ 35 Btu/ft² – sec; Q ≃ 30,000 Btu/ft² Total enthalpy = 11,400 Btu/ft² Char thickness = 0.7 inches for 5026/39 Hc ablator	AVCO Rovers Arc-Jet	$\dot{q}_{cw}$ ≅ 22 Btu/ft²–sec; Q = 22,000 Btu/ft² Total enthalpy = 11,000 Btu/lb$_f$ Char thickness = 0.5 inches on 5026/39 Hc	Representative flight char imposed on models Delamination of Mod 7 M; good char integrity of other materials, especially 480 1B Hc.
		2. Bondline Strains After Entry	Char Surface temperature ≃ 500° F, pressure below 20,000 ft altitude Max bondline strains on l.e. = 0.0020	Grumman T. Olsen Tensile Test Machine	Room temperature and pressure Bondline strains up to 0.0035	No visible effects

Figure 46 Typical Leading Edge Specimen

Figure 47 One Set of Flexure Models of the Candidate Ablators

cold soak, entry heating, pressure fluctuation and shock environments The facilities used are indicated in table 13. The instrumentation on each l.e. model was seven backface thermocouples, appropriately isolated to eliminate lateral conduction effects in the substructure. The opposite policy was used for the flexure tests; the models (figure 47) were very simple strips, one flexed in its initial form and one first charred and then flexed. The facilities in which these flexure models were tested are indicated in table 13. The instrumentation was also very simple, two strain gauges and two thermocouples per model.

In all models, l.e. and strips, the thicknesses of the various ablators (uniform over the models) were scaled according to density so as to afford a comparison of the results at the same unit weight. Of course, there were in all tests other appropriate measurements such as surface temperature, roughness, recession and mass loss measurements, and extensive photographic coverage including 16mm movies * of the arc-jet tests and the shock tests. Each ablator manufacturer bonded its own materials on the appropriate substructure.

The following provides a brief outline of the two series of tests.

a) Leading Edge

The aerothermal tests utilized the leading edge specimen shown in figure 48. This configuration provided the proper environment for the evaluation of the materials and at the same time maintained compatibility with the NASA/LRC Apparatus "A" facility. The nose radius was dictated by flow blockage considerations while the material thickness was limited by the ability to curve the flexcore honeycomb. With the exception of the 480-1B Hc the weight per unit area of ablator (W/A) was held constant so that the

* Films can be seen at the Thermal Protection Branch, NASA Langley Research Center, Hampton, Virginia.

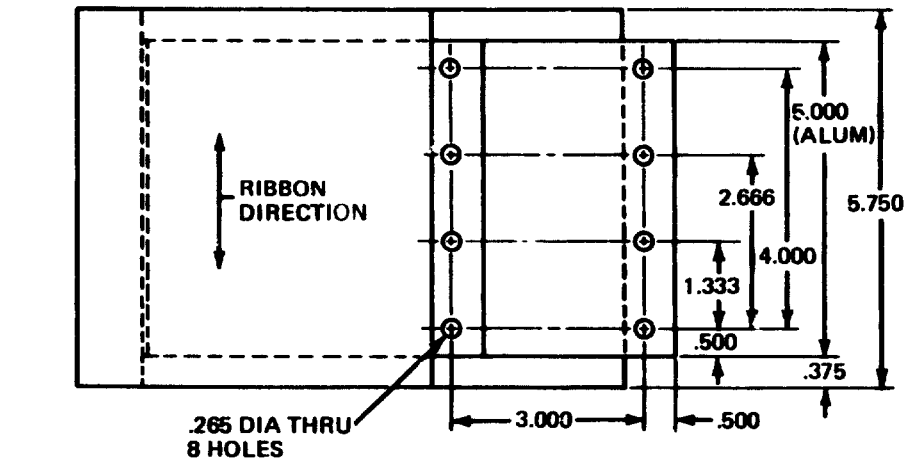

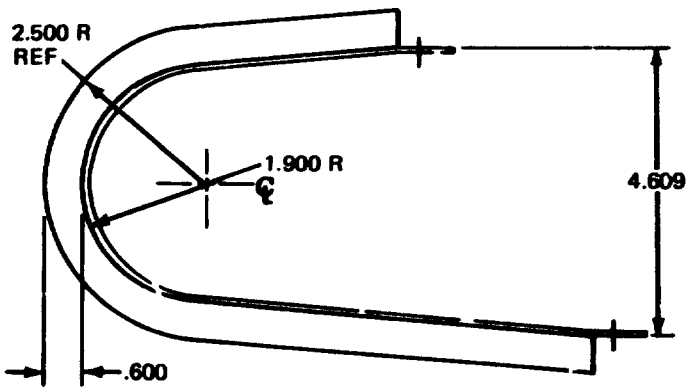

② MAT'L - 55 LBS/FT³ - NOMINAL DENSITY RANGE
OTHERWISE SAME AS PART #1

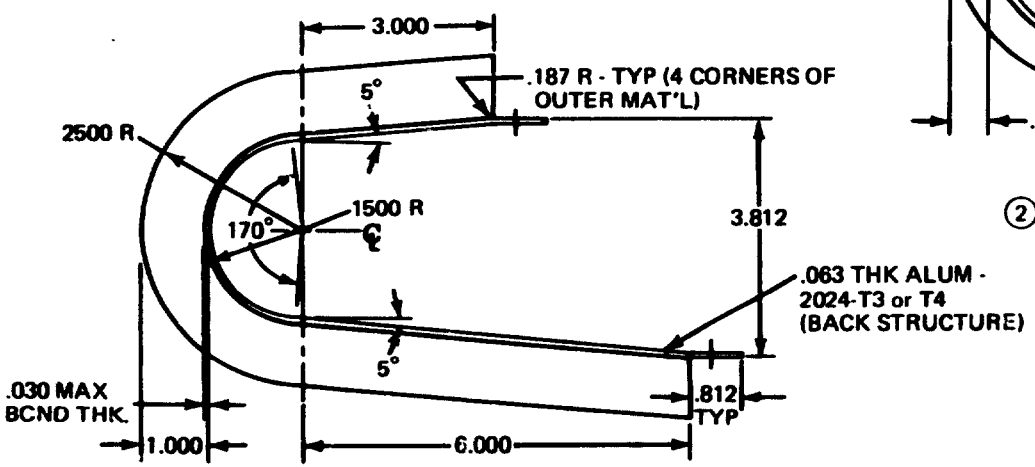

① MAT'L - 22 LBS/FT³ OR 33 LBS/FT³ - NOMINAL DENSITY RANGE

Figure 48 Leading Edge Test Model

relative thermal efficiencies could be determined.

The leading edge specimen was exposed to the various environments shown in figure 45. The different conditions required that the tests be conducted at various facilities. The test conditions indicated in table 13 are representative of the flight environment and comparisons between test and flight as shown there and in Sections 5.3.3 to 5.3.12.

b) Flexure tests

In order to determine the virgin and char flexural properties a series of beam tests were conducted. The tests utilized the specimen shown in figure 49 and were instrumented with thermocouples and strain gages to aid in determining thermal efficiency and strain limits (note that for all materials the weight per unit area was kept constant). Two sets of tests were run as shown in table 13. The reentry heating tests were conducted in the Avco ROVERS facility while all structural tests were conducted at Grumman.

In general, the simulation of the flight conditions was good, with the exception of the enthalpy simulation in the entry heating test. This was unfortunate and may well have penalized the epoxy materials in comparison to the elastomers.

A considerable amount of data worth studying was accumulated. A few significant samples are: the effectiveness* and soak-out temperatures in the entry test (figure 30), a summary of the ablation history (figure 51), the shape of two models after the entry test (figure 52), and the roughness values measured after the shock test (figure 53).

A brief statement on the results of the tests are collected in table 13. It

* Defined as $\dot{q}_{HW}\Delta\tau/(W/A)$, where $\dot{q}_{HW}$ is the stagnation-point hot-wall heating rate, $\Delta\tau$ the time for the stagnation point backface temperature to rise to 200°F and W/A the ablator weight per unit area.

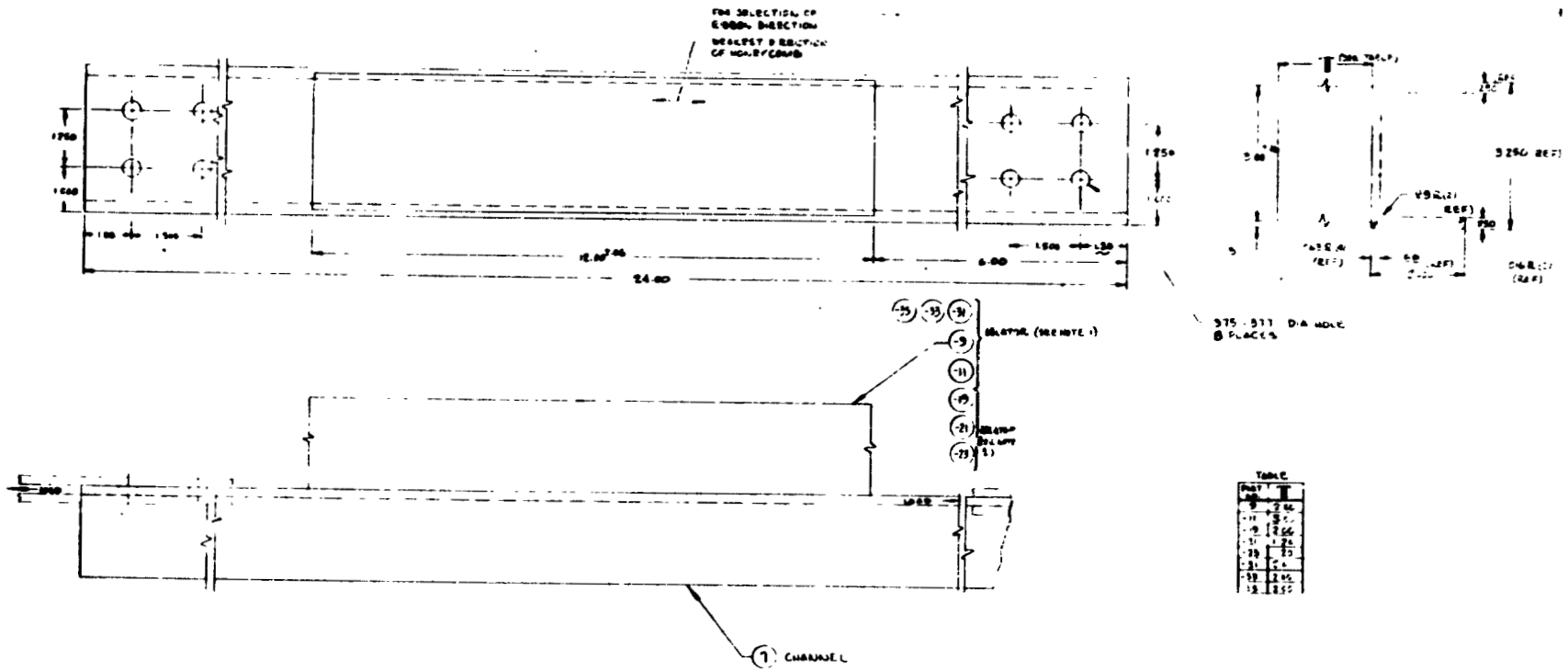

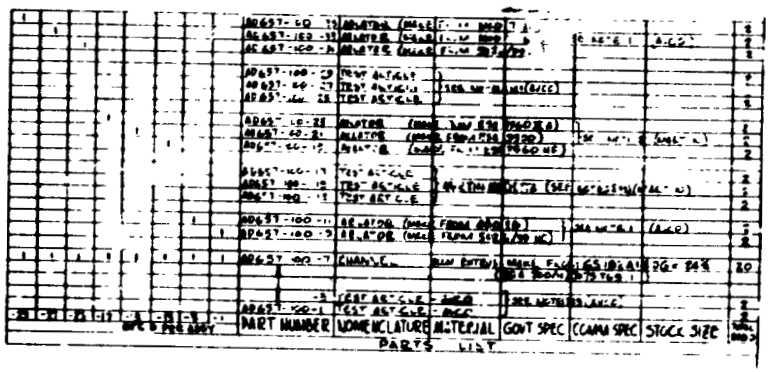

PARTS LIST

PART NUMBER	NOMENCLATURE	MATERIAL	GOVT SPEC	COMM SPEC	STOCK SIZE
AD657-100-1	TEST ARTICLE	INCO			
AD657-100	CHANNEL				

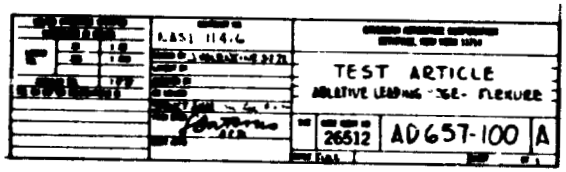

Figure 49 Flexure Tests Models.

COMPARISON OF INSULATION EFFICIENCIES

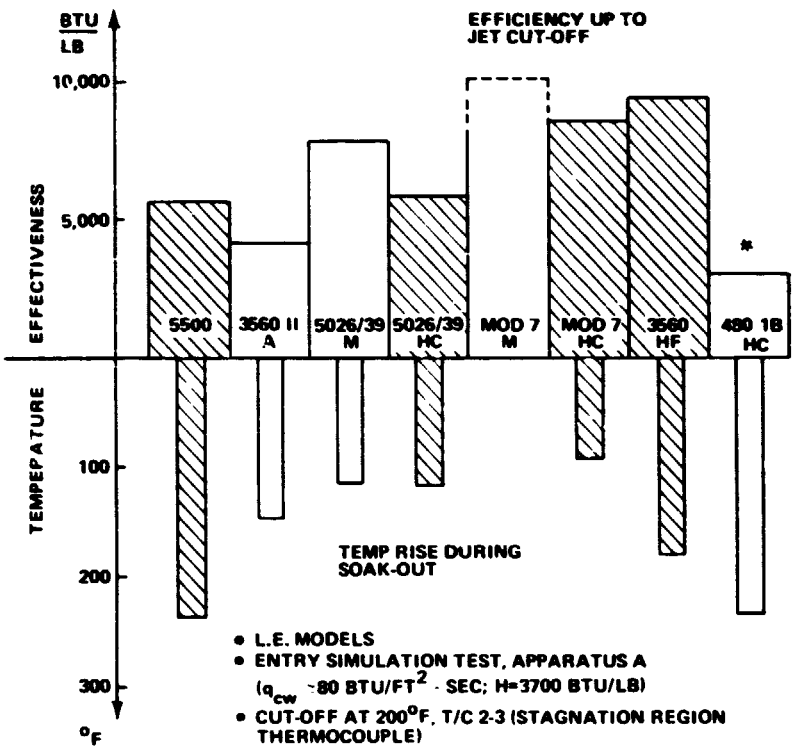

*NOT SCALED BY WEIGHT

Figure 50 Comparison of Insulation Efficiency of Candidate Ablators

L.E. MODELS: ABLATION HISTORY AT STAGNATION POINT

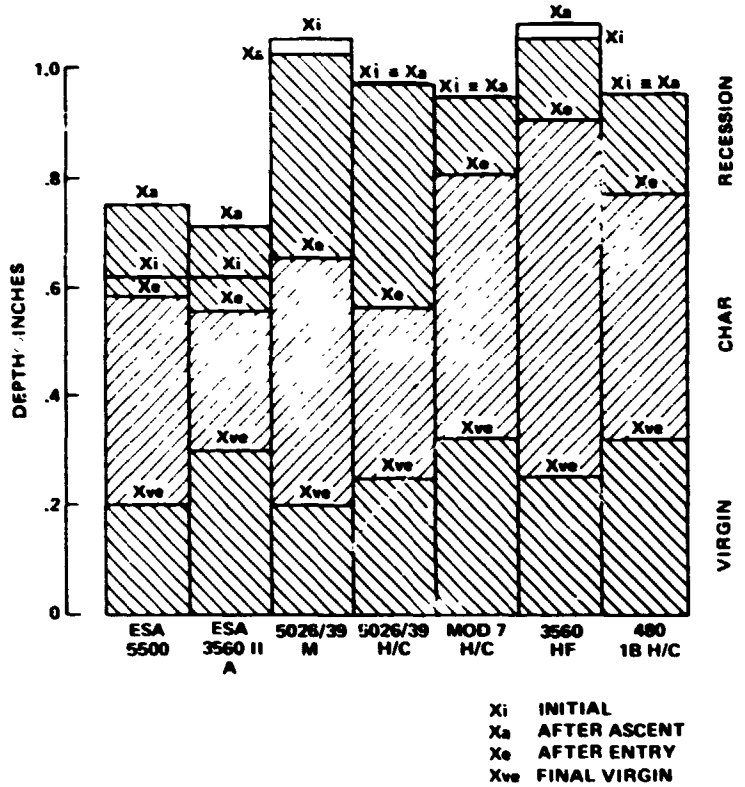

Figure 51 Comparison of Ablation Histories of Candidate Materials

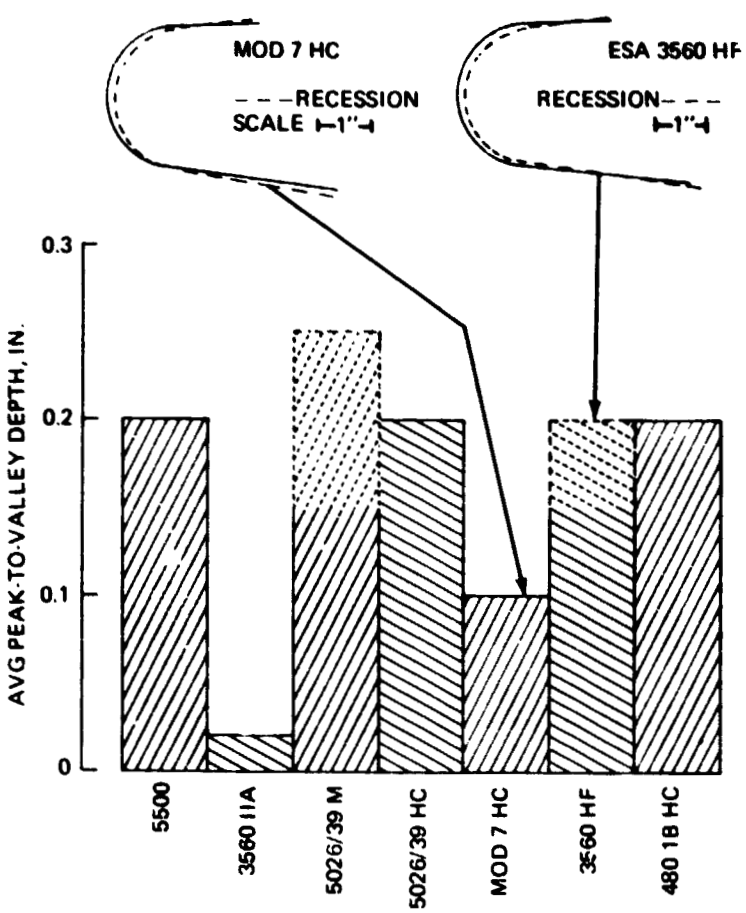

Figure 52 Typical Shape Change & Roughness of L.E. Models

is obvious that many tests went uneventful, without visible effects. One important lesson learned from the uneventful tests is that the testing sequence can be simplified to the first three steps of ascent heating, cold soak, and entry, eliminating both vibration and shock tests and flexure tests. Even though at the end of the vibration test one model, the ESA 3560 IIA, lost the entire cap down to the char-virgin interface, clear signs of a continuous crack at the char-virgin interface were visible before the test. Moreover, the flexure tests on the charred models failed to affect the delamination cracks that had occurred during charring of the Mod 7 M material.

More details on each of the tests are given below in Sections 5.3.3 to 5.3.12. The full documentation on test rationale, model design and test data report is given in the Package.

5.3.3 Ascent Heating of L.E. Models

The first test to be run in the leading edge models was the ascent heating simulation in the Avco ROVERS facility. NASA prescribed for simulation the flight environment corresponding to the Grumman 473 orbiter and a NAR trajectory, (see table 14a).

For this series of tests the ROVERS Arc made use of the square nozzle configuration using a two-dimensional nozzle of dimensions 4.5 by 4.5 inches. The environment shown in table 14b. was measured using a water-cooled copper calorimeter model of the same size and shape as the test models. Figure 53 shows the location of the various calorimeter plugs. The plugs designated 2-3,-5,-6, -7, and -8 are all located in the center line plane of the model. Plugs designated -1 and -4 were located two inches on either side of plug 2-3. All models were subjected to this environment for a total of 560 seconds. The extrapolated stagnation point heat flux rate was 9.5 Btu/ft^2-sec.

Table 14a Ascent Environments

Flight vs ROVERS Arcjet on L.E. Models			
	Dominant	GAC 473 Vehicle & NAR Traj	ROVERS Facility
$\dot{q}_{cw}$ Max BTU/ft^2 sec	14	9.5	9.5
P_{Max} at q_{cw} atm	5×10^{-4}	(*)	7.2×10^{-4}
H @ $\dot{q}_{cw}$ BTU/lb$_F$	10,200	↓	11,200
τ Max lb$_F$/ft^2	1.5	↓	(**)
q BTU/ft^2	6700	5300	5300
Time at q_{cw} sec	250	250	–
Test Time sec	–	–	560
(dP/dS) at $\dot{q}_{cw}$ atm/in.	0.44×10^{-4}		0.7×10^{-4}

(*) Not Calculated
(**) Not Estimated

Table 14b ROVERS Arc Test Environment

Station No.	Calorimeter No.	Location From Stagnation Point Inches	Cold Wall Heat Flux BTU/ft^2-sec
S5	1	-0 8722	6.13
S5	2 3	-0.8722	8.39
S5	4	-0.8722	7.03
S4	5	+1.091	7.53
S6	6	-2.835	1.53
S7	7	+5.207	0.54
S9	8	+6.707	0.29

Gas Enthalpy	– 11200 BTU/lb
Plenum Pressure	– 23.0 Torr
Pressure – Station 5	– 0.30 Torr
Pressure – Stagnation Point	– 0.55 Torr
Calorimeter Angle of Attack	– 0 degrees
Model Angle of Attack	– 5 degrees

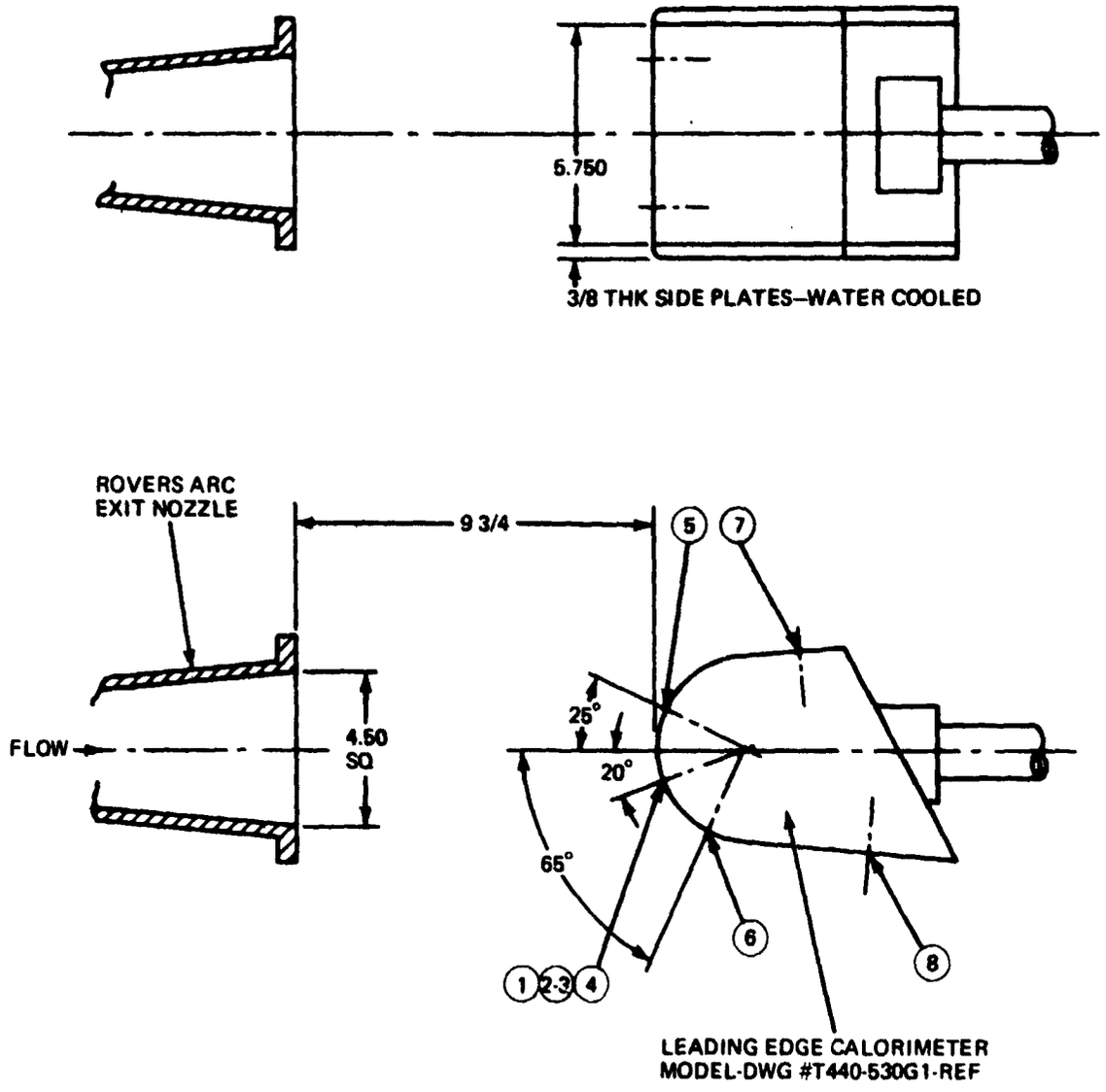

Figure 53 Leading Edge Calorimeter Configuration - Rovers ARC Facility

For each material tested the following data were noted:

a) Physical ablation characteristics.

b) Surface temperature response (stagnation point of model).

c) Char layer integrity.

d) Shape change (ten stations in each of five planes).

e) Backface temperature response (stations 1, 2-3, 4, and 5).

To obtain the above data, various instruments and fixtures were used. Table 15 presents a summary of the data.* Table 16a presents appropriate comments on the post-test appearance of each of the materials. Pictures of the materials after the test are given in figure 54.

In general, each sample discolored in the stagnation region where the heating was greatest. During each test, no obvious adverse ablative characteristic was noted by test observers. In all cases, sample decomposition products were generated which deposited on the cooler downstream surfaces. Surface temperature measurements were continually recorded and showed no discontinuities or abnormal behavior. Four rear surface temperatures (chromel alumel thermocouple peened into the 0.060 inch thick aluminum rear structure) were recorded (stations 1, 2-3, 4, and 5). Table 15 reports only the 2-3 station temperature rise for the 560 second time period. The other remaining thermocouples in the model showed a similar temperature rise.

* It is noted, that because of a machining error in the sample holder plate all test models were tested at an angle of attack of 5 degrees rather than zero degrees as the calorimeter model.

Table 15 Ascent Heating Test Summary for L.E. Models

Ascent Heating

Rovers Arc { $q_s \sim 9.5$ BTU/ft^2; $H_s \sim 11500$ BTU/lb; Test Time = 560 sec

Material	Density lb/ft^3	Material Thickness Inches	Peak Stag. Pt. Brightness Temp, ^{o}R	Sample Mass Loss, GMS	Rear Surface Temp Rise, ^{o}F Stag. Pt.	Station 2-3 Dimensional Change, Inches
Avco 480-18 H/C	21	0.949	1770	9.7	139	-0.006
Avco MOD 7 H/C	34	0.942	1734	22.9	60	+0.014
Martin 101-9B (ESA 3560 HF)	32	1.048	1740	24.4	46	+0.025
Avco 5026-39 H/C	35	0.970	1860	43.8	58	-0.004
Avco 5026-39 M	38	1.052	1853	43.9	50	-0.29
Martin 101-3A (ESA 3560 IIA)	56	0.618	1686	19.5	149	+0.090
Martin 101-1A (ESA 5500)	56	0.617	1734	17.7	166	+0.131

Table 16a Comments on General Appearance of the L.E. Models After Ascent Heating

Model No.	Comments
Avco 480-1B H/C	Darkened stagnation region becoming lighter in color as one moves down stream. Char appears solid with a few small areas where H/C separated slightly from cell material.
Avco MOD7 H/C	Whitish coating on stagnation region not too stable as it can be blown off
Martin [101-9B] ESA 3560 HF	Gray-whitish deposit on stagnation region. Some separation of H/C from cell material. Char appears stable. Some flaking occurred after the test and during handling.
Avco 5026-39 H/C	Dark charred heating pattern in stagnation region of model. Cell material in stagnation region receded below the H/C material (0.015"). Surface had a roughened texture. H/C material separated from cell material in stagnation region
Avco 5026-39 Molded	Dark charred heating pattern in stagnation region. Numerous cracks present in stagnation region running parallel with flow. Crack dimensions were about 1/16 x 1/8" wide by 2 inches long. Crack phenomenon decreased as one progressed downstream of model.
Martin [101-3A] ESA 3560 HA	Crusty surface layer with bubbles generated at the 45 degree stations on both the leeward and windward sides of the model. It appeared that delaminated sections were present as evidenced by surface discontinuities at four locations. Char zone appear solid to touch.
Martin [101-1A] ESA 5500	Cell growth evidenced over entire stagnation region – decreased downstream of stagnation region. Char layer cracked in a few cells.

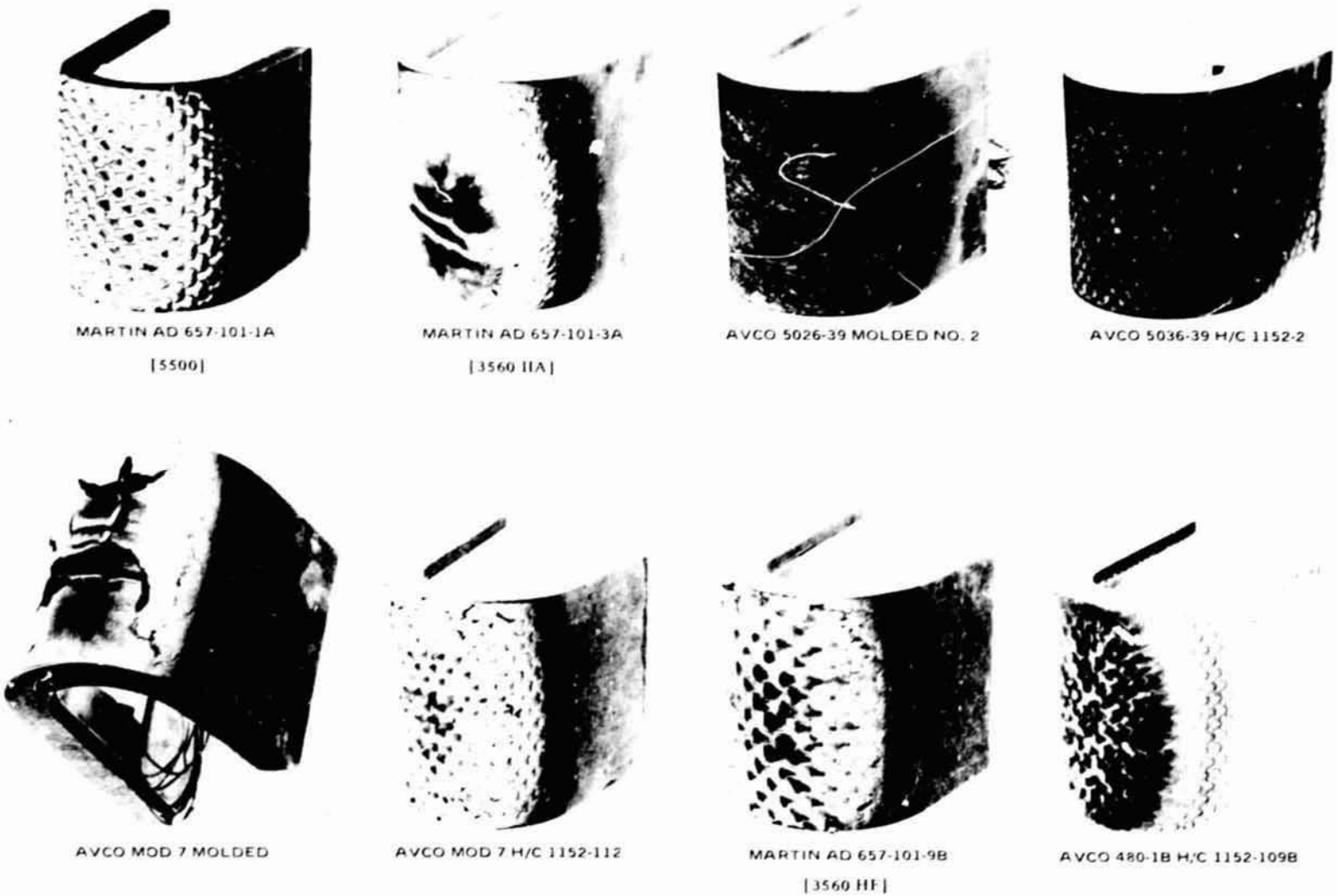

Figure 54. L.E. Models Appearance After Ascent Heating

5.3.4 Cold Soak of the L.E. Models

The test on the leading edge models called for a cold soak environment of two hours at a pressure of 10^{-7} atmospheres and a temperature of -200°F.

During the test it was found that the liquid nitrogen used to cool down the double walled 4' x 8' thermal-vacuum tank wall was leaking into the tank. After the target temperature was reached the liquid nitrogen input was stopped and the pressure dropped to its design value. Figure 55a shows the pressure/temperature values of the test during which the target conditions were met although not quite for the full two hours intended. Figure 55b shows the models in the chamber. Note that the models' ends are not tied, as the purpose of the tests was to investigate only the local compatibility of ablator and substructure.

Observations during the after tests of the models showed there were no apparent changes in either the ablator surface or to the ablator/substructure bond. Weights remained essentially unchanged. Appendix 3 gives the pertinent data on the test.

Although the cold soak duration during testing was not a full two hours it was decided not to run another cold soak test because 1) the conditions obtained were close to the target ones, and 2) prior tests on another set of L.E. models (Data Package) were cold soaked for seven days with no apparent change.

5.3.5 Entry Heating of the L.E. Models

The most important test to be conducted during the sequential series is the entry heating tests since it can determine 1) the effects of ascent heating on reentry performance 2) the thermal efficiency of the material and 3) the performance characteristics (including char stability) of the various materials under the most severe thermal environment. It is important to note that

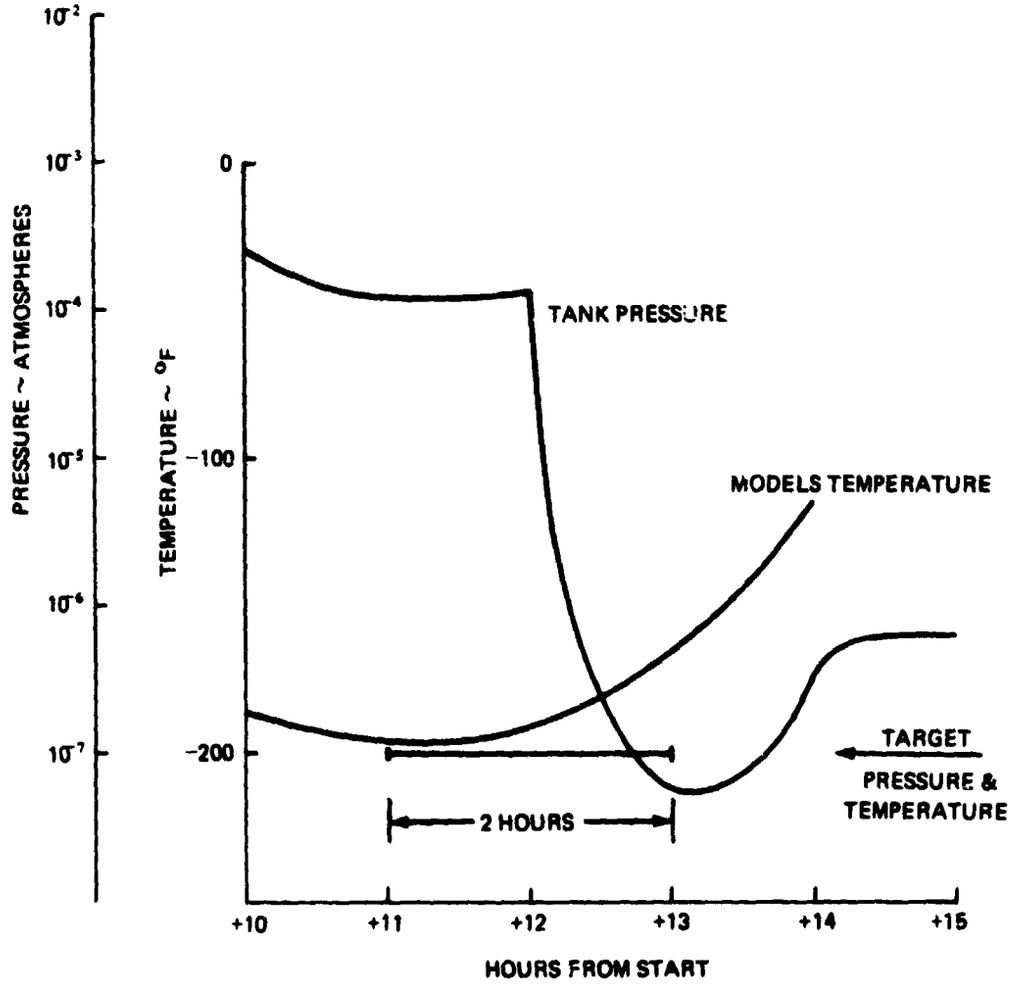

Figure 55a Environment Maintained During Cold Soak Test

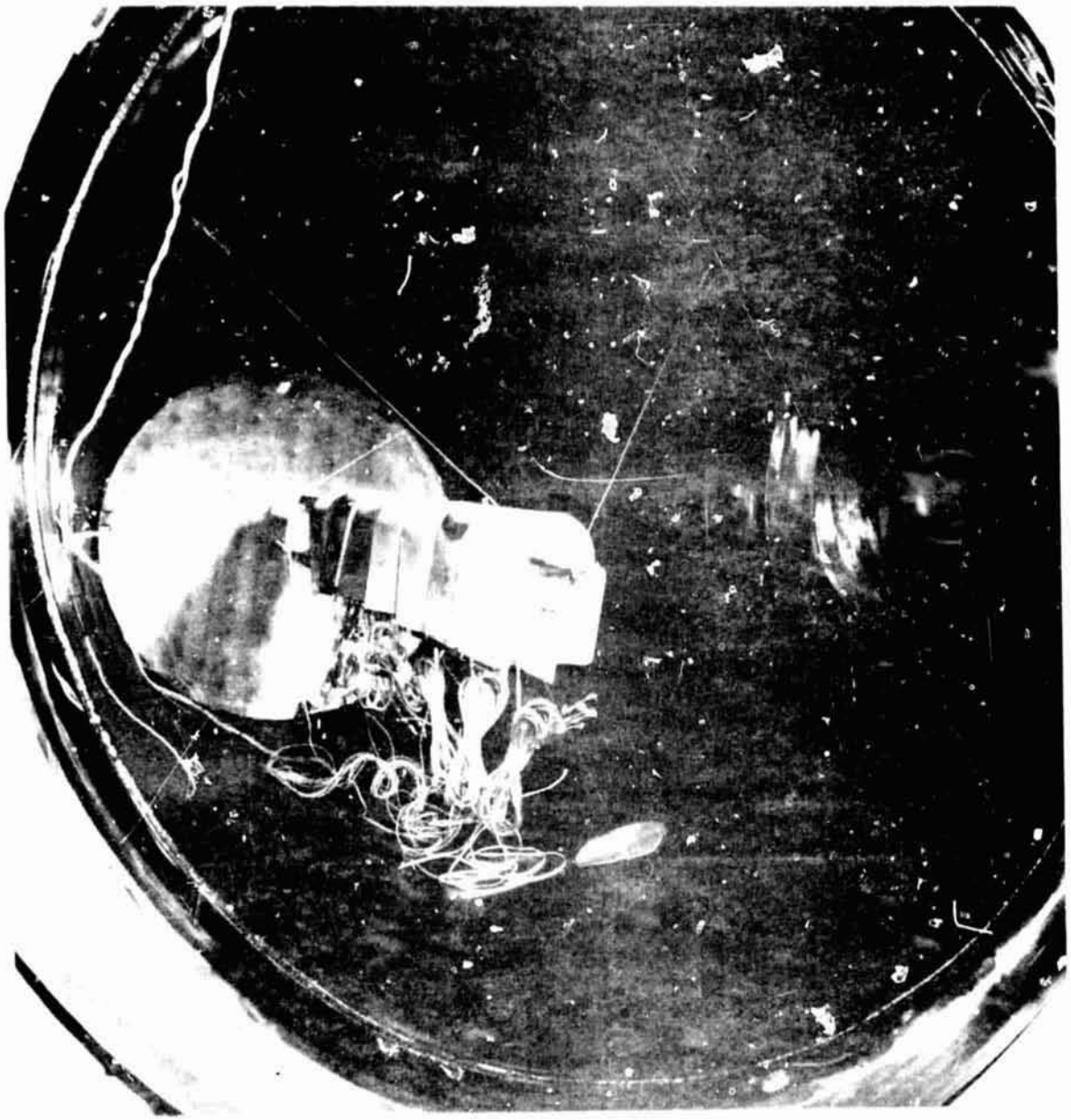

Figure 55b The L.E. Models in the Cold Soak Chamber

previously no significant data has been presented relative to ablator material performance in an entry environment on samples previously subjected to ascent and cold soak environments.

The reentry tests were conducted on the pre-conditioned leading edge specimen in the NASA/LRC Apparatus "A" Facility. The conditions selected for the test are shown in table 16b together with the comparative flight conditions. As can be seen the simulation is quite good except for the lower enthalpy and integrated heating experienced. Prior to testing the candidate materials, calibration runs were made using the leading edge calorimeter.

Table 17 summarizes the results of the reentry heating tests. The recession values represent an average near the stagnation point. Representative recession profiles are shown in figure 56, a to d for the ESA 3560 HF and Mod 7Hc; temperature histories at a typical location are shown in figure 57. Detailed weight, recession and thermocouple data are shown in the Data Package. Photographs of the specimen before and after test are provided in figure 58.

5.3.6 Vibration of L.E. Models

The vibration tests were conducted in the Thermo-acoustic Fatigue facility at NASA LRC. Figure 59 shows the acoustic levels attained in the facility at locations upstream, in front of and downstream the models respectively. Included in these plots are the target or flight acoustic levels which were exceeded in the test. During the test the surfaces of the seven ablative leading edge models were brought to 500°F via radiant lamps to complete the simulation of the flight conditions occurring in the latter part of entry. Figure 60

Table 16b Entry Flight vs Simulation Environment

	Flight (Dominant)		Test
	GAC Veh.	NAR C/D Orbiter	
$\dot{q}$ ~ BTU/ft^2 sec	70	60	80 (Coldwall) 60 (Hotwall)
P_{Max} ~ ATM	7×10^{-2}	*	7×10^{-2}
H ~ BTU/lb	10,750		3700
Q ~ BTU/ft^2	64,200		5400 → 23,000
Time @ $\dot{q}$ ~ sec	800		68 → 309
$dP/_{ds}$ ~ ATM/$_{in}$	2.8×10^{-2}		2.8×10^{-2}

*Unavailable

Table 17 Entry Heating Test Summary for L.E. Models

Entry Heating
NASA Langley
Apparatus A
$\dot{q}_s \sim 70$ BTU/ft^2 sec
$H_s \sim 3700$ BTU/lb

Material	Density lb/ft^3	Material Thickness Inches	Test Time (Sec) To Reach 200°F At Station 2-3	Average Stag. Region Ablation $\frac{(\Delta S_4 + \Delta S_5)}{2}$ Inches	Total Mass Loss GMS	$\frac{\Delta M}{\text{Time}}$ gm/sec	Remarks
Avco 480-1B H/C	21	0.949	68	0.111	33.2	0.488	During start of test (10 sec) melting and flow erosion started at both corners of model which progressed rapidly t. wards center run-cut at 68 sec. Stag. region eroded-large areas adjacent to water-cooled side plate receded in a non-uniform manner.
Avco MOD 7 H/C	34	0.942	261	0.085	90.7	0.348	No unusual surface effects except for minor surface roughening and particle removal. Stag. region was glassy silver white going to black on both Leeward and Windward sides. Some glassy areas present. Cell material below H/C .050" only in stag. region.
Martin 101-9B (ESA 3560 HF)	32	1.048	309	0.146	102.9	0.333	Surface roug ened-Gouging in spots-Very rough surface in Stag. region-Two holes present on 450 windward stations-1/8 dia x 3/8 deep-Cell material appears to be raised on both Lee and Windward sides.
Avco 5026-39 H/C	35	0.970	195	0 225	152.0	0.779	Silica flow evident over surface of stag region-recession in corners adjacent to side plates twice that at center-char layer hard and black on Lee and Windward sides-silica rivets deposited on 450 locations.
Avco 5026-39 M	38	1.052	283	0.310	199.1	0.704	Erosion between side plates and material-Stag region glassy-channeling occurred where cracks from ascent heating existed. Accumulation of silica deposits at 450 location.
Martin 101-3A (ESA 3560 IIA)	56	0.618	153	0.112	87.1	0.570	Erosion near side plates-Some shrinkage noted at stag line-Sample cracked badly over 2/3 of surface area.
Martin 101-1A (ESA 5500)	56	0.617	205	0.018	83.5	0.407	Loss of material in some cells-Material expanded in some cells and produced whitish color which was very brittle and fell off easily from both sides. It appeared that a crack went around the entire specimen at char/virgin interface.

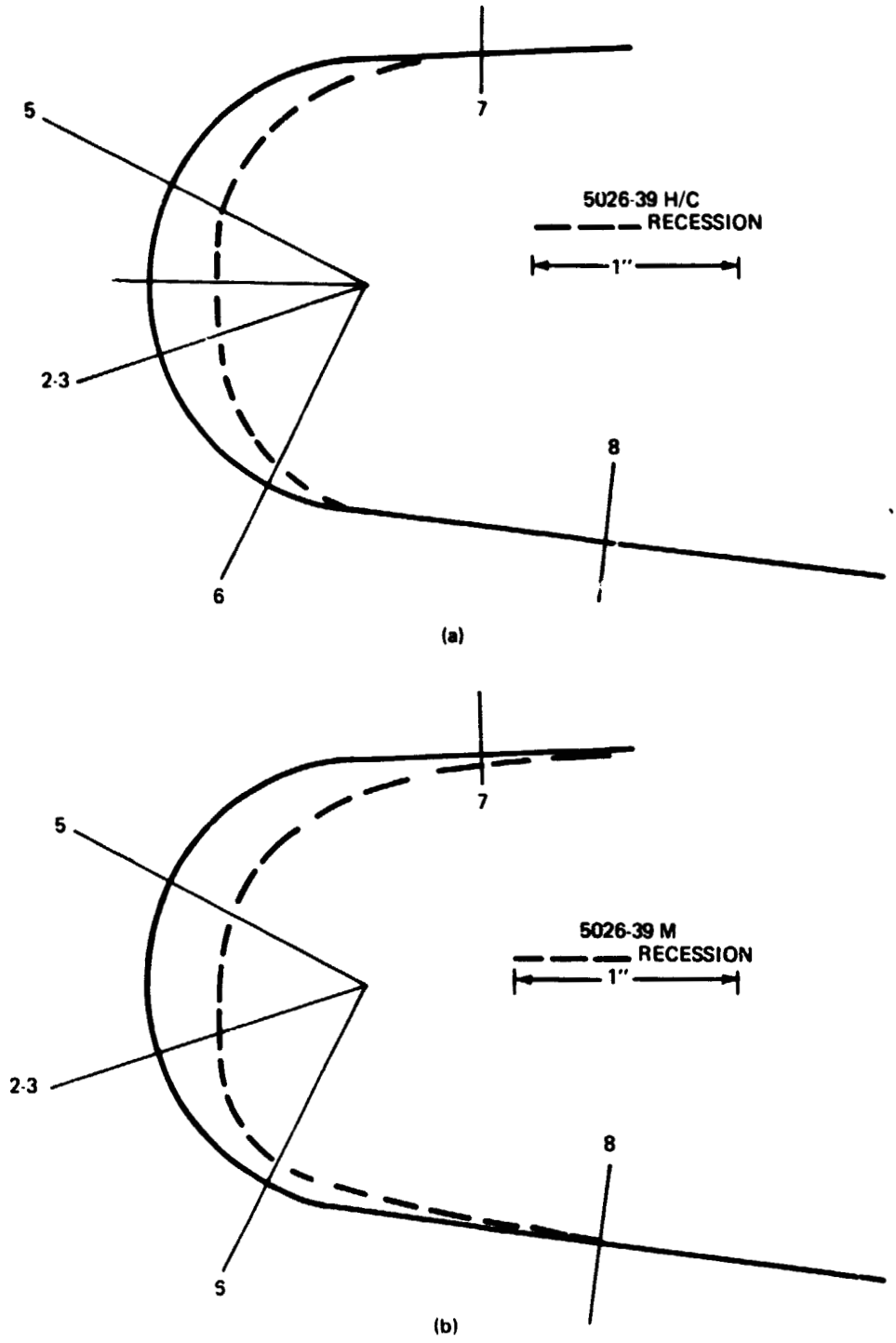

Figure 56 Shape Change of Leading Edge Models After Entry Heating

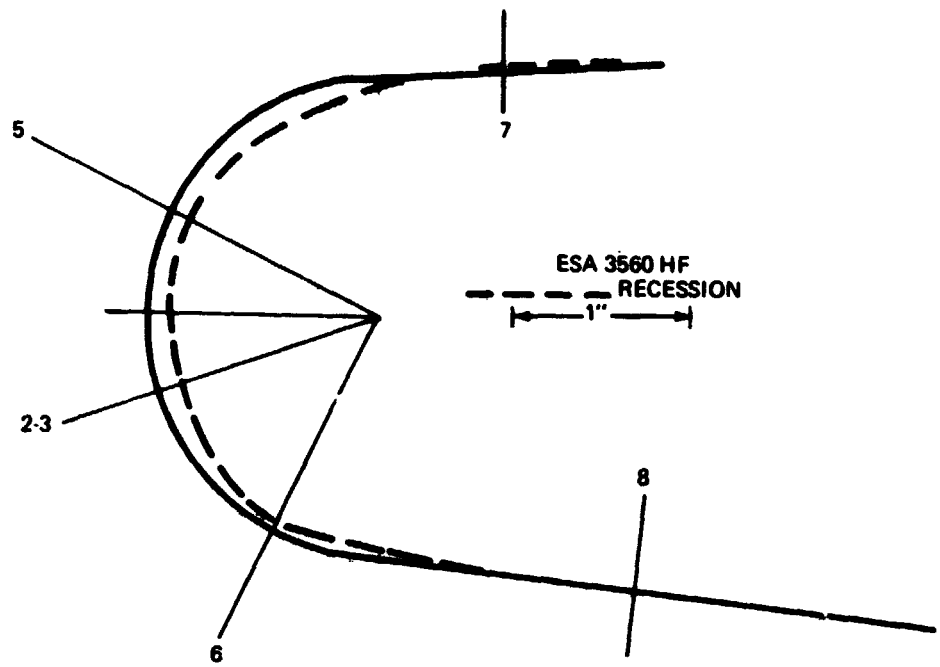

(c)

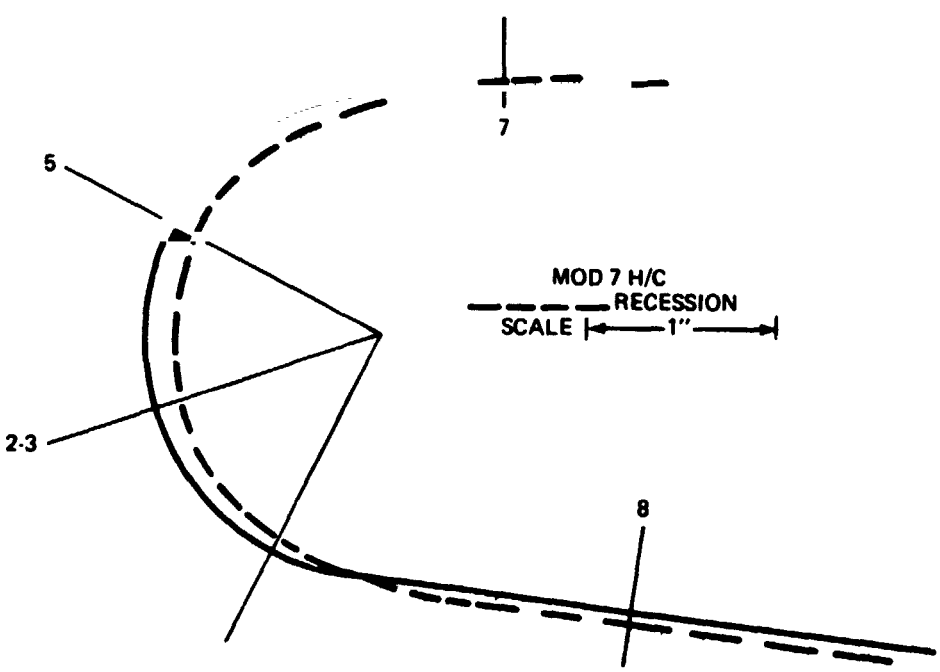

(d)

Figure 56 (Cont.) Shape Change of Leading Edge Models After Entry Heating

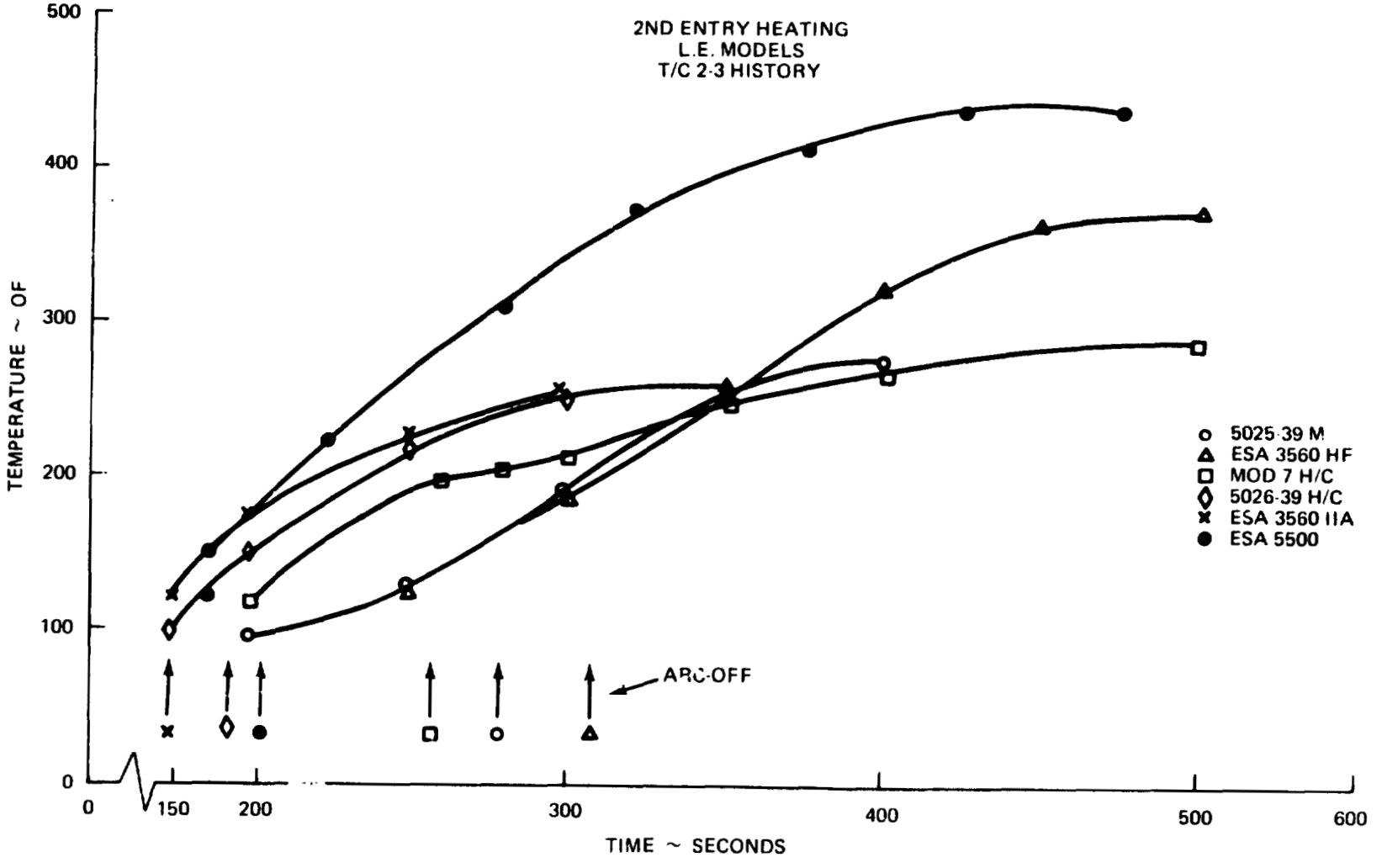

Figure 57 Stagnation Point Backface Temperature History During Entry Heating of L. E. Models

Figure 58 L.E. Models Appearance before and after Entry Heating
(Materials are: 5026/39HC, Mod 7 Hc and 3560 HF)

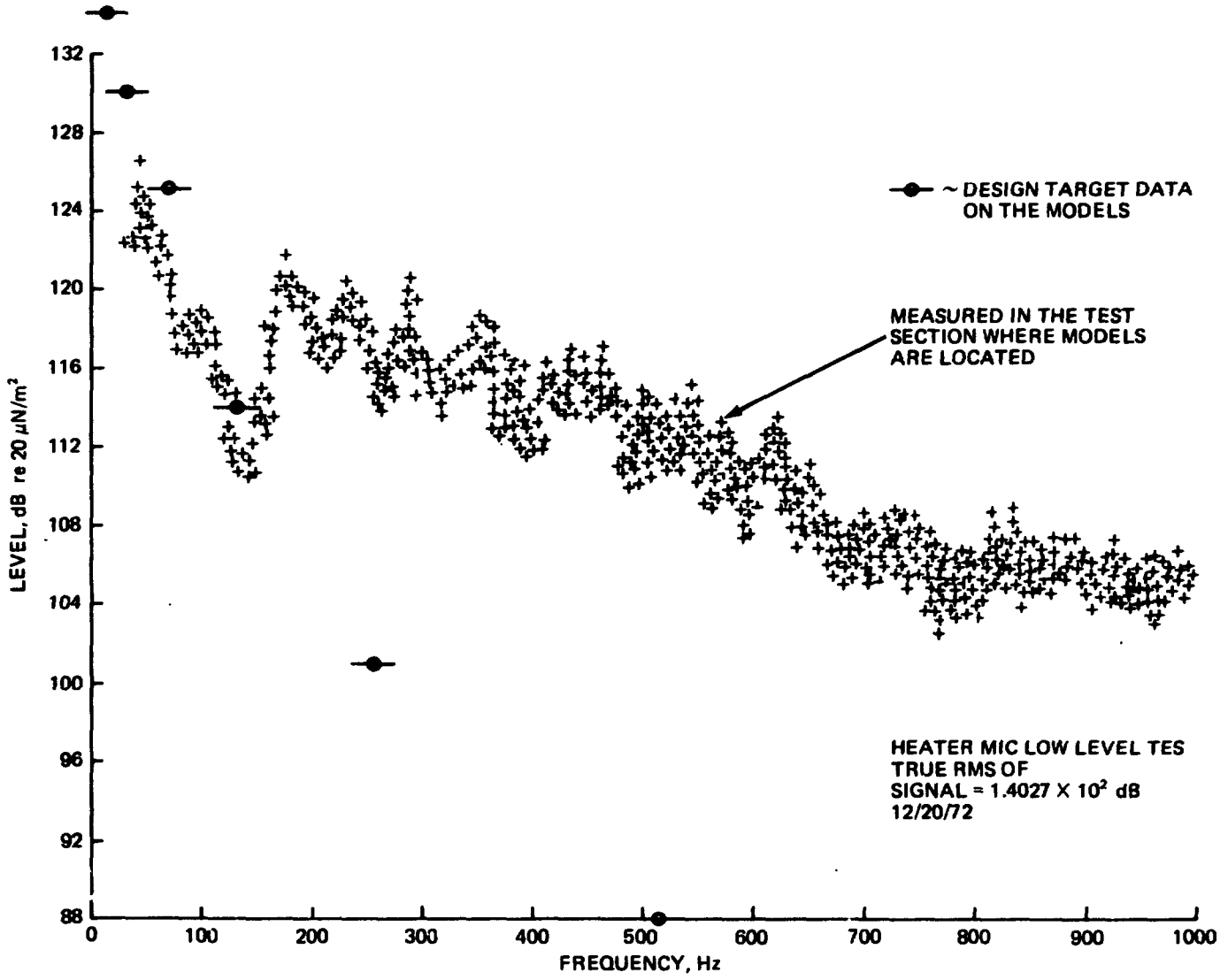

Figure 59 Comparison Flight Vs Test Vibration Environment on L.E. Models

and 61 give an idea of the installation of the models in the facility.

An examination of the models immediately after testing showed that none appeared affected by the thermal-acoustic test. Later upon removal from the facility, one model, the ESA 3560 IIA material showed that separation had developed at the char-virgin interface: the entire stagnation region cap came loose. The loosened cap was about .25 inches thick and covered approximately $\pm 30^{\circ}$ of the stagnation area.

5.3.7 Acceleration Tests of L.E. Models

After the thermal-acoustic tests the seven L.E. models were subjected to acceleration shock tests at Grumman simulating the landing conditions for the orbiter wing.

The test set-up is shown schematically in figure 62. Each specimen was subjected to 2 seconds of 17 Hz sinusoidal oscillation ±11 g's in amplitude twice in each of three axis. The order of the tests in each axis was numbered in the following:

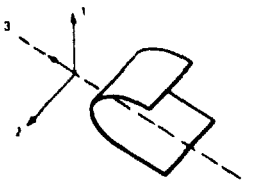

The installation of the models is shown in figures 63 and 64.

Other than a few small particles of charred ablator flying off during the tests, the L.E. models were unaffected in appearance or in weight.

5.3.8 Cutting of L.E. Models

After the L.E. models were tested under simulated orbiter shuttle flight conditions (ascent - cold soak - entry - thermal vibration-shock), the models were cut along the centerline normal to the L.E. to determine the depth of char and virgin material remaining. The models were cut through both ablator

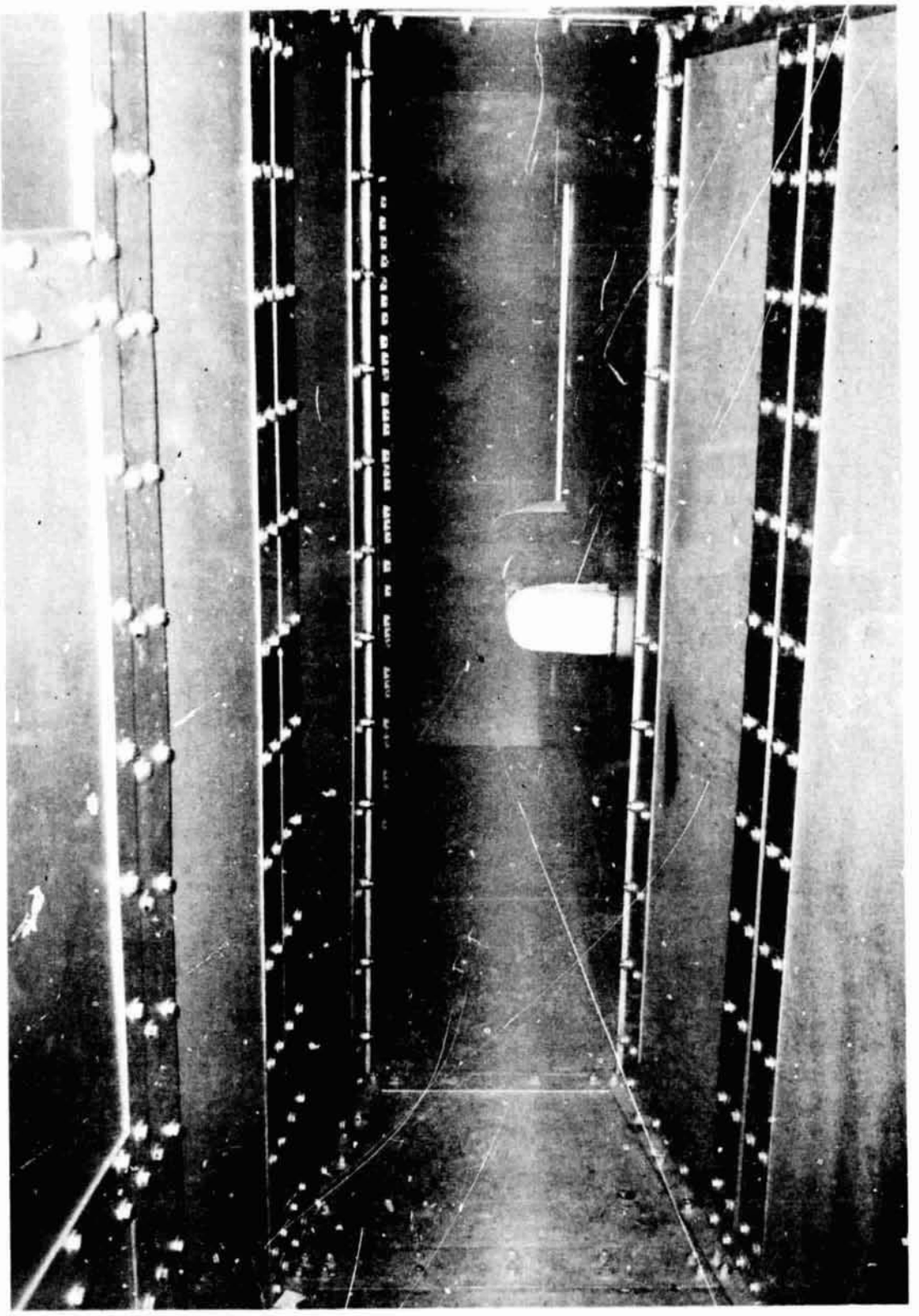

Figure 60 Vibration Test on the L.E. Models - the Models installed in the Thermo - acoustic Fatigue Facility

Figure 61 Vibration Test on the L.E. Models - Detail of the Models Installation

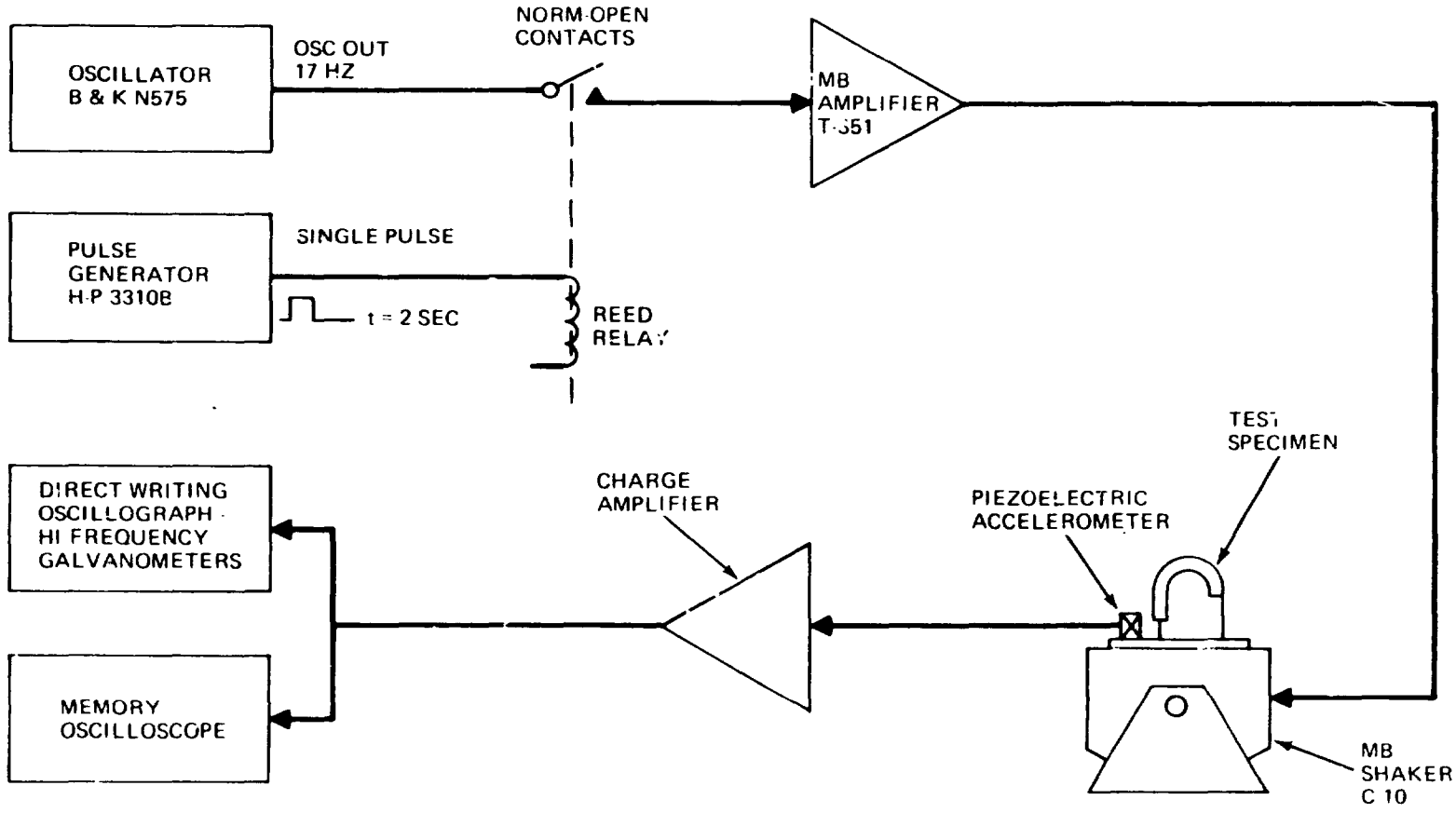

Figure 62 Block Diagram - Shock Test Set-Up for L E Models

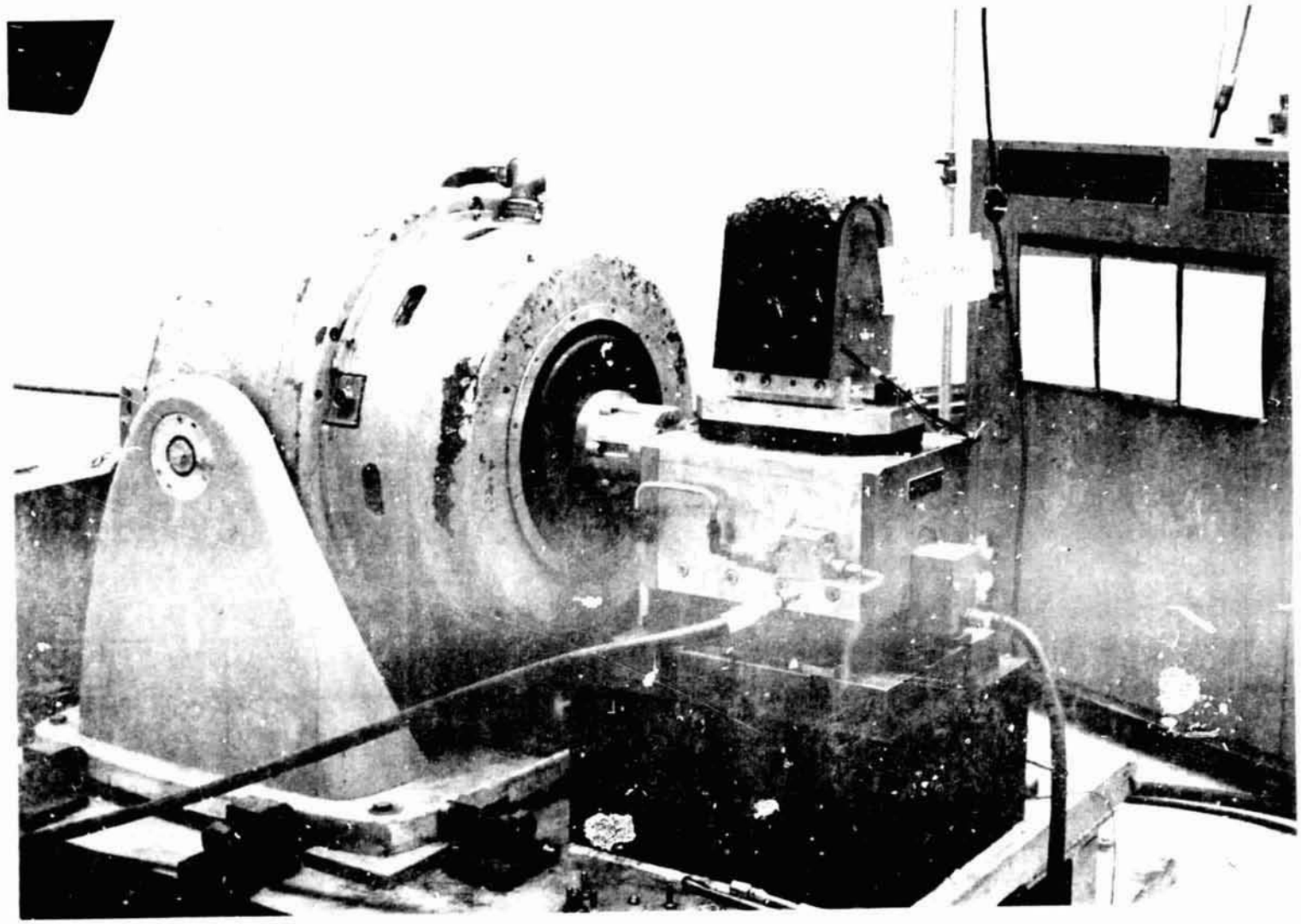

Figure 63 Set-Up for Acceleration Tests on the L.E. Models Acceleration in the Spanwise Direction

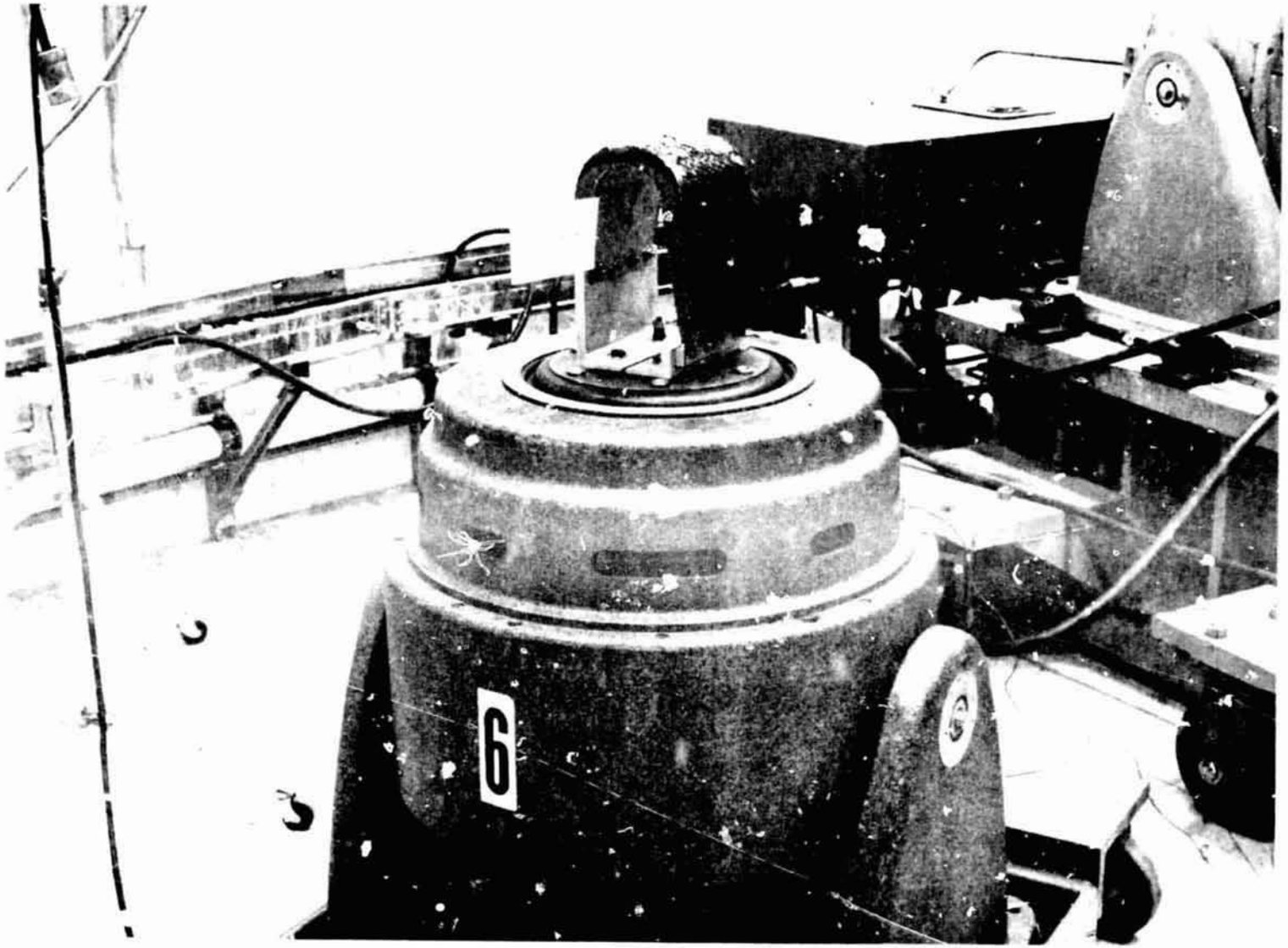

Figure 64 Set-Up for Acceleration Test on the L.E. Models - Acceleration in the Chord-wise Direction

and aluminum substructure with a diamond edged abrasive saw. Some models were repeatedly cut to examine the spanwise appearance of the char, of the Hc cells, etc.

Figure 51 gives a bar-graph history of the changes in depth of each material after ascent and entry and the final 'cut' of char and virgin material remaining.

Table 18 gives some observations on the fabrication, char layer, the char-virgin interface and the bond along the centerline cut of each L.E. model.

5.3.9 Flexure of Virgin Strips

The purpose of these tests was to examine the ablators behavior under the tensile strains induced by the deformations of the substructures. The substructure strains in flight had to be estimated at this stage as the substructure design was not yet available.

Figure 65 gives a comparison between the flight bondline tensile strains and those induced in the models. The model was somewhat unusual in that a strip of ablator was bonded on a channel beam which was pulled off the neutral plane so as to induce bending moments and strains. Figure 66 gives an idea of the installation of the models in the Olsen Universal Testing Machine. A bare channel was also tested for reference.

The tests showed no visible effects on any of the ablators up to bondline strains (along the strip direction) of 0.003. The models were not taken to failure.

5.3.10 Charring of Strips

In order to evaluate the strength of the char typical of that expected at low altitudes before landing it was first necessary to subject a set of flexural beams to a reentry heating environment. It was determined that satisfactory

Table 18 Observations of Cut L.E. Sections

Material	Bond	Fabrication	Char	Interface
Avco 480 18 H/C	Good	Voids ~ Many, Mostly at Bondline	– Stable ~ Random Cracks – Some H/C Cell Walls Gone	– Wavy (Non Homogeneous) Contour – Stable ~ Whitish
Avco MOD 7 H/C	Good	Voids ~ At Bondline At C/L and ¼ cuts	–Stable – A few Cracks	– Smooth (Homogeneous) Contour – Stable, Whitish
MMC 3560 HF	Good	No Voids	– Brittle – Many Cracks, Blowout Area Has Cavity 1/2 in Deep	– Smooth Contour – Weak, Light Grey
Avco 5026-39 H/C	Good	No Voids	– Brittle at Stag. Pt. – Small Random Cracks	– Stable, No Zone Apparent – Color Not Distinct From Char – Slightly Uneven Contour @ S.P.
Avco 5026-39 M	Good	No Voids	– Brittle – Many Cracks – Some Propagate Into Virgin Layer	– Stable, Darker Than Char – Uneven Contour @ S.P. – No Separation
MMC 3560 IIA	Good	No Voids	– Nose Cap Separated – Remaining Char Brittle	– Exposed S.P. is Like Grey Felt – Sides: Grey, Separation Line Evident
MMC ESA 5500	Good	Several Pinhole Voids	– Brittle ~ A Few Cracks – Separation From H/C Cells	– Uniform Contour – No Color Distinction – Separation Evident

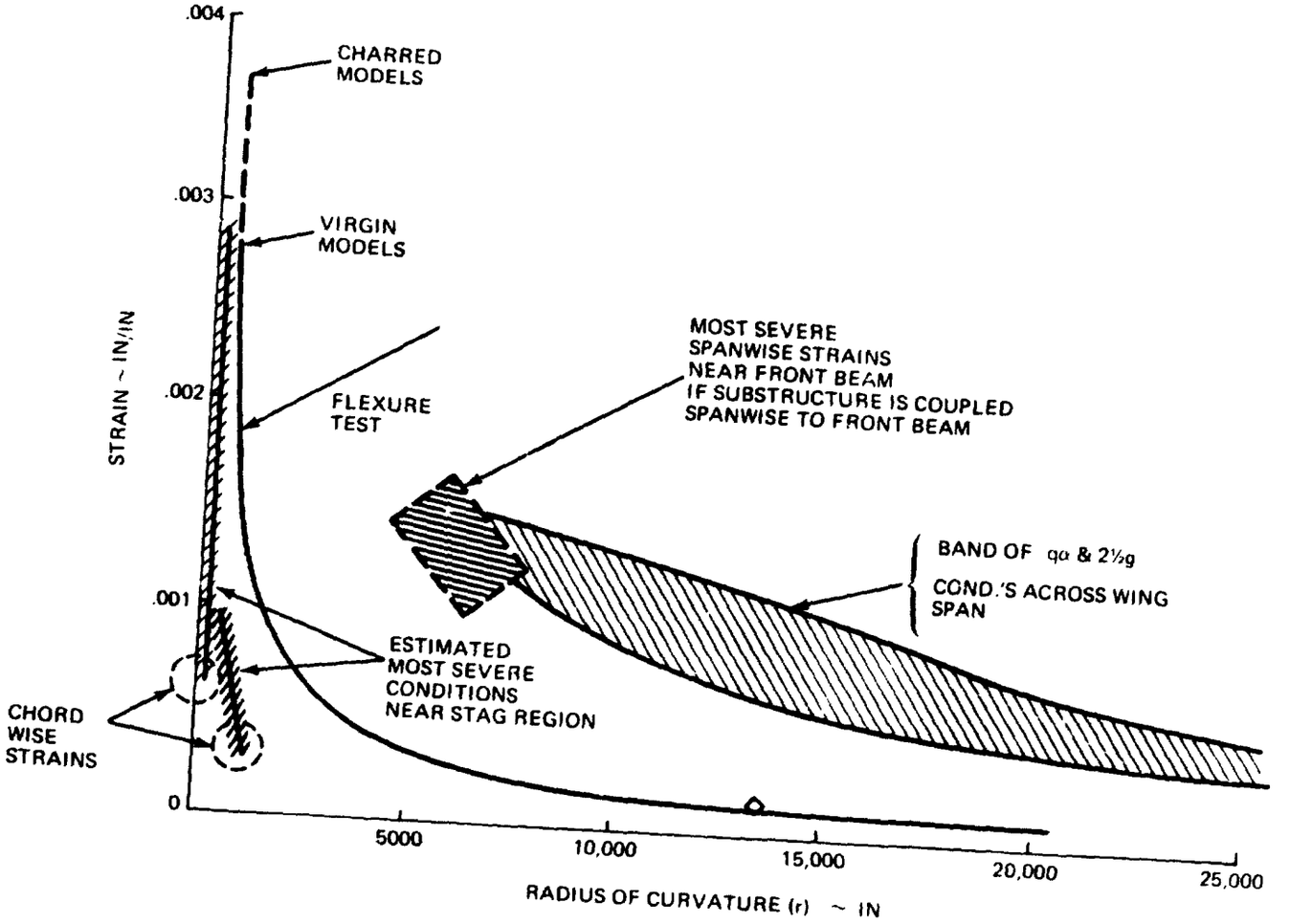

Figure 65 Flight (Estimated) Vs Test Tensile Strain Comparison

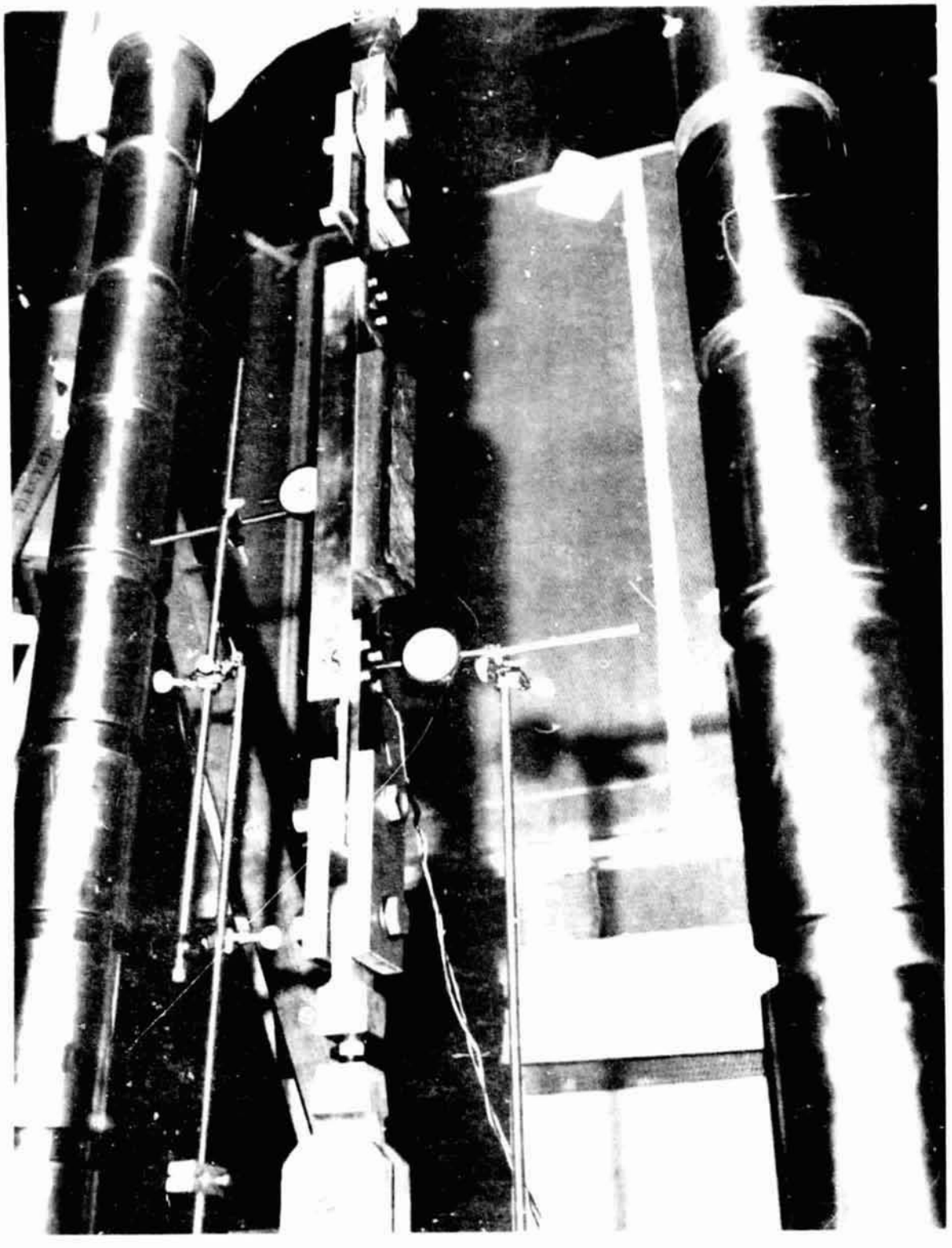

Figure 66 Strip Model mounted on the Olsen Machine

conditions which resulted in the formation of a realistic char could be obtained in the Avco ROVERS Arc facility, as shown in table 19.

The specimen was located at the exit of a nozzle as shown in figure 67. Thermocouples were placed in the aluminum channel at locations of 1.0 (T_1) and 6.0 (T_2) inches from the leading edge. In addition weight and thickness change measurements were made.

Table 20 summarizes the results of the test including weight loss, dimensional change data and general post test appearance description.

5.3.11 Flexure of Charred Strips

The purpose and procedure for these tests were as for the virgin strips.

There were no visible effects on all the ablators up to 0.0035 bondline strains. Close observation, during the test, of the surface or side cracks produced during charring indicated that the strain had no visible change on the crack dimensions or appearance up to $\epsilon = 0.0035$.

5.3.12 Cutting of Charred Strips

The observations collected after cutting the charred strips are summarized in table 21.

5.4 Evaluation Criteria

The first step in the evaluation of the candidate ablators consists of establishing the evaluation criteria which are of the usual two type, 'go/no-go' criteria (those which the material must meet to be applicable to the orbiter i.e.) and 'rating criteria' (those that will rank the ablators that are acceptable for this application). The evaluation criteria used here are presented in table 22, where the criteria are listed roughly in order of importance.

Table 19 Comparison, Flight vs Test, of Thermal Environment for Charring the Flexure Models

	Flight*	ROVERS Arc Facility
$\dot{q}_{cw}$ BTU/ft^2-sec	17 → 56	22**
Q_{cw} BTU/ft^2	16,000 → 52,000	22,000**
H BTU/lb$_f$	11,400	11,000
$\frac{dP}{ds}$ in the direction of the flow	Negligible	Small (not measured)
$\frac{Re}{L}$ ft^{-1}	1.9×10^4 (at 220 Kft)	1.6×10^4
Type of Flow	Laminar	(probably) transitional

*Windward flat region of L.E. during entry/no charring during ascent/dominant environment
**Average over model

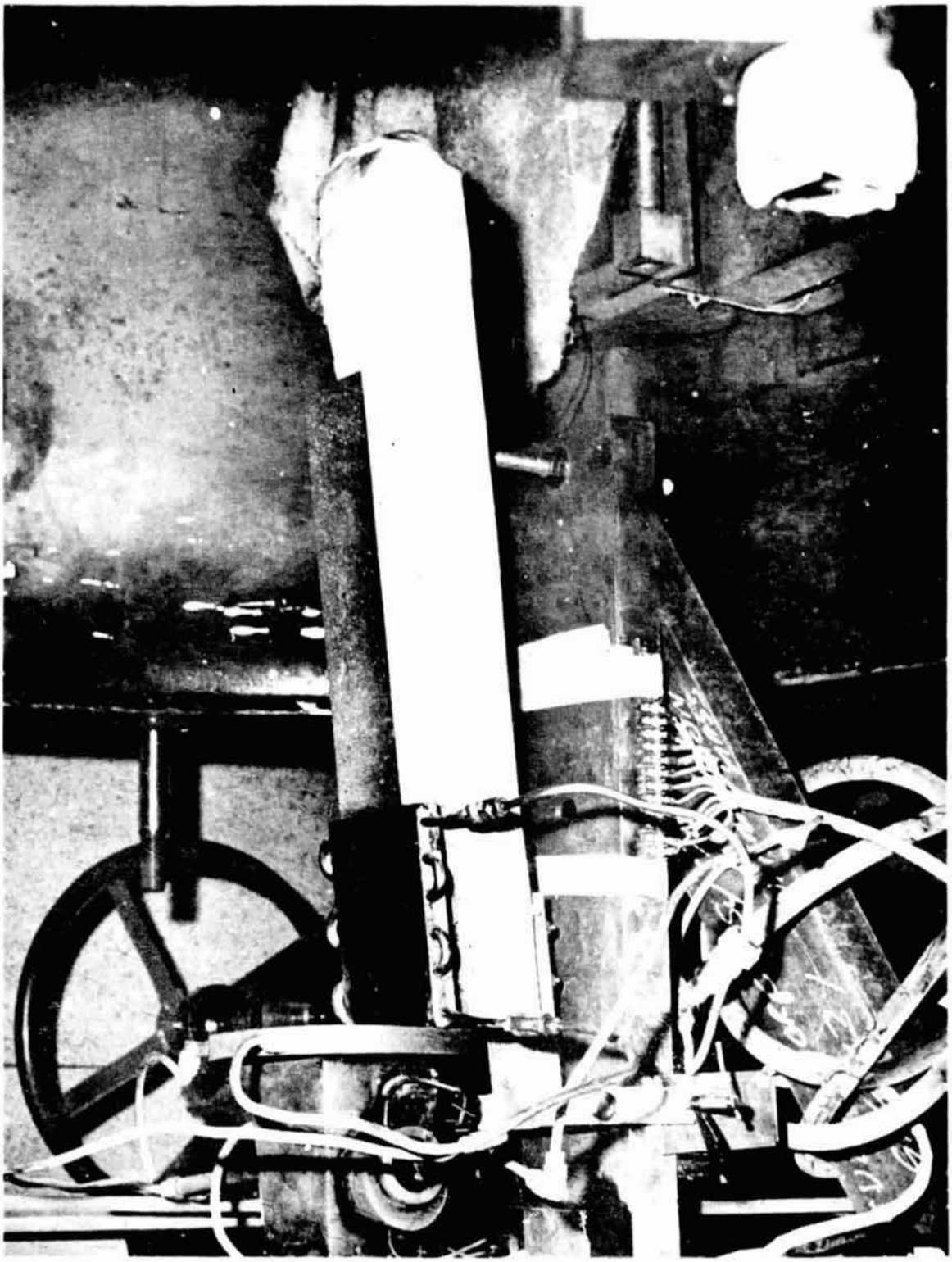

Figure 67 Charring of the Flexure Models – Installation in the ROVERS Arc-Jet Facility

Material	Test Time (sec)	Thickness (In.)*									Weight (Oz.)			Max Surf. Temp (°F)	Remarks
		Sta 1"			Sta 6"			Sta 11"			Initial	Final	ΔW		
		Pre	Post	ΔL	Pre	Post	ΔL	Pre	Post	ΔL					
Avco 480-1B H/C	1000	5.080	5.095	+.015	5.080	5.105	+.025	5.067	5.098	-.031	99	96	2	1800	Whitish streaks present at leading edge of model-turn black as one goes downstream-silica streaks protruded above surface - probably vented gasses at H/C interfaces and deposited downstream-slight separation of H/C cell material from H/C
Avco MOD 7 H/C	1000	4.292	4.332	+.040	4.304	4.296	-.008	4.314	4.343	+.029	83	83	3	1660	Char appeared smooth but numerous shocklets were present on the surface-color gray black to black-surface had numerous areas of silica mounds generated at Honeycomb walls-produced a roughened surface effect.
Martin (101-9B) 3560HF	1000	4.300	4.336	+.036	4.312	4.344	+.032	4.316	4.337	+.021	81	78	3	1735	Roughened, crusty solid surface-original color was brownish/red-transformed to blackish/whitish at L/E to black on rear half of model-silica globles present over heated surface-small crack in char layer in H/C cell.
Avco 5026-39 H/C	1000	4.295	4.236	-.059	4.300	4.236	-.064	4.300	4.247	-.053	82	77	5	1880	Uniform white crusty surface-H/C cell material depressed 1/8" - cracks in char.
Avco 5026-39M	1000	4.304	4.233	-.071	4.320	4.235	-.085	4.220	4.259	-.061	87	84	3	1770	Some erosion over 2" region of L/E numerous cracks in char and virgin material-char surface has a felt appearance.
Martin (101-3A) 3560IIA	794 206	3.510	3.679	+.169	3.500	3.689	+.189	3.510	3.663	-.153	83	80	3	1630	Numerous cracks, delaminations, craters, raised surface throughout.
Martin (101-1A) 5500	335 645	3.504	3.585	+.081	3.504	3.605	+.101	3.495	3.589	-.094	84	82	2	1800	Solid char, crack along length of sample - 1/8" to 1/2" crack laterally at midspan.
Avco MOD 7 Molded	1000	4.306	4.300	-.006	4.339	4.325	-.014	4.335	4.340	-.005	85	82	3	1650	Color of surface gray/black to black from leading to trailing edge-at 500 seconds numerous surface cracks had formed and generated numerous shocklets from front to rear of sample-Surface appeared to have lifted 3" from L/E silica around surface cracks - Char layer appears to have seperated from virgin material.

Table 20 Summary of Flexure Beam Arc Tests Rovers Facility

Table 21 Observations of Cut Charred Flexure Models

Material	Char Depth Calculated X_c* ~ In.	Measured Char Depth After Tests & Cutting			Remarks
		@ 1 In. From Front End	Mid Point	@ 1 In. From Back End	
Avco 480-1B H/C	1.051	.6 → .8	.6 → .9	.5 → .7	Large number of voids within HC cells
Avco MOD 7 H/C	0.502	.63	.65	.63	
MMC 3560 H/F	0.545	.52	.57	.60	
Avco 5026-39 H/C	.79	.52	.50	.46	
Avco 5026-39M	.502	ARTICLE DESTROYED IN FLEXURE TEST			
MMC 3560 IIA	.537	.5	.4	.42	
MMC ESA 5500	.442	.55	.52	.52	
Avco MOD 7M	.44	.49	.52	.48	

*From weight loss and dimensional change.

Note: Front end refers to edge nearest nozzle exit.

Table 22 Criteria for the Evaluation of the Candidate Ablators

'GO/NO-GO' CRITERIA	
• Reliability as TPS in screening tests	
• ~~"Acceptable" contamination of RSI*~~	
• Roughness after entry less than 0.4-0.5"	
• Recession after entry predictable (If char is rejected in large chunks, laminae or entire nose-cap segments, recession will be taken as non predictable)	
'RATING' CRITERIA	
• Costs (Dev and Prod)	- At nominal Traffic Model - Sensitivity to Traffic Model - Cost uncertainty and risks
• TPS Performance	- Bond & Cracks under strain - Insulation efficiency - Char stability and Cracks - Over-shoot capability
• ~~Effects on RSI weight and Cost~~ *	- ~~Contamination~~ - ~~Heating (transition shifting)~~*
• Degradation of aero charact	- Roughness - Recession
• Effects on Substructure Weight & Cost	- Strain Limit - Contrib to Stiffness
• Improvement potential of material • Production problems/overall risks	- Development status - Performance not yet tested, Etc.
*Lack of information	

'Reliability as TPS' means the confidence that the material inspires of being able to perform the TPS function; therefore it comprises such items as char integrity, char regularity in the cracks (if any) produced under flexure in the virgin state, etc. Naturally the fact that the judgement on the reliability is to be done from the results of the test performed, means that such factors as poor simulation or exclusion of a test (e.g., rain erosion) can influence the result.

Ideally, all the rating criteria should be reduced to either costs or imponderables. Weight, for example, should be reduced to cost via the usual notion of value of weight saving. Criteria such as degradation of aerodynamic characteristics caused by l.e. roughness should also be reduced to cost penalties, the procedure being often complicated and configuration-dependent, as indicated in Section 4. It turns out that such a systematic reduction to cost of each 'rating' criterion is not necessary to select the ablator.

Cost information on ablators is, of course, a subject of large uncertainties. Often the belief is expressed that it is just impossible to make realistic comparisons between costs offered for planning purposes by different manufacturers. To at least reduce the obvious excuses for discrepancies, a considerable effort was made at uniformity by (a) defining the bookkeeping system, i.e. in defining the items to be bookkept under a given heading, and (b) fixing the ground rules for pricing, i.e., l.e. area, number of flights, etc.

To compare the ablators, only ablator - connected items are priced under ablator costs. The items bookkept under 'development' and 'production' cost of the ablator are defined in table 23. The ground rules are spelled out in table 24.

Unfortunately, among the evaluation criteria there are two that are just listed for completeness but had to be neglected. Contamination effects on the RSI

Table 23(a)

COST ITEMS BOOKKEPT UNDER

DEVELOPMENT COSTS AND PRODUCTION COSTS

'Development costs' and 'production costs' involve only ablator-linked costs, specifically the items indicated in Table 23(b) ('development costs') and in Table 23(c) ('production costs' or $\$/ft^2$).

In particular, the substructure costs (fabrication, refurbishment, etc) are not be be included. But if a particular ablator, on account of its characteristics or the bond required, were to require extra manhours for refurbishment, then such extra costs should be bookkept against the ablator.

Table 23(b)

ABLATOR DEVELOPMENT COST ITEMS

1.0 Material Characterization (if any)

- 1.1 Property Measurements (Thermal, Structural)
- 1.2 Thermal Performance Evaluation (arc tests)
- 1.3 Thermal Performance Evaluation in representative sequential testing
- 1.4 Capability of Generating Design Charts
- 1.5 Structural Performance (cold soak, flexure tests)

2.0 Fabrication Studies (if any)

- 2.1 Investigation of Low Cost Fabrication Approaches
- 2.2 Preliminary Production Plan
- 2.3 Process and Fabrication Specifications
- 2.4 Set-up Pilot Plant Operations
- 2.5 Evaluate characteristics of pilot plant materials (properties)
- 2.6 Investigate and Define Repair Procedures

3.0 Quality Assurance

- 3.1 Define ablator acceptance criteria
- 3.2 Define acceptance criteria for ablator/bond attachment, seals and joints.
- 3.3 Define acceptance criteria for repairs

Table 23(c)

ABLATOR PRODUCTION COSTS ITEMS

1.0 Design and Fabrication of Final Tooling

2.0 Fabrication of Ablator

Table 23(d) for Molded
Table 23(e) for Honeycomb

3.0 Seals, Joints, Bolt Plugs etc.

3.1 Raw Materials

3.2 Tooling

3.3 Fabrication

3.4 Inspection

4.0 Packaging and Shipping*

5.0 On-Site Assembly Inspection

6.0 Field Repairs (as required)

*Account only for costs of shipping from production plant to KSC. For packaging assume that the crates used for delivering the substructures to the production plant will accommodate also the substructure-and-ablator panel. Therefore, such crates are not to be charged under the ablator production cost.

Table 23(d)

OPERATIONS IN HONEYCOMB ABLATOR FABRICATION

1.0 Procure and Inspect Raw Material (including honeycomb)

2.0 Clean and prime structure*

3.0 Bond H/C to structure

4.0 Cure and Inspect H/C bond

5.0 Prime H/C walls

6.0 Mix ablator and inspect

7.0 Fill H/C with ablator

8.0 Cure and inspect for voids, fiber clumps etc.

9.0 Post Cure

10.0 Rough and finish machine

11.0 Inspect dimensionally

12.0 Pore Seal and moisture barrier application

13.0 Final Inspection

*'Clean Substructure' means any cleaning operation starting from a substructure that (1) has been refurbished by scraping off the ablator but leaving perhaps as much as some 5 mils of silicone-based adhesive and that (2) has been structurally inspected.

Table 23(e)

OPERATIONS IN MOLDED ABLATOR FABRICATION

1.0 Procure and Inspect Raw Material

2.0 Mix ablator and inspect

3.0 Charge Mold

4.0 Cure and Post Cure

5.0 Remove from mold, trim and inspect for voids, fiber clumps, etc.

6.0 Clean and prime structure*

7.0 Bond ablator to structure and cure (unless mechanically attached)

8.0 Inspect bond

9.0 Rough and finish machine

10.0 Inspect dimensionally

11.0 Pore Seal and Moisture barrier application

12.0 Final Coating (if any)

13.0 Final Inspection

*'Clean substructure' means any cleaning operation starting from a substructure that (1) has been refurbished by scraping off the ablator but leaving perhaps as much as some 5 mils of silicone-based adhesive and that (2) has been structurally inspected.

Table 24(a)

Groundrules for L.E. Ablators Costs

1. Three traffic models, see Table 24(b)
2. 1971 uninflated dollars
3. The orbiter is 'frozen' (not 'rubber')
4. Typically use the wing L.E. main areas (not tail, nor special areas, e.g. fillets)
5. Ablative L.E. is not a back-up system for(and interchangeable with) carbon-carbon system, it is just a L.E. TPS to be attached at the wing front beam.
6. If needed, use a typical reference design such as the GAC 473 orbiter,
7. Use an area per vehicle of 600 ft^2.
8. Aluminum (not titanium) substructures
9. Use, for each ablator, thicknesses typically required for the phase C/D shuttle mission.

TABLE 24(b) - TRAFFIC MODELS

Traffic Model #1

(This is the first year of the NASA Traffic Model, or the DDT&E effort, increments I and II of the Phase C/D Shuttle program*)

6 flight tests
2 development orbiter vehicles (orbiter flight verhicles No. 1 and 2)
Schedule: CY 1978

Traffic Model #2

(Source: Mod 2 to SOW of contract NAS 1-11416, 'Ablative L.E. Research')

5 flight tests and 120 operational flights
2 operational orbiters
Schedule: not available
Flight rate: 24 operational flights per year for 5 years.

Traffic Models #3

(This is the entire NASA Traffic model to 447 flights or to CY 1988, or increments I to IV of Phase C/D shuttle program*)

6 flight tests and 441 operational flights
5 operational orbiters of which 2 are the upgraded/retrofitted development vehicles
Schedule and flight rate: see Table 24(c)

* Source: RFP No. 9-BC-421-67-2-40P, Space Shuttle Program, NASA MSC, p. 1-7 and 1-8

Table 24(c) Annual Flight Rate Model for Cost/Flight

Calendar Year	77	78	79	80	81	82	83	84	85	86	87	88
		6	15	24	32	40	60	60	60	60	60	30

Fiscal Year	78	79		80	81	82	83	84	85	86	87	88
Flights	2	4	7	20	28	36	50	60	60	60	60	60
Traffic Model Adjusted by ½ Year to FY	2	4	7	8 12	12 16	16 20	20 30	30 30	30 30	30 30	30 30	30 30

DDT&E (Increments I & II) → Increment IV →

Total Flights	Increment IV Flights
447	441
447	441

weight and cost had to be neglected because of total lack of data, while a detailed separate study would have been necessary to estimate the transition shift induced by l.e. roughness and the joints, especially the ablator-RSI joint. In this study we could not embark on those two separate questions, as indicated in Section 2.

5.5 Evaluation of the Candidate Ablators

When the eight candidate ablators are examined in the light of the 'go/no-go' criteria, four materials are eliminated as unacceptable. This is shown graphically in figure 68, where a judgement is marked for each test. Inadequate char stability and lack of regularity in the char appearance were the main problems. Specifically, the objectionable features in each case can be described with hopefully expressive words, as follows:*

ESA 3560 II A: delamination; irregular erosion; weak char-virgin interface; recession not predictable;

5026/39M: cracks, some deep into the virgin material, inconsistent char surface;

Mod 7 M: insufficient strength in the char-virgin interface; recession non predictable;

480 1B Hc: demolished material texture; excessive char melting.

Note that all three molded materials are eliminated, the elastomers, not surprisingly, because of weak char-virgin interface. The behavior of all four 'no-go' materials is consistent with previous information, in particular the

* The models and the extensive photographic coverage of the tests can be examined at the Thermal Protection Branch, Material Division of the NASA Langley Research Center.

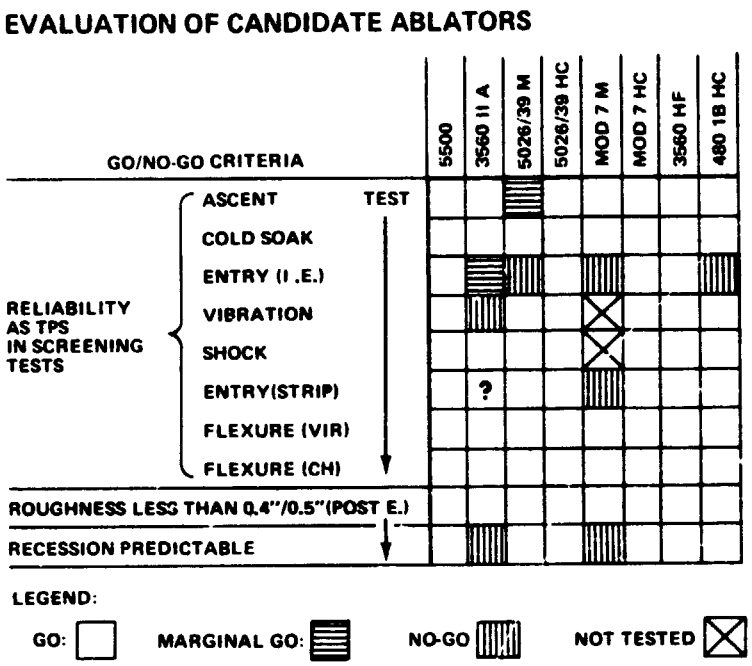

Fig. 68 Evaluation of the Candidate Ablators – Go/No-Go Criteria

ESA 3560 II A with the flight experience on the X 15 A-2 airplane.

The remaining four 'go' materials were examined against each of the rating criteria (table 22), except of course those neglected for lack of information.

As far as ablator costs are concerned, relatively good information was obtained from the manufacturers.** It amounted to the following: 1) at the nominal traffic model, the ESA 5500, the Mod 7 Hc and the ESA 3560 HF have the lowest cost. a few million dollars for the development cost and between 150 and 250$/ft^2 for the production cost (1971 dollars); the ESA 5500 and the ESA 3560 HF have somewhat lower production costs than the Mod 7 Hc;+ 2) the sensitivity to the traffic model is minimal; 3) the cost uncertainties are described as some 15% for the 5026/39 Hc and some 20 to 25% for the 3560 HF and the Mod 7 Hc, with the risks being clearly highest for Mod 7 Hc. The only conclusion that we could extract - when the necessary realism is exercised - is that the ESA 3560 HF, the ESA 5500 and Mod 7 Hc are attractive and that they are about equal in cost.

Concerning bond performance under the substructure strains, the flexure tests and the cold soak tests on the l.e. models showed that all the candidate materials are equally good. The tests covered adequately the flight-condition (the virgin strips were subjected to bonding strains of about 1.5 times the maximum strains;

** This information is not for general dissemination and therefore only vague statements are reported here. Obtained were the global value of development cost and $/ft^2 for three traffic models (5 Avco materials) and #2 and 3 traffic models (MMC materials), as indicated in the costing ground rules (Section 4).

+ This judgement, as the evaluation of the candidate ablators, is the responsibility of the first author only.

the cold soak was done with the models unloaded and untied at the ends; the charred strips were subjected to bondline strains about twice the maxima flight strains, however at room temperature).

In the area of insulation efficiency, the result of the l.e. test (figure 50) permits only one completely objective conclusion, i.e., that within the uncertainties of the measurements in the single test performed, Mod 7 Hc and the ESA 3560 HF are best and equal. However, if one wants to search for trends within the uncertainties, it appears likely that Mod 7 Hc is a more efficient insulator at least in range 60 to 100 Btu/ft^2-sec. (the Mod 7 Hc had lower soak-out temperature by some 80°F, lower surface temperature by some 500°F* and a thicker virgin layer left - figure 51; moreover in the first set of l.e. tests, the Mod 7 Hc showed generally lower temperature than the 3560 HF).

As far as char stability and cracks are concerned, we concluded--on an absolutely objective basis--from the tests on the l.e. models and the strip model that the Mod 7 Hc and ESA 3560 HF are best and equal, while the ESA 5500 exhibited excessive tendency to swell and the 5026/39 Hc displayed undistinguished performance and may well be unfairly penalized vis-a-vis the elastomers by the poor enthalpy simulation in this single screening test. Again, if one searches for trends within the uncertainties (2 tests, 20,000 - 27,000 Btu/ft^2, etc), the conclusion is that Mod 7 Hc appears to be somewhat better than the 3560 HF which exhibited (a) less regularity in the char appearance, (b) higher char depth, and (c) a more fragile char, when compared to the Mod 7 Hc.**

---

* The values actually were 2300°F for the Mod 7 Hc and 2890°F for the 3560 HF. This last value is a little surprising since it is even higher than that of the 5026/39.

** The 3560 HF models of the second set exhibited two irregular spots, essentially in the form of a 'hole'. A check of the X-ray picture of the model (done by Martin) showed absolutely nothing. The explanation of these 'holes' remains elusive.

As far as behavior under a heating overshoot (an increase of, say, 30-40%), no hard information was obtained in this study. However, some information can be extracted from the tests that were conducted on one set of l.e. models that had a different design for the side plates (with considerable effects of the sides of the model) and that were tested at heating rates representative of the extreme environment. Other difficulties with these data (see Data Package) are the ascent heating applied via radiant lamps and the very low enthalpy in the entry tests. In spite of these uncertainties, the data obtained in the entry test suggest that in a heating overshoot, (a) the Mod 7 Hc char appearance is somewhat better than that of ESA 3560 HF and (b) at high $\dot{q}_w$ the 3560 HF appear to develop 'tunnels', i.e. void channels into the material. Naturally this indication should be taken with caution, since the tests were conducted at $\dot{q}_w$ of about 107 Btu/ft^2-sec and this is considerably more than an overshoot. Moreover, the 3560 HF is not recommended for applications beyond some $\dot{q}_{cw} \simeq \dot{q}_{hw} \simeq 90$ Btu/ft^2-sec (Refs. 47 and 59) and therefore the indications from a high $\dot{q}_w$ test may be even less representative of an overshoot.

As far as degradation of aerodynamic characteristics, the roughness degradation for all four 'go' candidate materials is small and probably cost-free, as indicated by the roughness measured (figure 52) and the cost of the degraded aerodynamic characteristic (figure 53). The roughness of the 3560 HF and the Mod 7 Hc is about equal within the uncertainties. The degradation due to recession should also be small (at most a L/D loss of some 0.15) when the concept for minimizing shape change is used. Again, Mod 7 Hc and the ESA 3560 HF are best and equal (see figure 56).

There is no strain limit imposed on the substructure by any of the 'go' materials, since the maximum bondline strains in the l.e. substructure are about 0.002 and, in the flexure tests at room temperature with a typical char thickness, bondline

strains up to 0.0035 do not affect any of the candidate ablators. Therefore all the 'go' materials are equally good from this point of view.

As far as the ablators contribution to the stiffness of the substructure, this is merely an added qualitative merit of the ablator but not one that would result in savings in cost or weight of the substructure, since it is not conceivable of a realistic structural design that counts on the ablator structural contribution. In this sense, this criterion is a minor one. All the 'go' materials are equally good, and in fact a quantitative measure of this contribution (see figure 69) shows that Mod 7 Hc and the 3560 HF give exactly the same contributions.

By the criterion 'production problem/overall risks'* the best of the four 'go' is 5026/39 Hc since it is the one that has been fabricated in the largest quantity**, whose fabrication techniques have been developed in depth in a well funded program, and simultaneously is well characterized and well known. However, for what follows, we are interested in a comparison between Mod 7 Hc and the ESA 3560 HF. The Mod 7 Hc is a developed material formulation, but not a developed 'material system', as elaborated in Section 5.2. On the other hand,

---

* We have in mind, under this criterion, unexpected difficulties, surprises, uncertainties or probability of errors in planning and estimating and similar uncertainties that all amount to risks. We a e not accounting here for differences in the development between ablators and their predictable differences in effort required, since these are accounted under development costs of each ablator.

** To date, the total production of 5026/39 HcG has been around 15,000 ft^2 (30 Apollo Command Modules at about 400 ft^2/ship, plus odds and ends). The next highest production among the candidate ablators is for the 356. HF and is about 2,400 ft^2 (4 PRIME vehicles at 300 ft^2/article plus some 1200 ft^2 of development activities; the total is actually 3,200 ft^2 if we add materials of the same family such as those for the PAET 8 vehicles, the X15A2 and Viking.

- AS SHOWN IN FLEXURE TESTS
- VIRGIN ABLATORS
- AT BONDLINE STRAIN = 0.0017

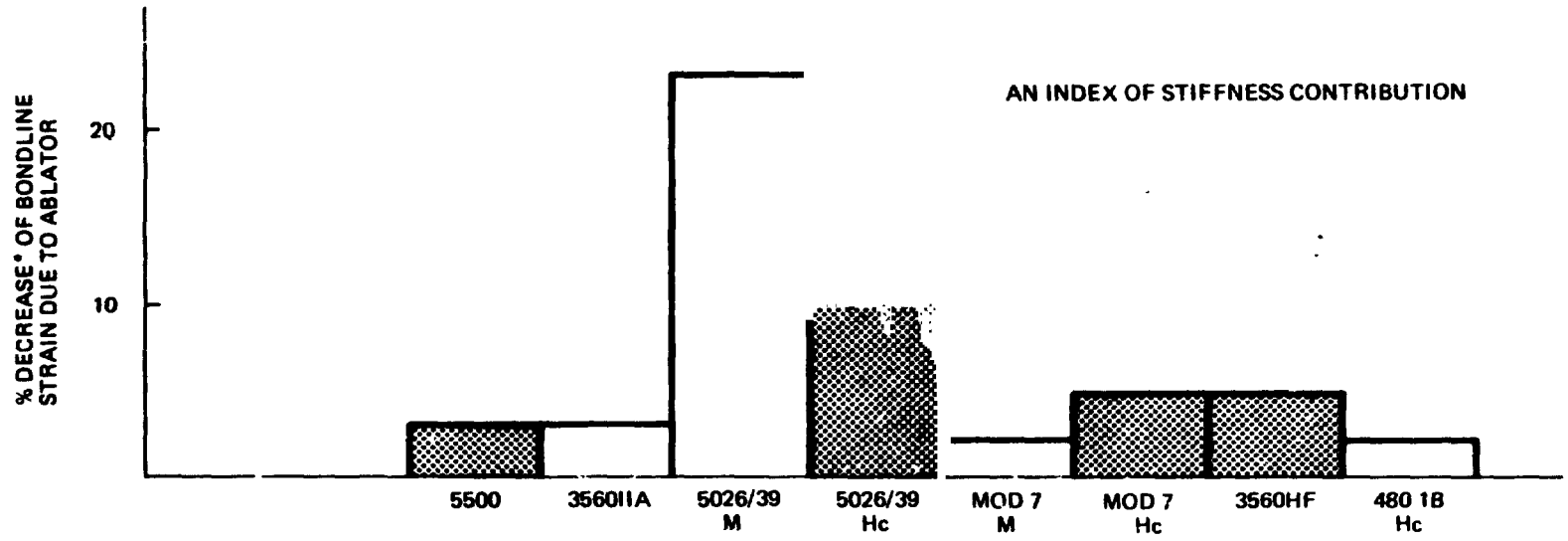

* RELATIVE TO BARE MODEL

Figure 69 Relative Contribution of Candidate Ablators to Stiffness of Substructure

the ESA 3560 HF is a 'developed system' produced for and flown successfully on PRIME. Therefore, the ESA 3560 HF has a clear edge as far as possible production problems and overall risks, while Mod 7 Hc is only marginal.

It is not necessary to stress how cloudy and complex the criterion 'improvement potential' is. Among other things, it depends upon whether there is time and support for the improvements envisioned; it is at least debatable whether there will be such support for an ablative l.e. for the shuttle orbiter, even though there was some for such research vehicles as the X15 A2 or PRIME. Moreover, in ablator development, even if there is a clear and obvious approach to formulation modifications, there is no guarantee beforehand that the expected improvement will in fact be realized. In parallel to this study, both the Martin Corporation and the Avco Company produced various modifications of the 3560 HF, Mod 7 M, ESA 5500, and 3560 II A. The initial results of many of these materials appear very disappointing, but only ascent heating and cold soak tests have been carried out so far (Ref. 56). Therefore the issue of improvement potential of the four 'go' materials is one of complete uncertainty.

Summarizing now, the rating criteria point fairly systematically at the two elastomers, Mod 7 Hc and ESA 3560 HF as definitely the best of the four 'go' materials at least within the data generated and the criteria considered. The performance of these two materials appeared very close, as shown in table 25. Again, we distinguish between an objective conclusion from the few test results with their many uncertainties and a likely trend that is noticeable within the data uncertainties.

5.6 Ablator Selection

It is clear from table 25 that not much difference is left on which to base a selection of one material over the other. Or, in a different light, the two

Table 25 Evaluation of the Two Best Candidate Ablators, Rating Criteria

	Objectively With Data Gathered:		Possible Trends In Data Gathering In Favor:
	3560 HF	Mod 7 HC	
Cost per unit area	Equal		3560 HF
TPS Performance:			
– Under Strain	Equal		Equal
– Insulation Efficiency	Equal		Mod 7 Hc
– Char Stab & Cracks	Equal		Mod 7 Hc
– Over-Shoot	No Info		Mod 7 Hc
Aero Characteristics	Equal		Equal
Effects on Substructure	Equal		Equal
Improvement Potential	?	?	?
Production Problems/Overall Risks	Better	Marginal	3560 HF
*Complex/Debatable Issue			

materials are close enough in properties and characteristics to perform in a very similar manner in the screening tests of this program, and therefore, hopefully in flight. The lack of objective performance differences makes them both equally attractive from the point of view of a technology study such as this (ground rule b), (Section 2).

Therefore, both materials, ESA 3560 HF and Mod 7 Hc, were selected for the development of two versions of the l.e. design. Actually, the versions are as similar as the performance of the materials. Questions not yet studied (e.g. contamination), or further tests may in the future suggest the selection of one material over the other.

6. WING L.E. DESIGN

For the purpose of this program the orbiter Leading Edge (L/E) was assumed to consist of all wing structure including TPS forward of the wing front beam. The leading edge system design included thermal and aerodynamic design of the selected heatshield as well as structural design of the L/E substructure and associated attachments to the wing front beam. In view of the fact that at the program inception there were several orbiter concepts in contention it was decided to maintain design flexibility such that the ablator L/E system arrived at would be as configuration independent as possible.

Consistent with this approach and due to program limitations a typical midspan L/E segment was selected for design evaluation. Interfaces were established for the TPS at the ablator/RSI juncture in the spanwise direction and between adjacent ablator segments in the chordwise direction. The design of the joints and seals along both boundaries was also included in the design task. As alluded to above the structural interface was taken to be the wing front beam with the design effort encompassing all wing structure forward of this point including attachment schemes to the front beam. Figure 70 illustrating a typical orbiter wing segment at midspan defines the areas which were covered under this program. This figure also presents the general configuration and nominal dimensions selected to represent a typical midspan L/E segment.

The following sections present the results obtained in the various tasks which led to the definition of the final design presented in Section 6-5.

6.1 L.E. REFURBISHMENT AND DESIGN CONCEPT

6.1.1 Refurbishment Concepts

The first task performed prior to conducting the detailed design trade-off studies was the selection of the L.E. refurbishment concept. (We call L.E.

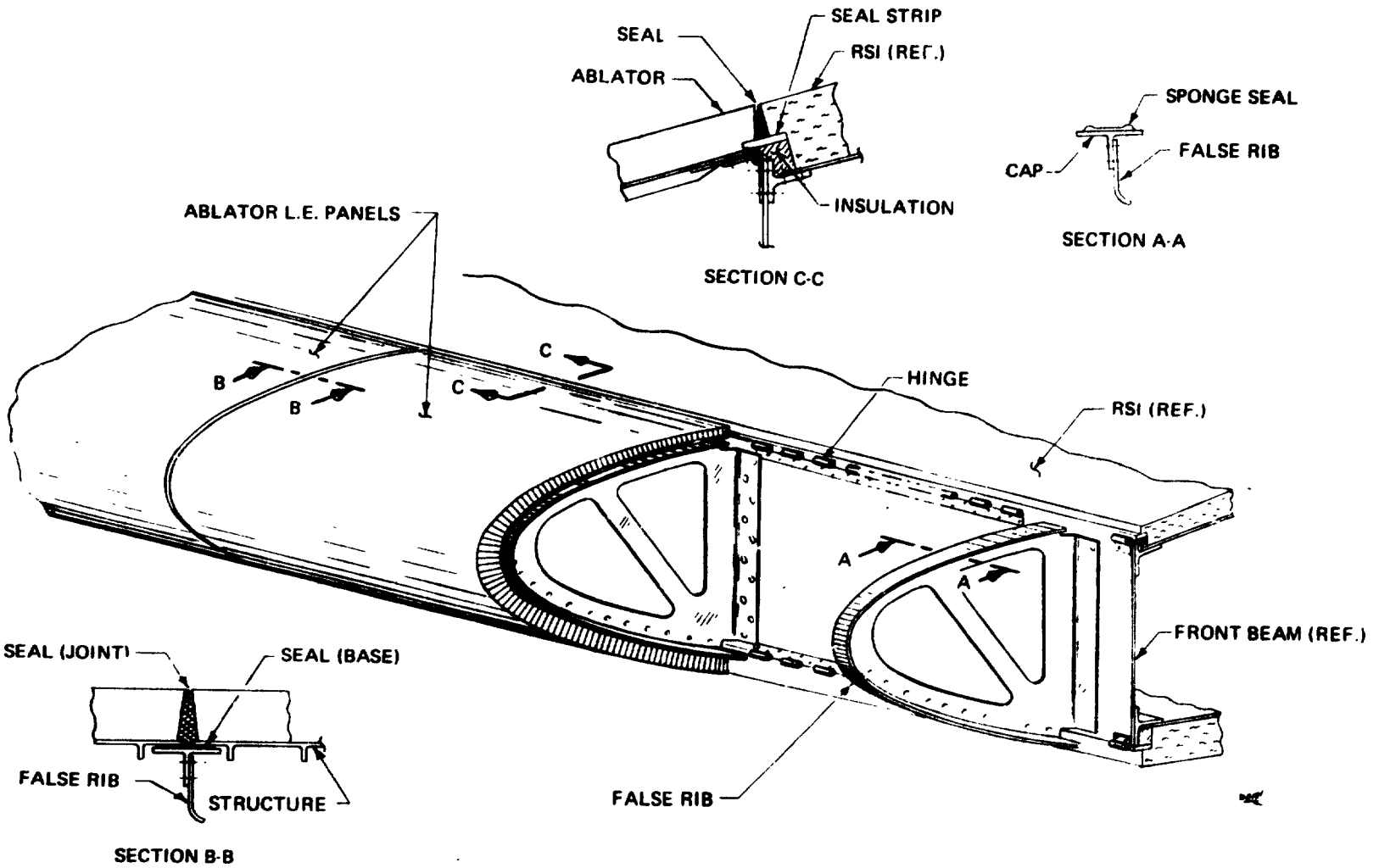

Figure 70 Areas Covered in Wing L.E. Design Study

refurbishment the procedure by which, after each flight, the orbiter l.e.s are repristinated to a flying condition).

Essentially, this task was a systems trade-off study where all potential concepts were identified and subsequently evaluated relative to all pertinent factors; ultimately leading to the selection of the single most promising concept. Although simple in concept this task proved to be one of the more difficult due to the large number of potential candidates and the number of engineering disciplines involved in the evaluation.

A variety of design concepts were considered ranging from systems which are refurbished on the vehicle to totally disposable systems. In general, the concepts reviewed can be grouped into three broad classes relating to the number of different operations done on the vehicle as opposed to work carried out at the ablator manufacturer's plant or at a refurbishment depot. From another point of view the three basic classes differ in the amount of leading edge structure that is permanently attached to the vehicle and is not removed after each flight.

Figure 71 presents a series of thirteen sketches illustrating, with the description in table 26, the various leading edge concepts evaluated in this program. In this figure the class division becomes evident. For example, those included under Type A have a nonremovable substructure and only the heatshield is removed after each flight. Under Type B, only part of the L/E substructure is removed and either reused off site or discarded, whereas in Type C the entire leading edge system forward of the front beam is removed and again one has the option of either reused off site or disposal.

There are substantial differences among the variants on such factors as cost, weight, vehicle turn-around time, reliability, etc. Table 26 lists some of

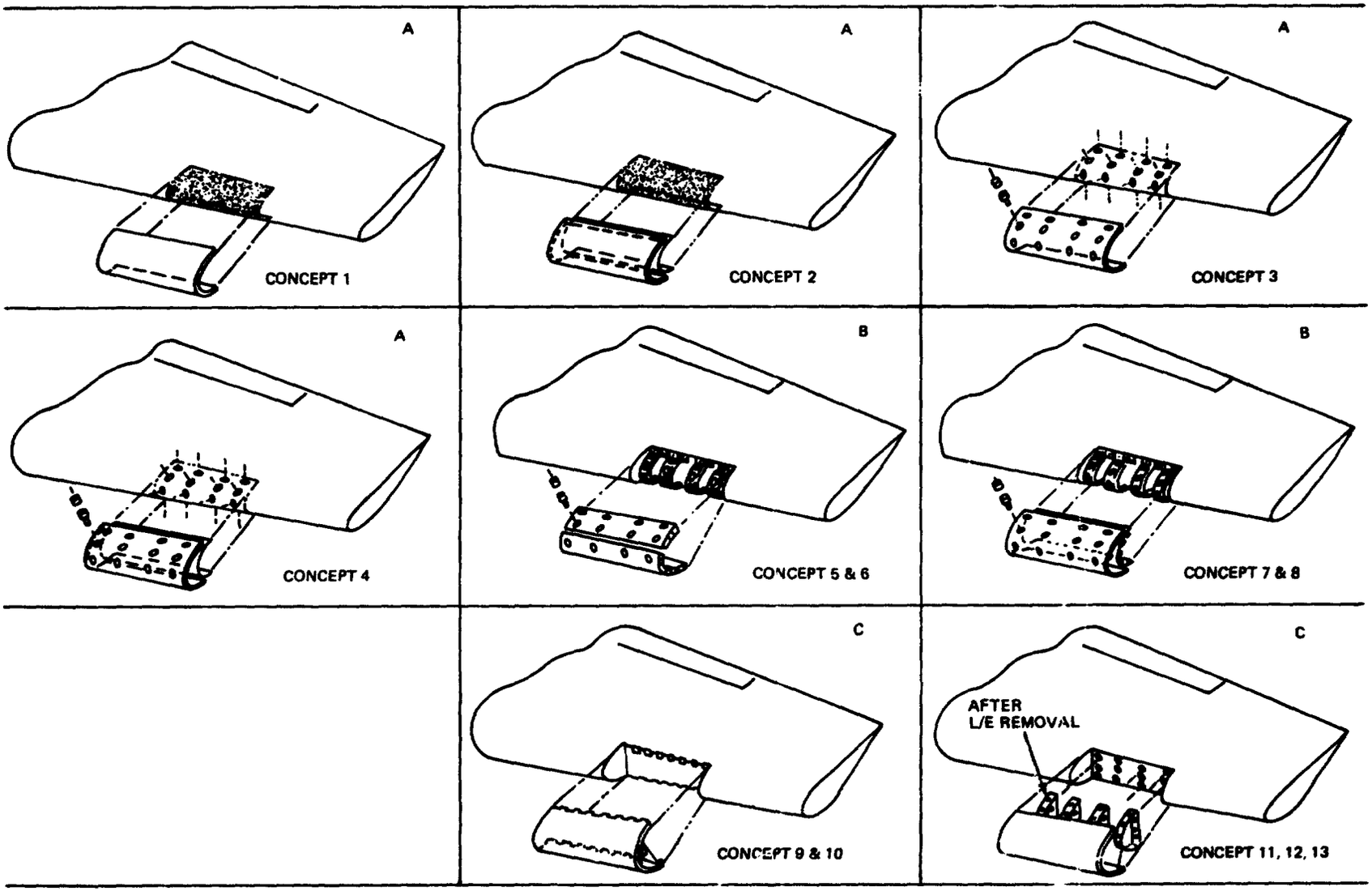

Figure 71 Leading Edge Refurbishment Concepts Studied

FOLDOUT FRAME

Table 26 Description of Refurbishment Concepts

Concept No.	Description	Advantages	Disadvantages
1	A honeycomb reinforced ablator without any carrier panel is bonded on site directly to the wing. The L/E substructure is permanently attached.	• L/E substructure never removed. • Only 7 substructures required (5 orbiters-2 spares) • Lightweight	• Direct bonding of ablator to wing on site undesirable • Difficult to inspect bond • Fabrication of a H/C reinforced ablator in curved configuration without backup structure is difficult. • Refurbishment difficult and time consuming • High initial cost of tooling for ablator fabrication
2	A Honeycomb reinforced ablator with a carrier panel is bonded on site directly to the wing. The L/E substructure is permanently attached.	• L/E substructure never removed. • Only 7 substructures required (2 spares) • Ablator cap relatively easy to fabricate	• Direct bonding of ablator to wing on site undesirable • Compound bonds required-ablator to carrier panel and carrier panel to wing. • Difficult to inspect on site bond. • Refurbishment difficult and time consuming. • Carrier panel could mean weight penalty • High initial tooling cost for ablator fabrication.
3	A Honeycomb reinforced ablator without a carrier panel mechanically attached to the wing. L/E substructure permanently attached.	• L/E substructure never removed. • Only 7 substructures required. • Ablator segments cleanly removed	• Many bolts required. • High initial cost of tooling for ablator fabrication • High cost associated with finishing bolt holes and making bolt plugs • Fabrication of H/C reinforced ablator in curved configuration without carrier panel difficult.
4	A Honeycomb reinforced ablator with a carrier panel mechanically attached to the wing. L/E substructure permanently attached.	• L/E substructure never removed. • Only 7 substructures required. • Ablator segments cleanly removed.	• Many bolts required. • Weight penalty due to carrier panel and number of bolts required. • High initial cost of tooling for ablator fabrication. • High cost associated with finishing bolt holes and making bolt plugs.
5 & 7	A Honeycomb reinforced ablator bonded to structural carrier panels mechanically attached to nonremovable ribs. Structural carrier panels are removed after each flight and refurbished in shop. 5 – Three piece ablator 7 – Single piece ablator	• Structural panels are retained and refurbished • Structural panels provide large part of tooling for making ablator. • Ablator to structure bond made in shop. • Ablator to structure bond easily inspected.	• Many bolts (structural connections) required. • If made in three sections would require extensive usage of seals. • Weight penalty associated with large number of bolts, seals and closures. • High cost of finishing bolt holes and bolt plugs.
6 & 8	A Honeycomb reinforced ablator bonded to structural carrier panels which are mechanically attached to non-removable ribs. Structural carrier panels and expended ablator are removed after each and discarded. 6 – Three piece ablator 8 – Single piece ablator	• Refurbishment of structural panels eliminated. • Structural panels provide large part of tooling for making ablator. • Ablator to structure bond made in shop. • Ablator to structure bond easily inspected.	• Many structural panels required for each flight. • Many bolts (structural connections) required. • If made in three segments would require extensive usage of seals; some in high heating areas. • Weight penalty associated with large number of bolts, seals and closure strips. • High cost of finishing bolt holes and bolt plu

FOLDOUT

	— [illegible] piece ablator 7 — Single piece ablator	[illegible] structure inspected.	plugs.
6 & 8	A Honeycomb reinforced ablator bonded to structural carrier panels which are mechanically attached to non-removable ribs. Structural carrier panels and expended ablator are removed after each and discarded. 6 — Three piece ablator 8 — Single piece ablator	• Refurbishment of structural panels eliminated. • Structural panels provide large part of tooling for making ablator. • Ablator to structure bond made in shop. • Ablator to structure bond easily inspected.	• Many structural panels required for each flight. • Many bolts (structural connections) required. • If made in three segments would require extensive usage of seals; some in high heating areas. • Weight penalty associated with large number of bolts, seals and closure strips. • High cost of finishing bolt holes and bolt plugs.
9	A Honeycomb reinforced ablator bonded in shop to easily removable monocoque L/E structure. Entire L/E is removed and refurbished off site.	• Structure provides large part of tooling for ablator fabrication. • Quick turn around time. • Requires no skilled labor on site. • Entire system can be inspected in shop prior to shipment to site. • Lightweight.	• Substructure is refurbished after each flight.
10	A Honeycomb reinforced ablator bonded in shop to easily removable monocoque L/E structure. Entire L/E is removed and discarded after each flight.	• Structure provides large part of tooling for ablator fabrication. • Quick turn around time. • Requires no skilled labor on site. • Entire system can be inspected in shop prior to shipment to site. • Lightweight. • Cost of refurbishing substructure eliminated.	• A new substructure is required for each flight.
11	A Honeycomb reinforced ablator bonded in shop to easily removable semi-monocoque substructure. Entire L/E is removed and refurbished off site.	• Structure provides large part of tooling for ablator fabrication. • Quick turn around time • Requires no skilled labor on site. • Entire system can be inspected in shop prior to shipment to site.	• Substructure is refurbished after each flight. • Slightly heavier than monocoque design.
12	A Honeycomb reinforced ablator bonded in shop to easily removable semi-monocoque substructure. Entire L/E is removed, ablator and skin panels are subsequently removed (ribs retained) and replaced with a new panel.	• Structure provides large part of tooling for ablator fabrication. • Cost of refurbishing of skin panels eliminated. • Entire system can be inspected in shop prior to shipment to site.	• New skin panels required for each flight. • Slightly heavier than monocoque design.
13	A Honeycomb reinforced ablator bonded in shop to easily removable semi-monocoque substructure. Entire L/E is removed and discarded after each flight.	• Structure provides large part of tooling for ablator fabrication. • Quick turn around time. • Requires no skilled labor on site. • Entire system can be inspected in shop prior to shipment to site. • Cost of refurbishing of skin panels eliminated.	• New L/E structure required for each flight. • Slightly heavier than monocoque design.

FOLDOUT FRAME 2

the advantages and disadvantages of each concept and the results of the design trade-offs are summarized in the following section.

6.1.2 Weight, Cost and Concepts Evaluation

Having identified and reviewed each design the concepts were rated relative to their cost, weight, risk factors (e.g. reliability, fabricability, maintainability) and requirements (turn-around time required). As can be seen this evaluation considered the primary driving factors of cost and weight as well as other items requiring judgement (i.e., reliability, maintainability, etc), all of which must be considered in making a final decision. In preparing the rating schemes the following ground rules were observed, which were set out in Section 2:

a. The traffic model would consist of 447 flights.

b. The L/E would employ a single ablator covering 600 ft^2.

The following assumptions were also used:

a. The results for the ablator material Avco Mod 7 reinforced with fiberglass honeycomb were also applied to the ESA 3560 HF.

b. For handleability the L/E would be made up of discrete segments approximately 36" long. Later design studies supported this decision.

c. When the substructures are not discarded after each flight, only nineteen substructures will be fabricated.

Table 27 presents a summary of results obtained from this evaluation and figure 72 displays a comparison of weight and cost.

Costs in terms of 1971 uninflated dollars were generated on a dollars per square foot basis using the area and traffic model presented above. To arrive at a true total program cost/ft^2 it was necessary to include the cost of refurbishment along with the basic costs associated with the fabrication of the ablator and substructure and the costs have been segregated accordingly. Precisely

Table 27 Data for Trade Off of Refurbishment Concepts

Group	Concept No.	Weight			Normalized Cost (%)				Risk Factors					Requirements
		Heat Shield	Structure	Total Wt.	Heat Shield	Sub Structure	Refurbish.	Normalized Total Cost	Reliability	Ease of Refurbish	Ease of Inspection	Ease of Repair	Fabricability	Vehicle Turn Around Time
		lb/ft^2	lb/ft^2	lb/ft^2										Days
A	1	5.37	1.13	6.50	62	1	37	100	Poor	Poor	Poor	Poor	Poor	16
	2	6.23	1.13	7.36	54	1	37	92	Poor	Poor	Poor	Poor	Good	16
	3	5.11	1.14	6.25	68	1	6	75	Fair	Fair	Fair	Fair	Poor	4
	4	5.72	1.14	6.86	59	1	6	66	Fair	Fair	Fair	Fair	Fair	4
B	5	5.44	1.25	7.29	63	11	6	81	Fair	Fair	Fair	Good	Fair	4
	6	5.44	1.85	7.29	63	12	6	82	Fair	Good	Fair	Good	Fair	4
	7	5.40	1.85	7.25	62	12	6	80	Fair	Fair	Fair	Good	Fair	4
	8	5.40	1.85	7.25	62	12	6	81	Fair	Good	Fair	Good	Fair	4
C	9	5.37	1.13	6.50	53	12	3	68	Good	Fair	Good	Fair	Good	4
	10	5.37	1.13	6.50	54	12	3	69	Good	Good	Good	Fair	Good	4
	11	5.37	1.85	7.22	56	12	2	70	Good	Fair	Good	Fair	Good	4
	12	5.37	1.85	7.22	57	13	2	72	Good	Good	Good	Fair	Good	4
	13	5.37	1.85	7.22	57	15	2	74	Good	Good	Good	Fair	Good	4

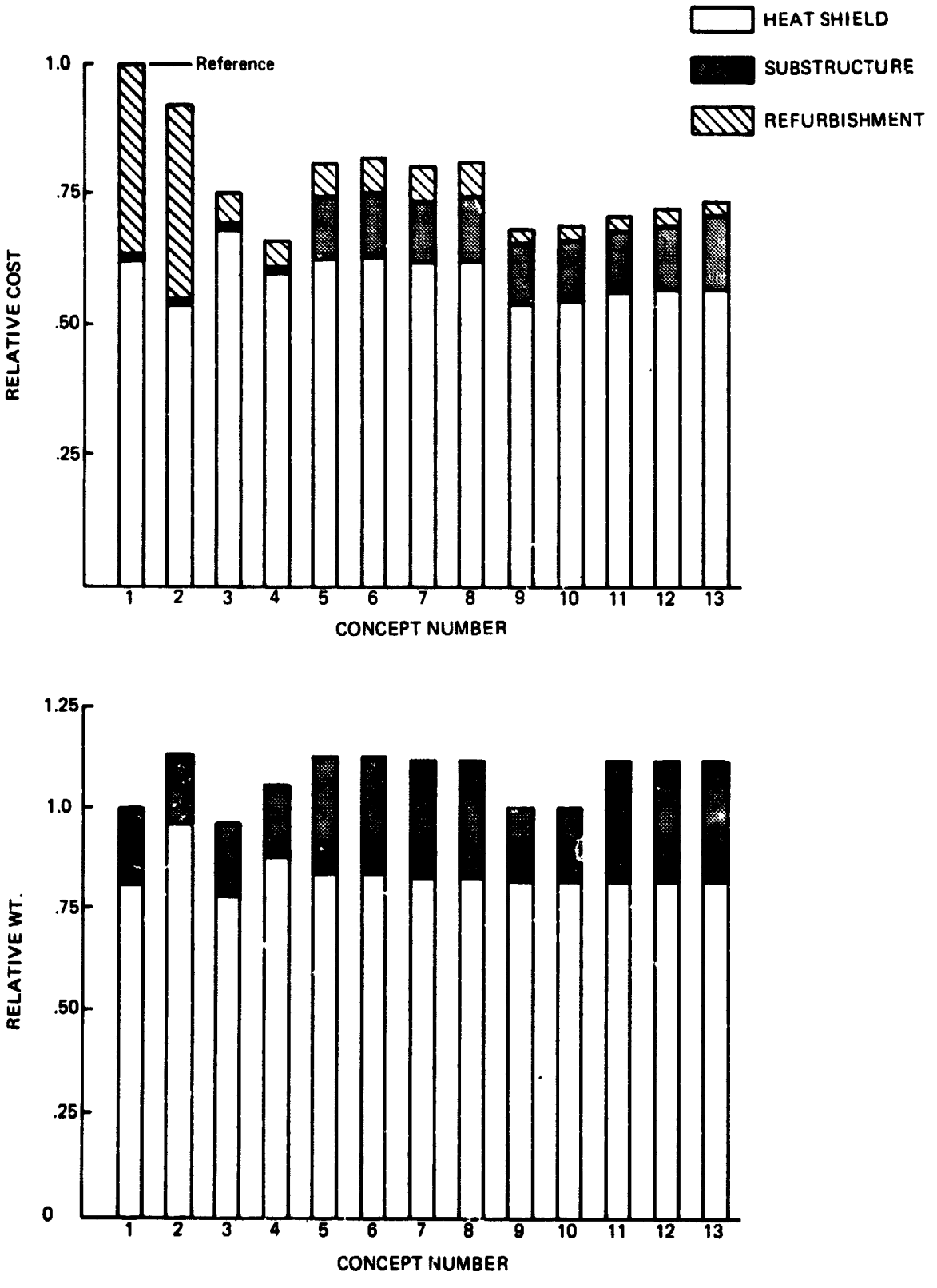

Figure 72 Weight and Cost Comparison of Refurbishment Concepts

what items have been bookkept for the various cost elements is indicated in table 28. It should be pointed out that in the cost bookkeeping as defined here, "refurbishment" and the associated refurbishment costs are taken to include only those operations directly traceable to the removal and replacement of the leading edge TPS system on the vehicle. Consequently, the costs incurred (if any) for removing the charred ablator from the substructure after a leading edge assembly has been removed from the vehicle have been accounted for under the cost of the substructure. For the refurbishment cost of table 27, table 29 presents a detailed man-hour breakdown for each of the operations covered under refurbishment costs. In addition to providing the basis for the refurbishment costs this information was also used to estimate the total turn-around time required to replace the leading edge TPS which is also listed in table 27.

Weight estimates were prepared for both the Mod 7 Hc heatshield and the aluminum substructure. The bookkeeping used in preparing the weight estimates is indicated in table 30. In general, and as expected, the heatshield weight is nearly constant whereas variations are noted in the estimated substructure weights. Although all the structures presented are relatively light-weight when considered in terms of the primary structure, there exists a reasonable percentage difference between some concepts which sould have an impact on the overall vehicle weight. Of course, the total L/E system weight does not reflect such large variations since the heatshield contributes greater than 75% of the L/E total weight.

The remaining items included in table 27 are less tangible but nonetheless important in the overall selection process. These items can be looked upon as risk factors and rely heavily upon experience, understanding and judgement. Some of the items considered are reflected in the cost data presented earlier

Table 28 Items Bookkept Under Cost

(a) Heat Shield & Substructure

Heat Shield Cost: includes all the items indicated as ablator production cost in connection with the ablator costs (see Section 5.4); includes also carrier panel (if any) and relative bonding operation.

Substructure Cost: includes all items in the production of the substructures including spares (not DDT & E or start up). Specifically:

1. Tool design.
2. Tool fabrication
3. Material.
4. Production.
5. Manufacturing management.
6. Packaging and shipping of new substructures (Grumman – Avco).
7. Quality control (inspection, acceptance, certification).
8. Manufacturing documentation.
9. (If substructures are reused) refurbishment cost.
10. (If substructures are reused) packaging and shipping of substructures from KSC to Avco).
11. (If substructures are reused) depot cost for the reuse of the substructure.

(b) Refurbishment Costs

Refurbishment Costs: the cost of all operations needed to remove and replace any part that needs to be removed and replaced plus the cost of maintaining storage areas, equipment, etc., needed for the operations. These costs are only recurrent costs, not DDT & E or start up. Items included:

1. a) Take-off from vehicle the l.e. segment (or anything that need be taken off for replacement).
   b) Ship it to storage area.
2. Inspection of l.e. area after removal (for example: in concept 1, inspect substructure after removal of charred ablator, in concept 7 – 13, inspect front beam).
3. Ship new l.e. (ablator, ablator panel, l.e. segments, etc.) from storage.
4. Install new l.e.
5. Install joint seals.
6. Final inspection of installation by vehicle manufacturer.
7. Cost of storage for new l.e. parts (ablator panels, ablator, l.e. segments, etc., depending upon the concept).

Neglected were:

8. Cost of depot space for the refurbishment of the vehicle when ablator removal is to be done on site.
9. Storage for discarded l.e. parts.

Table 29 Itemized Man-Hours Needed for L.E. Refurbishment

Concept		Refurbishment Cost Items(1)								
		← m-hr/ft^2-Flight →							$/ft^2-Flight	
Type	No.	1	2	3	4	5	6	Item 1 to 6	7	Source of Data
Ⓐ	1	7.4(a)	–(b)	0.04(c)	0.75(g)	0.17(d)	0.35(c)	10.25	0.37(e)	
	2	↓	–	↓	↓	↓	↓	↓	↓	
Ⓑ	3	0.5(f)	0.04(c)					1.60		
	4	↓	↓					↓		
	5					0.25		1.69		
	6					↓		↓		
	6a					0.17		1.60		
	6b					↓		↓		
Ⓒ	7									
	8									
	9									
	10									
	11	↓	↓	↓	↓	↓	↓	↓	↓	

Notes:

(1) As per bookkeeping in Table 28.

Ref. 1: Hammon, J.M. and Yoshino, S.Y., Space Shuttle TPS Refurbishment Techniques, Space Division, Rockwell Int., SD 73-SH-0044, March 1973

Ref. 2: Personal communication from B. Frumkin, Grumman

Ref. 3: Personal communication from R. Heizigenstadt, Facility Dept., Grumman

a. Routing of ablator, scraping of bond, cleaning of substructure for a 30 pcf Hc elastomer, bonded with silicone-type adhesive on l.e.-type curvatures: estimated at 7.4 m-h/ft^2 (as reported in Ref. 1 for curved and non-curved areas, silicone-type adhesive and a 16 pcf Hc elastomer; inspection in Ref. 1 is also included but is here bookkept under item 2).

b. Inspection as per Ref. 1: 1.9 m-h/ft^2.

c. Ref. 2.

d. For the midspan segment, length of seals: chordwise 4 55 ft per l.e. segment (1 side per segment); spanwise at front beam 31" (at least 2 per l.e. segment, 4 for concepts 5 and 6); area of l.e. segment: 11.83 ft^2; rate of installation 0.2 m-h/ft (ref. 2).

e. Storage area per segment 10 ft^2; 3 segments stacking in crates; 44 segments per vehicle, 1 set per vehicle available all the time; 146.6 ft^2 of storage area required per vehicle; cost of storage area = 3$/ft^2-year (Ref. 3); number of years for NASA traffic model (increment IV): 11; number of flights of vehicle: 89; cost of storage area per flight: 0.37 $/ft^2-flight.

f. B. Frumkin, W. Berkson, G. Wadkinson, Task time estimates for TPS panel replacement. Grumman Inter-office memo, B35-400-M0-43 (29 Oct. 1970). This is a global estimate that does not differentiate between attachment schemes.

g. Ref. 2. This is a gross estimate that does not attempt to differentiate between attachment schemes (including bonding). It results in about 9 m-h per segment.

Table 30.

Bookkeeping of Weight Items

Heat Shield Weight: includes the weight of all the items book kept under the cost. Specifically:

1. Ablator.
2. Bond between ablator/carrier panel and substructure.
3. Coating (if any).
4. Seals, including internal insulation strips (if any).
5. Bolts and plugs.
6. Carrier panel and bond between carrier panel and ablator (if any).

Substructure Weight: includes the following:

1. Substructure proper to the wing front beam.
2. False ribs.
3. Attachments weight (hinge pin, quick release mechanism).

in the table, only insofar as one can predict their impact on weight and cost; however, it is necessary to examine these factors in the light of the uncertainties in prediction. Moreover, all factors that may contribute to deviations from nominal operations must be considered in the light of the risks taken. This gives further insight into the understanding of the individual concepts. Since there is no exact or absolute rating system available for these items it was decided to rank them on a good/fair/poor basis. Given time it is possible that a more exotic rating system could have been arrived at, but, the end result would be about the same. In examining table 27, it should not be inferred that the specific rating assigned to each concept is absolute from the overall design standpoint but, rather, based upon our combined judgement this is how it ranked relative to the other concepts presented. For example, giving a poor rating to concept one for reliability simply means that its reliability relative to the other concepts presented is judged to be lower.

The risk factors selected cover the more important aspects of the design with admittedly some overlap. In making the evaluation the following factors were considered for the various topic headings; reliability, ease of refurbishment, ease of inspection, ease of repair and fabricability.

Reliability is the confidence level one can assign to the final piece of hardware in accomplishing its intended mission. Items considered were design complexity, amount and type of inspection required, caliber of inspection procedures available, and the type of labor and work area in which the fabrication was conducted.

Ease of refurbishment is taken to mean how difficult and time consuming would be the job of refurbishment. Although this would be reflected in the costs

to some degree the effect of cost was not factored into this rating. Rather, items related to preparing the vehicle for flight were considered, such as removing and replacing the leading edge and refurbishing the substructure. Concepts rating high in this category obviously would be those where the leading edge is easily removed and discarded.

Ease of inspection involved the amount of inspection required, the caliber of the inspection techniques available, the importance of the inspection, and the amount of confidence one could assign to the inspection having been performed. Here, concepts where to accessibility for inspection was possible during the bulk of the assembly cycle rated highest.

Under ease of repair it was assumed that a complete segment on the vehicle would have to be removed and replaced. The amount of effort required and difficulty encountered in performing this task was rated here.

Fabricability considered the relative amount of difficulty expected in developing and implementing a fabrication scheme for the assembly of the leading edge. This included tooling development and the various molding, trimming and finishing operations required to produce a complete piece of hardware.

6.1.3 Refurbishment Concept Selection

In its entirety table 27 presents a good overview for all the potential refurbishment concepts considered. Taken individually the elements in the table show that (a) from both the weight and cost aspects (figure 72) the ablative heatshield is the driving force; it constitutes about 75% of the system weight and accounts for 80%, on the average, of the total system costs, (b) with the excepticns of Group A, for equivalent designs whether the substructure is refurbished or discarded does not influence the overall substructure cost dramatically, (c) vehicle turn around time is prohibitive for

direct bonding to the vehicle (Group A, Concept 1 & 2) and the least time is required for concepts where the entire leading edge system is removed and replaced and, (d) concepts where the bulk of the fabrication activity is confined to work performed in a refurbishment depot or at the ablator manufacturers plant rate the best from an overall risk point of view.

Taken collectively these elements show that Concepts 1 & 2 are strongly objectionable from the required turn-around time since the target time for the vehicle is between 150 and 250 hours (see Section 2). Additionally, the cost and reliability factors for these two concepts are also unacceptable when compared to the other alternative approaches. The combined aspects of system weight and cost can be used to eliminate all the Group B concepts as well as Concepts 11 through 13 in the Group C classification. It should be pointed out here that this elimination process is directed at obtaining a minimum weight, cost system within the framework of acceptable risk factors and turn-around time. Consequently, the fact that a particular concept is eliminated does not necessarily mean that it is undesirable or unworkable but rather based upon the data presented it was concluded that a more attractive system is available.

Accordingly, having made these cuts, four candidates remain, Concepts 3 and 4 of Group A and Concepts 9 and 10 in Group C. Although Concept 3 is the lightest it is also the most expensive. Cost alone is insufficient to eliminate this concept since low weight can result in considerable cost savings when assessed on an in-orbit-payload basis. Looking further, however, it is observed that the overall risk factors associated with this concept are high. In fact, the desirability of fabricating an ablative heatshield in this configuration without a back-up structure is in question, notwithstanding the use of embedded mechanical fasteners without a back-up structure. These concerns are reflected in the high cost for the heatshield as well as the fair reliability and poor

fabricability rating assigned to this concept. This combination of factors was considered sufficient justification to eliminate Concept 3.

Of the three remaining concepts, namely Concepts 4, 9, and 10, there was only a need to select Concept 4 or Concept 9 since Concept 10 differed from 9 only relative to whether the substructure was reused or discarded after each flight. It was felt that in the event that Concept 9 proved to be the most desirable the decision on whether to reuse or discard the substructure could be deferred to a later time. On the other hand Concept 4 being in Group B represented a totally different approach to vehicle refurbishment as compared to Concepts 9 and 10 taken collectively.

Weightwise Concept 9 is slightly lighter than Concept 4 and it also has a more favorable risk factor rating taken across the board. Additionally, the vehicle turn-around time is somewhat less for this concept. The only negative factor pertaining to Concept 9 relative to Concept 4 is that its total cost is slightly higher. In the final analysis it was concluded that the lower system weight would more than compensate for the modest difference in total system cost. This combined with the other desirable features lead to the selection of Concept 9 as the best refurbishment concept. The decision as to whether a totally disposable system (Concept 10) or a reusable substructures approach (Concept 9) would be the most attractive is left open at this point in time. It would seem, however, that based on these initial estimates for the substructure costs, reusing the substructures in a totally removable leading edge holds a very slight cost advantage.

6.2 Attachments

In view of the fact that a totally removable monocoque leading edge system was selected as the candidate design, all leading edge to front beam attachment

schemes investigated were directed at this type of concept. Besides examining the primary attachment of the leading edge to the wing front beams, the connection (if any) between adjacent leading edge segments was also evaluated. The details of this evaluation and selection process are presented in the following sections along with the governing design criteria.

6.2.1 Design Ground Rules

As with all trade-off studies a set of design ground rules were prepared prior to evolving the attachment schemes. It was intended that these rules define specific operational requirements of the leading edge of the shuttle orbiter, more than the obvious good practice of designing for hardware integrity and maintainability. Accordingly, the following ground rules were specified.

1. No more than two extra segments need to be removed in order to remove a given segment.

This rule is a compromise between the two extremes of sequential and random removal (see schematic, figure 73) should a segment require reinspection and/or removal before flight. The arguments against sequential removal are: a) the time and expense of removal of all the segments; b) the desire to limit (for reliability) to twice the handling of a segment even if during inspection there were a need to remove more than once a given segment. On the other hand, completely random removal is somewhat too stringent a requirement that is not really justified per se and may eliminate outright potentially interesting attachment concepts.

The implementation of the semisequential approach set forth above would require key segments (externally removable) at every sixth L/E element in order to meet the no more than two segments be removed to remove a given segment. This is illustrated in figure 74, where left to right removal sequence would

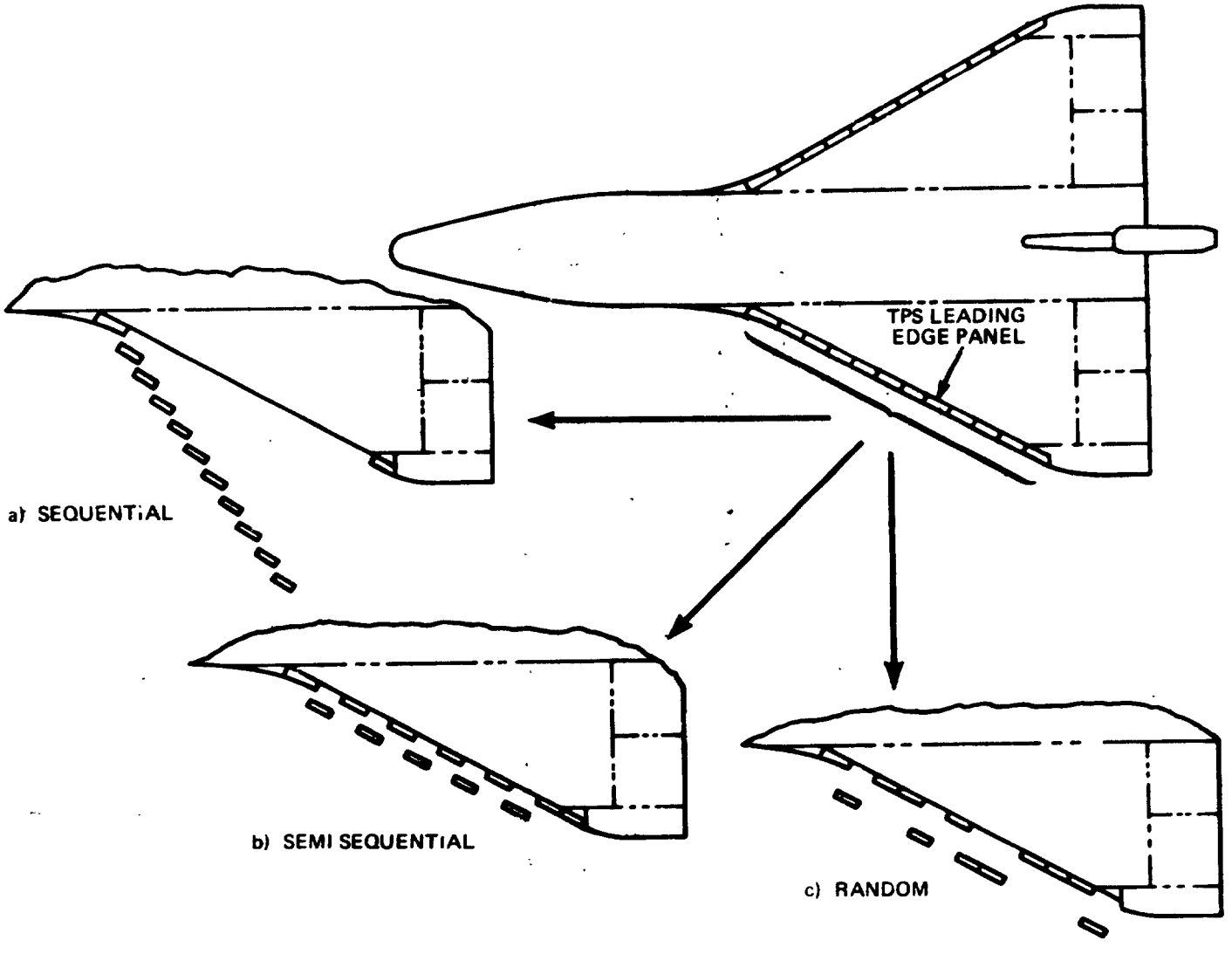

Figure 73 Leading Edge Installation Concepts

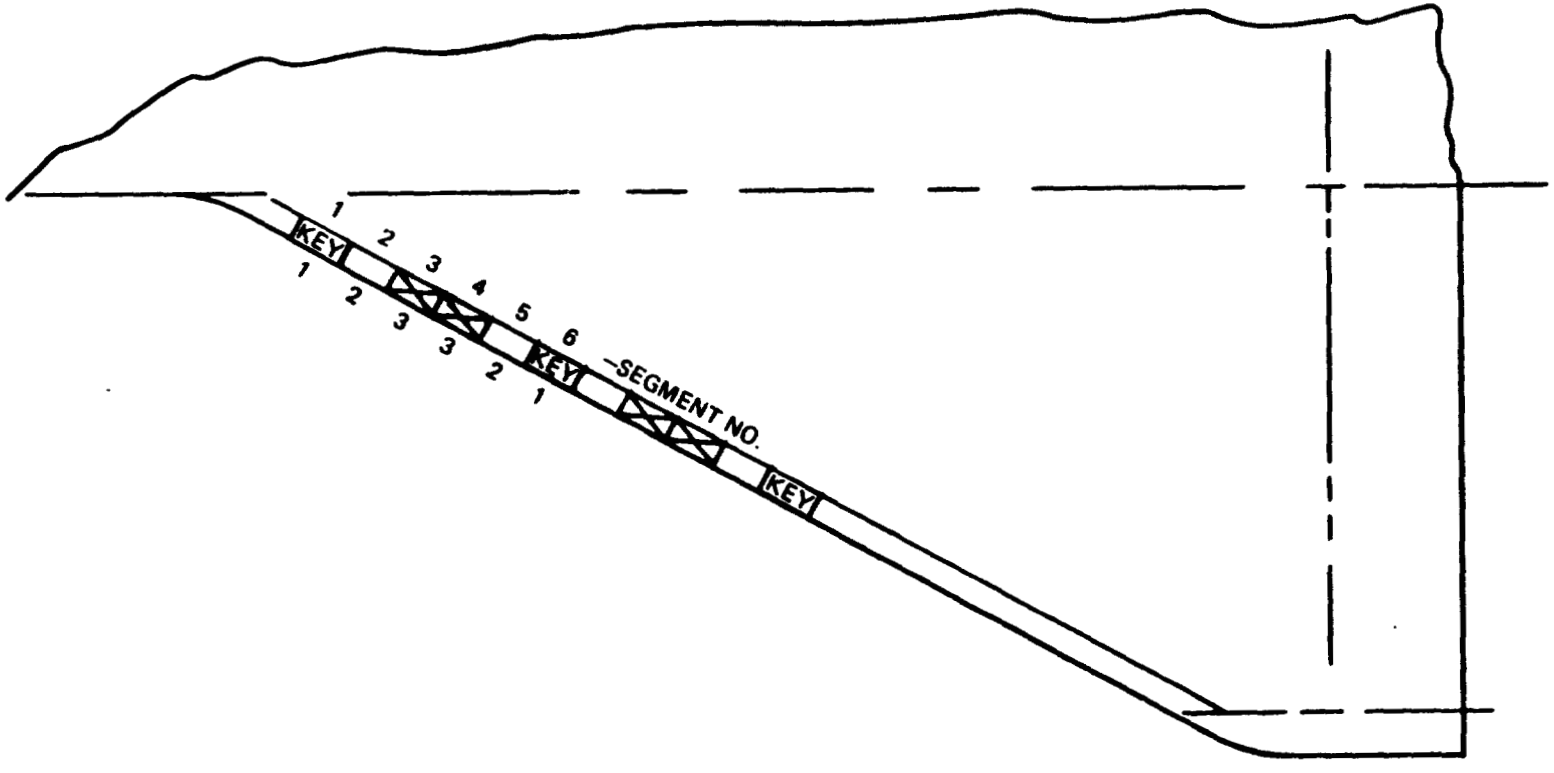

Figure 74 Semisequential Leading Edge Segment Removal

be employed to remove the third inboard segment, whereas a right to left approach would be utilized to remove the fourth inboard segment. A repeating spanwise pattern of this type would be needed as a minimum to meet this ground rule. It should also be possible to install segments in each wing simultaneously so that with a reasonable operation (e.g., 2 shifts and 2 crews of 8 each) the l.e. refurbishment time is well within orbiter turn-around limits (150 to 250 hrs.).

2. No access to the front beam shall be relied upon from inside the wing, as had been envisioned at one time during Phase B of the Shuttle Program. This rule is justified by the desire:

a. To maintain flexibility of the ablative l.e. design with respect to the orbiter configuration in that the attachment should be applicable to a double-delta orbiter where access to the (thin) forward wing may not be possible or to orbiter configurations with l.e.'s of small radii ($\sim$ 3 - 4 inches).

b. Assure that the ablative l.e. design can be easily adapted to one that is interchangeable with the carbon/carbon system or to one that admits RSI ahead of the front beam, though the ground rules (see Section 2) do not require to consider these possibilities. The most natural adaptation to such a case would be to substitute a nose spar for the front beam in our design. However, accessibility to the nose spar from inside the wing may well be impossible.

c. To provide independence of the l.e. refurbishment from the refurbishment of rest of the vehicle, which is strongly suggested by the tight turn-around time required for the orbiter (150 to 250 hrs.). Independence

assures parallel rather than series operations.

d. To eliminate, at least for the l.e. refurbishment, the somewhat exotic operation for having a person crawl into the wing through the gear opening.

3. No removal of a RSI tile or a plug through the RSI shall be required for the segment attachment. The reasons for this rule are:

a. Independence of the l.e. refurbishment as stated in Number 2c. above.

b. Good design practice for reliability. The RSI tiles ideally need not be removed except after a hundred flights or so while the ablator is changed after each flight; therefore, if a plug is needed it should be through the ablator and not the RSI.

6.2.2 Leading-Edge-to-Wing-Front-Beam Attachment Schemes

In general there are three basic approaches which can be employed to make the primary attachment between the leading edge and the front beam. These include direct bolting, continuous attachments, and quick release mechanisms as illustrated in figures 75 through 78.

The most fundamental approach is by direct bolting as depicted by figure 75. There are a number of variations which could be made on this basic concept, however, consistent with ground rules Nos. 2 and 3 all access to the bolts must be made through the ablator L/E. Obviously, all segments would not have to employ bolts passing through the H/S and covered by bolt plugs as shown in figure 75. Rather, external bolting could be used for selected L/E segments (every sixth segment - ground rule No. 1) with internal bolting (see figure 76) employed for intermediate segments. Of course such an approach carries with it the requirement that access to these internal bolts

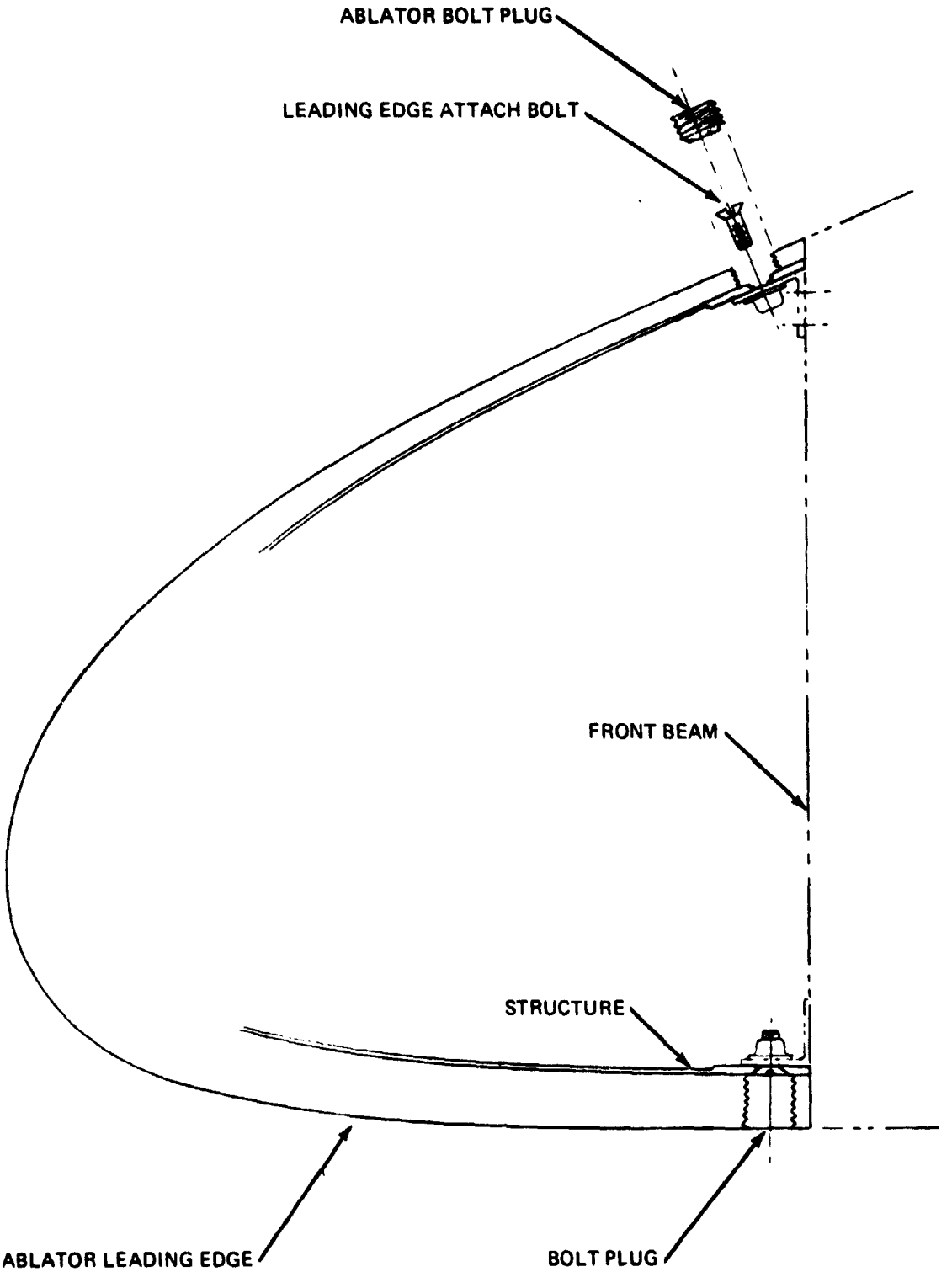

Figure 75 Bolt On ~ External Access

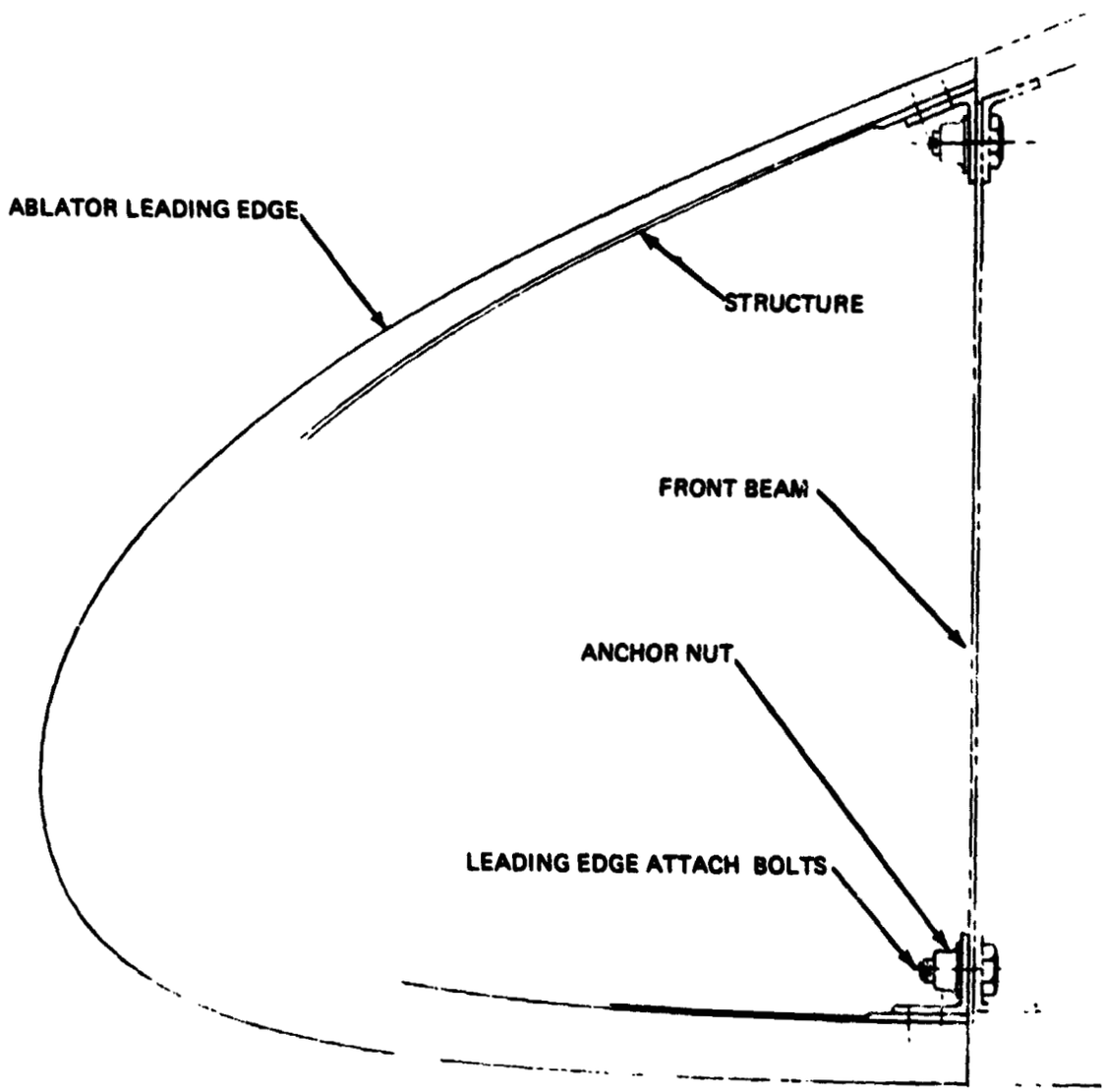

Figure 76 Bolt on ~ Internal Access

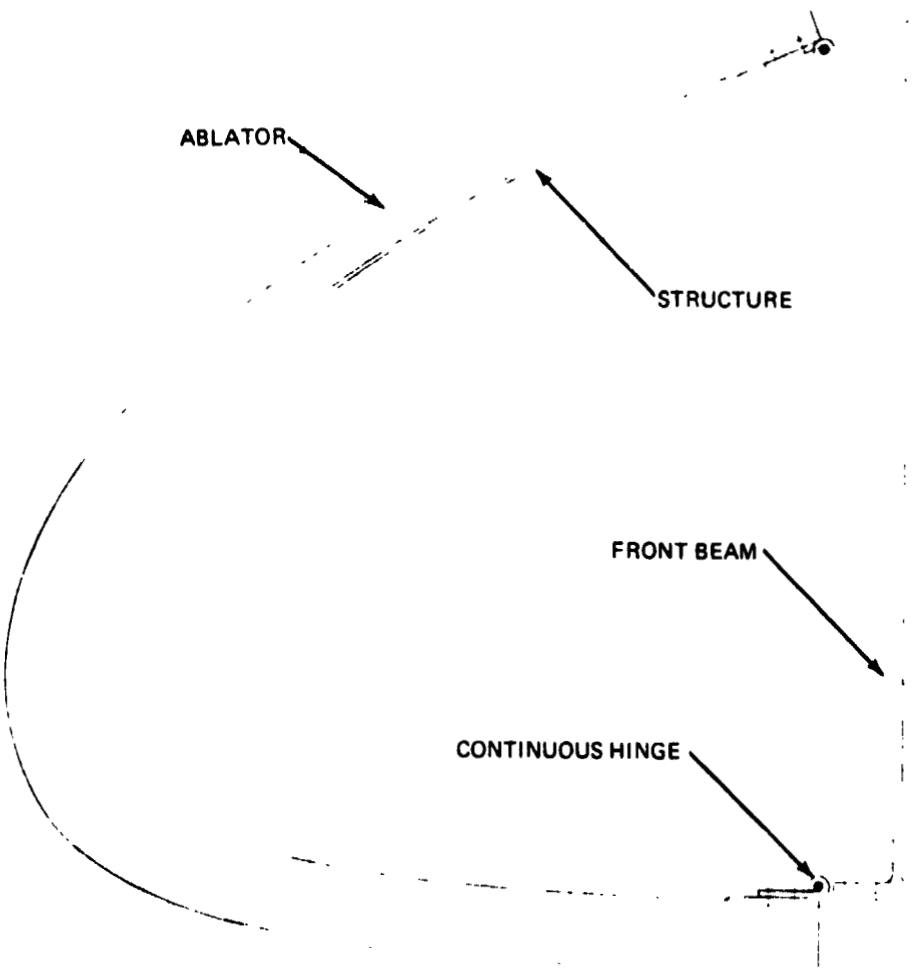

Figure 77 Hinge Pin

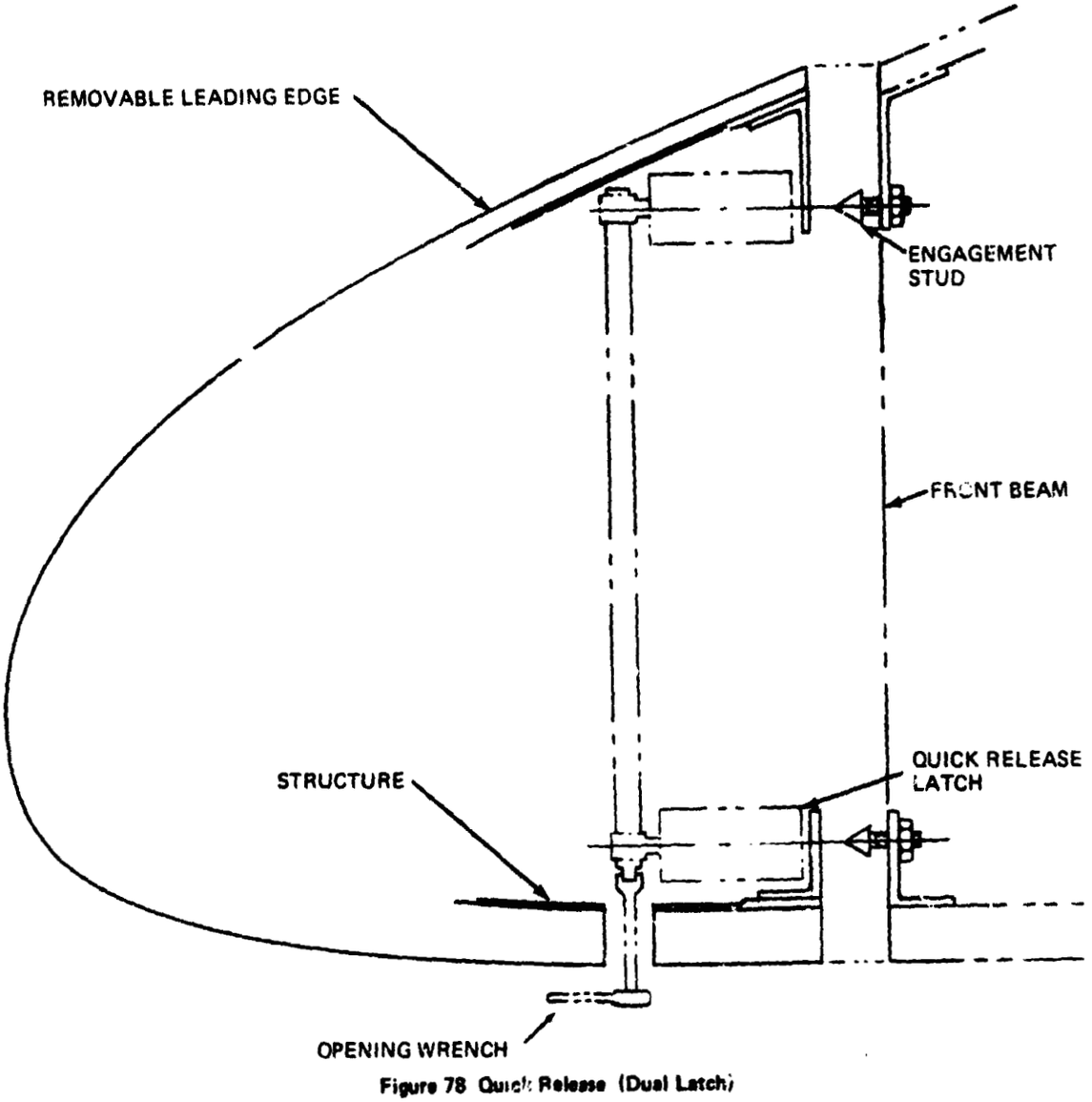

Figure 78 Quick Release (Dual Latch)

drawal of the upper and lower hinge pins. This concept has the obvious advantage of quick removal and also quick replacement. Attendant with the pin removal, however, is the need for internal access necessitating an alternative removal scheme for selected key segments (regarding ground rule No. 1). This could be accomplished by combining the direct bolting approach for the key segments (every sixth) and hinge pins for the remainder.

The third attachment scheme identified encompasses the broad area of quick release mechanisms. In some instances these fasteners would be used in much the same manner as the external bolting scheme depicted in figure 75 with the added advantages of faster refurbishment and greatly simplified ablator penetration. Typical of this type are the Pres-Loc and Dzus fasteners shown in figure 78. The Pres-Loc fastener can be engaged and released by applying a force through a 0.10" diameter hole in the ablator. The difference in engaging and release force provides a means of engagement verification. The standard Dzus fastener again requires only a small hole (.188") through the ablator and engagement and release is effected by a one-quarter turn of the hexagonal nut. Alternative quick-release attachment schemes considered included dual latching release hinge assemblies and the Plus Latch System. The dual latch release hinge is simply a type of short hinge where the pins are spring loaded and can be quickly disassembled by sliding back and latching the pin in the release position. This scheme again requires internal access. The Plus Latch System is shown in figure 79 and combines the desirable aspects of external operation, self-alignment and draw-down capability.

6.2.3 Trade-Off Studies of L.E.-to-Front Beam Attachments

Qualitatively the pros and cons of the various schemes are indicated in table 75. From an examination of the more obvious selection criteria it becomes apparent that in order to make an intelligent selection of the L/E attachment,

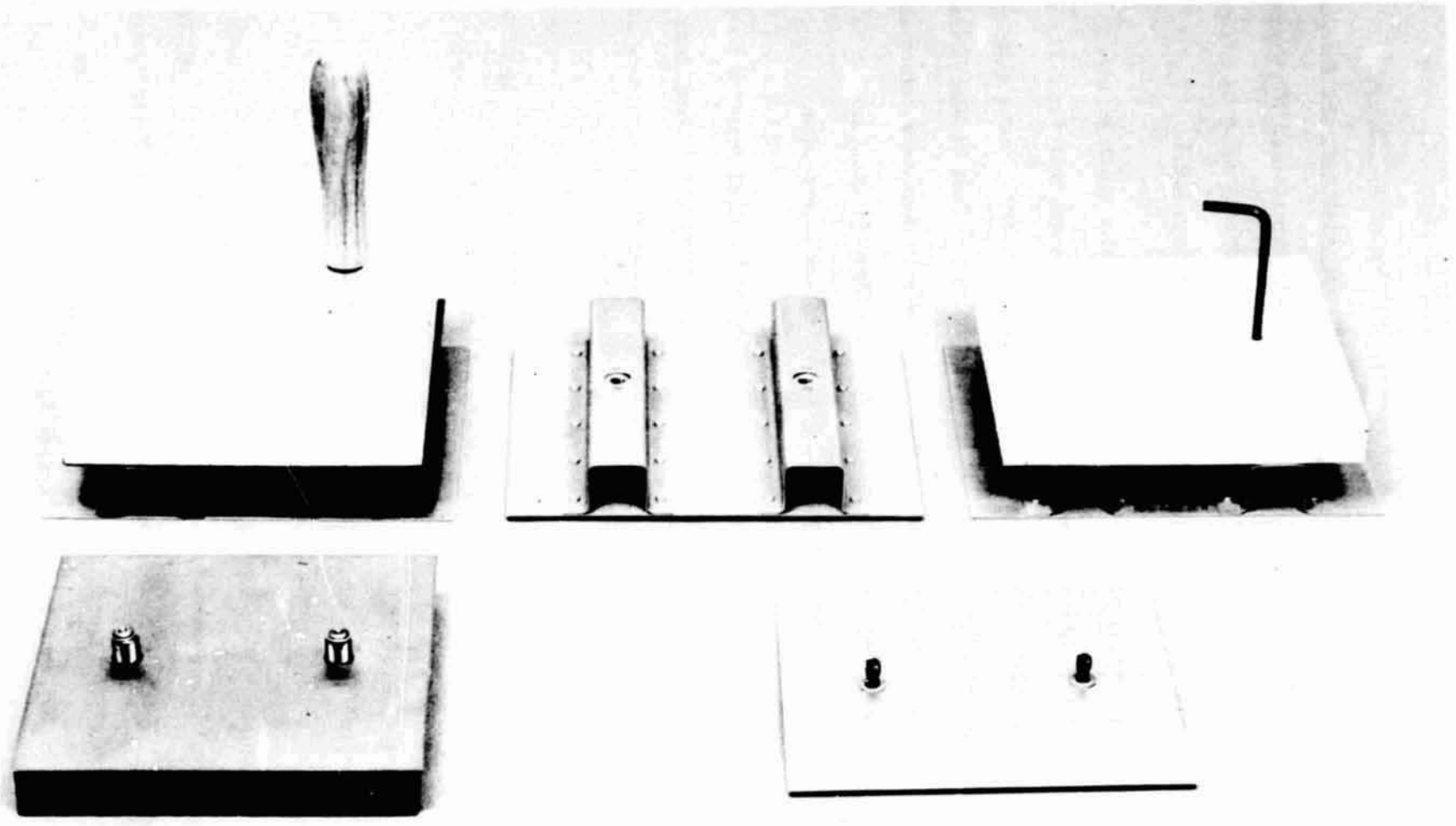

Figure 79 Pres-Loc and Dzus Quick-Release Fasteners in a Flat Panel Application

a more in depth investigation would be needed. For instance, calculations indicated that the structural loads at the front beam attachment are modest such that all attachment schemes presented are viable candidates. Furthermore, with some minor alterations, each of the approaches proposed could be designed to satisfy all the basic ground rules set forth in Section 6.2.1.

Also, with the exception of the Hartwell Plus Latch System which employs a mechanism to activate the attachment, it could be concluded that the difference in weight between the various other schemes would be minimal. Costs also proved to be inconclusive since on the one hand bolts are less expensive than the quick release mechanisms, whereas with quick release fasteners refurbishment time for the vehicle would be less. Here the piano hinge seemed to be more favorable both in terms of initial cost and refurbishment time.

Higher reliability of bolts and the piano hinge could be cited relative to the quick release mechanism, bu this would only be conjecture since there has been little experience acquired with quick release fasteners in this type of applicator.

The key question should be one of ease, simplicity, consistent rapidity of the operation of installation and removal of the typical segment. The schemes appear essentially comparable from this point of view.

This was borne out by the evaluation of the schemes using the two Avco leading edge mock-ups (Ref. 2). Figure 80 shows Mock-up No. 1 which contained bolt plugs to fasten the H/S panels, and a combination of bolts and piano a hinge to attach the nose cap. Figure 81 shows Mock-up No. 2 consisting of two leading edge segments. The left hand segment is attached using the Plus Latch System shown disassembled in figures 81 b and c. The nose cap of the right hand segment employed the dual latch hinge shown disassembled in figures 81 d and e.

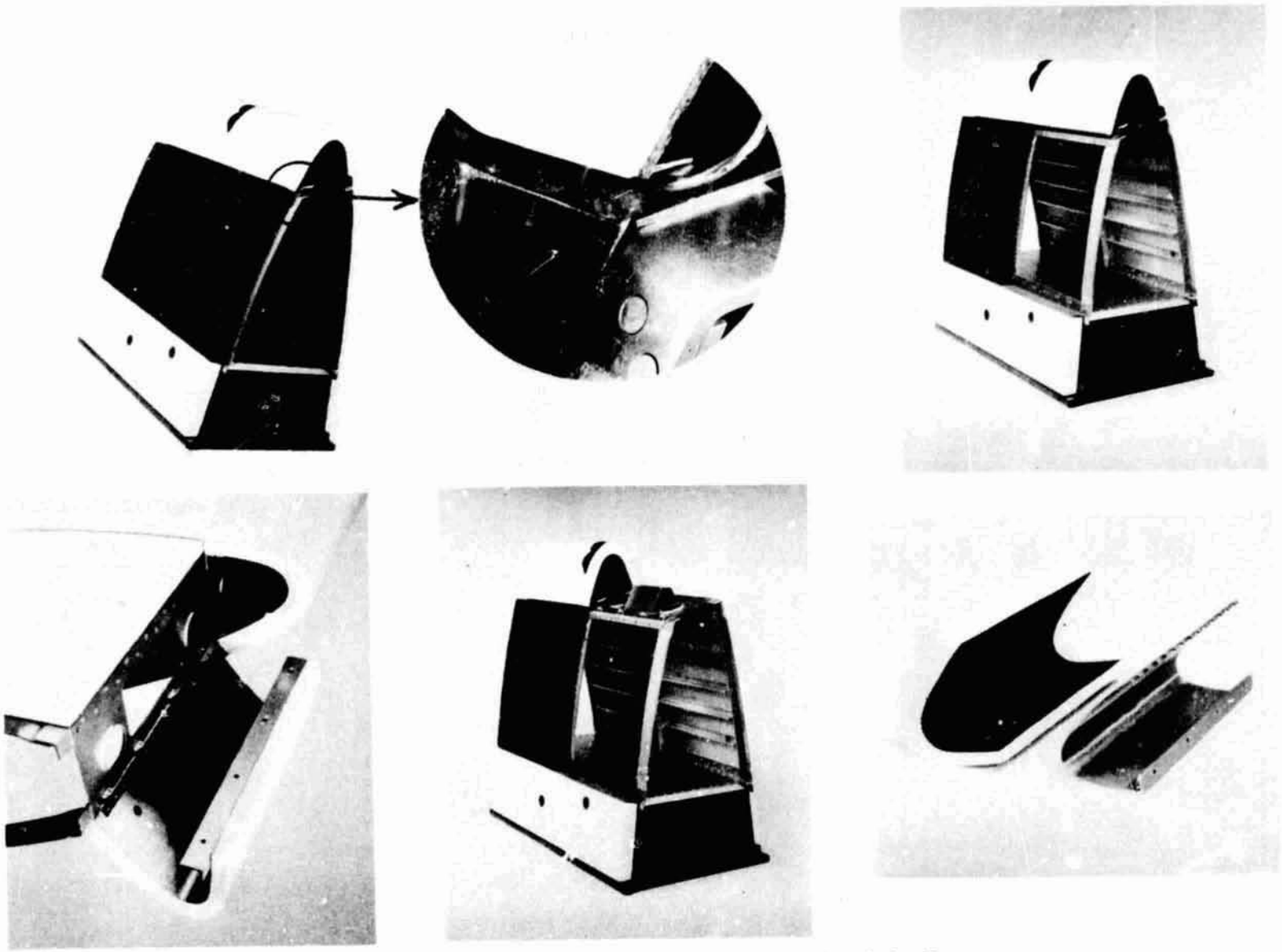

Figure 80 Nondetachable Forward Structure Mock-Up. Ablator Panels Attached to Structure

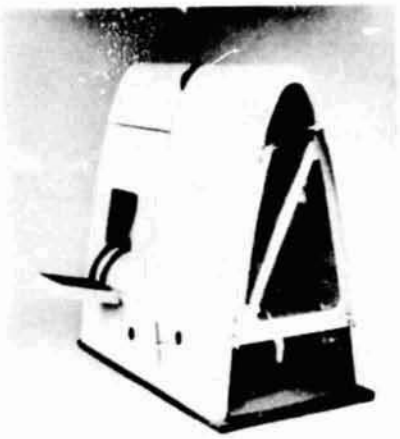

a

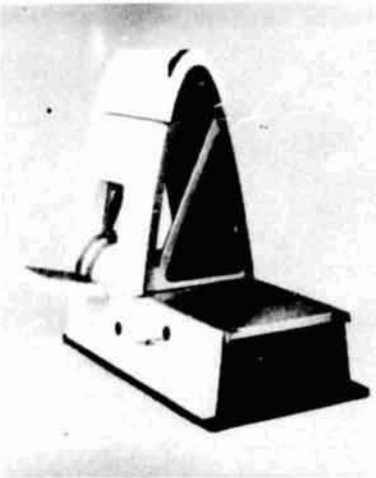

b

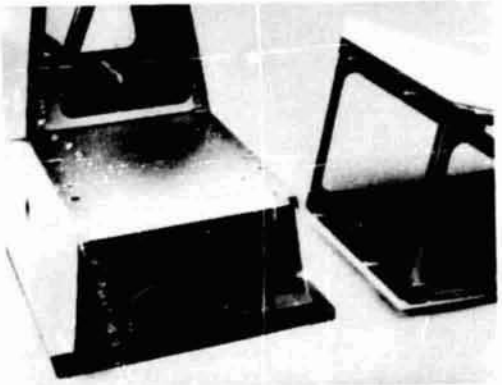

c

d

e

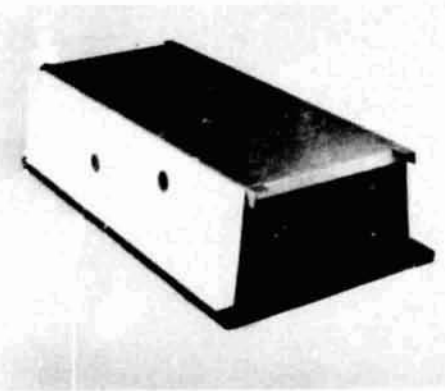

f

Figure 81 Detachable Forward Structure Mock-Up

Naturally, mock-up tests are carried out in somewhat ideal conditions, definitely better than the operational environment and therefore caution is required in interpreting the results.

The one item that tended to discriminate between the schemes was the structural concept selected for the design of the substructure, i.e. uncoupling the leading edge from the front beam in the spanwise direction (see Section 6.4.2).

For the bolted or quick release method of attachment a means had to be implemented to allow for free spanwise expansion. One approach envisioned was to fix the segments at their midspan and use slotted holes for the remaining connections. This would allow for free expansion in both spanwise directions with the center tie providing a fixed reference point. Such an approach was eliminated because of the concern registered by the Grumman design personnel relative to unsatisfactory performance of slotted holes in this type of application. Grumman's recommended procedure for connections which have preferred directions of movement is to use flexible members which allow movements through deformation. As a result the proposed scheme would still have a central fixed tie but the ends would have connections with built in spanwise flexibility. Alternatives to this would be to have connections at either end of the segment only, with one end fixed and the other floating. In either case the number of bolts or fasteners per segment would be minimal (4 to 5), making both the connection detail more complex as well as affecting the structural design of the leading edge. With these discrete connections the leading edge structure would have to be reinforced at the upper and lower edges along the attachment interface in order to distribute the surface loads into the connections. Additionally, since both positive and negative pressures were considered, these edge members would have to form an integral part of the leading edge assembly. With the rib stiffened designs selected (see Section 6.4)

this added member tended to complicate the fabrication procedure.

In comparison the piano hinge concept provides a continuous means of attachment which can accommodate free spanwise relative motion between the front beam and the leading edge. Moreover, the continuous edge support is structurally more desirable for reacting the relatively uniformly distributed spanwise pressure loads experienced by the leading edge segments resulting in a clear structural design.

The combined attributes of low initial cost, short vehicle turn-around time and overall design simplicity make the piano hinge an attractive concept. This attachment scheme readily lends itself to a semi-sequential installation and removal approach. The strongest objection to the piano hinge concept is a general feeling that the pin might be difficult to remove after being subjected to the severe flight environment. It was noted that most prior applications of this approach for attaching flaps, cowlings and ailerons allowed the part to be rotated while extracting the pin a freedom that does not exist in this application. Counter arguments in favor of the piano hinge were: the pin would be used only once, its length of about 30"-36" is not excessive; the method of installation and removal includes a small drill attachment which could rotate the pin while being inserted or extracted; and finally since the pin is protected the flight environment would be probably less severe than equivalent components on conventional aircraft.

6.2.4 Selected L.E.-to-Front-Beam Attachment.

The piano hinge concept was selected because of the simplicity of the structural design and the absence of strong objections with regard to the difficulty of inserting the pin over and over again in the hinges fixed with the wing. The hinge will be of stainless steel.

For standardization in design all leading edge segments will be held in place using the piano hinge. For all but the key panels the leading edge portion of the hinge will be permanently attached to the L/E with rivets and these segments will be installed on the vehicle in a sequential manner. In the case of the key panels, located at every sixth segment, (ground rule No. 1) the hinge will be bolted to the leading edge. These bolts will be externally accessible through the ablative heat shield by the removal of bolt plugs. During refurbishment the bolts would be removed and the entire hinge would remain on the vehicle.

The use of the hinge pin to attach the key panels provides for a consistent method of obtaining the spanwise uncoupling. Additionally it also affords an opportunity for totally sequential refurbishment where all segments, with the exception of the initial segment, can be removed simply by withdrawing the hinge pin. The question of the segments' removal and installation procedure will be taken up later, once the number of segments is defined, in Section 6-6.

6.2.5 Selected Segment-to-Segment Attachments

The possibility of employing a positive connection between segments in the chordwise direction to couple them together in the spanwise direction was also investigated. As the design developed it became readily apparent that there was no need for such a connection, in fact all arguments were to the contrary. Structural design calculations showed that it would be more advantageous to allow each segment to act independently both from the standpoint of minimizing the mechanical loads as well as allowing for differential thermal expansion. Systems requirements also dictated that the fewer the connections the better for quick vehicle turn-around.

As a result, the only piece of structure used in the joint area is a false rib (see figure 70) which was included to close off the rear surface of the

joint and act as a former to provide a means of alignment for the L/E segments during assembly. There is no positive attachment between the L/E and these ribs but they will tend to retain the continuity of the L/E across the joint when subjected to air loads.

6.3 Ablator Design

The main contributor to the weight of the leading edge is the ablator material. Therefore, it is critical to review the design considerations and define the safety factor rationale so that a reliable (but not overly conservative) design is produced. This section describes the approach used in defining the reference design together with the final results. All results shown here are based on the Avco Mod 7 Hc and ESA 3650 HF materials.

6.3.1 Design Thermal Loads

Table 31 summarizes the heating data for various locations on the Grumman 473 orbiter leading edge that were utilized in sizing the ablator heat shield. Maximum values are presented for ascent (nominal and abort-to-orbit) and reentry (nominal and dispersion). For ascent the nominal condition provides the highest integrated heating with only slightly lower rates than the abort-to-orbit case. For reentry the integrated heating for both the nominal and dispersion case is quite close with the dispersed heating rates, about 20% higher. The heating values shown in table 31 and used in defining the heat shield requirements do not include the effects of shock impingement (see Section 2).

Of additional interest is the relationship between the ascent and reentry heating. Table 32 summarizes the heating at the midspan region for various locations around the leading edge. As can be seen the maximum total heating occurs where the reentry heating is a maximum. It is also important to note

Table 31 Summary of Leading Edge Heating Stagnation Line of GAC 473 Orbiter Wing

Trajectory	$\dot{q}_{Max}$ (Btu/ft^2-sec)			Q_{Total} (Btu/ft^2)		
Ascent	Tip	Mid-Span	Root	Tip	Mid-Span	Root
Nominal	12.4	12.4	12.4	6,100	6,100	6,100
Abort to Orbit	14.2	14.2	14.2	4,440	4,440	4,440
Reentry						
Nominal	51	51	45	64,200	64,200	57,100
Dispersion	60	60	52	64,300	64,300	55,200

Table 32 Summary of Heating Distribution at Mid-Span Location (GAC 473 Orbiter)

Location (% Chord)	Nominal Ascent (Btu/ft^2)	Nominal Reentry (Btu/ft^2)	Total (Btu/ft^2)
-10.0	548	643	1191
-5.0	1035	1288	2323
-3.0	1645	1927	3572
-2.0	2135	3215	5350
-1.5	2745	4503	7248
-1.0	3660	5142	8802
-0.5	5185	11572	16757
0	6100	41795	47895
+0.5	5915	64300	70215
+1.0	3355	63010	66365
+1.5	1707	61084	62791
+2.0	915	57869	58784
+3.0	548	48224	48772
+5.0	548	23788	24336
+10.0	548	17363	17911

that the ratio of ascent to total heating varies from 45% at the leeward joint to 8.4% at the stagnation point to only 1 - 3% along the windward side. It is obvious, therefore, that ascent heating must be accounted for in defining the heat shield thicknesses particularly in the leeward regions where the effect may be quite pronounced.

6.3.2 Thickness Predictions Charts

To establish some initial estimates of heat shield thickness, calculations were performed using the Avco charring ablation code (Computer Program 2500). The transient environment as defined in Section 3.5 and the material properties as shown in Section 3 of Volume 2 were used in the calculations. The results of these calculations are shown in figure 82 which indicates the thickness requirements of the Avco Mod 7 and ESA 3560 HF as a function of maximum structure temperature (allowing for soak out) for two integrated heating conditions. Figure 83 indicates the local weight (lb/ft^2) for the two materials as a function of integrated cold wall heating for a limiting structure temperature of 350°F. The two conclusions to be gained from these data are (1) Avco Mod 7 HC and ESA 3560 HF have apparently the same thermal efficiency, and (2) the ablation thickness on the leading edge will vary from about 1-3 inches over the contour of the surface.

In order to establish ablator thicknesses on the leading edge it is necessary to determine the effect of ascent heating. The effect varies over the leading edge due to the relationship between ascent and reentry heating shown earlier (see table 32). Figure 84 indicates the result of this study for the Mod 7 Hc material. Two conditions are shown, one for the case of reentry with virgin material and the second for reentry with an ascent char. The curves indicate that approximately 0.16 inches must be added to the virgin material thicknesses in areas where the ascent heating is $\approx$6,000 Btu/ft^2 while in lower

ABLATOR REQUIREMENTS FOR A GIVEN MAXIMUM STRUCTURE TEMPERATURES

ABLATOR + 0.03" BOND + 0.06" ALUMINUM

- INITIAL TEMPERATURE = 100°F
- 473 ORBITER, NOMINAL ENTRY TRAJECTORY

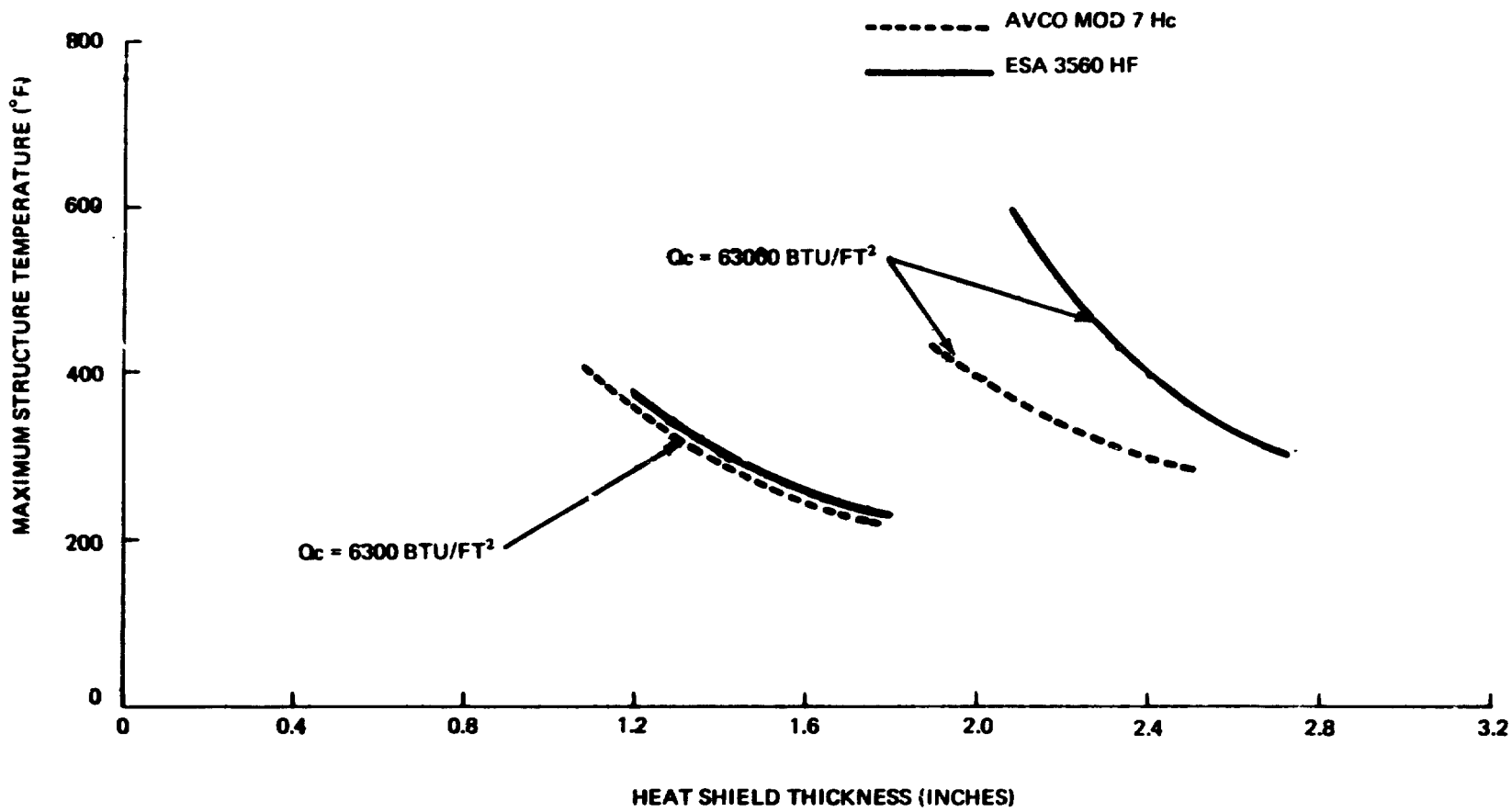

Figure 82 Ablator Requirements for a Given Maximum Structure Temperature

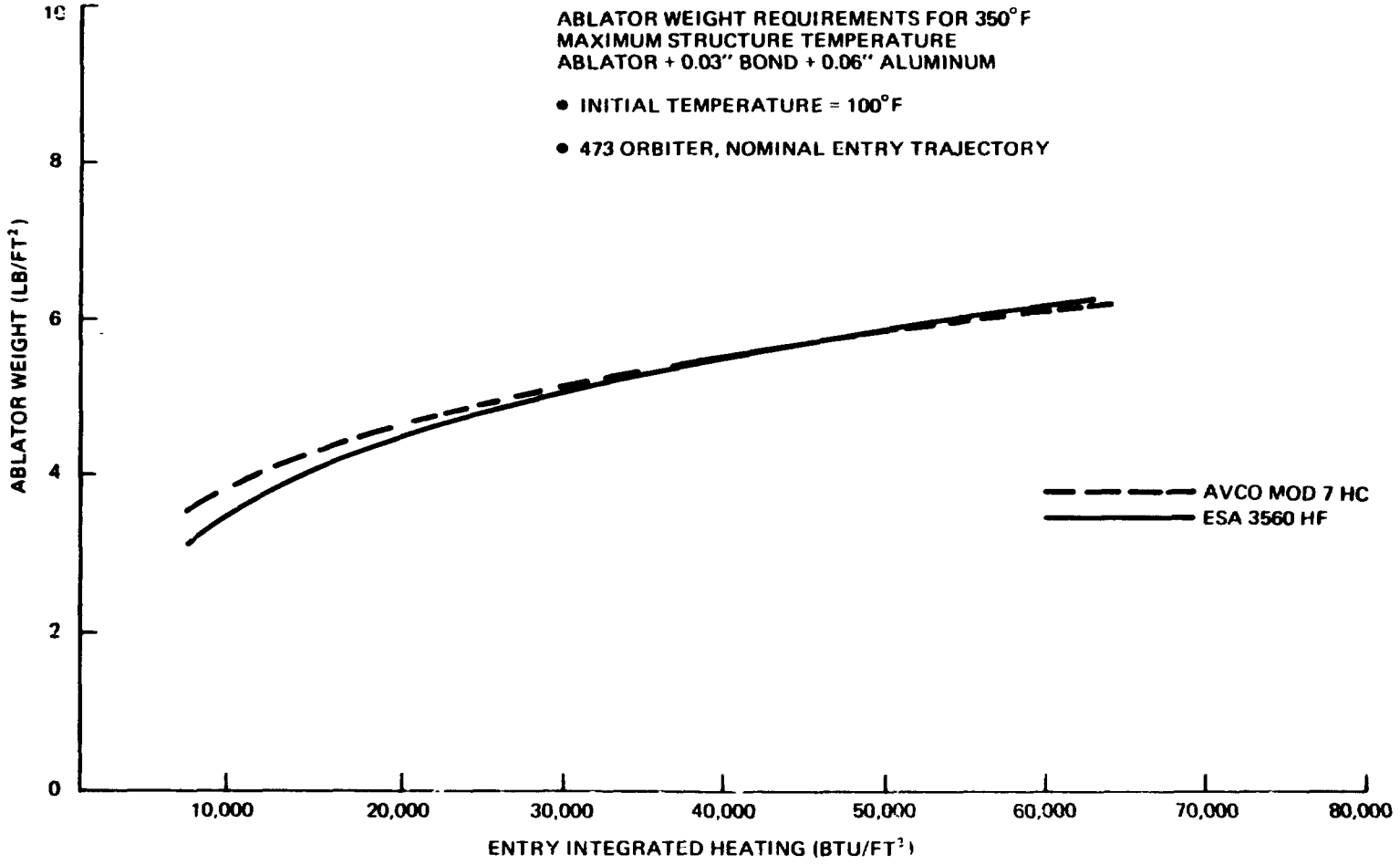

Figure 83 Ablator Weight Requirements for 350° F Maximum Structure Temperature

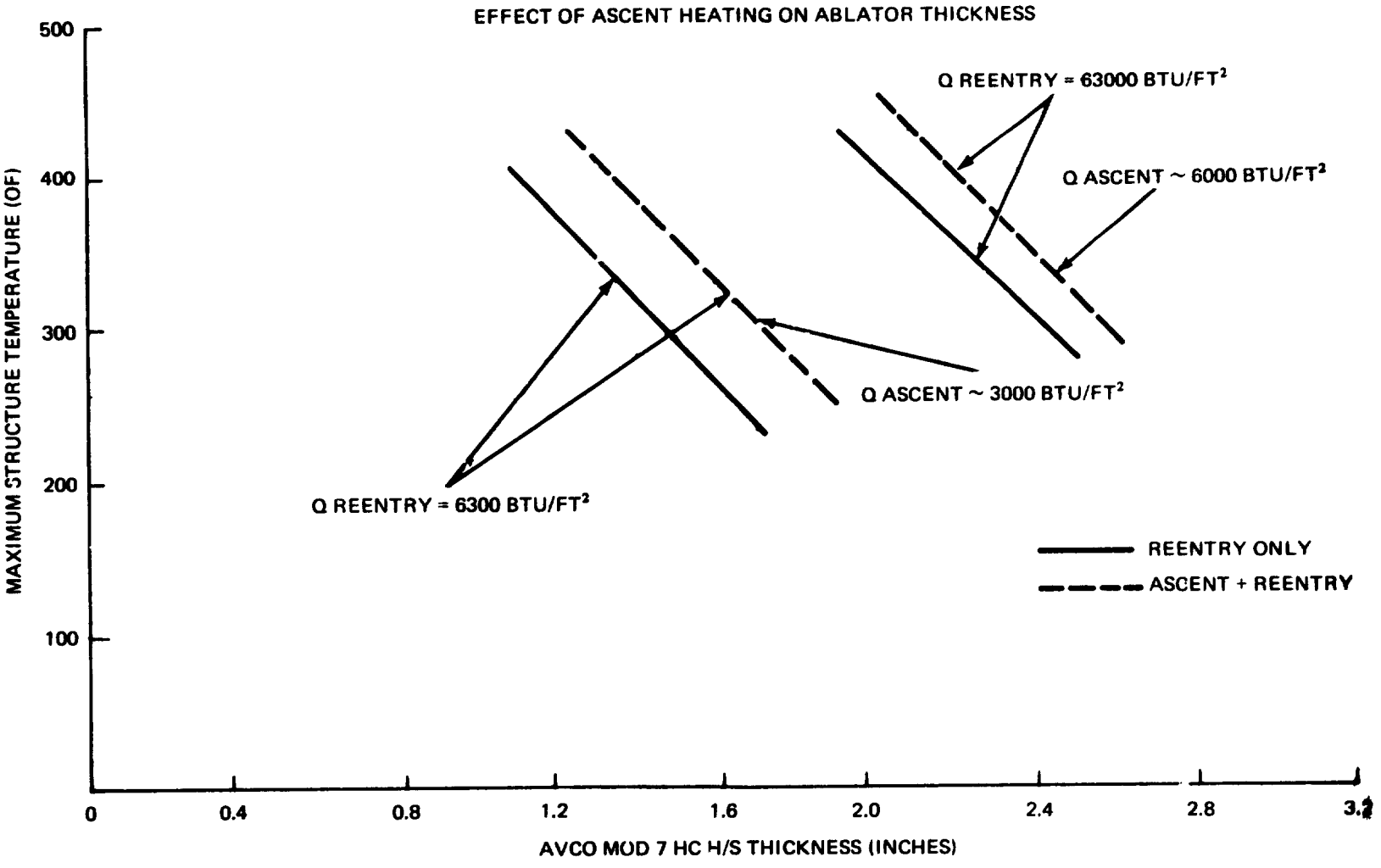

Figure 84 Effect of Ascent Heating on Ablator Thickness

heating areas (≈3,000 Btu/ft^2) additional 0.26 inches are required. This apparent inversion is due to the fact that in the locations where ascent heating is low the heat shield is relatively thin, hence the percentage of material which is charred during ascent is greater than in regions of higher ascent heating where the reentry environment controls the thickness. Figure 85 shows the Mod 7 Hc char thicknesses developed during ascent as a function of heating level. While these data were examined for Mod 7 Hc only, the magnitude of the increase in thickness for the ESA 3560 HF should be similar.

Figure 86 indicates the heat shield requirements for various total heating levels (ascent and reentry) for both Mod 7 and ESA 3560 HF using a bond line temperature of 350°F. This curve was employed in defining the heat shield thickness variation around the vehicle. Figure 87 shows the char depth levels that can be expected with the various heat flux levels. Note that for the reentry environment currently anticipated for the leading edge negligible recession is predicted for either Mod 7 Hc or ESA 3560 HF. The total char thickness is seen to constitute about 60% - 70% of the thickness for a bond line temperature of 350°F, with 0.6 to 0.8 inches of virgin material left after entry.

6.3.3 Safety Factor Rationale

In order to establish a realistic design for the ablator leading edge it was necessary to define safety margins which will provide adequate confidence of success while at the same time not being unduly conservative. There are several approaches used in defining the safety factor including using multipliers on the aerodynamic heating (e.g., Ref. 59), using conservative properties (e.g., Ref. 60), and also adding a specified material thickness (e.g., Ref. 59).

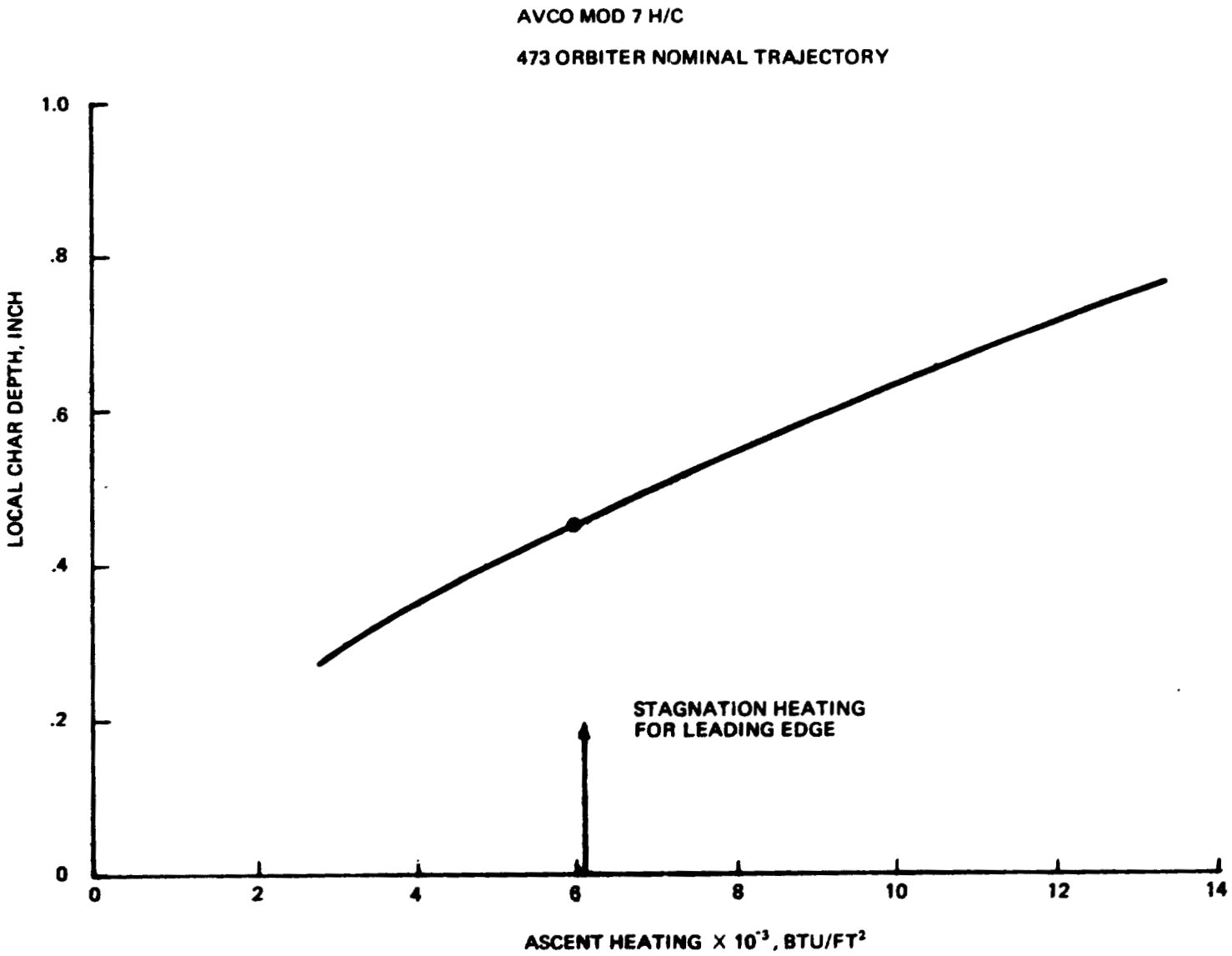

Figure 85 Ascent Char Data For Leading Edge

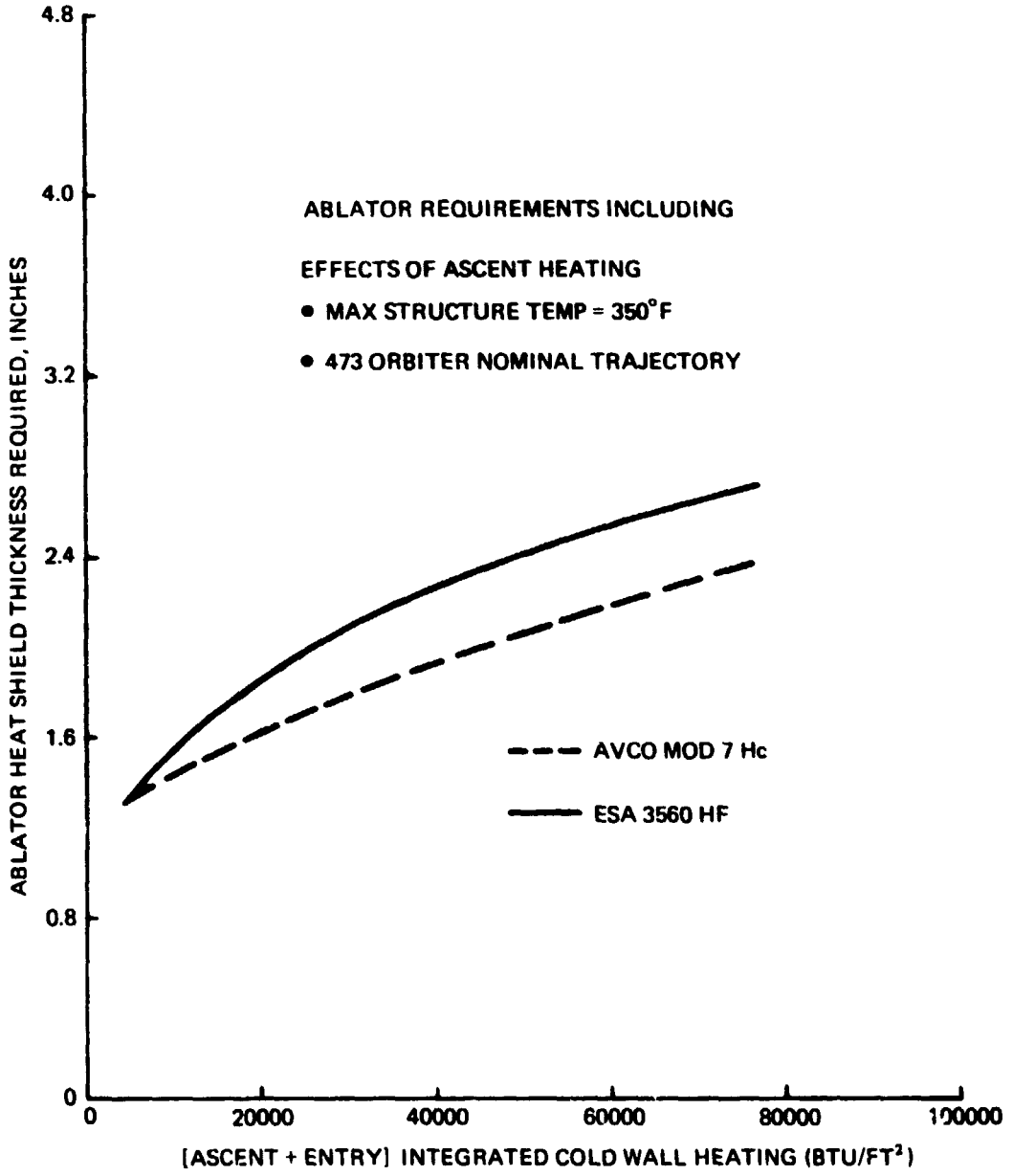

Fig. 86 Ablator Thickness Requirements

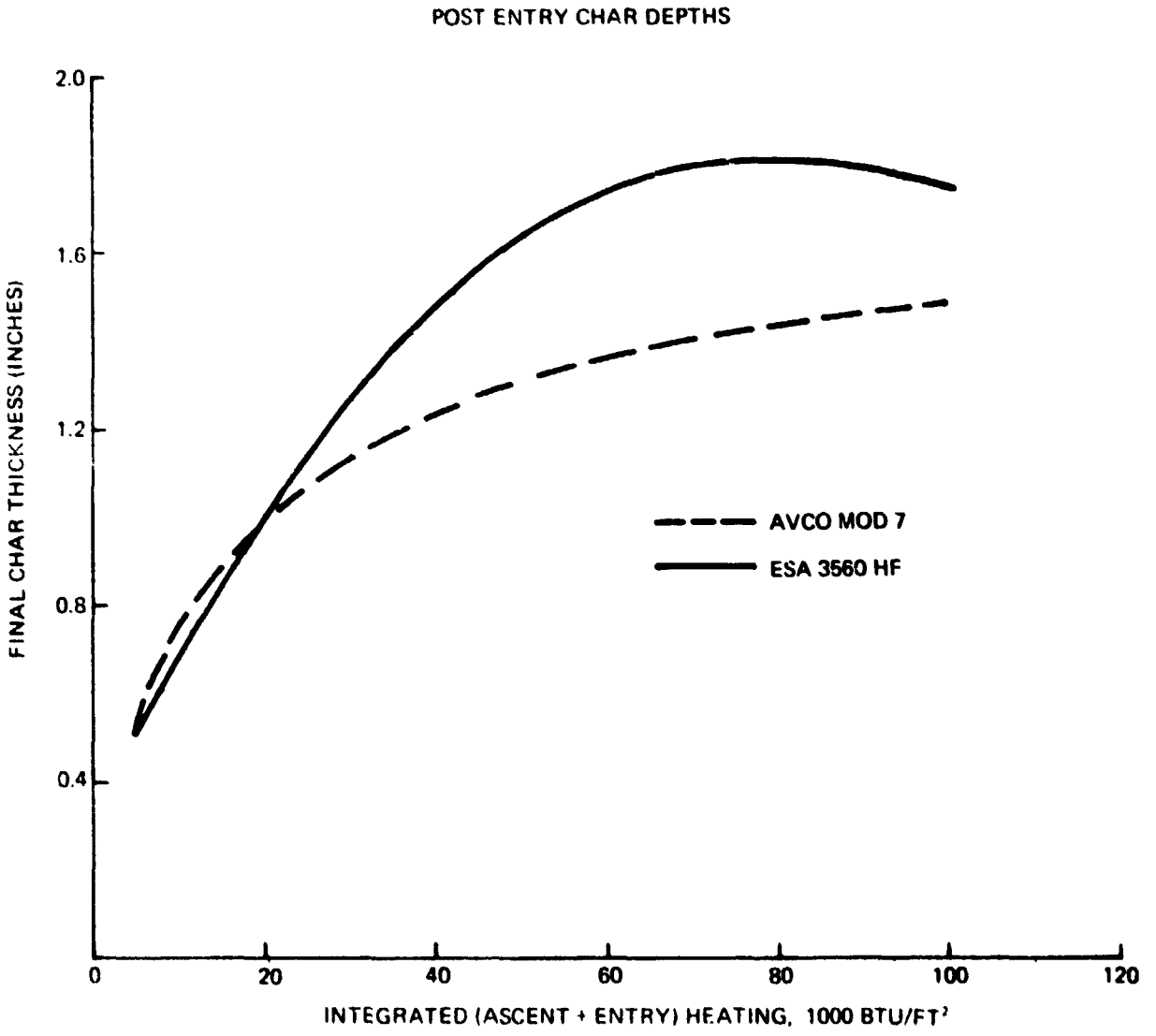

Fig. 87 Post Entry Char Depths

For the design developed in this program the following procedure was used:

1) A multiplier of 1.10 was used on the heating to account for a 10% uncertainty currently considered reasonable for the l.e. of the orbiter (e.g., Ref. 61).
2) An additional thickness was added to the nominal thickness so that a 25°F margin is produced in the maximum structure temperature (i.e. design is based on 325°F). This additional thickness is 0.10 inches.

This approach was used since it accounts for the only uncertainty that can be reasonably defined (i.e. 10% on heating) while at the same time providing a 25°F margin for uncertainty in properties, analytical techniques, accuracy, etc. A 50°F margin would have caused significant weight increases, chiefly on the leeward side, and was thought to penalize considerably the design. It should be noted that there is an additional area of conservatism that is inherent in the design.

The design was based on a "soak out" condition, and the structure temperature does not reach 350°F until after 2500 seconds (nominal touchdown) when the final mechanical load is experienced due to shock. Note that as shown in figure 88 at touchdown the temperatures are 284 and 334° F for the Mod 7 Hc and ESA 3560 HF respectively. These data would indicate that the safety factor, at least for the crew, for the Mod 7 may be somewhat higher than the ESA 3560 HF.

Still another area of safety, at least for the leading edge, follows from the different temperature histories in the ablator and the RSI. It seems that with the projected (and rather conservative) RSI thickness at the ablator/RSI

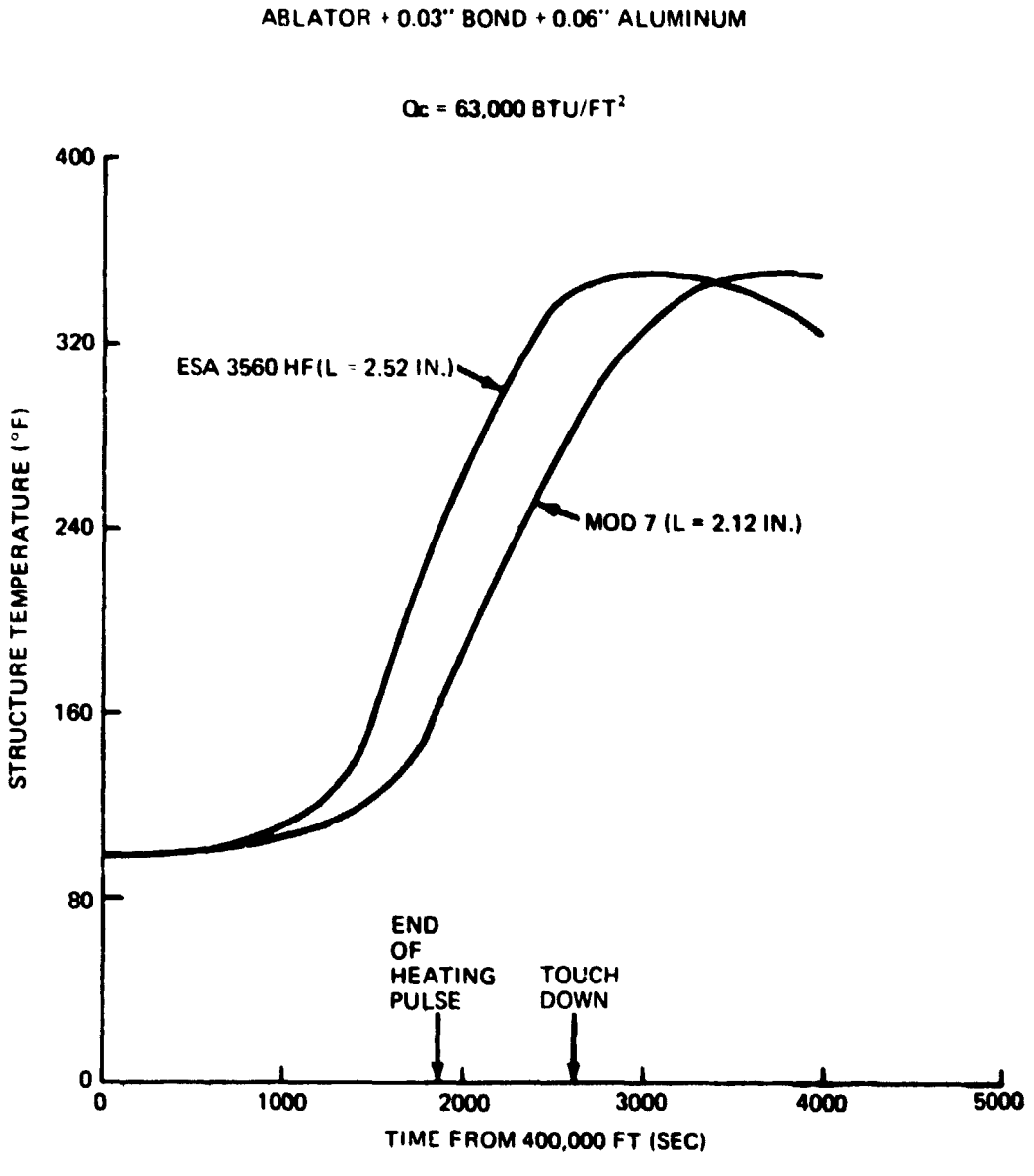

Fig. 88 Structure Temperature Histories.

interface (some 2 to 3 inches), the wing structure will be considerably cooler than the l.e. substructure, thereby setting up lateral conduction to the benefit of the l.e. Therefore especially near the ablator/RSI joint the l.e. substructure will have this added safety.

We feel that the safety factor rationale described above is a reasonable one.

6.3.4 Single Ablator

One of the general rules used during the performance of the effort was that a single ablator (i.e. one material) would be used in the leading edge areas. While this rule appeared to be reasonable in view of the objectives and scope of the program it nevertheless precluded investigation of alternate approaches (i.e. two ablator systems) which could prove to be attractive. In this section we set out brief qualitative comments on the two-ablator system. The most obvious alternate two material system would be comprised of the selected honeycomb ablator in the high heating region (i.e. Mod 7 Hc or 3650 HF) with the introduction of lower density (ρ= 15 lb/ft^3) unreinforced ablator in the reduced heating regions away from the stagnation point. Such an arrangement is shown in figure 89. Whether or not this concept would be advantageous from an overall systems standpoint depends on several factors and the pros and cons of such an approach are listed in table 33. As can be seen, the use of a dual ablator system provides lower weight and material cost but introduces additional complexities into the design. The extent of cost savings (if any) resultant from such a design must include the effects of the additional refurbishment and manufacturing efforts required.

The potential advantages of a dual system will be reduced as the area forward of the front beam covered by ablator is reduced. For example, the present TPS concept used in the shuttle wing is composed of a relatively small area of

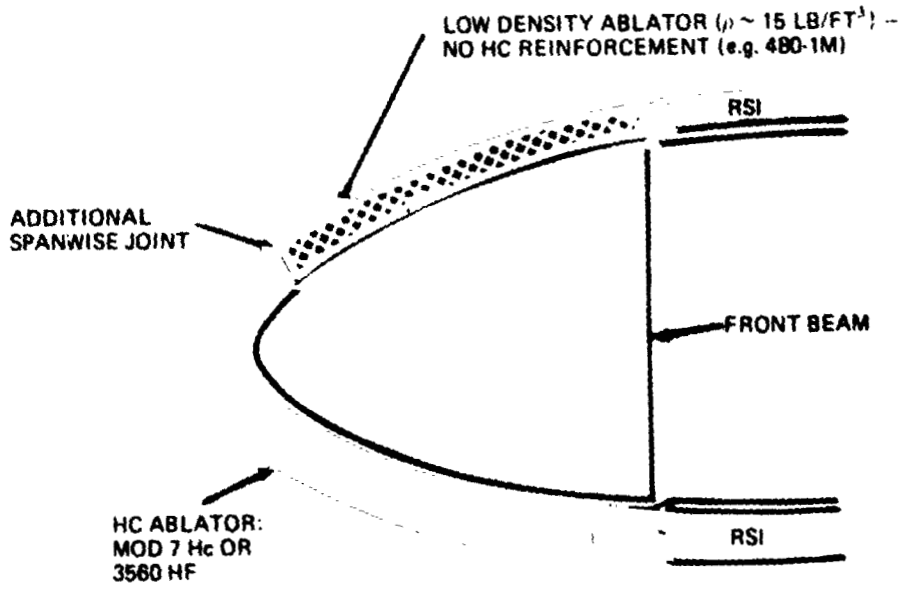

Fig. 89 Double Ablator Leading Edge Concept

Table 33 Tradeoffs in Double Ablator System

Advantages	Disadvantages
A. Lower Weight • Use of low density material will be more efficient.	A. More Complex Bonding Operations • Bonding requirements may be different.
B. Lower Material Cost • No honeycomb. • Lower thickness required because of higher efficiency	B. More Manufacturing Operation Required (Cutting tooling, etc.) C. Additional Span Wise Joint Required D. More Complex Structural Detail at Interface of two Ablator Materials (Dissimilar thickness requirements); more comple· thermal design for minimum weight.

oxidation inhibited carbon/carbon and the remainder of the leading edge (i.e. the region forward of the front beam) is protected by RSI. For this design it would appear to be more practical (and in fact lower in cost) to utilize a single honeycomb material rather than attempt to optimize the concept by incorporating a second material for a relatively small area.

6.3.5 Shape Optimization

One of the major concerns in the selection of an ablator for use on the leading edge is the potential degradation in subsonic performance due to surface recession. The most attractive approach would be to utilize a material which recedes a negligible amount and therefore produces a very small shape change. An alternate concept would be to size the virgin material in such a way so that the shape that exists after reentry is that desired from a subsonic aerodynamic performance standpoint. This latter approach however requires that the recession performance of the vehicle be predictable and this is where a difficulty arises.

The matter would be simpler if experimental data obtained in splash tests, in flat samples and without ascent heating could be used for the l.e. with precharring. Unfortunately this does not appear possible, since in general the elastomers l.e. models tested here showed non-negligible recession, while it has been known for some time that elastomeric materials in flat configuration without precharring recede very little or in fact even expand at relatively low heat flux levels in the order of 50 Btu/ft^2-sec (e.g., Refs. 62 thru 65). Table 34 provides a summary of typical test data (Ref. 63-65) obtained in splash models without precharring at the Avco ROVERS Arc Facility on Mod 7M. The conclusion reached from these data is that only a small amount of recession will occur on the leading edges and perhaps even some expansion will be noted. It is important to recognize that the data shown in table 34 are in

Table 34 Typical ROVERS Arc Test Data on Mod 7M Splash Test-No Precharring

Test No.	Cold Wall Heat Flux (Btu/ft^2-sec)	Enthalpy (Btu/lb)	Test Time (Seconds)	Surface Recession or (Gain) Inches
(479-122)-1	51	10,200	610	(0.014)
(479-122)-2	113	10,400	505	0.015
(479-122)-3	150	9,950	475	0.015
686-7	98	8,400	162	(0.05)
686-8	100	8,400	161	(0.06)
687-17	31	8,500	234	(0.06)
687-18	30	8,500	372	(0.01)
559-4	82	11,300	300	(0.048)

agreement with other data generated at Avco on other elastomeric materials. Note also that the data cover the heat flux and integrated heating range typical of the leading edge (i.e. $q_c \simeq 70$ Btu/ft^2-sec., Q_c 60,000 Btu/ft^2).

Of course, the situation would be even simplier if theoretical data from typical quasionedimensional charring codes that neglect mechanical removal could be used for the present case of l.e. with precharring. Of course, in such codes surface recession is predicted after modeling data similar to those shown in table 34 are used in defining the thermal models. In the case of Mod 7M and the 3560 HF it was found that up to integrated heating levels of 60,000 Btu/ft^2 negligible recession is anticipated in flat samples, no precharring and no mechanical error. However, when data from the tests on the leading edge models with precharring are reviewed, it is clear that the prediction is inadequate. Table 35 summarizes the surface recession of the leading edge model center line for both the Mod 7 and ESA 3560 HF materials. While some expansion is noted in the lower heating regions it is quite obvious that significant recession occurs in the stagnation region.

Therefore, the difficulty announced above is that we have only one set of data on which to base the prediction.

Moreover, even with this set of data, there is the problem of the extrapolation to flight conditions since the total entry heating on the model was only some 16,000 Btu/ft^2 (hot wall) versus a flight value of some 55,000 Btu/ft^2 (cold wall). If the stagnation-point test data are extrapolated to the total heating expected on the vehicle ($Q_c \sim 60{,}000$ Btu/ft^2) it would be expected that [illegible] and 0.45 inches of Mod 7 He and ESA 3560 HF respectively would recede during reentry . However, in view of the previous arc test data where insignificant recession was observed in flat samples without precharring; we feel that the

Table 35 Recession in Ablator Leading Edge Models During Reentry Test at LRC (L/E Models Precharred)

Position		Avco Mod 7 H/C*	Recession or (Gain)Inches ESA3560HF**
	S1	(.023)	(.016)
	S2	(.033)	(.007)
	S3	(.005)	.035)
Stagnation Region	S4	.069	0.13
	S5	.101	.161
	S6	.009	(.004)
	S7	(.016)	(.017)
	S8	(.009)	(.018)
	S9	(.004)	(.005)
	S10	(.014)	(.004)

*Test time = 261 seconds
**Test time = 309 seconds

recession which occurs on the leading edge models during the leading edge tests is in fact mechanical removal of the char layer which was developed during ascent exposure. Therefore we expect that the shape change recorded on the leading edge models would in fact remain at these levels (i.e. negligible further recession) if the Q_c were simulated and should not be extrapolated. This of course should be checked by appropriate tests. It whould be pointed out that the theoretical prediction of recession on the leading edge accounting for mechanical removal of the ascent char is difficult if not impossible based on the limited amount of leading edge data and one set of data including precharring. Considerably more testing of the recession characteristics of these two materials in pressure gradient environments when precharred is required to validate the explanation of the recession measured on the l.e. models and to develop, if desired, the appropriate modeling of the mechanical removal.

In view of this discussion, it is concluded that the most recession that will occur is about 0.10 inches (from table 35) and will drop off rapidly from the stagnation point and in fact some expansion will exist on the windward and leeward sides. Therefore, no adjustments were made to account for this minor recession in the design because of its expected minimal effect on system performance.

6.2.6 Ablator Requirements

Using the data from figure 86, the design safety factors and rationale from Section 6.2.3 and the assumption that the substructure is of aluminum with 350° F maximum temperature, ablator thickness distributions were defined as a function of chord position around the leading edge at the tip, midspan, and root locations. These data are presented in table 36 for both the Avco

Table 36 Leading Edge Ablator Thickness Requirements

Chord Location X/C (%)		Mid-Span		Tip		Root	
		MOD7HC	ESA3560HF	MOD7HC	ESA3560HF	MOD7HC	ESA3560HF
Leeward	10.0	0.93	1.00	0.95	1.02	0.77	0.84
↑	5.0	1.06	1.14	1.08	1.16	1.02	1.11
	3.0	1.21	1.30	1.24	1.33	1.10	1.18
	2.0	1.36	1.44	1.38	1.46	1.26	1.34
	1.5	1.52	1.61	1.54	1.62	1.40	1.45
↓	1.0	1.55	1.67	1.58	1.69	1.48	1.54
Leeward	0.5	1.71	1.94	1.73	1.95	1.65	1.83
℄	0.0	2.13	2.56	2.14	2.57	2.10	2.49
Windward	0.5	2.41	2.84	2.43	2.85	2.35	2.73
↑	1.0	2.37	2.81	2.38	2.83	2.28	2.69
	1.5	2.33	2.76	2.34	2.77	2.24	2.67
	2.0	2.28	2.71	2.29	2.73	2.21	2.61
	3.0	2.23	2.60	2.24	2.61	2.16	2.49
↓	5.0	1.80	2.12	1.81	2.13	1.79	2.07
Windward	10.0	1.70	1.94	1.71	1.95	1.67	1.89

Mod 7 Hc and ESA 3560HF materials. The corresponding weights will be given in Section 6-6.

The assumption of aluminum substructures (and 350°F maximum temperature) will be verified in Section 6-4.

6.4 SUBSTRUCTURE DESIGN

6.4.1 Design Criteria

This section summarizes the criteria which were established as a basis for the structural design of the orbiter leading edge. Structural design limits were established for critical design parameters such as strength, stiffness, strain and safety factors and are defined below.

Stress - The structure shall be capable of withstanding the combined limit loads without causing yielding, heatshield cracking or excessive deformation. Furthermore, at ultimate loads the structure will not rupture, collapse or otherwise produce a catastrophic system failure.

Combined Loads - The external mechanical, thermally induced and pressure loads shall be combined in a rational manner and in no case shall the ratio of the allowable load to the combined limit loads be less than 1.40.

Factor of Safety - The factor of safety for all mechanical loads shall be 1.5 and the factor of safety for all thermal loads shall be 1.2.

Stiffness - The structure shall have sufficient stiffness so as to limit the maximum deflection at any point normal to the surface, to ±.20 inches when measured from the static position at ultimate load conditions.

Heatshield Strain - During the ground handling, ascent, staging and in-orbit phase, the strains in the heatshield and its attachments shall not exceed their failure limits at combined ultimate loads. Also, during entry, horizontal, flight and landing heatshield strains shall be maintained below

failure limits in the virgin material and at the char interface for the ultimate load conditions.

Heatshield Stiffness and Strength - Naturally, such contribution from the charred ablator is not factored in the design. However, no position has been taken on the question of whether or not to take advantage of the stiffness contrilution of the ablator during the initial phase of ascent. This question is left open for a study in which the level of detail is considerably higher than here. Of course, it becomes a question of design policy as to whether or not the heatshield should be relied upon to provide structural support as well as thermal protection.

Maximum Structural Temperature - 350°F for aluminum and 600°F for titanium. Note that we rule out the possibility of designing for these maximum temperatures at landing only, allowing for higher temperatures after landing (provided that the l.e. substructure are not reused after each flight, the l.e. substructures are thermally isolated from the wing structure and a set of metal l.e. is provided for a ferry flight to the refurbishment depot). The maximum temperatures are reached approximately at landing so that this concept is not useful.

Recommended Design Criteria - NASA recommended design criteria (Ref. 62) and proposed modification thereof (Ref. 61) have also been followed. These are the only two 'specification-like' documents that are presently available and that are appropriate to a technology study such as this. We consider inappropriate to follow the specifications of the current shuttle program hardware procurements.

6.4.2 Structural Concepts

Conventional aircraft leading edge designs normally consist of simple curved metallic or fiberglass skins stiffened when required by either a combination of light spanwise stringers and discrete full depth ribs or by closely spaced

shallow ribs. Since in most cases the leading edge in an aircraft is non-structural and simply provides an aerodynamic shape the selection of the L/E construction is influenced more as matter of choice than by design requirements. On the other hand, the leading edge for the orbiter has specific structural and systems requirements which can strongly influence the final design.

As in all aerospace structures weight is of paramount importance. In addition deflection constraints, thermal loads and limiting ablator strains exert a strong influence on the design. Potential loading conditions (see Section 3.3) consisted of aerodynamic pressure loads both positive and negative, acoustic and inflight vibration loads, thermally induced loads and spanwise wing bending loads acting independently or in various combinations.

From a review of these loads, it was concluded that a design concept in which the l.e. is uncoupled from the wing front beam in the spanwise direction would be desirable. That is, a design in which there would be no spanwise shear transferred between the front beam and the leading edge at their attachment points. In doing this, the high spanwise tensile and compressive strains induced in the wing skins due to overall wing bending would be virtually eliminated from the l.e. Instead, only localized skin curvatures would result in the l.e. at the attachment points where the curvature compatibility between the two elements is enforced by the attachment. This has the positive effect of eliminating the need for incorporating relatively heavy spanwise stringers in the leading edge for stability, had the spanwise coupling existed. Correspondingly, a lighter weight design concept should result.

A second desirable feature of this approach is that it removed the possibility of developing spanwise thermal stresses between the front beam and the l.e. due to the different thermal histories of front-beam and l.e. Also, the strength

and stiffness and hence the complexity of the l.e. attachment scheme can be reduced thereby making the attachment lighter.

In view of this design decision, the predominant loading condition became the aerodynamic pressure loads directly exerted on the l.e. To take these loads, three structural concepts were examined. The first consists of discretely spaced deep ribs supporting a lightweight skin (figure 90). The second concept involves using a thin skin supported and stiffened by closely spaced shallow ribs. A third concept which was included for comparison was a sandwich design; although, fabricability, operational requirements, specifications and costs could most certainly have eliminated this last concept, it being potentially the lightest weight concept provides a lowest limit on the structural weights against which to gauge the other concepts.

As it developed preliminary calculations indicated that to achieve a reasonable rib spacing in the deep rib concept (i.e. 12" - 15") the pressure loads were sufficient to require that spanwise stiffeners be incorporated between ribs. This requirement became necessary in order to limit the heatshield strains. Further evaluation of this concept indicated that the weight of the skins and the spanwise stiffeners alone would be comparable to the weight of the entire shallow rib design. Skin and stiffeners weights in the order of 1.5 lb/ft^2 were indicated which was equivalent to the weight of one of the heavier shallow rib designs and was significantly heavier than the sandwich concept.

Consequently, it was decided at an early stage to eliminate the deep rib concept from further evaluation and concentrate on trade-offs between ribs stiffened designs while carrying the sandwich designs along for comparison. The following sections present in detail the results obtained from these studies.

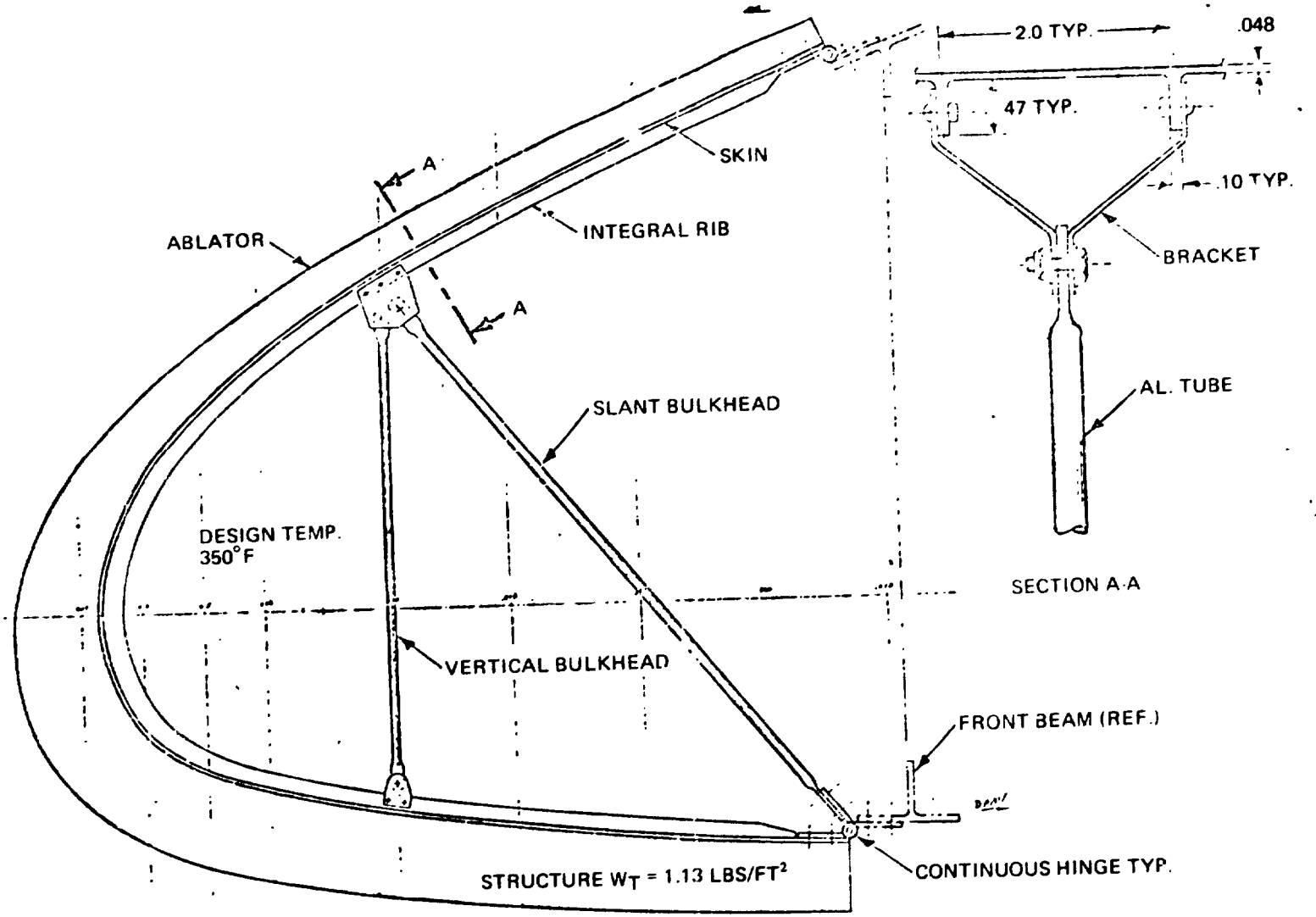

Figure 90(a) L.E. Structural Designs: Integral Stiffened Al./Slant Bulkhead

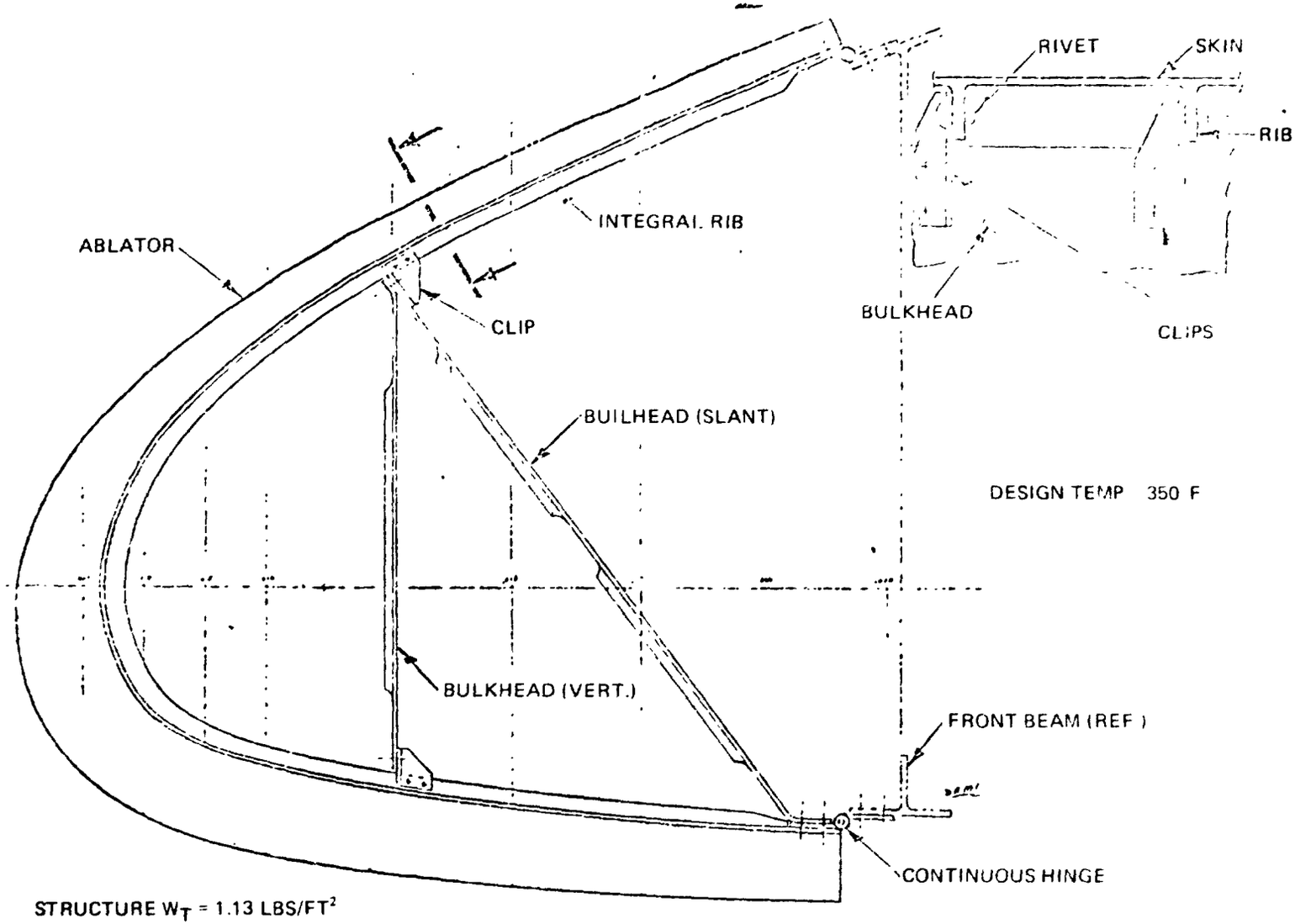

Figure 90(b) L.E. Structural Designs: Integral Stiffened Al./Sheet Slant Bulkhead

6.4.3 Scope of Structural Analysis

Limits had to be established on the scope of the structural analysis that can be fitted into a 'first-cut' study such as this. We decided to carry out the structural analysis and design for the static loads and postpone the study of the thermal stresses, dynamic loads and fatigue (if the substructures are reused) to the next step after this study. This is a reasonable scope for this initial development and is consistent with the structural work done on most the Phase B - beginning of Phase C orbiter configurations. Moreover, for the structural concept developed thermal loads appear less important, as seen in Section 6.4.2.

6.4.4 Static Loads and Criteria for Trade-off Analyses and Substructure Design in This Study

For trade-off analyses the following design constraints were employed in all calculations*:

1) Only the 2-1/2 g and the maximum q^{α} load conditions were considered and taken as ultimate loads (i.e. 1.5 x limit loads)
2) The stiffness and strength provided by the virgin heat-shield during ascent would not be included in the analysis, and
3) To account for strain limitations imposed by the heat-shield the maximum calculated strain at one half of an inch from the structure surface shall not exceed .5%.

*These represent reasonable simplifications. The initial motivation was also to accommodate the need to start this effort while the ablator had not yet selected. Of course, these simplifications are necessary for initial trade-off studies.

Constraint 1 is consistent with normal preliminary design practice where only those loads considered the most severe are initially used. Although it must be admitted that the heatshield will contribute to the strength and stiffness of the substructure eliminating it, the preliminary design evaluation is not totally inconsistent. The question only arises during the initial phases of flight, where the mechanical loads are similar in magnitude to the post entry 2-1/2 "g" condition considered. As a result, the designs generated without the heatshield stiffness contribution will be conservative as long as stress or strain limitations imposed by the heatshield are factored into the calculations. Constraint 3 satisfies this requirement and was determined on the basis that in no case shall the uncharred material be allowed to fail. The .5% allowed strain represents the lowest of the maximum allowable strains for all candidate ablators of this study.

For the sizing of the final design, it was further checked that when the ablator strength and stiffness is included, the stresses induced in the ablator are acceptable. The design ultimate loads for the max q^{α} and 2-1/2 "g" post entry conditions used are presented in figures 91 and 92. As can be seen in these figures, both loading conditions are comprised of both positive 'collapse' pressures and internal 'burst' pressures. When combined, these pressures produce a chordwise varying pressure field reaching maximum pressures of up to 4.5 psi which cause both local deformation and overall chordwise bending of the l.e. For the purpose of these analyses, no spanwise variation of the design loads was considered. Any spanwise variation would be minor in view of the fact that typical segments of the l.e. would be in the order of only 40" long or less.

Initial sizing was accomplished using simplified models and closed form solutions followed by more detailed evaluation using finite element models of chordwise segments.

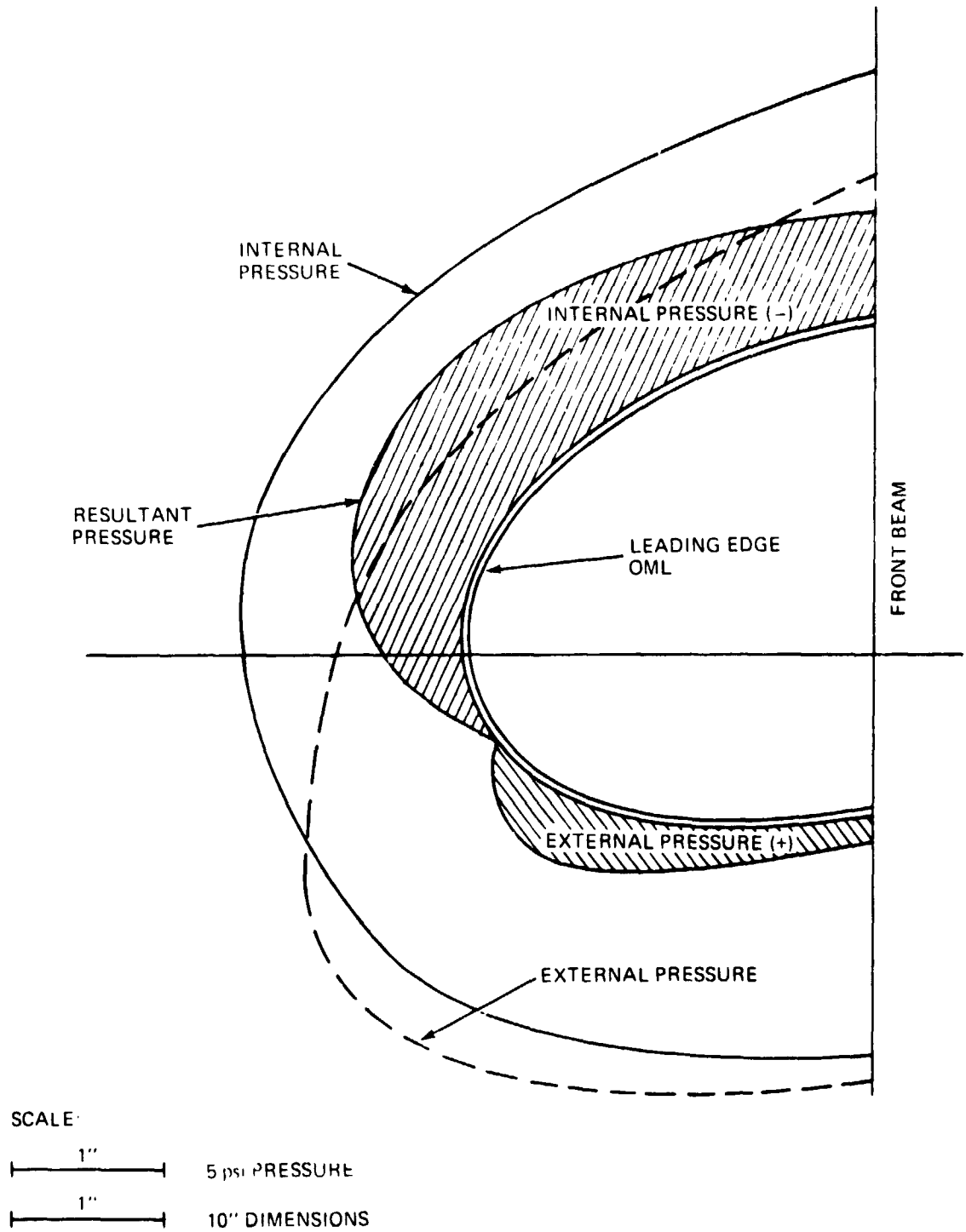

Figure 91 Ultimate Static Loads At Midspan Used For Structural Tradeoffs - Max qα (+) & qα (–) Condition

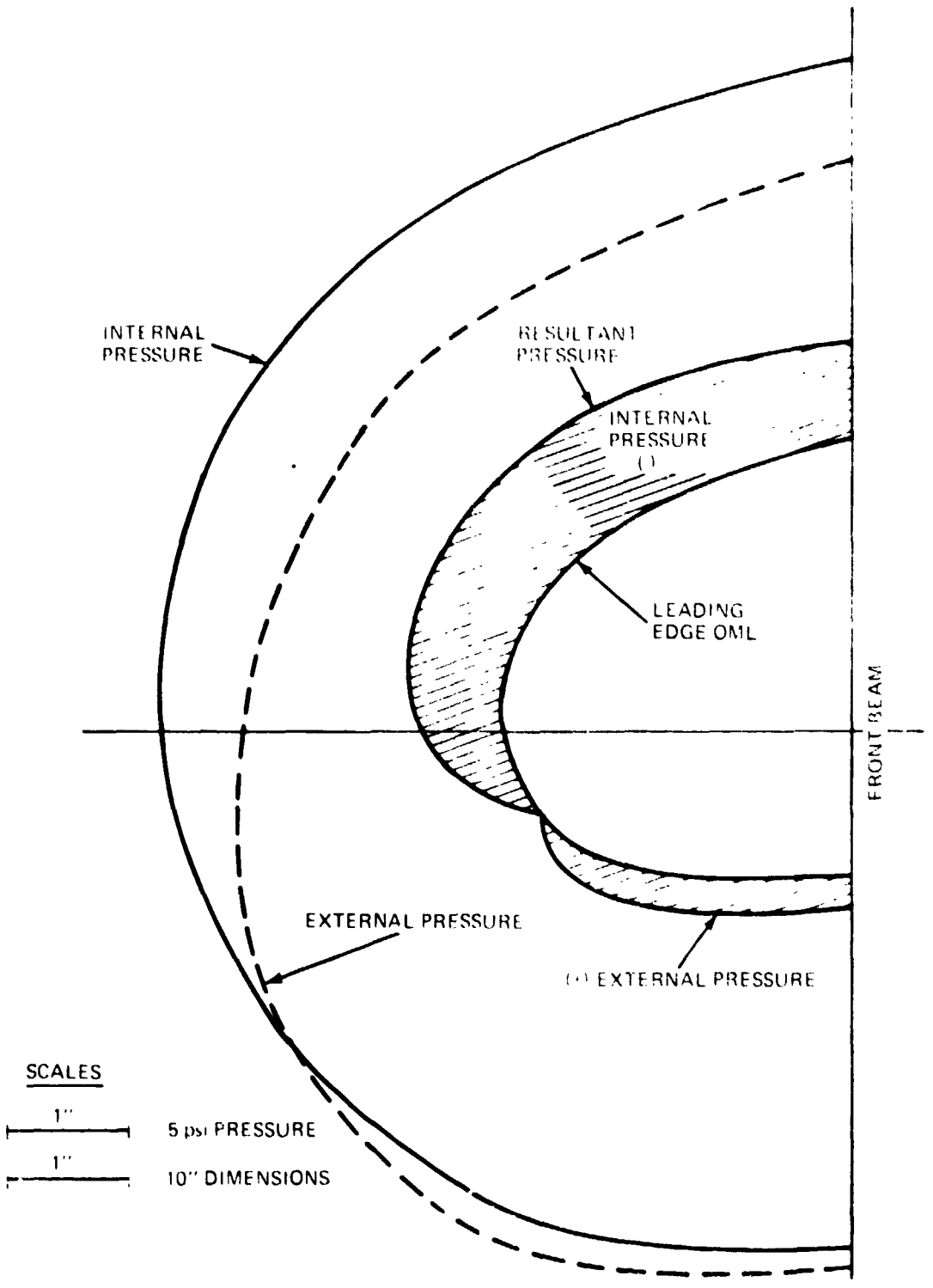

Figure 92 Ultimate Static Loads At Midspan Used For Structural Tradeoffs 2 1/2 g Condition

6.4.5 Development of Candidate Rib-Stiffened Designs

Trade-off studies were performed for two rib-stiffened designs considering both aluminum and titanium as potential substructure materials. For the aluminum designs a maximum backface temperature of 350°F was assumed whereas maximum temperatures of 350°F and 600°F were investigated for the titanium designs. The distinguishing features of the two design concepts are illustrated in figures 90 and 93.

Figure 90 illustrates the Integrally Stiffened Slant Bulkhead Design concept where shallow closely spaced integral ribs are used to react the local pressure loads and the slant bulkhead serves to limit the overall l.e deflections. The zee stiffened design is depicted in figure 93 where the skin is supported by deeper relatively closely spaced ribs which combine to react all loads. Essentially, the trade-off between these respective concepts reduces to whether it is more efficient weightwise to increase the overall depth of the individual ribs to limit the deflections and stress as opposed to reducing the rib weights and incorporating some or all of this weight in a bulkhead.

As noted earlier a sandwich design was also considered and this concept is illustrated in figure 94. For the sandwich design only aluminum face sheets with a maximum temperature of 350°F were evaluated.

In these initial trade-off studies the analyses were conducted for the purpose of determining the relative merits of one design configuration versus another and each therefore was constrained by the same requirements and assumptions as indicated in Section 6.4.4.

With these ground rules firmly established optimization studies were conducted within each design considering such items as rib pitch, skin thickness, rib depth and bulkhead stiffness and location for the rib stiffened concepts.

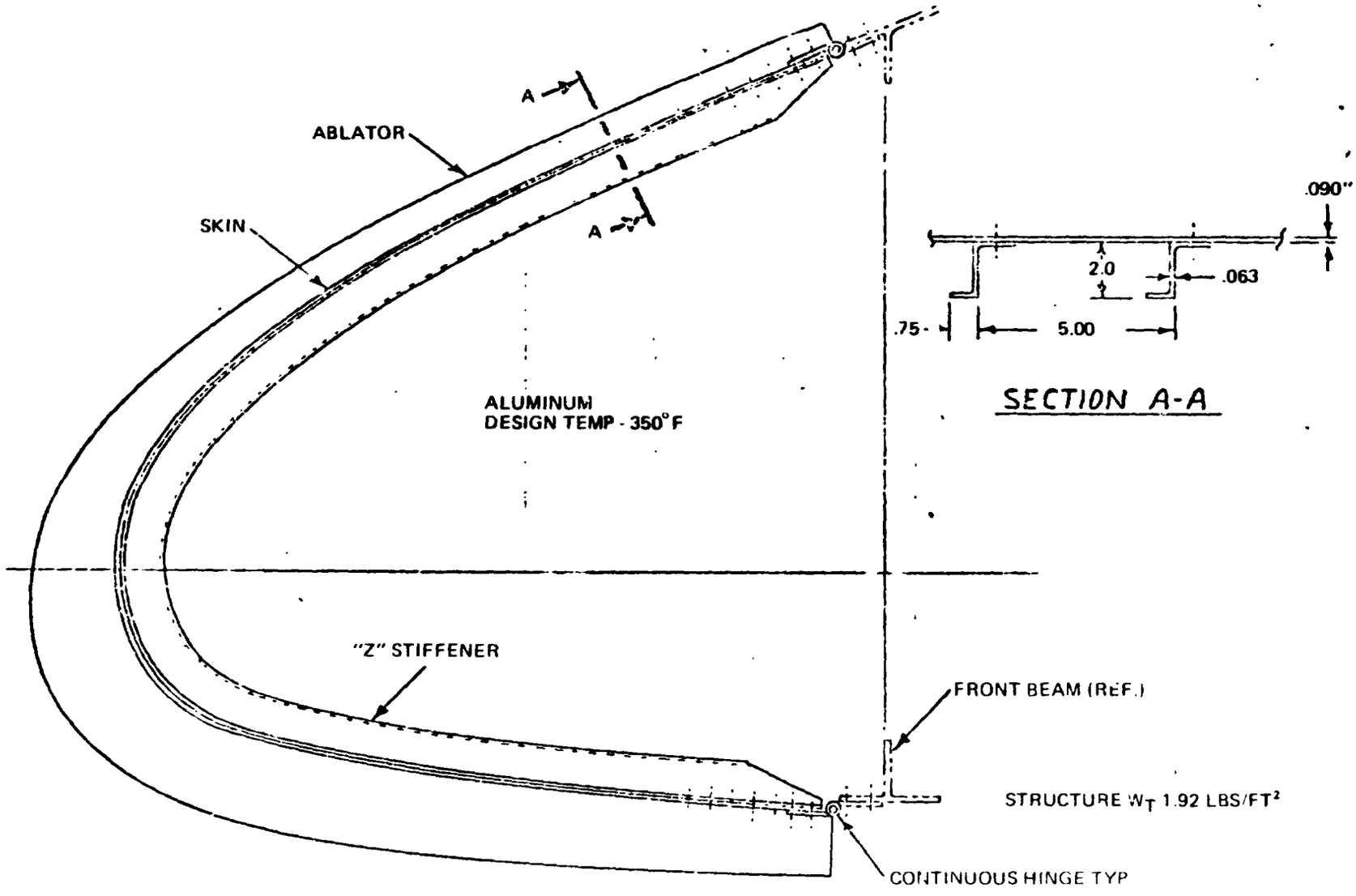

Figure 93(a) L.E. Structural Designs: "Z "Stiffened L.E. Structure - Aluminum

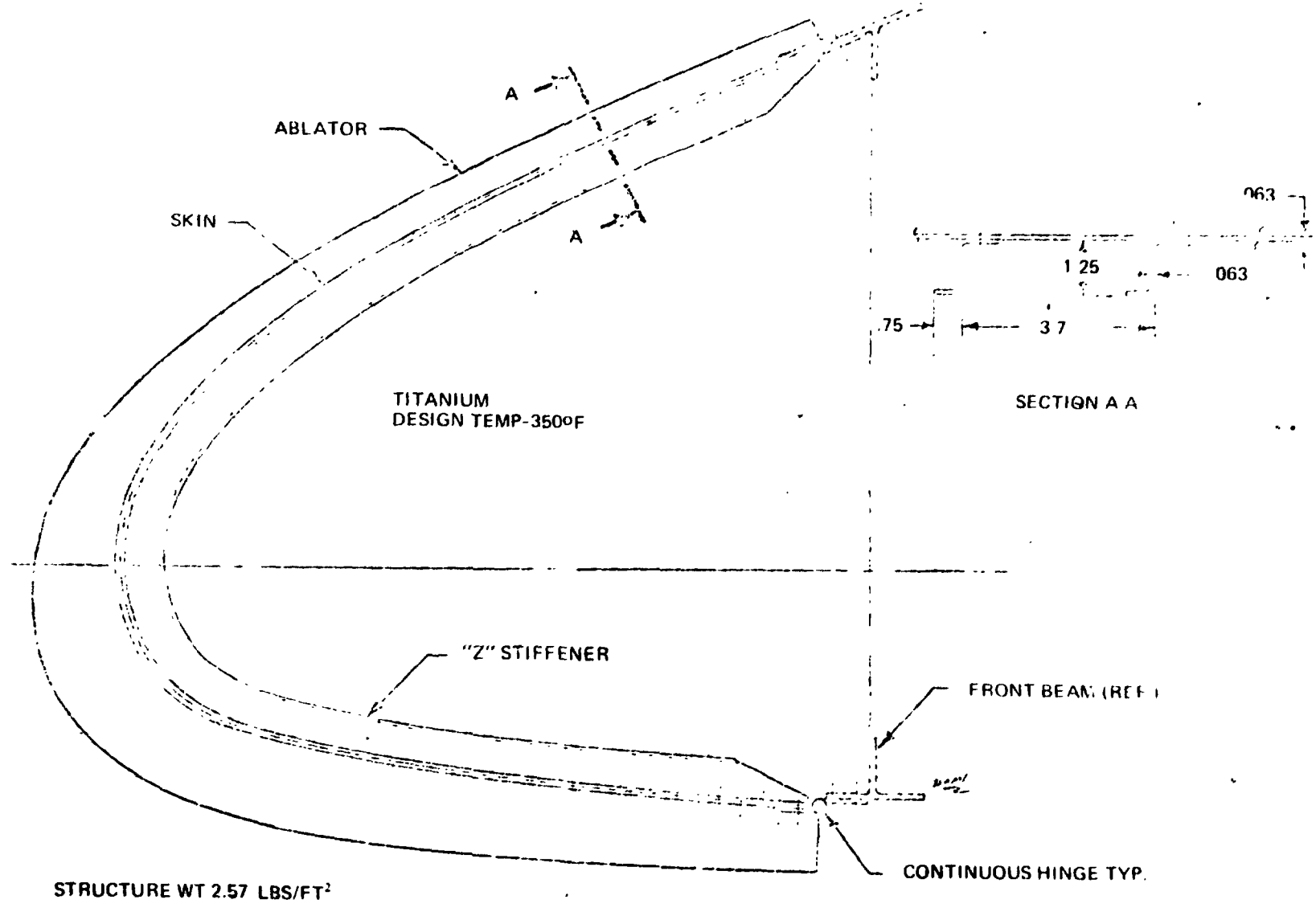

Figure 93(b) L.E. Structural Designs: "Z" Stiffened L.E. Structure - Titanium At 350°F

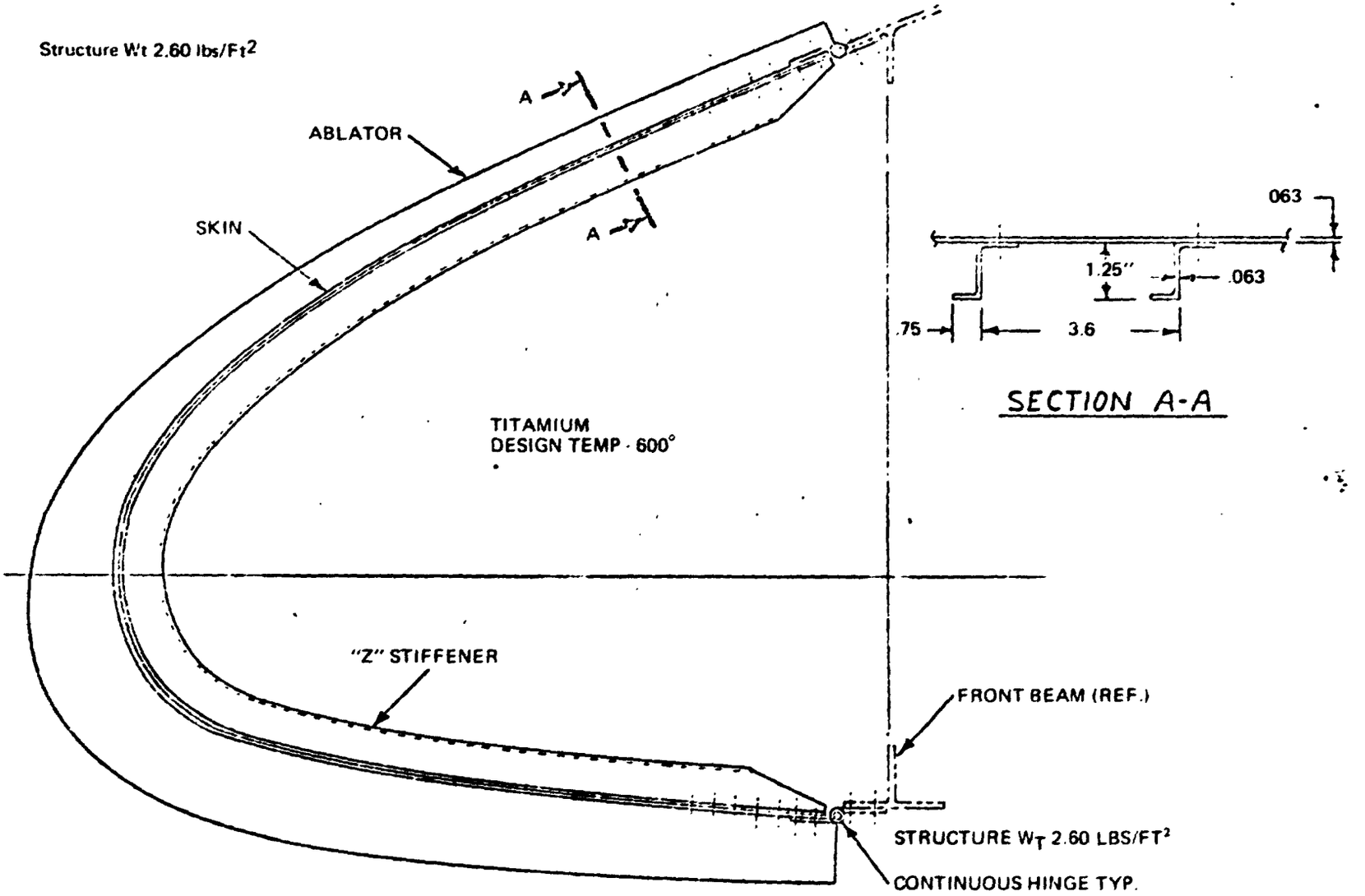

Figure 93(c) L.E. Structural Designs: "Z "Stiffened L.E. Structure Titanium at 600°F

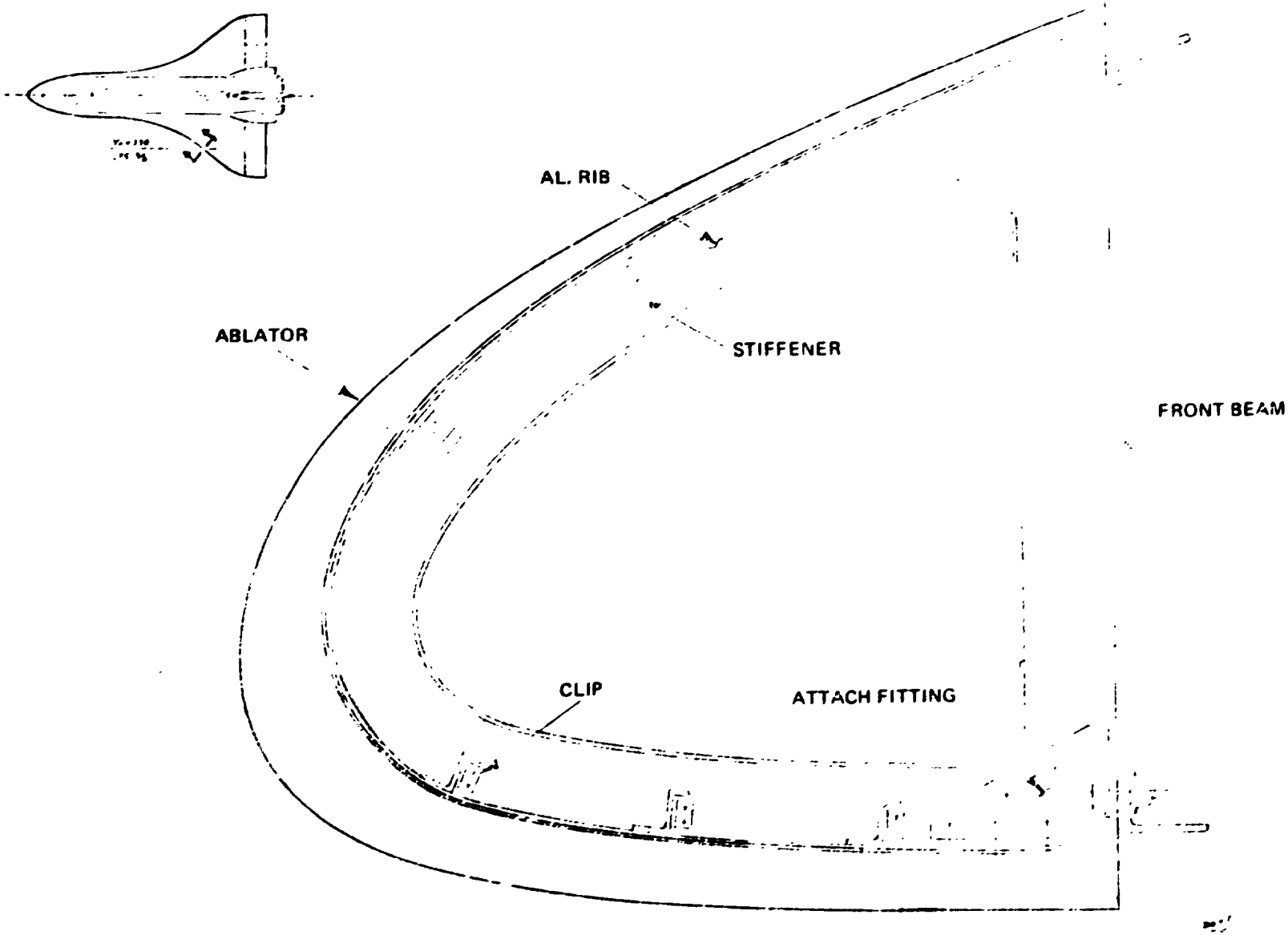

Figure 93(d) Deep Rib/Spanwise Stiffened

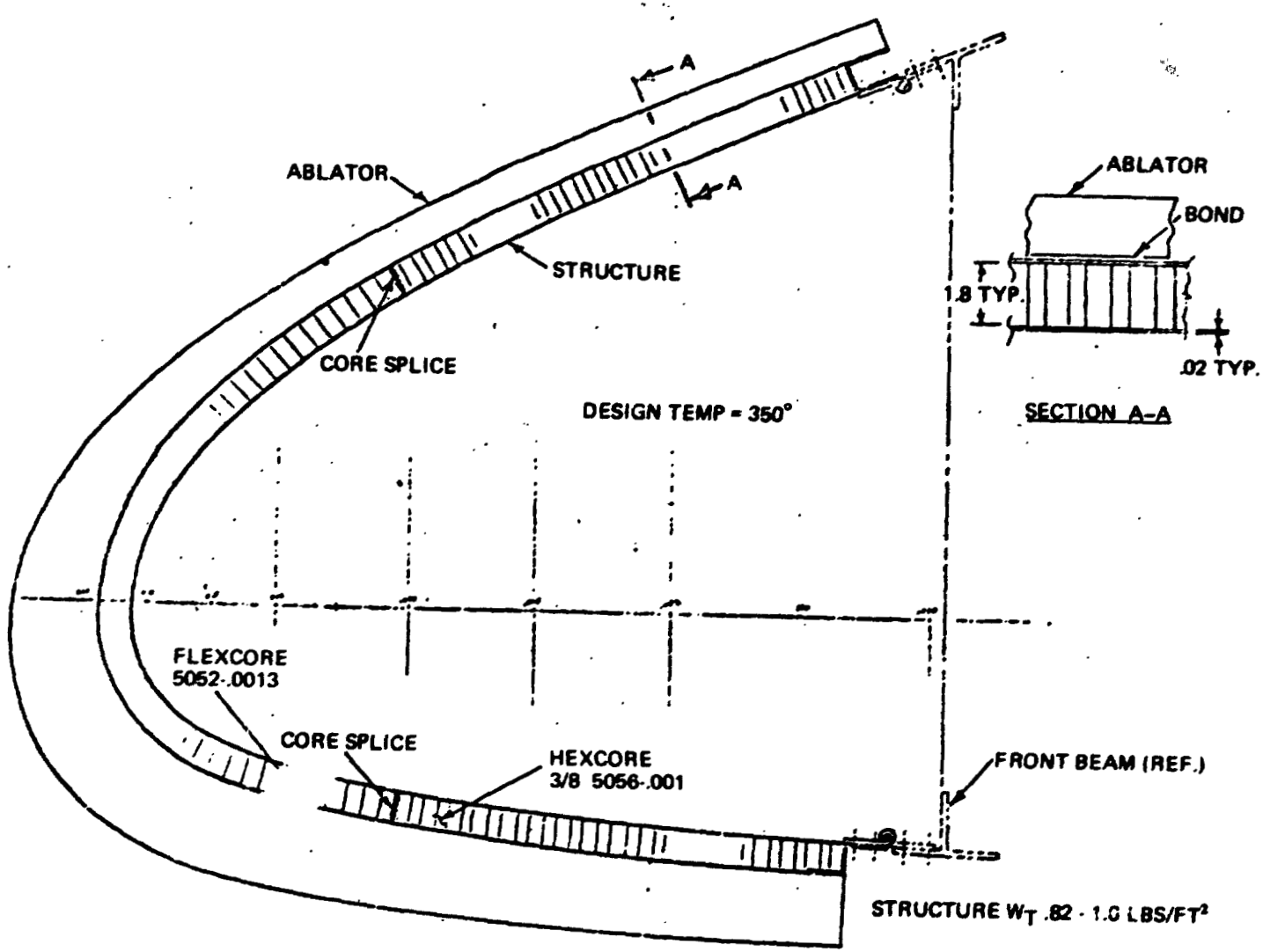

Figure 94 L.E. Structure Designs: Al. Sandwich L.E. Structure

For the sandwich concepts core depth and face sheet thickness were investigated.

Table 37 presents a summary for the more promising designs evaluated showing the relative weights and calculated values for heatshield strain and maximum deflection of each. Highlights of these designs are discussed below with detailed calculations included in Appendix 4.

Integral Stiffened Al/Slant Bulkhead Design

The design concepts shown in figures 90(a) and 90(b) (figure 90(b) being one of two versions of the same concept) were found from among the configurations evaluated to have the best characteristics of lightweight and deflection stiffness with good prospects for low cost. The controlling aspect of this design configuration was the strain allowable of the heatshield (.5%) with a resultant maximum deflection of 0.14 inches. An increase in the allowable strain for the heatshield would result in a weight saving of about 10% for a heatshield strain allowable of 2-1/2% and the deflection of 0.20 inches would then become the governing factor.

Various modifications of the integral stiffened concept could be incorporated to ease possible manufacturing problems but may increase manufacturing costs prohibitively.

One approach would be to decrease the depth of the outstanding leg in the area of maximum curvature to facilitate bending or stretch forming. This would also require an increase in the depth of the outstanding leg in the flatter portion of the structure and add a machining step that would not exist with the reference design.

Sandwich Structure Design

The sandwich structure design concept shown in figure 94 is as usual the

Table 37 Summary of Preliminary Design Concepts

Design	(lb/Ft^2) Substructure Weight	H/S Strain		Maximum Deflection
		Spanwise	Chordwise	
"Z" Stiffened Aluminum	1.92	.5%	.1%	13
"Z" Stiffened Ti 350° F	2.57	.47%	.14%	19
"Z" Stiffened Ti 600° F	2.60	.50%	.14%	.19
Aluminum Sandwich	.82	–	.23%	.20
Integral Rib/Slant Bulkhead-Al	1.13	.50%	499%	.14

lightest design from among the concepts evaluated. The controlling aspect of this design was the deflection requirement of 0.20 inches with a resulting mechanical heatshield strain of 0.23%. With the exception of possible thermal strain incompatibilities between the structure and heatshield due to a possible large thermal mismatch between the two faces of the panel, the sandwich design would probably be the best approach if costs are determined as being acceptable.

Zee Stiffener Designs

Three zee stiffened designs were evaluated: (figures 93 (a), (b) and (c) one aluminum and one titanium for service temperatures of 350°F and one titanium for a service temperature of 600°F.

All three configurations were constrained to the use of standard sheet thicknesses and standard extruded zee stiffeners.

The results of the analysis indicated that, within the constraints used, a minimum weight aluminum design was not dictated by either deflection (.13 in.) or allowable heatshield strain (.10%) in the chordwise direction. The optimum weight for the titanium designs however were dictated by the allowable deflection of 0.20 in. The titanium design configurations therefore cannot gain any weight savings due to an increase in allowable heatshield strain and the aluminum design weight savings will amount to about 3% of the reference design weight for an allowable deflection of 0.20 inches instead of 0.13 inches.

The use of spanwise intercostals was considered for the purpose of reducing the weight of each design however, this approach was not pursued for the following reasons.

For the reference aluminum design the shell weight (skin) accounts for 68% of

the total weight. The stiffness contribution of the shell in terms of chordwise bending is about 75% of the total bending stiffness. The use of intercostals will allow a reduction in the thickness of the shell however, this will also reduce the chordwise bending stiffness of the total structure which will require increasing the stiffness of the zee stiffeners and therefore the weight of the stiffeners.

The purpose of the intercostals would be to reduce the spanwise deformations of the shell between Z stiffeners which would in turn permit a reduction in the thickness of the shell. In order for the intercostals to be effective they would have to be deep in order to have adequate stiffness and would have to be spaced probably as close as 4 to 5 inches apart. In any case, the weight associated with the use of intercostals is totally ineffective with regard to the chordwise deformation of the leading edge structure and therefore not considered as being an efficient use of material.

Although a detailed analysis of the use of intercostals was not conducted, it is rather doubtful as to whether a weight savings could be realized and whether the weight savings would justify the costs of fabrication of such a multi part structure.

Another complication involving the use of intercostals would be the negative effect the depth of the intercostals would have on the induced strain in the heatshield due to wing flexure. The analysis contained in Appendix 4 illustrates the importance and effect of structure depth and should be referred to.

For the reference titanium designs the shell weight is approximately 58% of the total weight and accounts for about 42% of the total bending stiffness. The same comments apply relative to feasibility of an intercostal design however, the efficiency may be greater when considering titanium as opposed to aluminum.

6.4.6 Titanium vs Aluminum

Both titanium designs, rib stiffened and Z stiffened, are significantly heavier than the aluminum designs, thereby eliminating from further consideration, the titanium concept designed for a backface temperature of only 350° F. However the total system weight, (i.e. heatshield and substructure) must be considered when comparing the 600°F backface temperature titanium design with the 350°F maximum temperature aluminum designs since a higher backface temperature would result in a thinner and hence lighter heatshield.

Comparing the total 6.50 psf weight of this i.e. concept operating at a maximum temperature of 350° F to the 6.47 psf for the 600° F backface temperature titanium design, it is evident that the titanium design is still significantly heavier, when the additional insulation requirements and the attendant complexities of the titanium design are considered.

Examining costs for materials and fabrication of the substructure the titanium design is conservatively estimated to cost approximately 1.5 times that of the Z - stiffened aluminum design. Because of the higher weight and high cost assigned to the high temperature titanium design it was eliminated from further consideration.

6.4.7 Tradeoff of Aluminum Designs and Design Selection

As expected, on the basis of weight (table 37) the lightest structural concept is the aluminum sandwich design, but, as alluded to earlier this concept was not included as a serious i.e. candidate but rather was carried along in the preliminary design cycle to provide an estimate of the structural efficiency for the other concepts. Excluding the aluminum sandwich, the second lightest substructure evaluated is the integral rib stiffened design with the slanted bulkhead followed by the Z - stiffened aluminum design.

When comparing the two aluminum designs one should not expect that because of

the different weights of substructure, i.e. a slightly different heat capacity for each substructure, the heatshield thickness is significantly affected. In this instance, the heat capacity of the ablator is greater than the aluminum, therefore, an increase in the heat capacity of the substructure would not lead to a large enough reduction in heatshield thickness to compensate for the higher structural weight. Furthermore, the heavier aluminum design consists of a thin skin supported by relatively deep, discrete ribs which are less effective in distributing the heat input so as to reduce the heatshield thickness measurably. Consequently, for minimum system weight the superior aluminum design is the integral rib design.

As far as costs for material and fabrication, in limited quantities (7 shipsets) the Z -stiffened aluminum design would be the least expensive to fabricate, however, in volume production it was estimated that the fabrication costs of both designs would be comparable. As shown earlier in table 27, for limited quantities of seven ships sets (i.e. refurbishing for all subsequent flights) the cost of the substructure is inconsequential when amortized over the 447 flights. In terms of overall program costs, the only time the cost of the substructure exerts a strong influence is in those cases where a totally disposable l.e. system is contemplated. As a result it was concluded that on a cost tradeoff both aluminum designs are equivalent. In addition, both designs could either be refurbished or discarded for the same relative cost.

Therefore, the final selection criterion reverted back to a weight tradeoff resulting in the selection of the lightweight integrally stiffened aluminum design.

6.5 JOINTS

The design of both the chordwise joints between adjacent leading edge segments

and the spanwise joint at the ablator leading edge/RSI interface form an integral part of the overall leading edge system. In arriving at an acceptable joint design and its associated seal, if needed, all facets of the system must be considered, involving such diverse items as seals materials selection, structural requirements, thermal protection, aerothermodynamic effects and installation and inspection.

For example, if a special seal is required in the joint then a seal material must be selected which is compatible with the adjacent materials (ablator and RSI) such that it does not adversely influence the TPS in the regions near the joints. Furthermore, the joint must be designed to perform thermally in a manner equivalent to the local heatshield to prevent local hot spots. Aerodynamically the joint must not affect the flow characteristics in the leading edge area to cause premature transition to turbulence or downstream contamination of the RSI. Structurally the joint must maintain its own integrity while accommodating differential expansion and the mechanical loads introduced by the abutting leading edge segments. And finally, manufacturing of the joint and seal must be considered along with their impact on the overall installation and final inspection procedures. Consequently, the joint design process requires that a concept be selected which satisfies all aspects of the leading edge system. To illustrate this, table 38 lists some of the more important considerations for the joint design relative to the various phases of the mission.

Figure 95 depicts a typical wing leading edge consisting of a number of individual ablator segments. In this illustration the chordwise joint is perpendicular to the wing front beam, while the RSI joint runs parallel to the front beam. Due to the wing sweep angle ranging from 80° inboard to 50° from midspan to the tip the flow direction will in general be oblique to both

Table 38 Factors Influencing the Design of a Leading Edge Joint/Seal

OPERATIONAL PHASE	DESIGN CONSIDERATIONS
1. Prelaunch	a) Should not complicate installation of L.E. Panels b) Ease of installation – min. interference with other subsystems c) Time compatible with turn around time allotted L.E. d) Ease of inspection
2. On Pad	a) Resist environment – seal against rain b) Easily repaired/replaced, if damaged
3. Ascent	a) Resist rain, hail b) Withstand acoustic and vibration environment c) Resist effects of char – must not protrude or contaminate
4. Tank Separation/Docking In-orbit	a) Resist shock and vibration b) Cold Soak – expand to maintain contact with ablator segments
5. Reentry	a) Protect sub-structure thermally b) Compress as ablator segments expand keep load low c) Not protrude above ablator/RSI surface d) Recession (if any) must be compatible with ablator/RSI e) Must not contaminate adjacent TPS surfaces f) General surface condition must be aerodynamically acceptable
6. Post-entry/landing	a) Must not affect sub-sonic aerodynamic characteristics b) Resist rain, hail c) Resist landing shock loads

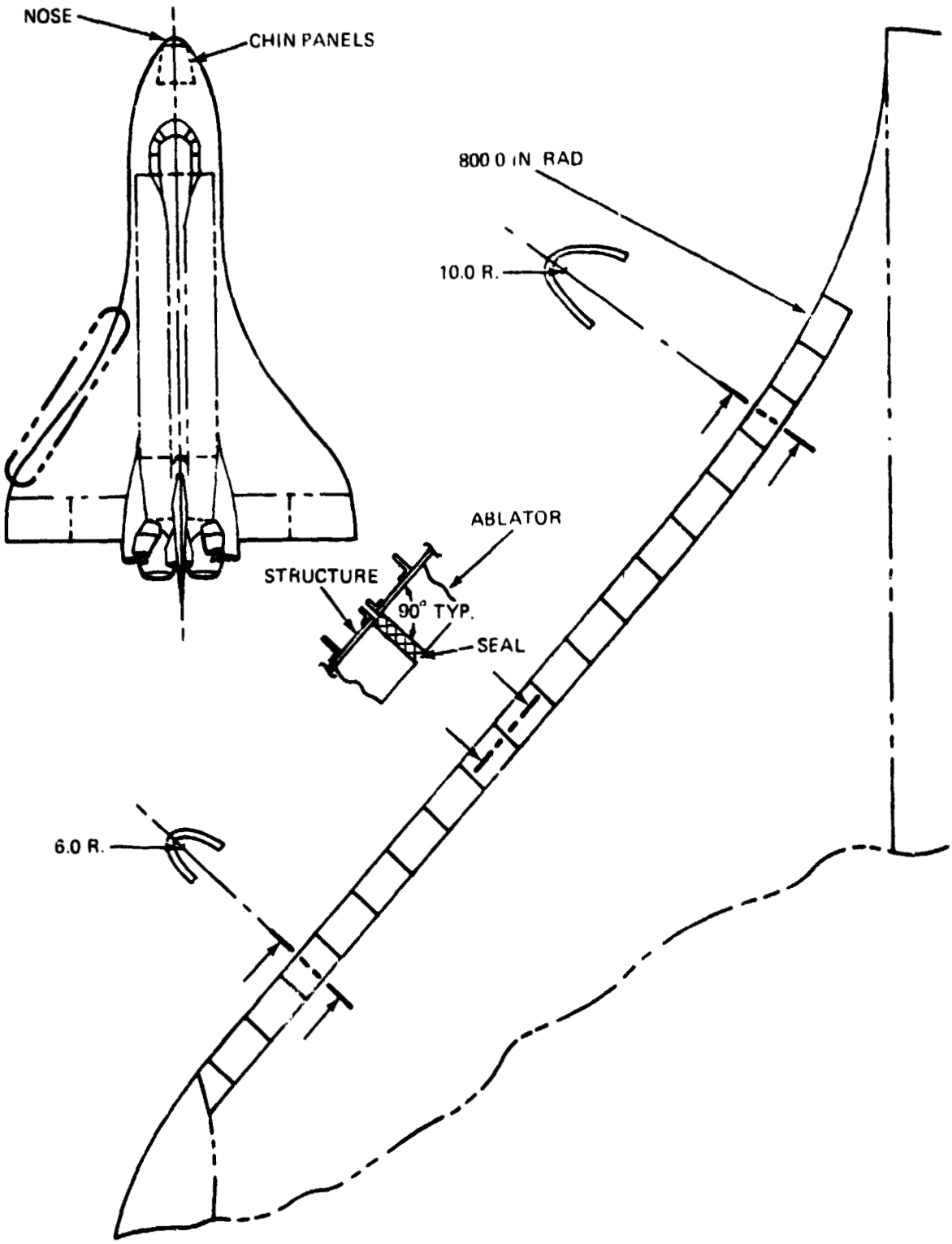

Figure 95 Typical Wing Leading Edge

joints. This tends to minimize the joint design problem for filled joints as compared to joints which run parallel to the flow, as long as the surfaces are flush or have a slight downstream facing step. Such a step can be easily provided by setting design tolerances which always insure that the joints be at worst flush and in most cases present a slight rearward step.

For the purposes of this program, in the selection of the joint designs, both ablator to ablator (A/A) and ablator to RSI(A/RSI), special emphasis was given to the good design rule of keeping the design as simple and inexpensive as possible without sacrificing performance. Two basic approaches were examined, namely: controlling the space between adjacent segments (gap width) such that no seal would be required, or using a seal material in the joint and thereby relaxing the restraints on gap width control. The concepts examined and the rationale for selecting the final A/A and the A/RSI joint designs are presented in the following sections.

6.5.1 Ablator/Ablator Joints

6.5.1.1 Gap Sizes

Ideally, it would be desirable to have a continuous leading edge with no chordwise joints, however, such a situation is physically impractical. Consequently, a compromise must be made which attempts to minimize the number of joints while satisfying a number of physical and thermal/mechanical constraints.

Factors which affect the chordwise joint design are the length of the individual l.e. segments, the thermal environment, wing flexure and the choice of a seal. The length of the l.e. segments is controlled to some extent by practical considerations such as fabrication limitations and simple handling requirements where size and bulk weight are important. As indicated earlier in the

refurbishment studies, the physical size and weight of each segment was limited such that they could be easily handled by no more than two burly men. In addition to these practical considerations, the section length will dictate the amount of differential expansion that will occur during thermal exposure and wing flexure. This differential expansion between the front beam and the leading edge controls the gap size between adjacent segments where under cold soak conditions the gap size will enlarge and conversely during heating the gap size will decrease.

Figure 96 illustrates the general behavior of the chordwise gap between adjacent ablator segments as a function of l.e. length when exposed to the extremes of cold soak and entry heating. This figure was prepared for various initial assembly gap sizes assuming the l.e. as uncoupled from the wing front beam in the spanwise direction, as in the selected attachment scheme. It was assumed that the aluminum substructure controlled the overall expansion and contraction of the l.e. and that during cold soak and entry heating the l.e. substructure would attain its maximum equilibrium temperatures of -250° F and +350° F respectively while the wing front beam remained at a nominal temperature of 70° F. This latter assumption is extremely conservative since although one might expect the leading edge to respond to temperature variations more rapidly than the wing front beam a lag of the magnitude assumed is extremely unlikely. However, this assumption was justified on the basis that if a gap seal could be designed to satisfy these conditions, it would certainly perform in the less severe real environment. Figure 96 indicates that for any given initial gap size there is a critical leading edge length at which the segments come into contact during entry heating. This condition was considered to be undesirable since it could lead to interaction between the segments and could possibly promote premature failure of the charred portion of the ablator.

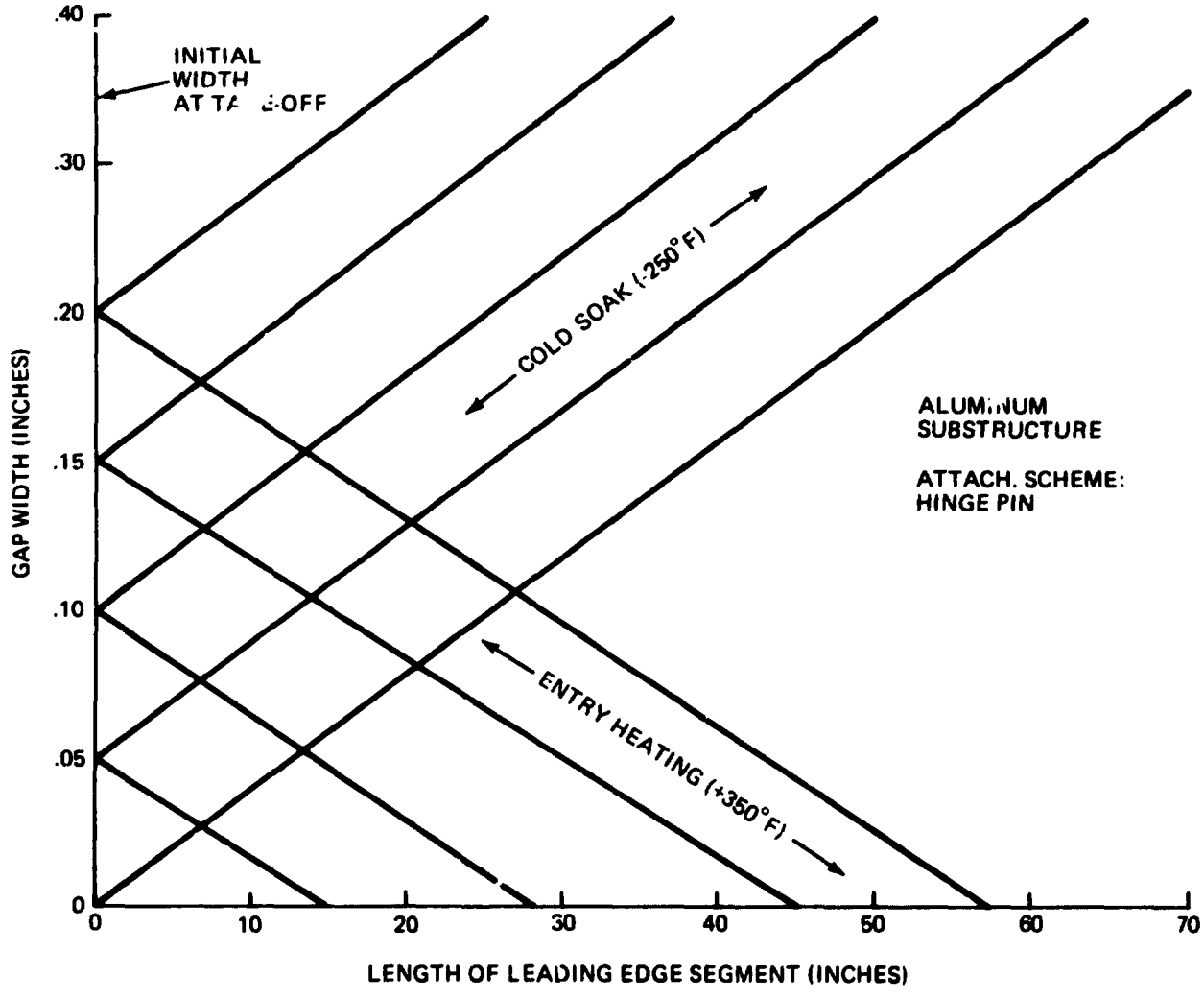

Figure 96 Flight Changes Of Gap Width Between L.E. Segments Due To Thermal Environment

Actually, no condition approaching a zero gap width could occur for the joint designs envisioned (see below) because all concepts employed a form of flexible seal in the gap which would impose a finite gap width on the design under all flight conditions. For the cold soak condition the figure indicates that the gap width constantly increases as a function of leading edge length.

The changes in gap width due to wing flexure must also be considered. These changes arise by virtue of the fact that the l.e. is essentially uncoupled from the front beam in the spanwise direction. As a result any spanwise curvatures in the front beam are not transmitted into the leading end, but rather, the l.e. bridges these curvatures by a series of linear segments. Consequently, any bending of the wing will cause the gap to open on the upper surface and close on the lower surface or conversely depending upon the direction of bending. Figure 97 illustrates how the gap width will vary as a function of wing span. This figure was prepared using predicted curvatures produced during the most severe wing bending condition (i.e. max. q^{α} figure 91) and accounts for the depth variation of the leading edge as a function of span. For conservatism it was assumed that the seal material would be sufficiently stiff to prevent any gap closure during wing flexure, thereby forcing the leading edge to pivot about its outer extremity rather than the front beam neutral axis which causes the maximum opening of the joint (see figure 97 insert). As can be seen in the figure the maximum change in gap width occurs out at the wing tip where the curvatures are the most severe with little or no changes indicated inboard of the midspan position. Also, for wing bending as was the case for differential thermal expansion the longer leading edge segments result in larger changes in gap width. Fortunately, the cold soak and maximum wing flexure design conditions do not occur simultaneously. In fact, an examination of figures 96 and 97 shows that the cold soak condition controls the maximum gap opening for all

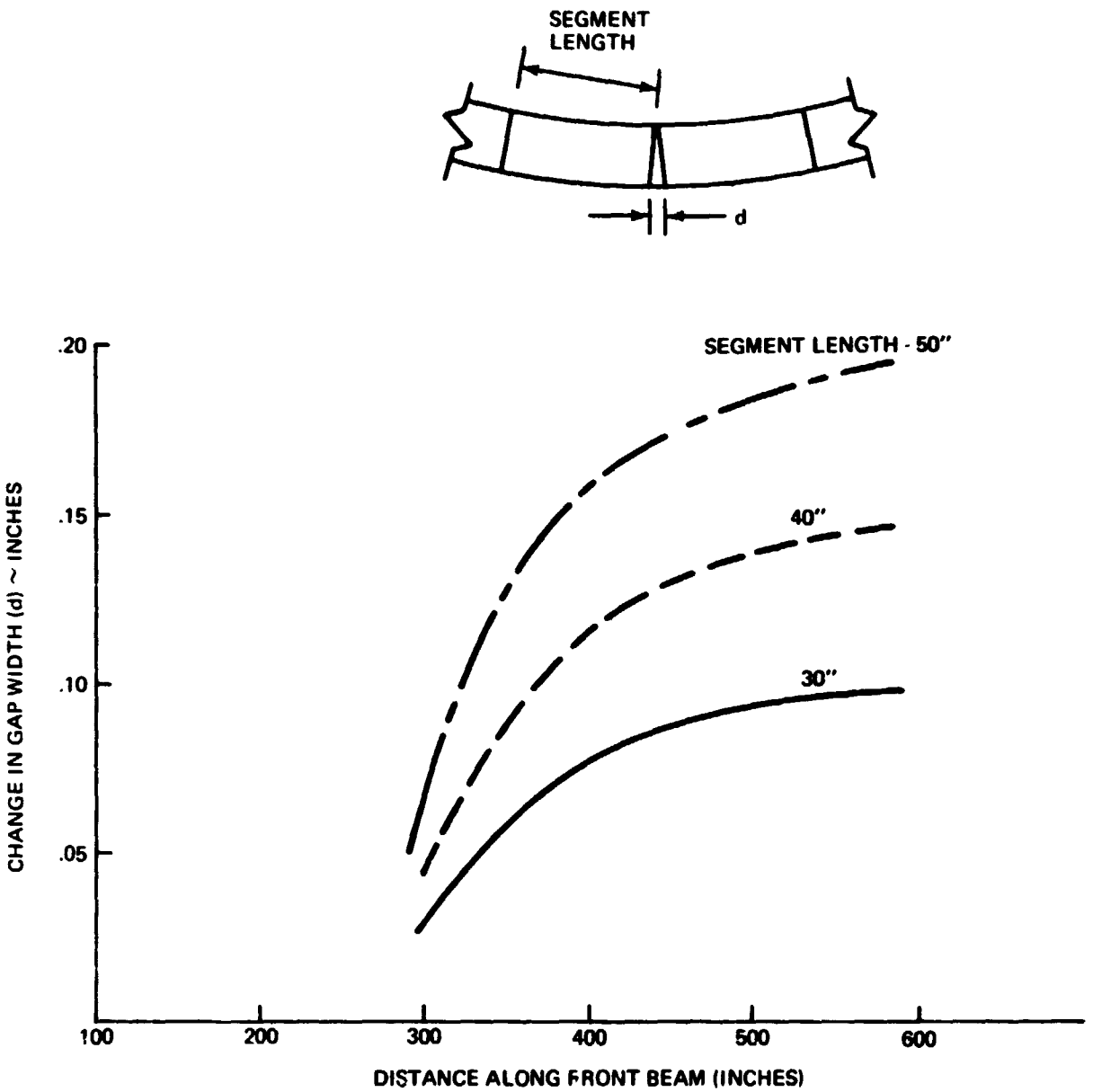

Figure 97 Flight Changes In Gap Width Between L.E. Segments Due To Wing Flexure

lengths considered even in the region of the wing tip. Consequently only thermal excursion need be considered to size the gap.

Combining these two conditions with the thermal heating requirements it was possible to place some design constraints on the leading edge gap size. To begin with, thermally it would be desirable to minimize the size and extent of the joint. From the thermomechanical viewpoint, during the entry heating the joint must maintain a width sufficient to prevent the seal from extruding or from compressing to the point where it causes excessive compressive strain between adjacent ablator segments. Also during cold soak and wing flexure, the seal must be flexible enough to expand to fill the gap such that it does not become dislodged or displaced prior to reentry.

With these as design constraints the problem resolved itself into selecting a leading edge length and associated assembly gap width which would be compatible with the compressible seals envisioned. Since it was established that the seal must always fill the gap, this required that the seal be installed with an initial compression such that it could expand during cold soak. Although seemingly minor, this initial compression of the seal could lead to some rather high compressive forces being applied during assembly due to the large surface area of the seal. In fact for some relatively compressible seals considered, the assembly forces required to compress the seals to the desired levels approached 200 lb (see Section 6.5.1.3). Consequently, this became an important consideration in the overall selection of the seal.

Leading edge lengths less than 20" were eliminated simply on the basis of practicality. In examining l.e. lengths greater than 40", one is forced to employ either a high initial precompression of the seal or to enlarge the initial gap width to .20" and larger. For example, for a 50" segment, the gap width opens by .20" during cold soak. To fill this gap under ideal conditions, assuming complete expansion of the seal, would require an initial gap width of .20" for a seal compressed by 50% during installation. This does not allow for the embrittlement of the seal at -250°F nor has any allowance been made for any residual compression in the seal during cold soak to retain its position. Therefore the gap widths expected for l.e. lengths greater than 40" would have to exceed .20" or the seal precompresion would have to be greater than 50%. Neither of these alternatives were acceptable. Consequently, the leading edge length was confined to the range of greater than 20" and less than 40" per segment.

Initial gap widths of .30" or greater had already been eliminated and, with the segment-length bands set, it would appear from figure 96 that initial gap widths of much less than .15" would be undesirable since they would lead to relatively high seal compressive stresses under the assumed entry heating conditions. In fact, at a .10" initial gap width, the seal would be fully compressed during entry heating for segment lengths greater than approximately 28".

Consequently, the initial gap width range selected for evaluation was set at between .15" and .20" which is compatible with the 20 to 40" segment length. This would result in a situation where there would never be a possibility of the leading edges coming into intimate contact and the initial compression of the seal during assembly would be in the order of 50 to 60%.

6.5.1.2 Joint Concepts

a. Controlled Gap Width Design (No Seal)

The first approach investigated for the chordwise ablator/ablator (A/A) joint design was the concept in which the gap width is controlled and no seal is employed. Typical concepts for this type of design are shown in figure 98 where the intent is to prevent the entry to the substructure of hot gases by creating a narrow indirect path. For the leading edge A/A chordwise joints this approach was deemed impractical for the following reasons:

Even though the l.e. joint is not parallel to the flow, in the nose region the flow will impinge directly into the joint and in all likelihood this would dictate a very small (.01-.04 inch) gap (Ref. 66, 67). Dimensions of this magnitude are not practical when you consider vehicle structural tolerance build-up and ablator segment shrinkage/growth. Larger gap would probably be required, in conjunction with this, to inhibit flow directly into the gap with modified designs such as a half lap or other joint design similar to those depicted in figure 98, but the gaps would still be impractically small. Both of these are expensive to fabricate within reasonable tolerances. Also, calculations indicate that in the stagnation area depth of char would be

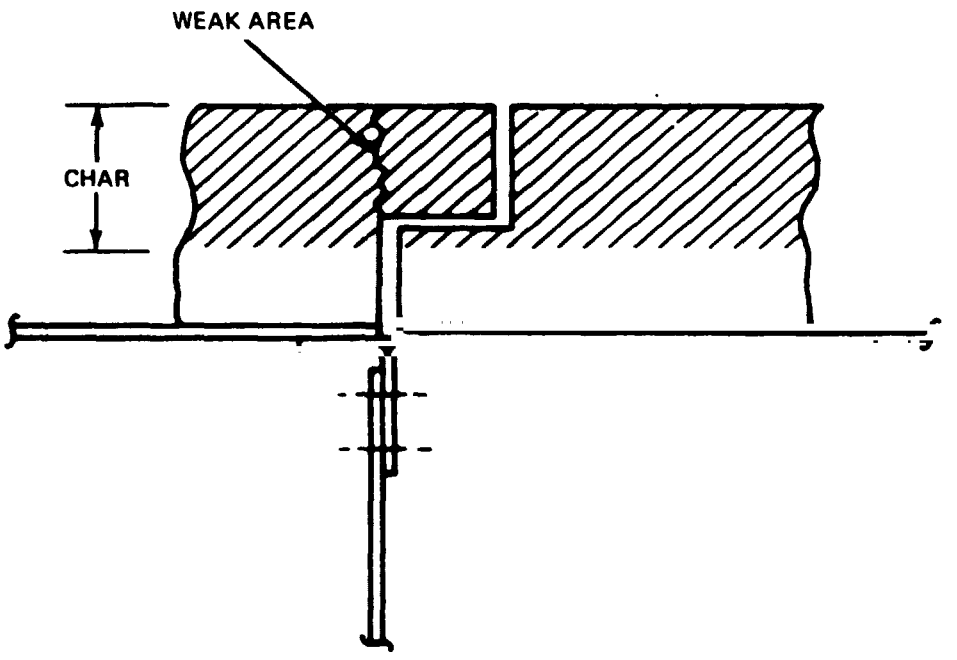

HALF LAP JOINT

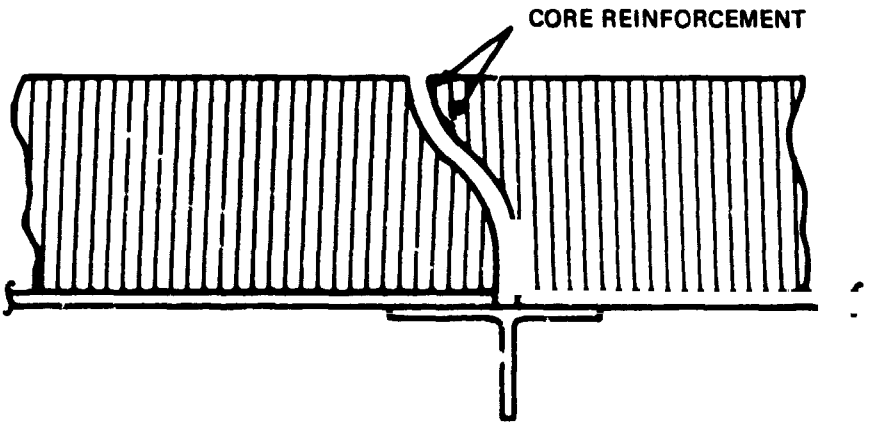

BEVEL JOINT

Figure 98 Controlled Gap Width A/A Joints

deeper than the overlap plane making the outer overhanging ablator strip weak and subject to loss during flight. The honeycomb reinforcement does not improve this situation to any great extent.

Therefore, the approach involving the insertion of a filler material in a gap having dimensions of a more practical magnitude (.1-.2 inch) is the one selected for the A/A joint.

b. Seal Materials and Concepts

Seal Materials: Several materials were considered for use as a high temperature seal between the leading edge segments. Leading the list were the RTV materials which have undergone extensive flight evaluation as A/A seals on the Apollo vehicles (Ref. 68-69). Their performance has been good and they are easy to work with, are castable and not overly expensive. On this basis, this material is considered a prime candidate.

Silica and zirconia are high temperature materials that, when utilized in a felt or woven mat form, can easily be compressed to absorb closing of the gap. An attractive characteristic of this class of materials is that they do not expand to any great extent upon heating and/or compression, therefore they are not likely to protrude into the air stream. Also, these materials are not likely to contaminate the adjacent TPS in any way. Preliminary testing has verified these two latter characteristics and for these reasons and due to the availability, silica felt is considered an attractive candidate.

Metals, such as Hastelloy X, Haynes 25 and Haynes 188, fabricated in the form of a wave spring, offer an attractive approach from the standpoint of protrusion, contamination, and force applied to the edges of the ablator. Forming this seal to the l.e. contour would require extensive tooling, and thermal performance for parallel or near parallel flow has not been determined. Such a

spring with the metal perforated and encased in RTV or silica felt offers another possibility.

Seal Concepts: Combined with the materials selection there are specific performance requirements pertaining to the seal design which also must be considered in determining the overall joint/seal concept. Ideally the seal should be capable of absorbing manufacturing tolerances for initial assembly purposes, expand as the ablator segments shrink during cold soak, and compress as the ablator segments and structure heat up during entry. Throughout this environment, the load (pressure) that the seal exerts against the edges of the ablator must be small enough such that the ablator, even in the charred state, does not fail.

There are two approaches to accomplishing this:

1) Fill the cavity with a soft compressible material, such as silicone foam in a partially compressed state, such that will expand in the cold soak or
2) Insert a mechanical seal in the cavity such that the material deforms in the bending mode or by bellows action, thus allowing movement at a low or controlled force.

Figure 99 shows a typical joint configuration between two adjacent l.e. segments employing a compressible filler material. The cavity between segments has tapered sides which act as a mechanical trap to retain the seal material. In this particular illustration the cavity is filled after the leading edges have been installed with a pressure-operated caulking gun. The caulking material is envisioned as a modified RTV having a reduced density and a viscosity such that it will not run out of the cavity. In the cured state, it would be a soft, easily compressible material similar to existing RTV sealers and

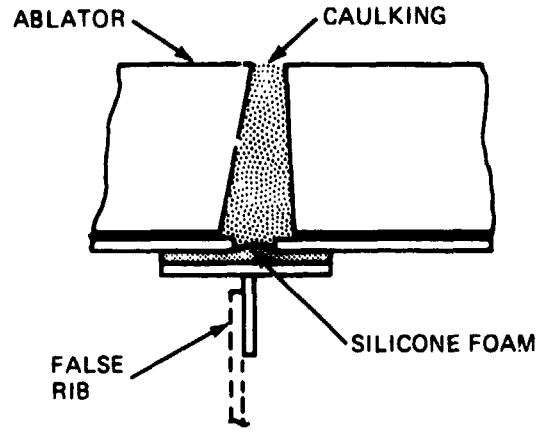

(a)

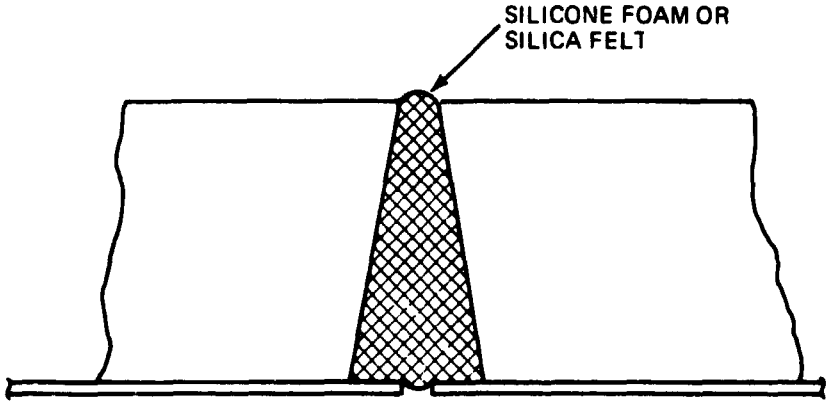

(b)

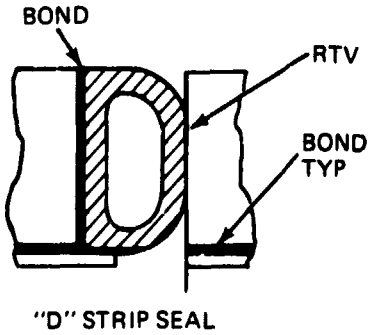

"D" STRIP SEAL

(c)

Figure 99 Compressible Seal Concepts for A/A Joints

adhesives.

Alternative compressible seal designs shown in figure 99 (b) and (c) would involve insertion of preformed seals (gaskets) using a silicone foam or silica felt material. Unlike the caulked seals these preformed seals would be put in place and initially compressed during installation of abutting segments. One disadvantage of these approaches is that the compressive force required during installation increases rapidly as the percent volumetric compression increases, thus, this may cause some difficulty during installation. However, from a thermal performance standpoint, this design appears to perform very well. It also would provide one of the better moisture seals.

Two general types of mechanical seals were also considered; one being the wave seal using either RTV silicone or super alloy metals and the second being a labyrinth type of seal employing a silicone material. Typical wave seal configurations are shown in figure 100, and consist of a premolded corrugated seal strip which is mechanically trapped in place during leading edge installation and absorbs expansion/contraction by bending. The wave seal as shown in figure 100 (a) has been previously fabricated in straight and leading edge configurations and installation has been demonstrated on full scale mock-ups (see figs. 80 and 81, Ref. 2).

A variety of labyrinth type seals are shown in figure 101. These seals allow for the greatest amount of differential motion while at the same time providing the least resistance to relative motion. Sealing is accomplished by the interlocking components which tend to prevent any hot gas penetration to the substructure. Also, several of the concepts shown can be put in place after installation of the leading edge panels. The primary disadvantage of these seals is cost, both in terms of initial tooling and subsequent fabrication.

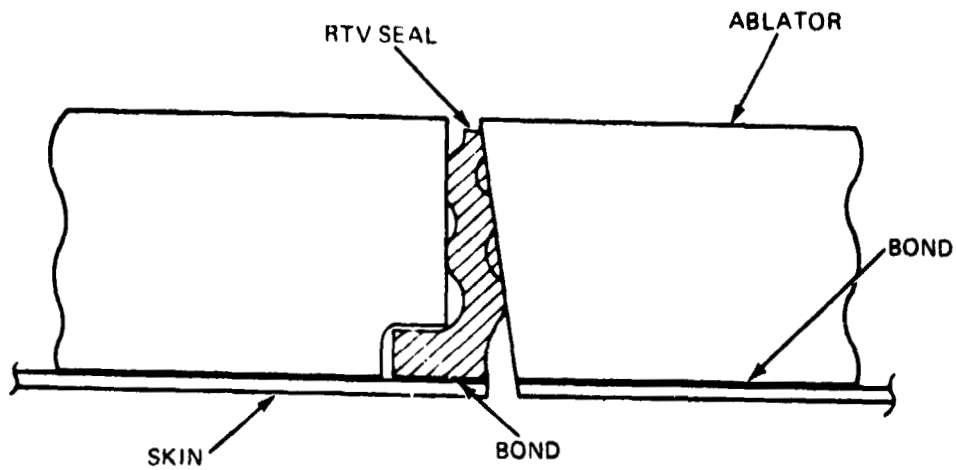

(a)

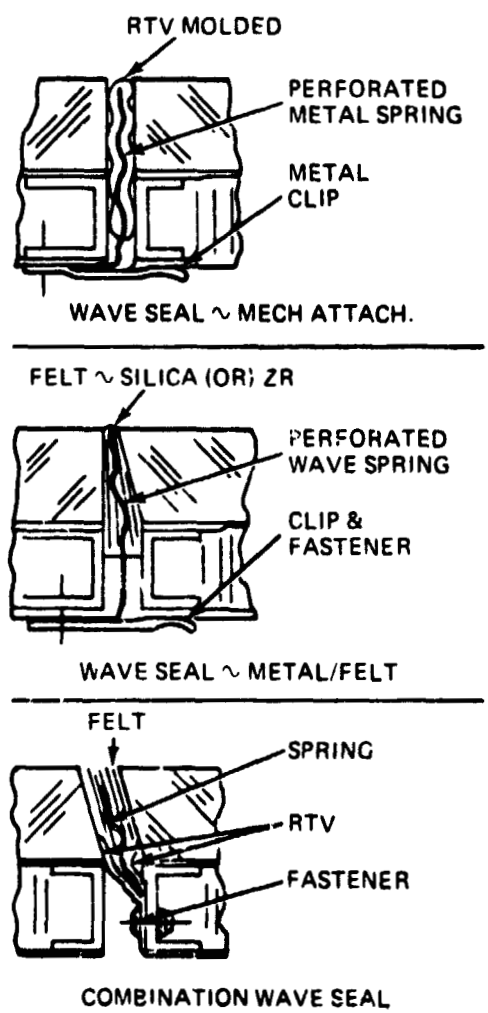

Figure 100 Wave Seals For A/A Joint

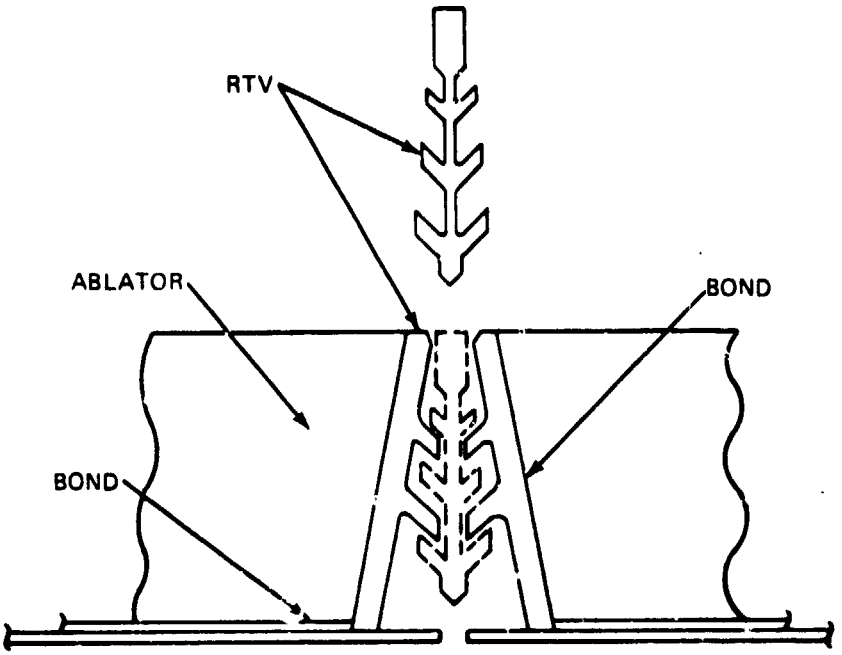

(a)

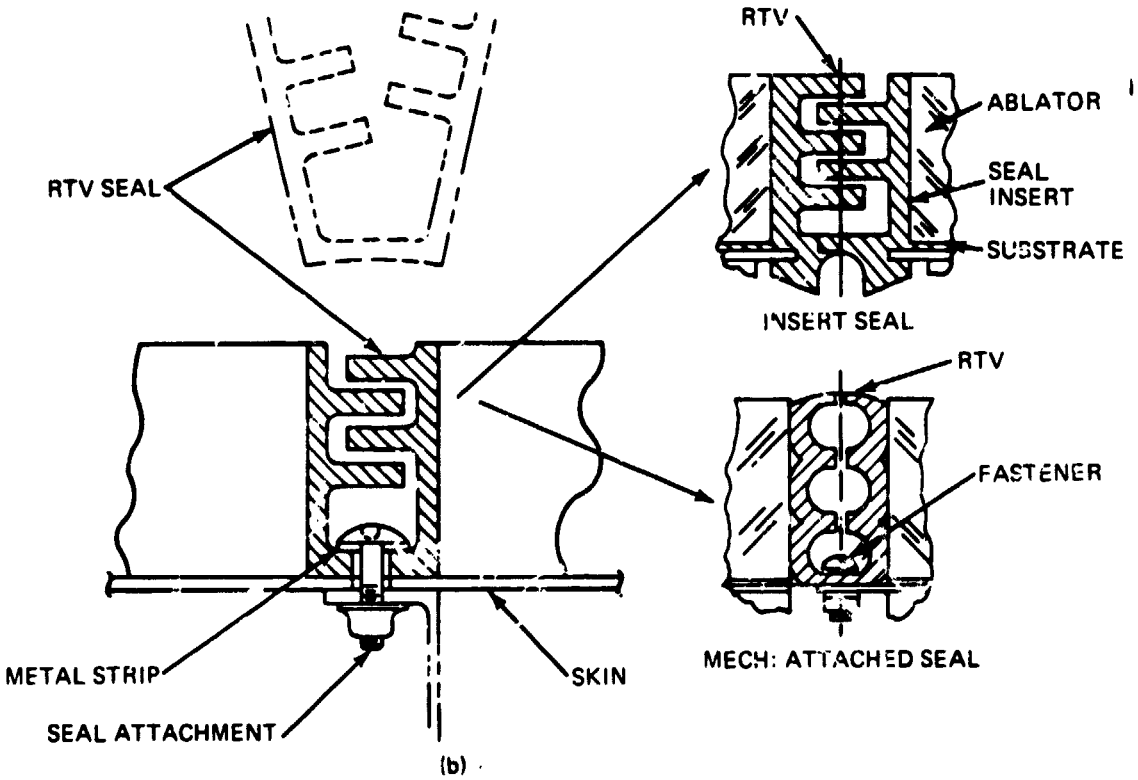

(b)

Figure 101 Labyrinth Seals For A/A Joints

c. Gap Configuration

Just about the simplest means of obtaining a positive holding pressure on the seal without resorting to secondary fastening or other schemes for mechanical entrapment, consists of leveling the edges of the ablator to entrap the seal.

6.5.3 Seal Evaluation and Trade-off Studies

Of the seal concepts presented in the previous section the compression seal and the wave seals represented the simplest and least expensive concepts. Therefore it was decided to pursue the evaluation of these two concepts in more detail. The labyrinth seals though somewhat more sophisticated did not afford any significant advantages over the other two methods, consequently the projected higher cost of fabricating these seals was sufficient justification for eliminating them from further consideration.

Evaluation studies conducted consisted of mechanical testing of candidate seal materials, screening via available thermal tests, on splash specimens, and final validation via arc testing of leading edge models with seals in a LaRc arc test facility.

a. Seal Compressibility Evaluation

A series of tests (Ref. 66) were run to determine the relative compressibility of the following seal designs (See figure 102):

a) Wave Seal - RTV 560

b) Silicone Foam

c) Silica Felt

d) Hastelloy "X" Wave Spring

The test consisted of a six inch length of simulated joint as shown in figure 103 and measurements were made of deflection versus applied load (See fig. 104).

C-4

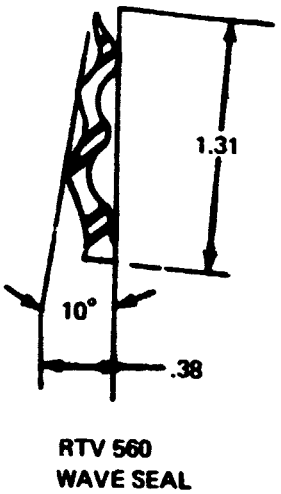

RTV 560
WAVE SEAL

(a)

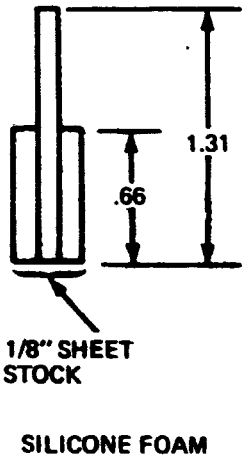

SILICONE FOAM

(b)

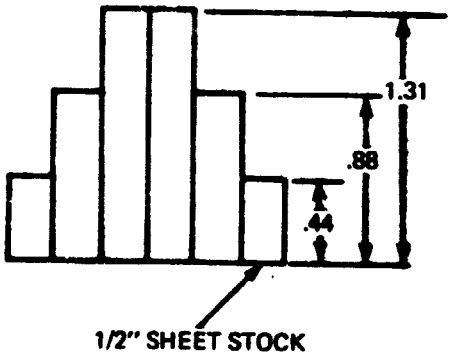

SILICA FELT STRIPS

(c)

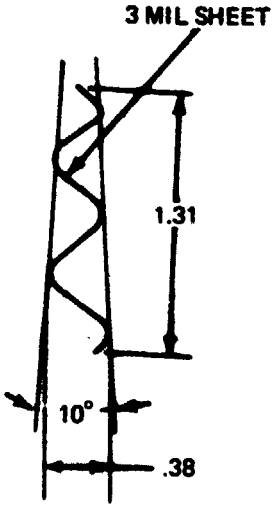

HASTELLOY X
WAVE SEAL

(d)

Figure 102 Seal Compressibility Test Specimens

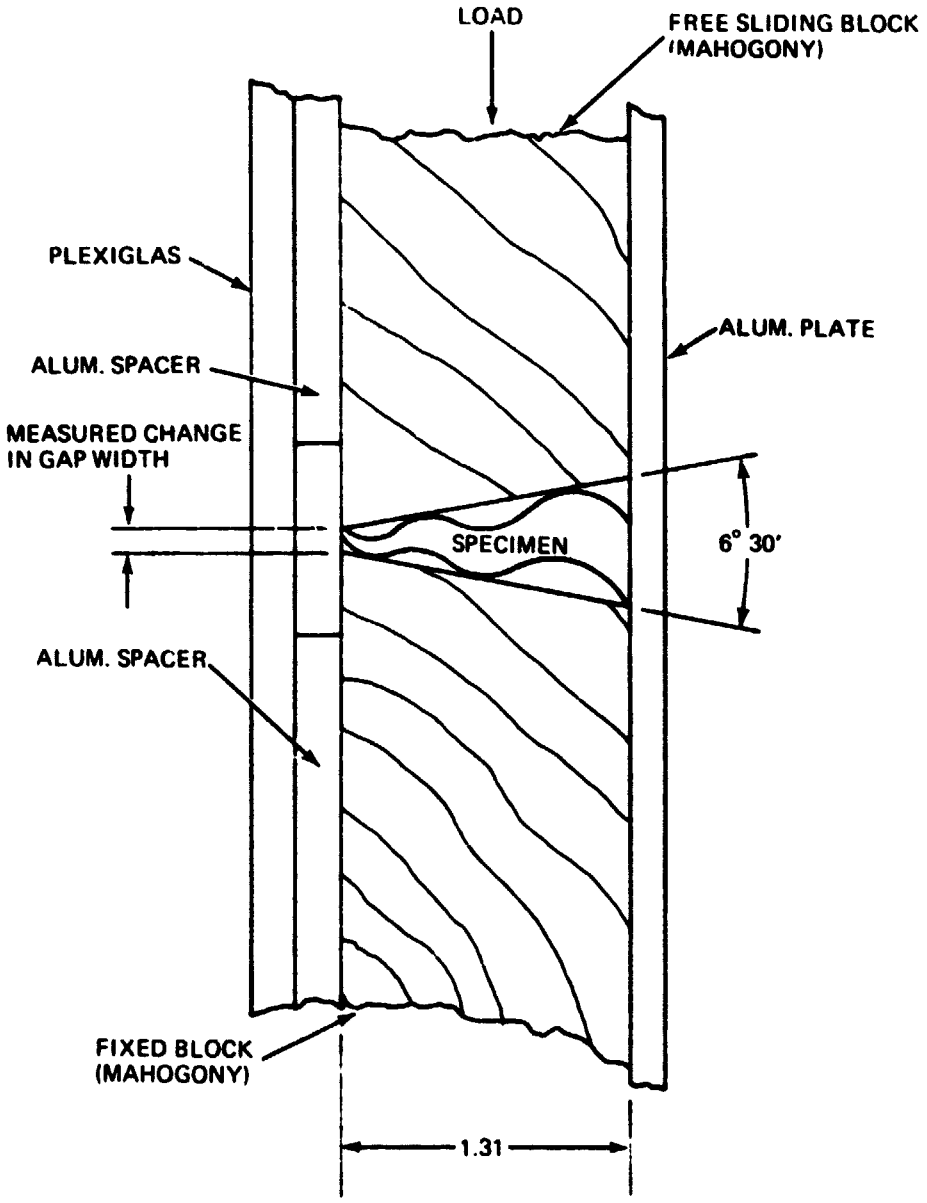

Figure 103 Test Fixture For Seal Compressibility

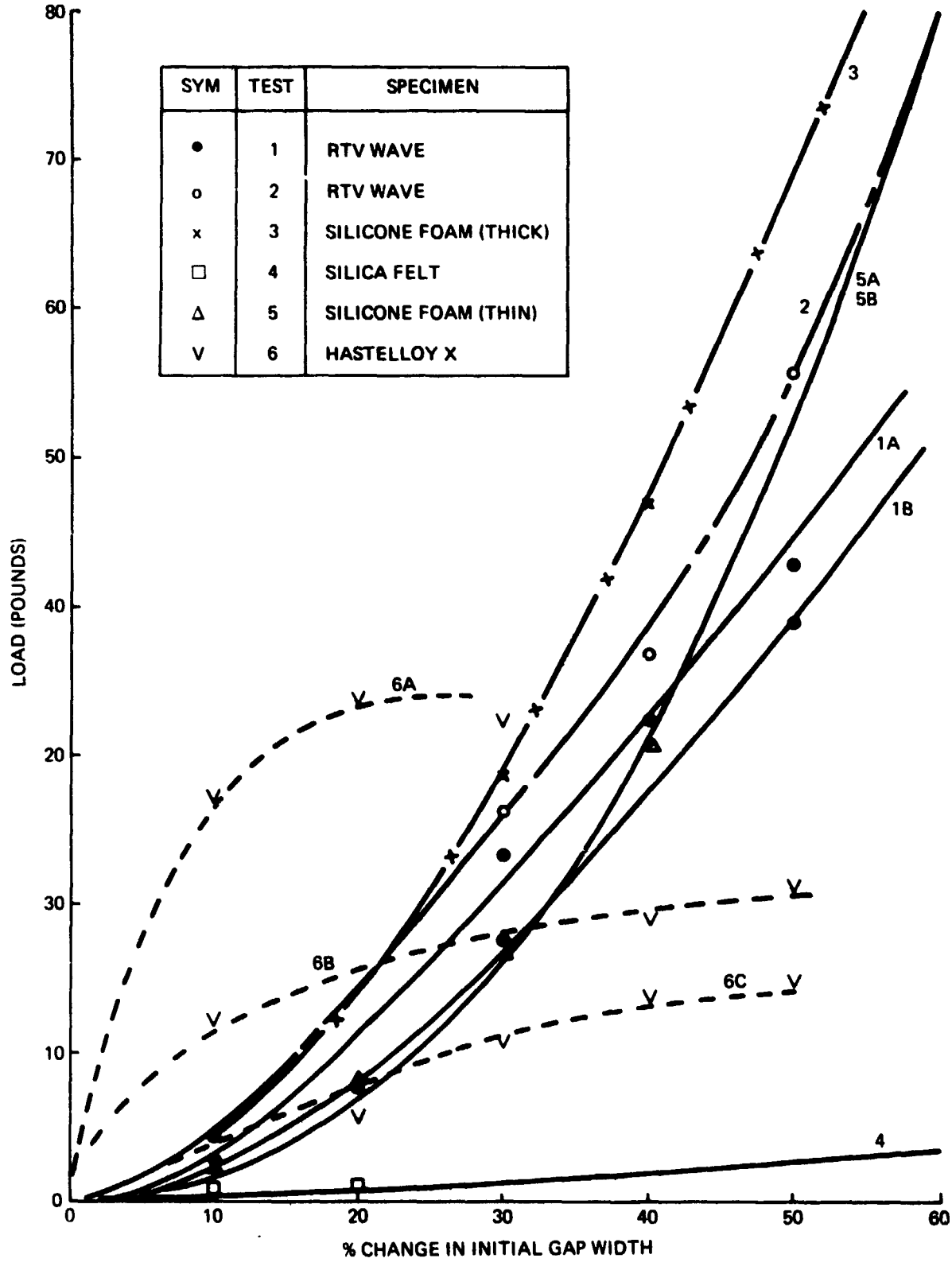

Figure 104 Results Of Seal Compression Test

Tests were performed using an INSTRON Model TTC-M1 Universal Testing Machine.

Test No. 1 was conducted on a wave seal molded from RTV 560, as shown in figure 102, and was set up to stop load application at a gap dimension of 0.060 (the approximate seal thickness). The test was repeated a second time with the curves labeled 1A and 1B in figure 104 showing the behavior for the first and second cycles respectively. Test No. 2 was conducted on the same specimen varying the load from 0 to 100 pounds, allowing the gap to close less than the .060 above.

Test No. 3 was conducted on a specimen consisting of three strips of 1/8" silicone foam. See figure 102 (b).

Test No. 4 used the test specimen shown in figure 102 (c) (6 pieces standard Astro mat (tradename), style No. 550).

Test No. 5 used a modified version of the configuration used in Test No. 3. The two outer pieces of silicone foam were made of 1/16" sheet rather than the 1/8" previously used. The test was repeated once.

Test No. 6 used a wave seal similar to that used in tests 1 and 2 but was fabricated from 3 mil thick Hastelloy (see figure 102 (d). This test was set up to stop loading when the seal was compressed 50% of its initial dimension. In the first test (Curve 6A) the tip of the wave seal contacted the test fixture (plexiglas plate) before 50% compression was reached, so the test was halted and the fixture was modified. It is interesting to note that at the conclusion of the first run (6A) the seal had taken a set of .047. Four hours later, at the start of run 6B, it had almost completely recovered. At the conclusion of run 6B, the seal again had a set of .047. The load required to achieve 50% deflection dropped in each run.

In all tests the initial gap used was that resulting from the weight of the test fixture (1.3 lb) resting on the seal.

It can be readily seen from figure 104 that the silicone foam is likely to build up large loads against the ablator and/or RSI edge as the seal material is compressed in excess of say 40 to 50 percent of its original (free state) gap dimension. This can be controlled through proper selection and pre-compression of the original assembled dimension. Of particular interest is the very low initial and negligible load buildup, even up to 80 - 90% compression, for the silica felt seal (see figure 104 and 105).

b. Preliminary Screening via Thermal Test Data

It was fortunate that some Avco test data (Ref. 70, 71) were available for an initial thermal evaluation of the candidate seal materials.

Five specimens of Avco 5026-39 Hc ablator with various seals installed had been tested, in the ROVERS Arc facility, for entry heating without precharring or cold soak. Four of these were seal candidates mentioned in the previous section and one was a reference ablator. The specimens had been fabricated at Avco utilizing standard Avco 5026-39 Hc ablator material. These specimens were 3 inch diameter, flat-faced cylinders measuring 1.25 inches thick and were bonded to a 0.25 inch thick fiberglass backing plate. A ten degree total angle, tapered slot measuring 0.100 inch width on the front surface was cut for the full diameter and for the full thickness of four of the specimens. Each of these specimens was then provided with a different type of seal. The four types of seals tested were:

a. Caulked

b. Silicone Foam

c. RTV Wave Seal, and

d. Silica Felt

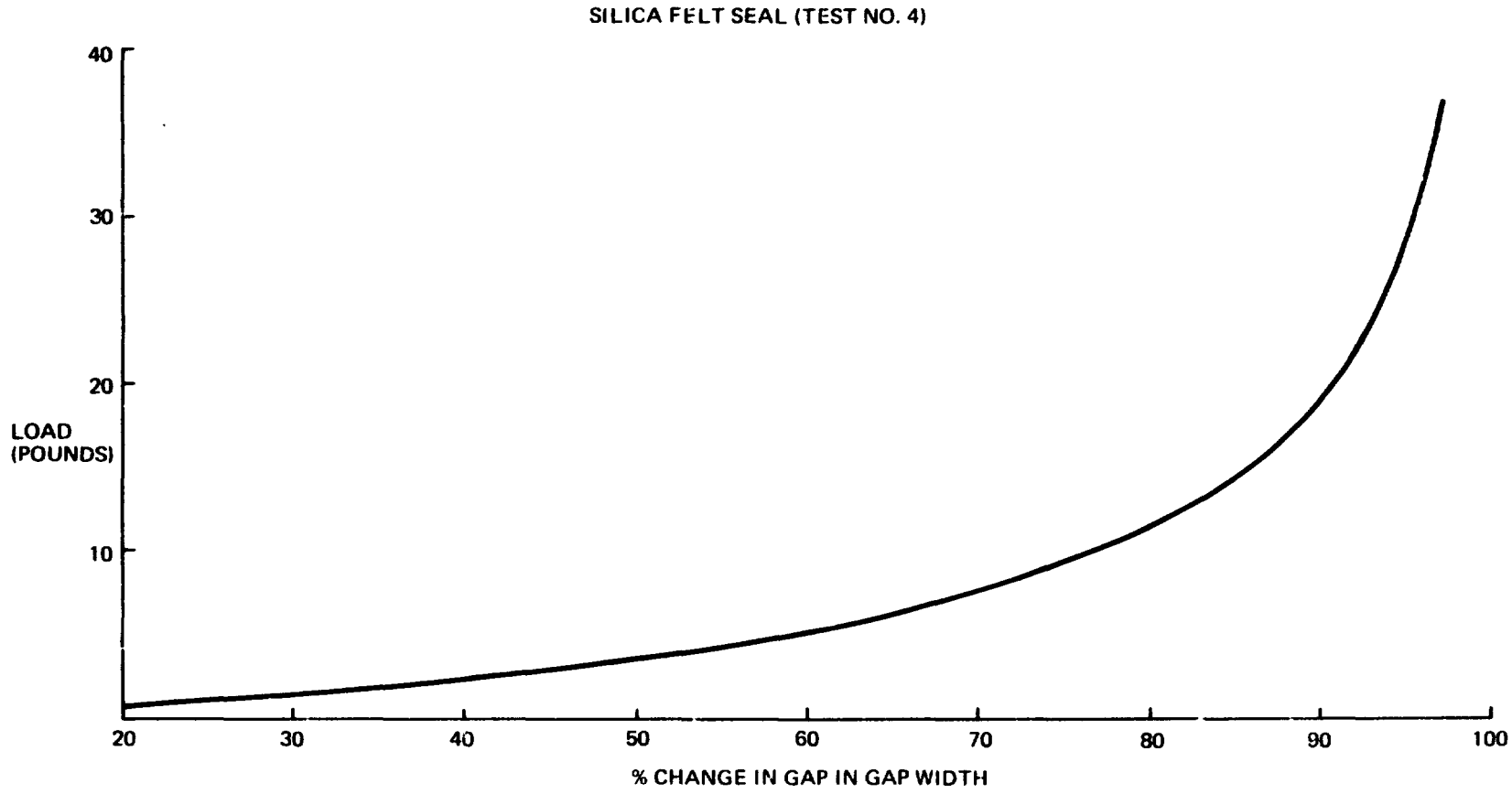

Figure 105 Compressibility Of Silica Felt

Note that this combination represents a gross manner, the two basic approaches considered here. For example, the wave seal has built in voids as do a number of designs and therefore, thermal performance will be similar. Figure 106 defines the test specimen configuration and instrument for each of the test specimens.

All specimens had been instrumented with two chromel-alumel thermocouples located at the interface of the ablator meterial and the fiberglass backing plate and positioned so that one was directly behind the seal on the specimen centerline and the other was offset one inch from the centerline and located in the ablator meterial. A recording pyrometer was utilized to monitor the surface brightness temperature throughout the test period. Motion pictures of the exposed surface at various time intervals are also available (Ref. 72).

The test specimens were weighed, measured and photographed (figure 107(a) & (b)) prior to installation. They were then installed in the square model holder with insulating strips wedged between the specimen and the holder and the spaces left were filled with fiberfrax insulation to reduce conduction between the sample and the model holder. The model holder was then attached to the remotely operated, overhead injector and adjusted to position the front surface of the test specimen in the center of the arc jet and at a distance of 10 inches downstream from the plane of the exit nozzle (3 x 3 inch section).

The test conditions were nominally a heat flux of approximately 60 Btu/ft^2-sec. at an enthalpy of approximately 12 - 13000 Btu/lb. Each specimen was injected into the plasma stream and exposed to the heating environment for a pre-set time of 600 seconds. This was followed by a cold-soak period of at least 500 seconds. After testing, the specimens were removed from the model holder, weighed (to determine mass change), measured (to determine thickness change),

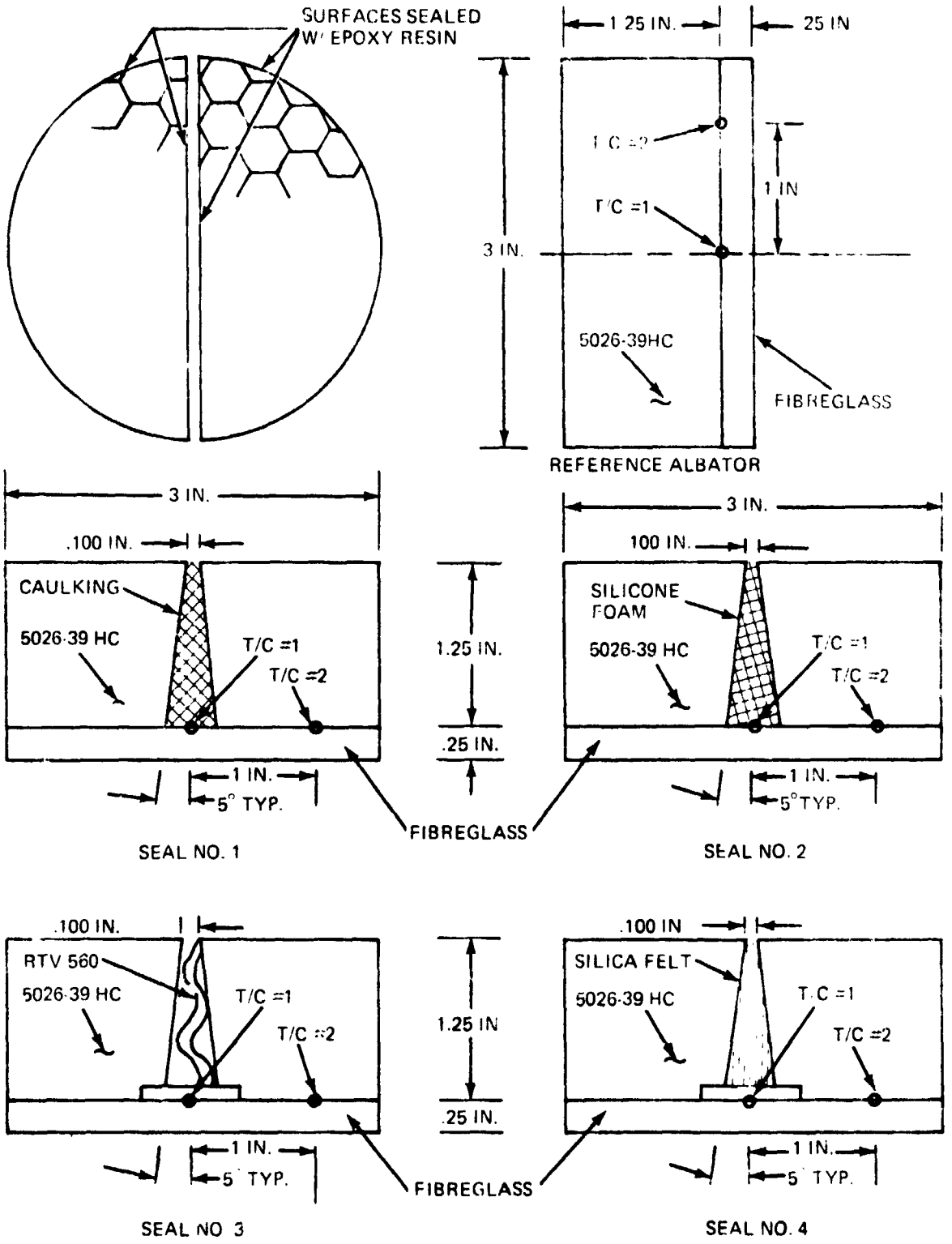

Figure 106 Details of Seal Construction and Instrumentation of Previous AVCO Seal Tests

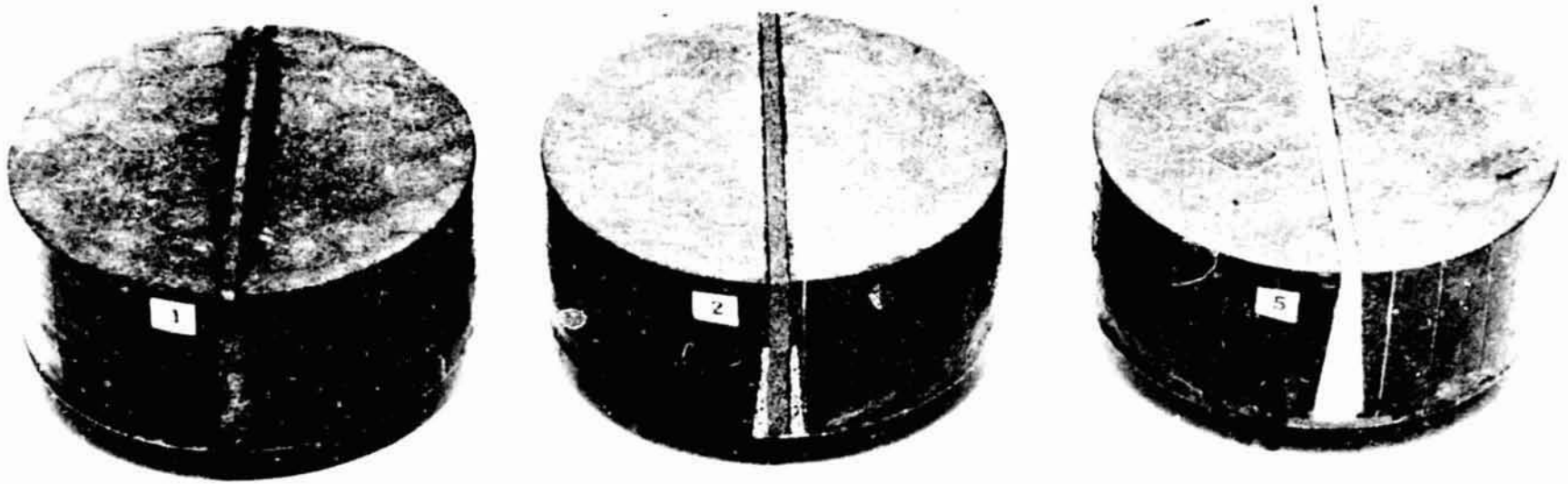

Figure 107(a) AVCO Seal Test Data: Pre-Test View of Specimens-1, -2 and -4 (#22944G)

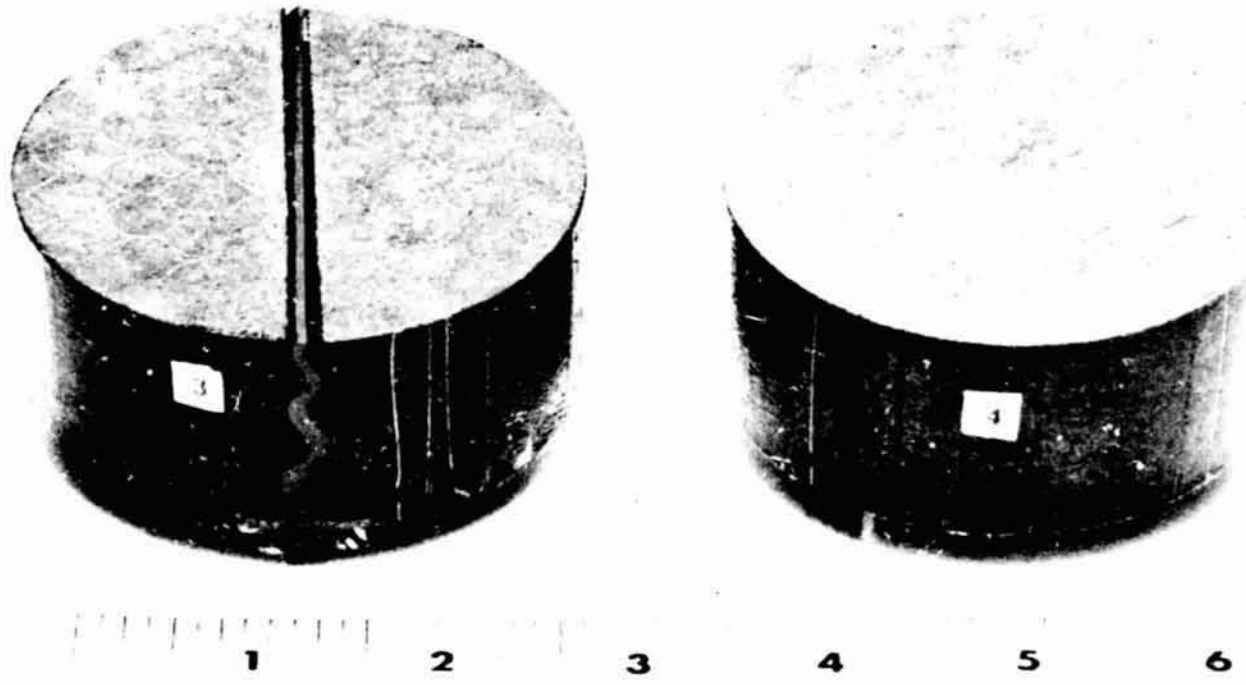

Figure 107(b) AVCO Seal Test Data: Pre-Test View of Specimens -3 and -5 (#22944H)

comments pertaining to the surface appearance of the ablator and of the seal noted and post test photographs taken of the surface (see figures 108(a),(b) & (c). Backface temperature data from thermocouple No. 1 (located on the specimen centerline directly behind the seal) is presented as temperature rise as a function of time in figure 109.

No severe degradation of test specimen surfaces was noted during the test series. No unusual effects were noted in viewing the motion pictures. Some contamination of the charred ablator surface in the seal area was noted on all specimens except the silica felt which remained very clean. The RTV wave seal protruded above the surface from early in the test run and upon cool-down was extended approximately .10" above the ablator surface. Both the caulked and silicone foam seals showed some cracking in the charred surface and evidence of slight pulling away (shrinking) from the ablator edges.

It is noted from observing the temperature dat that seal No. 2 (silicone foam) had the lowest rate of temperature rise (0.1 degree Fahrenheit/second at test time) and seal No. 4 (silica felt) had the highest slope (0.2° Fahrenheit at the corresponding mid-test time). The silicone foam seal design (No. 2) also produced a slightly lower total backface temperature at the end of the test period than the reference ablator material did.

c. Selection of Candidate Seals

Based upon these preliminary mechanical and thermal evaluations, two seal concepts were selected for further evaluation using leading edge models simulating the actual joint contour in a sequential test including ascent, cold soak and entry. The two selected were the silicone foam and the silica felt seals. Table 39 presents a summary of the most important factors considered in making this selection.

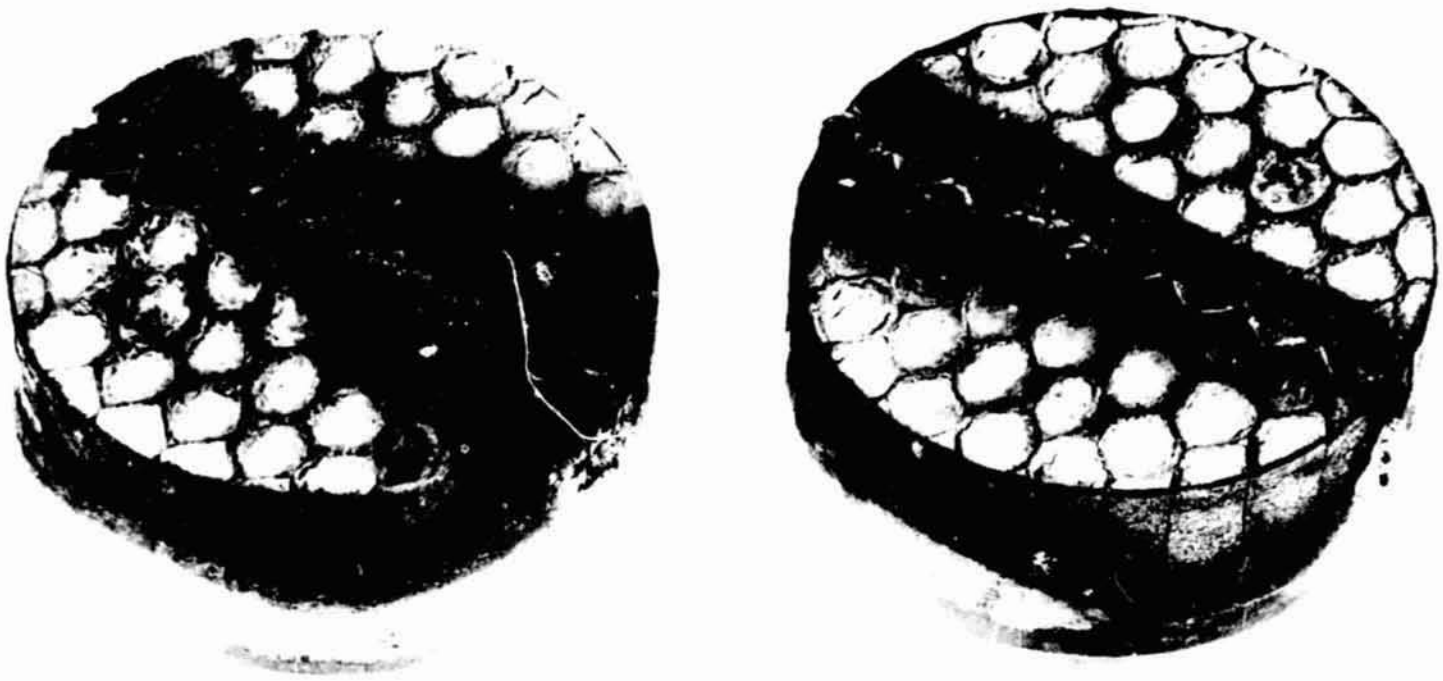

I
CAULKING
SEAL

II
SILICONE
FOAM

LEADING EDGE SEAL CANDIDATES

Figure 108(a) AVCO Seal Test Data: Post-Test View of Specimens -1 and -2 (#22950A)

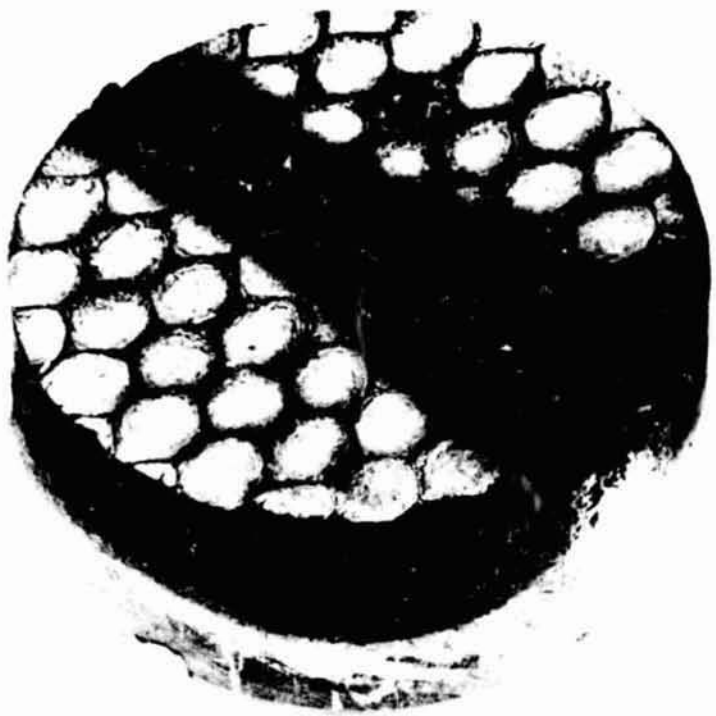

III
RTV-560
WAVE SEAL

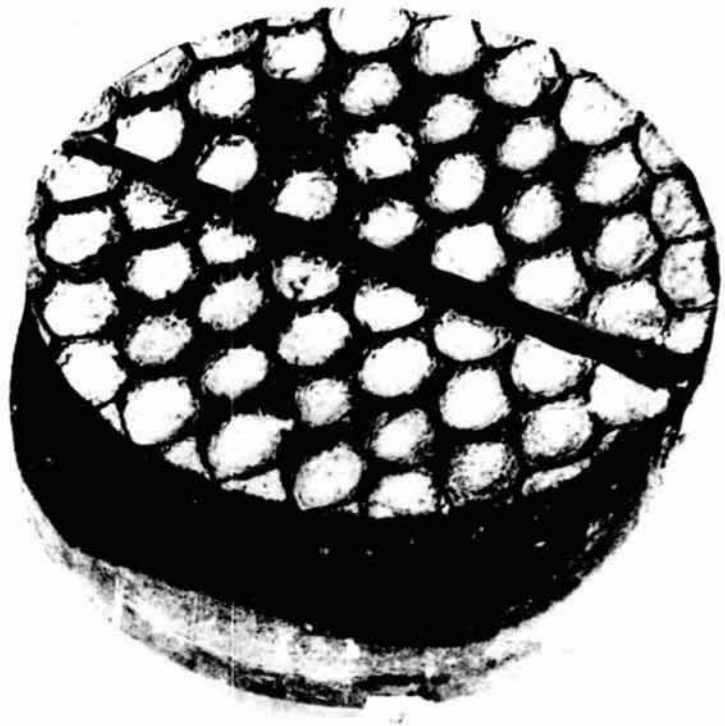

IV
SILICA FELT

LEADING EDGE SEAL CANDIDATES

Figure 108(b) AVCO Seal Test Data: Post-Test View of Specimens -3 and -4 (#22950B)

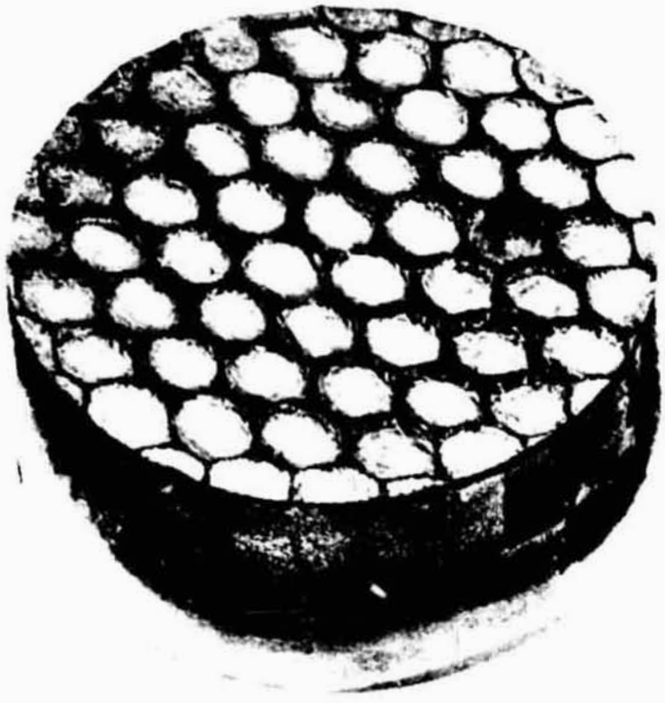

V
REFERENCE
MATERIAL

LEADING EDGE SEAL CANDIDATES

Figure 108(c) AVCO Seal Test Data: Post-Test View of Reference Ablator Specimen (#22950C)

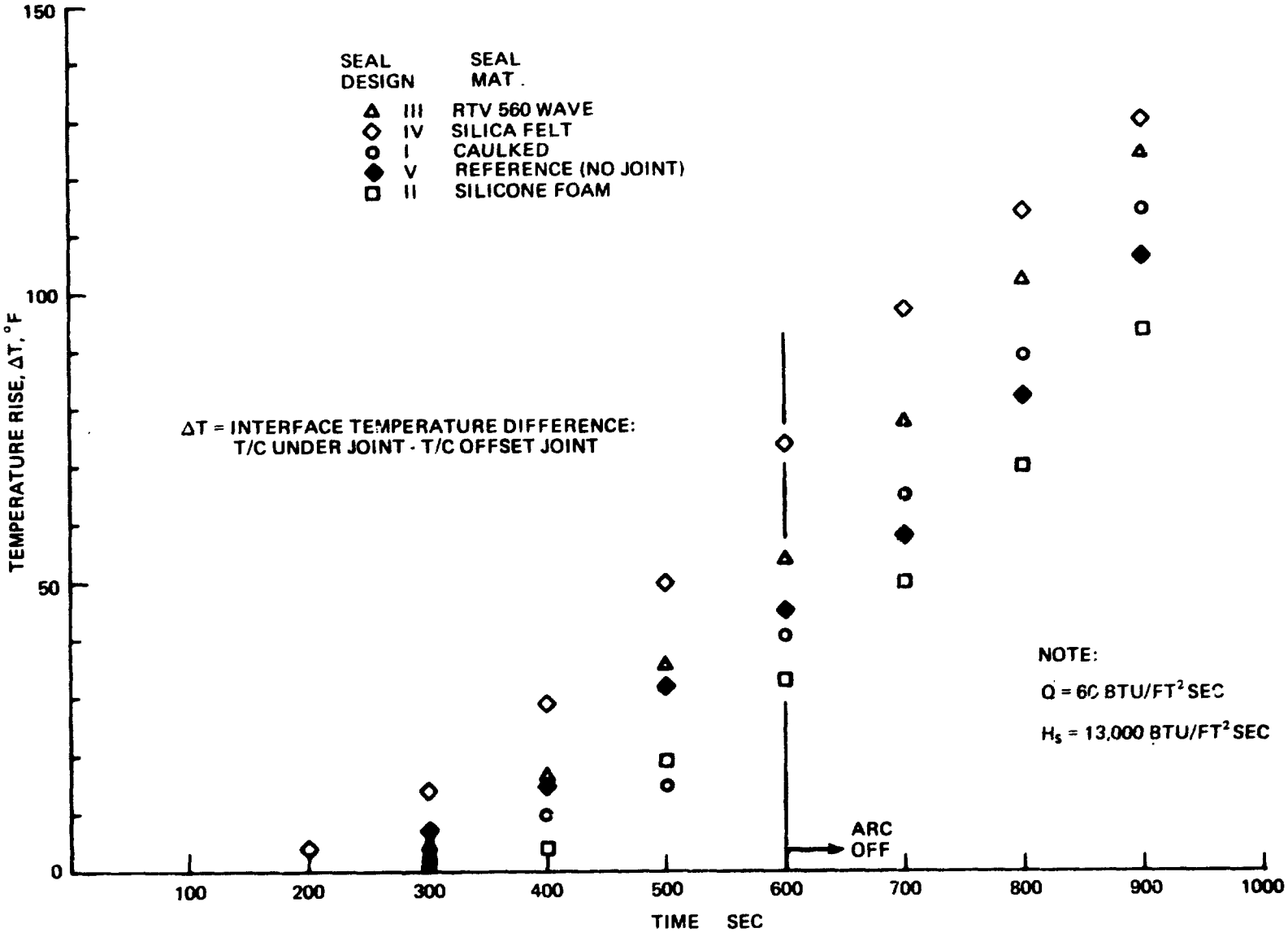

Figure 109 Rear Surface Temperature Rise on Seal Material Tests (Previous AVCO Tests)

Table 39 Ablator To Ablator Seal Comparisons

	Caulked	Silicone Foam	RTV Wave	Silica Felt
Thermal Performance	Good (3)	Excellent	Fair	Poor
Moisture Seal	Good (3)	Excellent	Fair	Poor
Ease of Inst.	Excellent (4)	Poor	Good	Fair
Ease of Inspection	Fair (2)	Good	Good	Good
Cost	Excellent (4)	Good	Fair	Good
Contamination	Poor (1)	Poor	Poor	Excellent
Growth (Protrusion)	Good (3)	Good	Poor	Excellent
Total Rating	20	19	14	18

Although the compressibility of the silicone foam was somewhat lower than desired its recovery after loading was very good. Thermally, it performed better than all other materials tested. The reverse was true for the silica felt seal which was by far the most compressible material, but its thermal performance (insulation efficiency) was less satisfactory. However, other points in its favor were that the silica felt seal did not show any contamination effects or protrude above the surface or become embrittled after the arc testing.

The caulked in place seal showed good thermal performance, but, because there had been some problems encountered in curing the seal material at room temperature (Ref. 73), it was decided this concept required further development and therefore would be inappropriate for our design. The metallic wave seals were eliminated because of their poor recovery rate after loading.

6.5.1.4 Seal Evaluation in Leading-Edge Models

As an aid in making the final decision on the two best seal candidates, two leading edge models containing a typical joint with seals in the Mod 7 Hc ablator were fabricated for ascent, cold soak and entry tests. However, the essential step in the sequence, the entry heating to be conducted in a NASA Langley arc jet, could not be carried out within the span of this study because of schedule conflicts in the Langley facility.

Only the results of the first step of the sequence were conducted within the span of the study. In the first step alone, very little is expected to turn out. In any case, the model design is shown in figure 110 and the complete test rationale, test procedure, and results are presented in the Data Package. Both models were exposed to the ascent heating environment in the Avco ROVERS facility (and then submitted to NASA LaRc).

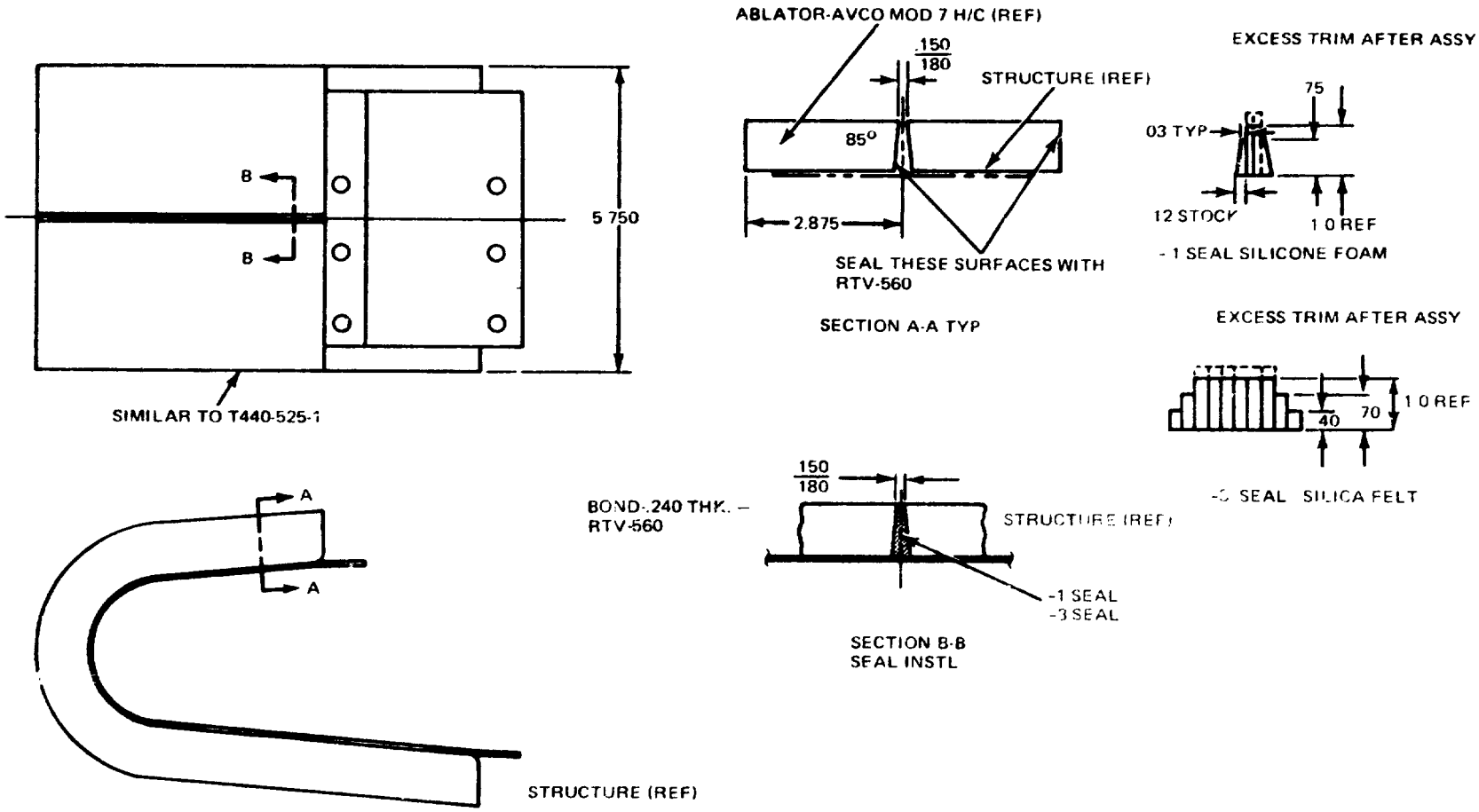

NOTE

1. ALL DIMENSIONS OF DRAWING NO T440-525-1 APPLY AFTER ASSEMBLY

D	04614	

Figure 110 Models Designed For A/A Joint Evaluation

Ascent heating test results for both models for a stagnation point heat flux of 9.7 Btu/ft^2-sec showed a maximum rear surface temperature rise directly beneath the seals of 42° F and 32° F for the silicone foam and the silica felt seals respectively after 560 seconds. Thermocouples located under the ablator offset spanwise 2" from the seals showed identical readings indicating no adverse thermal effects under the seals for these test conditions. Post test examination of the models showed that the silica felt seal was somewhat rigid to the touch near the surface and had a tendency to separate from the Mod 7 Hc ablator ablator (see figure 111). The silicone foam seal had a tendency to swell and protrude above the Mod 7 Hc ablator. There was also some surface separation between the two strips forming the seal in the nose region as shown in figure 112. With the exception of a thin flaky coating which appeared on the stagnation region, the surface of the ablator looked good after the test.

6.5.1.5 Selected Ablator/Ablator Joint Concept

Because of the unavailability of the leading-edge model data, the selection had to be made based on the basis of past experience and data accumulated to this point.

Based upon the test data generated, model fabrication experience, and working with both seal materials, there appeared to be little justification for selecting one material over the other. If anything the results tended to favor the silica felt material. Although the thermal performance of the silicone foam was somewhat superior to the silica felt in the splash tests, both materials performed about equally well in the leading-edge configuration during ascent heating. The compressibility of the silica felt was shown to be substantially higher than the silicone foam making it more desirable for installation as well as relieving any stresses between adjacent leading edge segments. Also, no contamination was observed on the adjacent ablator after either test using

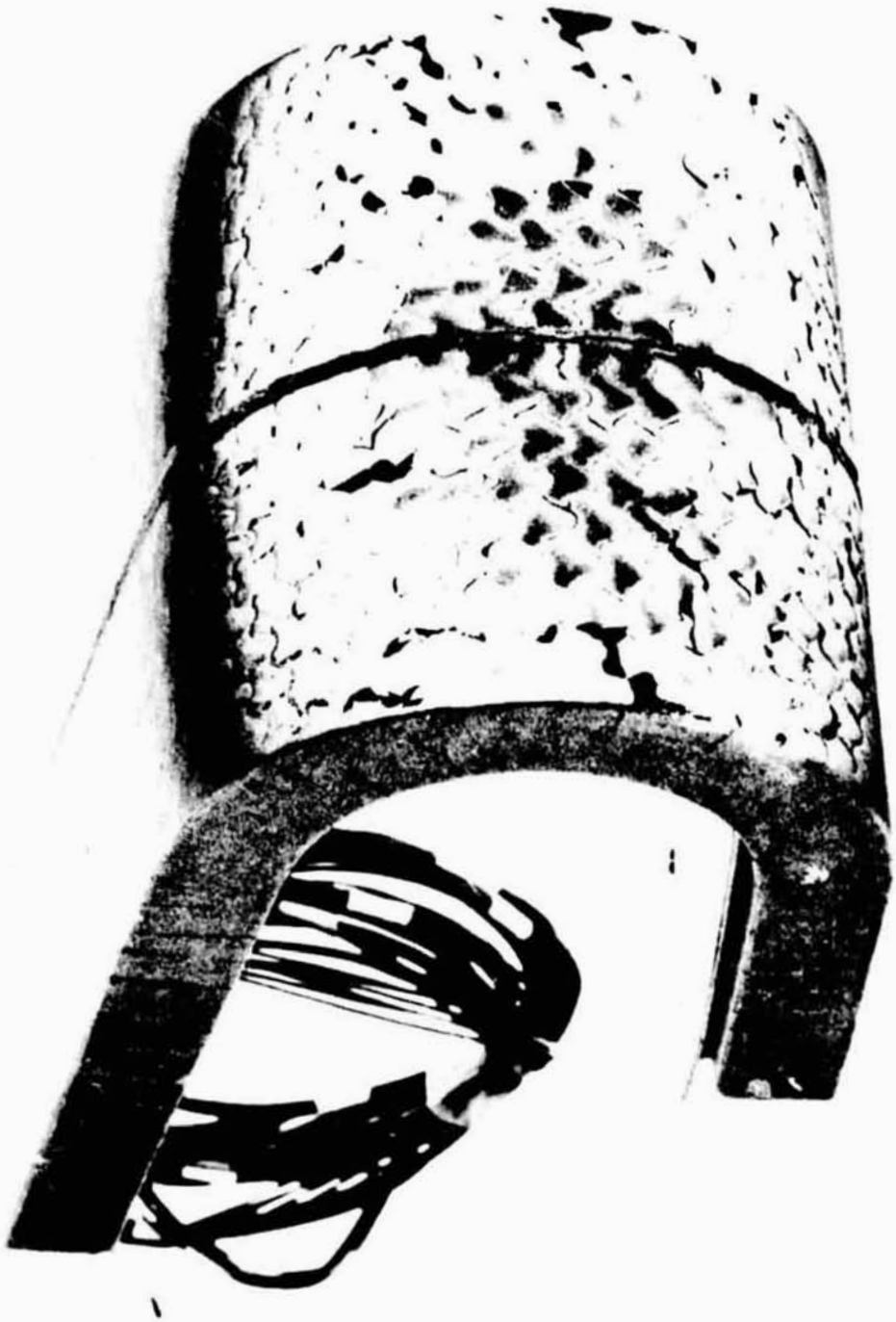

Figure 111 Post Ascent Appearance of A/A Silica Felt Seal Model

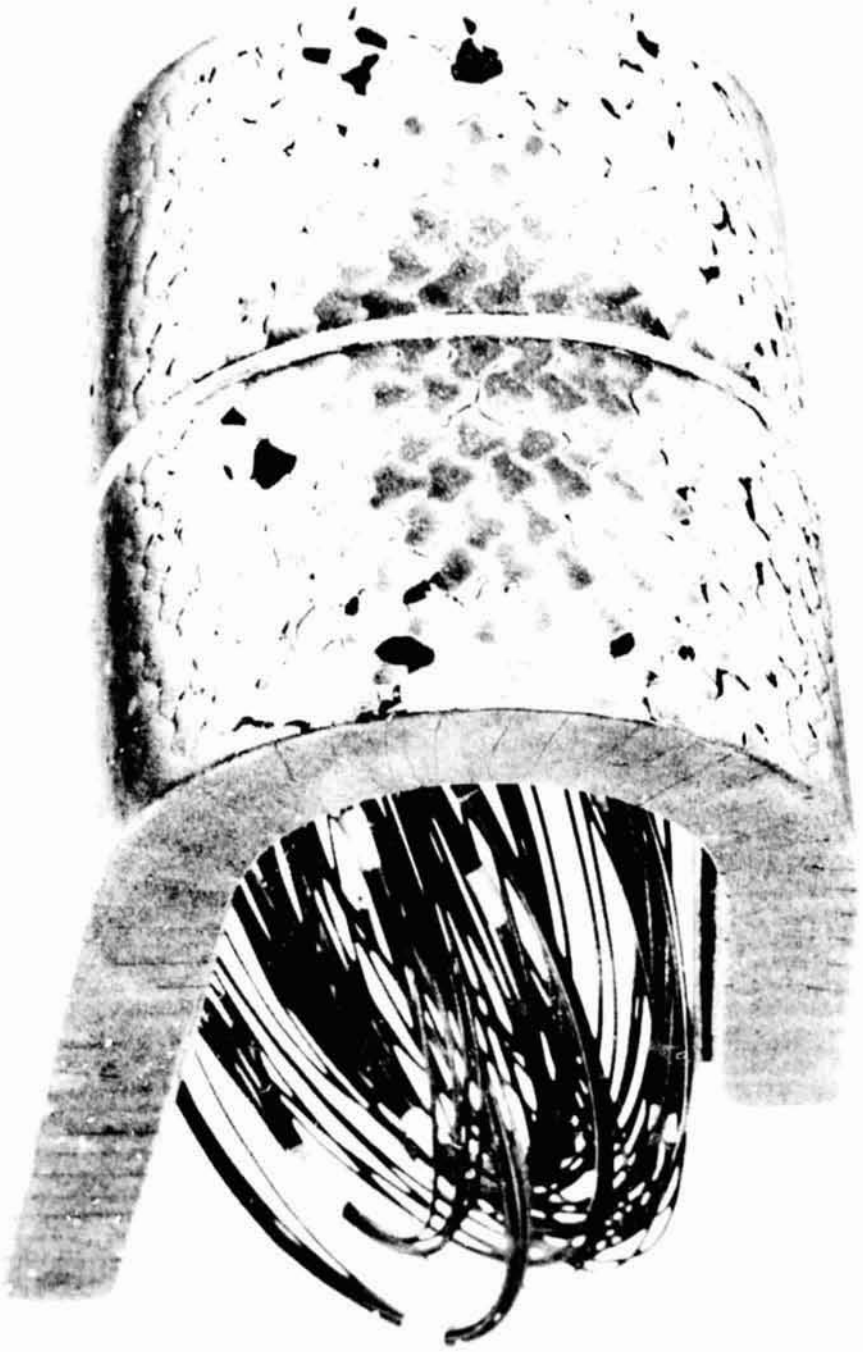

Figure 112 Post Ascent Appearance of A/A Silicone Foam Seal Model

the silica felt whereas some deposits were observed after the splash tests with the silicone foam material. Finally, the surface appearance of the silica felt was good unlike the silicone foam which showed a minor tendency to protrude above the surface.

In spite of all these positive features, there was one crucial unknown relative to the silica felt; namely, the performance of this relatively porous material under entry heating and the simultaneous l.e. pressure gradients and shears which could cause flow along and possibly down into the joint. The silicone foam seal on the other hand, having a closed cell structure, did not have an equivalent potential weakness. Moreover, the RTV class of materials have been flight proven as seals on the Apollo vehicle.

Without this vital piece of information (which would have come from the l.e. tests), and since one seal had to be selected for the final design, it was decided to go with the more well characterized and proven material; namely, the silicone foam seal.

The joint configuration chosen consists of beveling the edges of the ablator to entrap the seal, because it is about the simplest means of obtaining a positive holding pressure on the seal. Minimum gap widths of the OML of the ablator were set at 0.15", because it is a compromise between assembly tolerances, thermal expansion requirements, and minimum gap width for entry heating.

The operational procedure to install the joint during the l.e. refurbishment will be taken up in Section 6-6.

6.5.2 Ablator/RSI Joints

6.5.2.1 Joint and Seal Concepts

Some differences exist in the criteria affecting the design of the ablator to

RSI joint and seal as compared to the ablator/ablator joint and are as follows:

a. Due to the location, the heating is lower

b. Unless excessive spanwise flow develops over the wing, little or no parallel flow will occur

c. The allowable compressive force the seal exerts against the RSI must be lower than for the ablator since it is expected the RSI be more susceptible to damage

d. The thermal expansion/contraction across the joint is less than ablator/ablator designs

e. The upstream ablator must not recede so as to generate a forward step

The above differences immediately open up the possibility of controlling the gap width and not using any seal material in the cavity. Therefore there are two basic approaches to the A/RSI joint: a) controlled gap width joints; and b) joints with seals.

In selecting the gap shape and in developing the joint schemes, one must keep in mind what can be feasible--from a fabrication aspect--for the RSI. Considerable freedom seems to be available in the gap shape, since the current thinking on the RSI-RSI tile joints include rather sophisticated concepts, as is shown in figure 113. (from Ref. 74). Note that the schemes in figure 113 are all for unsealed gaps and that the tolerance control for the RSI-RSI tiles joints is expected to be superior to the RSI-ablator joints. Therefore the disadvantage noted in figure 113 for the bevel joint disappears if the gap is sealed.

Two criteria were considered in developing the schemes presented below:

1) Even though the ablator is Hc reinforced, it is not desirable the ablator to be cut as in the strip concept

of figure 113, since the charred thickness would be higher than the 'bridge' height (figure 98)

2) It would be desirable to eliminate the situation in which the RSI bridge is subjected to loads that increase the danger of fracture of the RSI overhand part. In other words, it would be desirable not to rely in closing the gap as in the lap and strip concepts of figure 113.

a. Controlled Gap Width Designs

The first of many basically similar designs is shown in figure 114. This involves an ablator strip adjacent to the RSI which is mechanically attached to the leading edge structure. One reason for the higher density non-ablating strip is to allow for the ablator change (recession or swelling) and yet guarantee a small rear-facing step at the joint to protect the RSI from a localized overheating at the corner of the file. The other reason is to be able to adjust the gap between l.e. and RSI and therefore eliminate the seal. The screws which attach this strip are in over-size holes allowing the ablator strip to be adjusted in the chordwise direction so as to control the width at the gap between the strip (leading edge) and the RSI. An additional seal strip is incorporated in the lower portion of the TPS adjacent to the structure.

Since the gap between the adjustable strip and the ablator edge will vary, depending upon the amount of adjustment, it is planned to gun (caulk) this after installation of the leading edge.

Figure 115 is basically the same as above except the ablator strip can be adjusted externally through the removal of threaded ablator plugs rather than requiring leading edge removal.

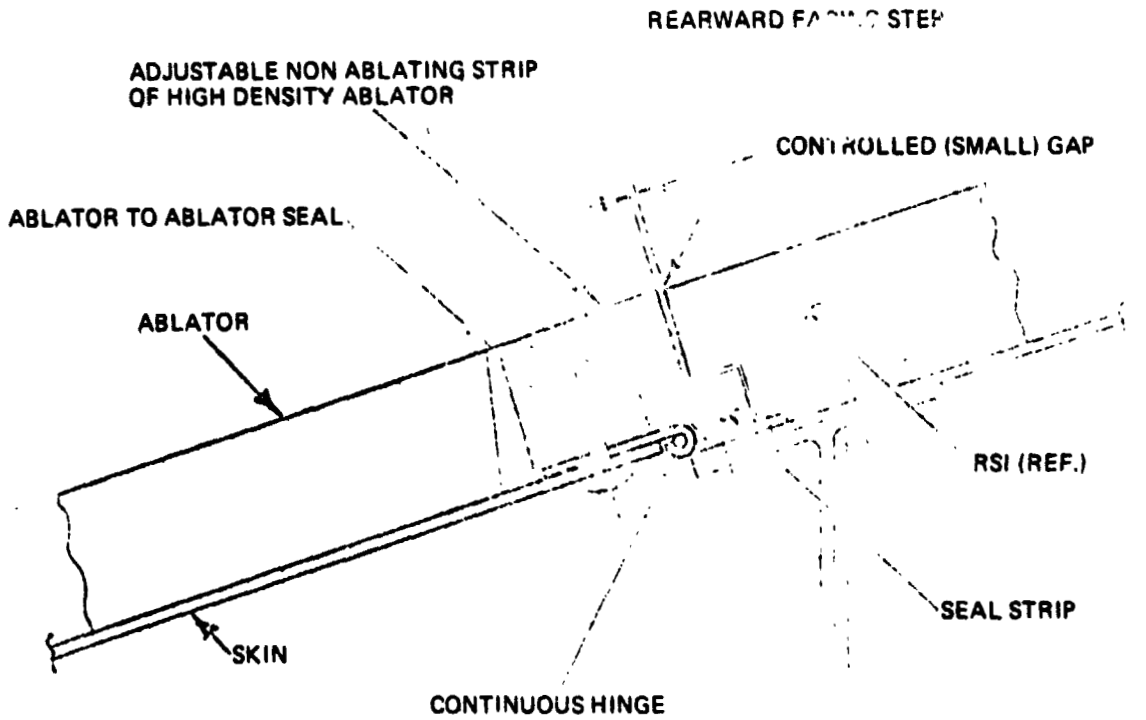

Figure 114 Ablator/RSI Joint: Controlled Gap with a Mechanically Attached Ablator Strip

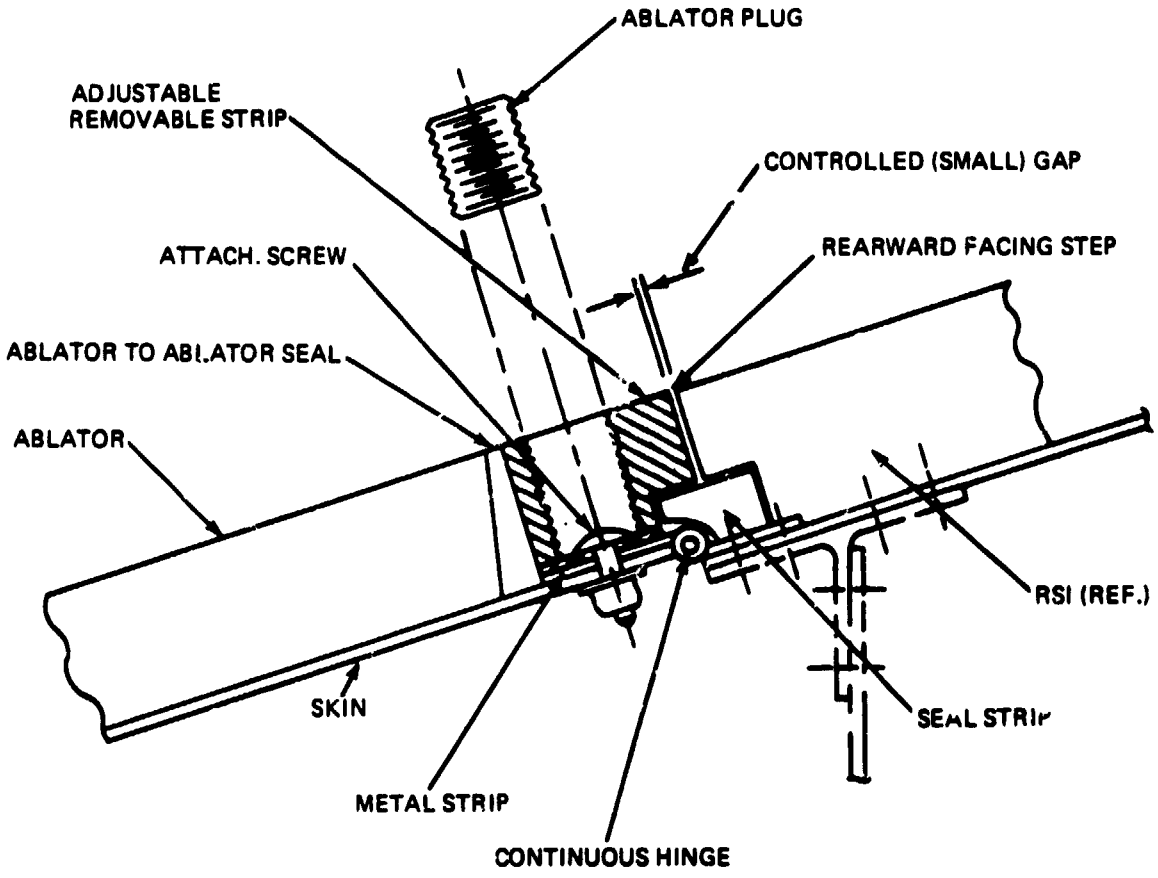

Figure 115 Ablator/RSI Joint: Controlled Gap With An Externally Bolted Ablator Strip (Metal Strip)

Figure 116 incorporates a seal design identical to that of figure 115 above, however, removal of the adjustable strip exposes the leading edge attachment bolts which attach the leading edge structure to the hinge. The hinge is maintained for purposes of structurally uncoupling the leading edge from the wing.

b. Joints with Seals

The second approach is depicted in figure 117. This approach utilizes seal strip in depth as well as, filling the gap to the surface; in this case, with silica felt material. The load exerted by the felt on the RSI, due to thermal growth and/or vehicle tolerances appears to be small as a function of compression of the felt (see Section 6.5.1.3). It is believed that this felt filler will not recede or expand into the air stream.

Figure 118 shows the incorporation of a metal wave spring seal which is mechanically attached via a number of screws along the length. Figures 119 and 120 incorporate the use of RTV as the seal material. The "Y" seal of figure 119 is bonded into the ablator edge and is in place when the l.e. panels are installed. The seal of figure 120 is a similar approach to that depicted in figure 119 and can be inserted after the leading edge panels are in place.

6.5.2.2 Ablator/RSI Joint Trade-off

With the selection of Mod 7 Hc and the 3560 HF as the ablative materials, no recession is predicted at the ablator to RSI interface; i.e., at the front spar. Since the primary reason for the higher density non-ablating strip in the designs of figures 114 through 116 was to allow a material change to maintain a smooth outer surface (no recession), less complicated designs would appear adequate. Moreover this approach requires the use of bolts (an unhappy

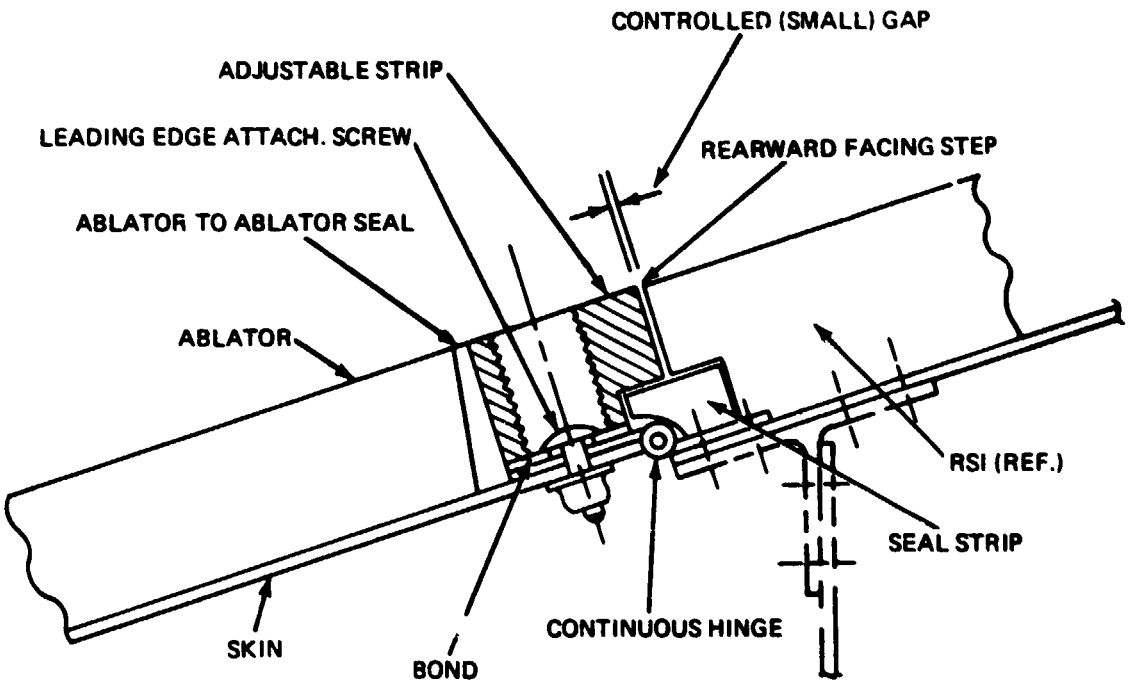

Figure 116 Ablator/RSI Joint: Controlled Gap with an Externally Bolted Ablator Strip (Bond Variant)

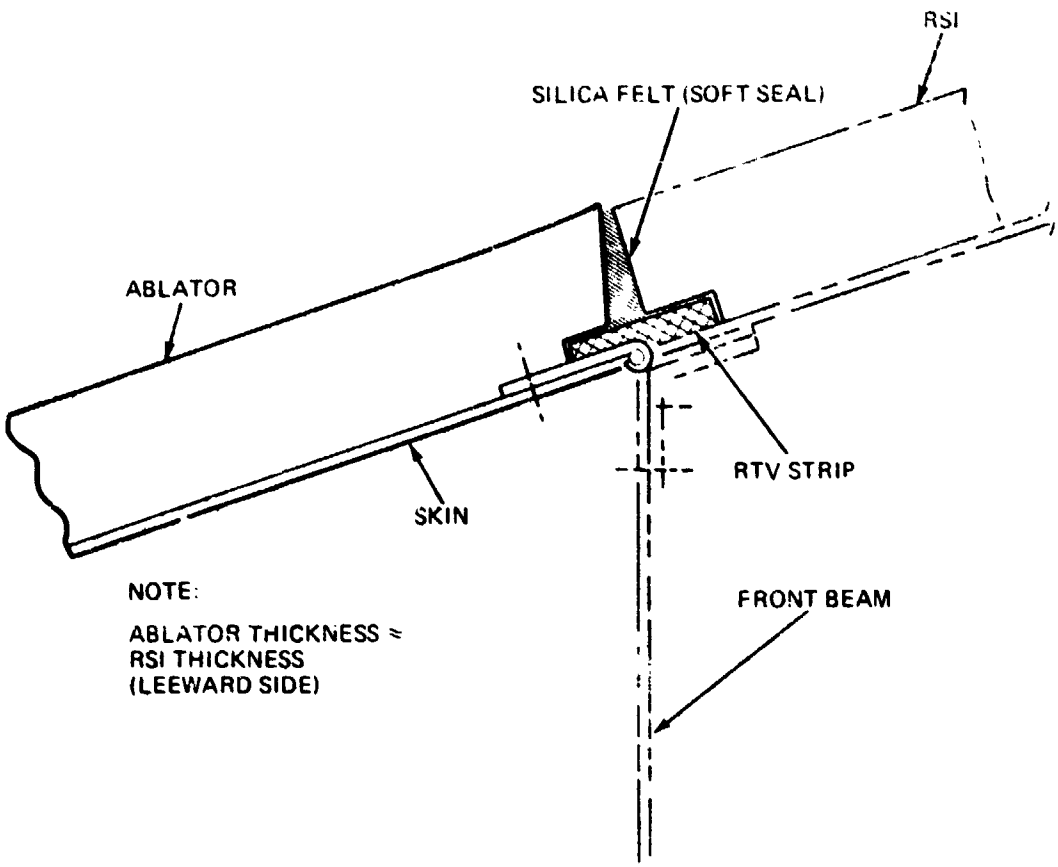

Figure 117 Ablator/RSI Joint: Silica Felt Seal

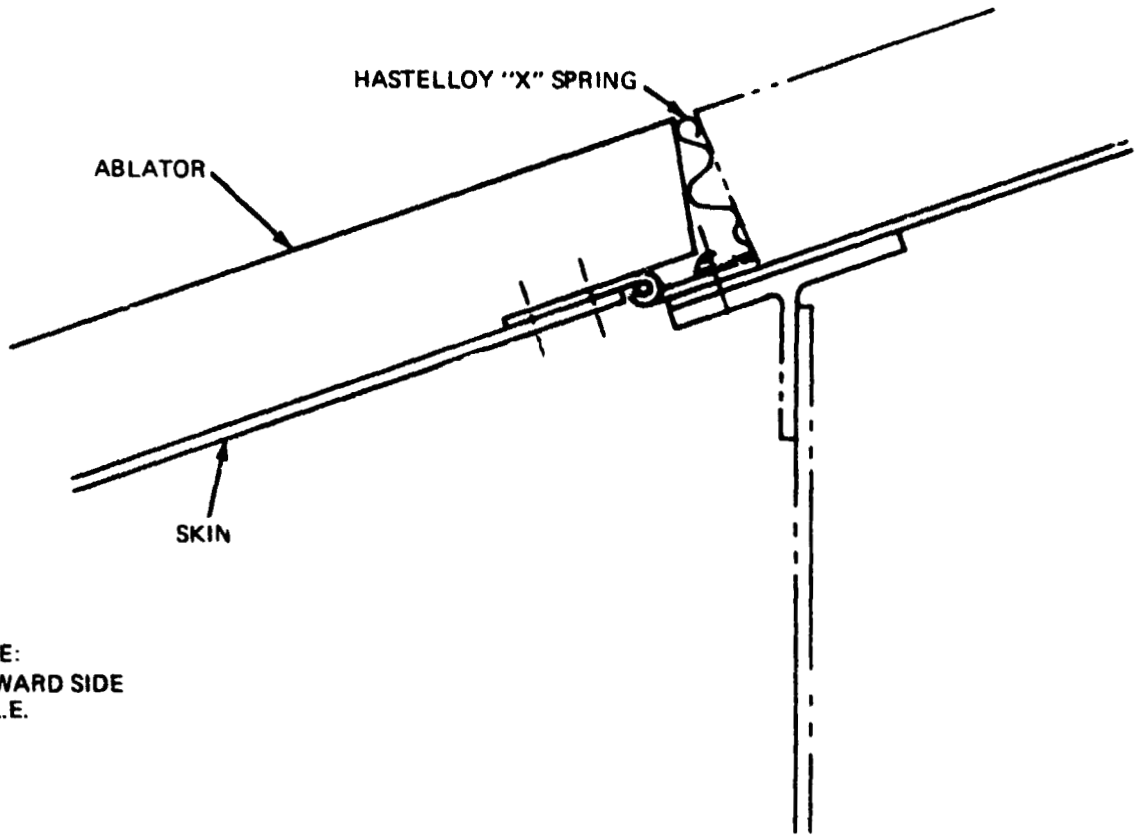

Figure 118 Ablator/RSI Joint: Metallic Wave Seal

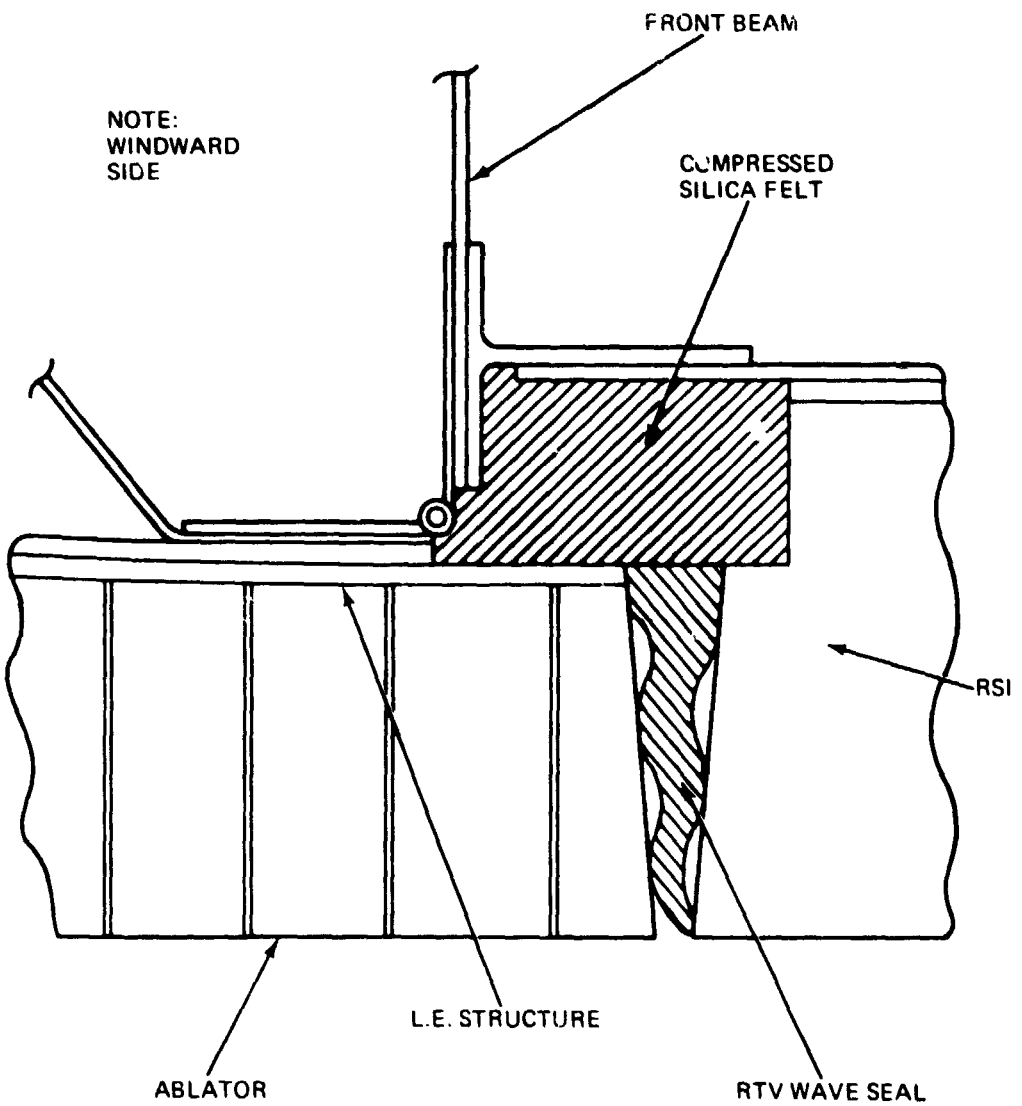

Figure 119 Ablator/RSI Joint ~ Gap Sealed with RTV Wave Seal

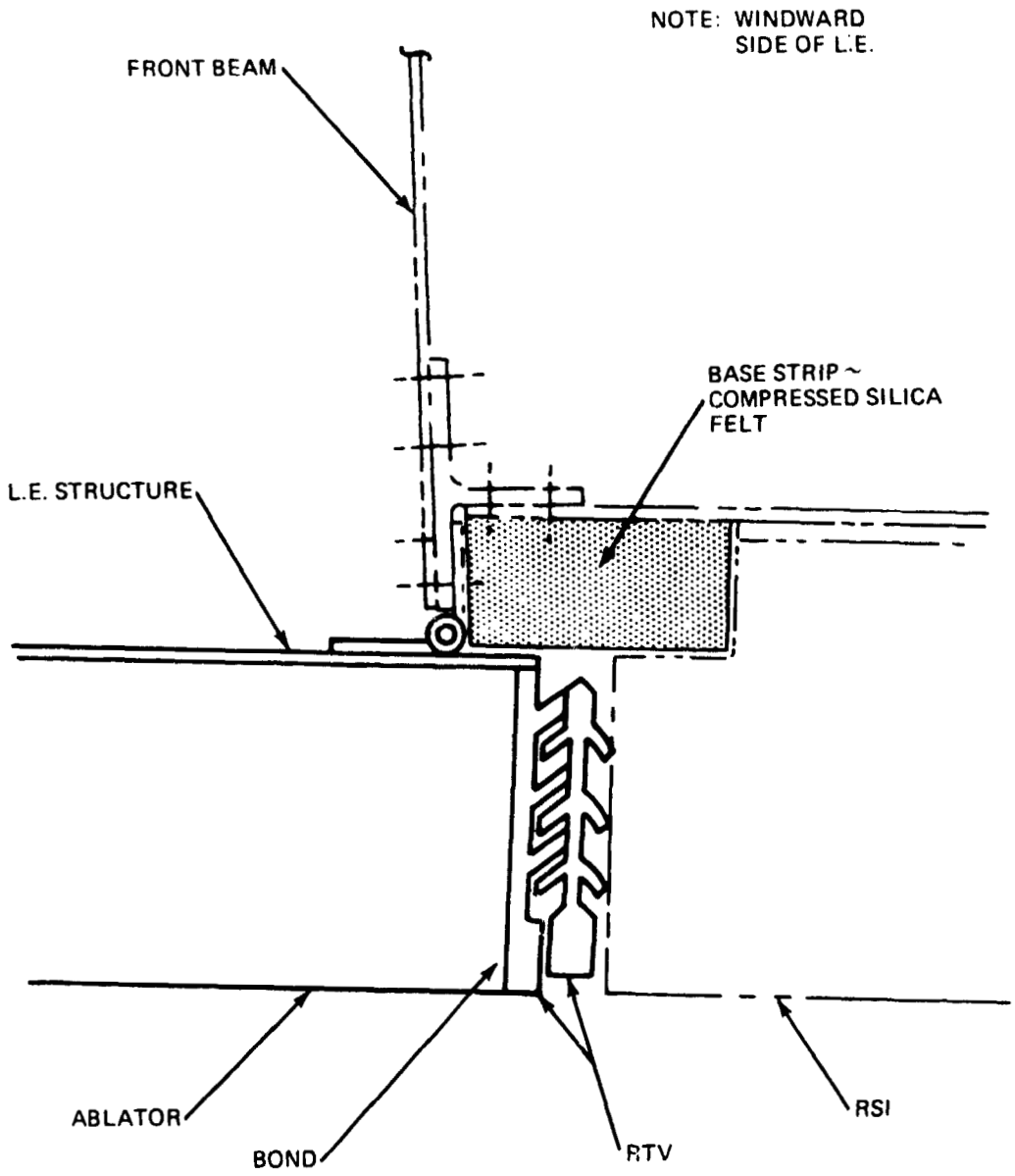

Figure 120 Ablator/RSI Joint: Gap Sealed With Labyrinth Seal

complication after the bolts were eliminated for the more important function of attaching the l.e. to the wing). A simpler version consists of carrying the leading edge ablator directly up to the RSI interface with a controlled width unsealed gap similar to those envisioned for the gaps between adjacent RSI panels. This was eliminated for several reasons. Among these was the fact that for the RSI the gap width could be controlled more closely during installation since each RSI tile is bonded in place. Secondly, the heating at the front beam would be higher than that experienced over the bulk lower surface. Lastly, this joint was between two dissimilar materials.

Of the sealing joint schemes presented (figures 117 to 120), the silica felt appears to offer the most advantages, specifically, low compressibility, no contamination, ease of installation and no protrusion above the gap as noted in connection with the A/A joints. Moreover, with the lower heating and less likelihood of spanwise flow there was little concern about flow down into the seal as was the case in the chordwise leading-edge seals.

As a back-up to this design the RTV wave seal appeared to be a strong candidate. In addition to its good thermal performance in the splash tests, it offered lower compressibility than the other remaining materials. This was a strong factor in selecting ablator to RSI seals in order to avoid damage to the RSI.

As a result, the seal joint approach was selected i.e. a simple narrow gap with a compressible material appears the most direct approval. The two seal materials, silica felt and RTV wave seal were identified as the two attractive candidates.

6.5.2.3 Two Candidate Designs

The complete joint design for upper and lower wing surface consists of beveling the edges of both the ablator and the RSI at the juncture to entrap the seal and using the scheme of figure 120 for the area underneath the seal. This is an

added bit of conservatism over the simpler, but less safe design of figure 119. On the upper surface (leeward side) where it is expected that the thickness of the ablator and RSI will be nearly equivalent the joint line will occur above the front beam directly over the hinge (see figure 121). To provide an added margin of protection to the hinge and seal off the leading edge cavity a narrow strip of RTV 560, will be placed directly beneath both heatshield overlapping the joint.

On the lower surface (windward side) where the RSI is expected to be markedly thicker than the ablator, the hinge connection will still occur at the front beam, but the ablator and leading edge substructure will be carried slightly aft of the connection. (see figure 121). This will protect the lower connection. Below the silica felt seal, it was decided to fill the void formed by the leading edge overlap with a low density insulator rather than attempt to cut a special RSI tile for the area.

These two designs were identified as the two candidates which merit experimental evaluation with a small scale simulation of the windward joint area. The results of these tests would be used to make the selection of the design.

6.5.2.4 Test Evaluation of the Two Ablator/RSI Designs

As with the ablator/ablator seal models, scheduling problems in the LaRc arc jet made it impossible to run these tests within the time-frame of this program. The arc test models designed for the evaluation of the silica felt and the RTV wave ablator/RSI seal are shown in figure 122. Rationale and details are given in the Data Package. These models were fabricated and submitted to NASA. The planned test sequence is cold soak and entry heating (there is no charring during ascent).

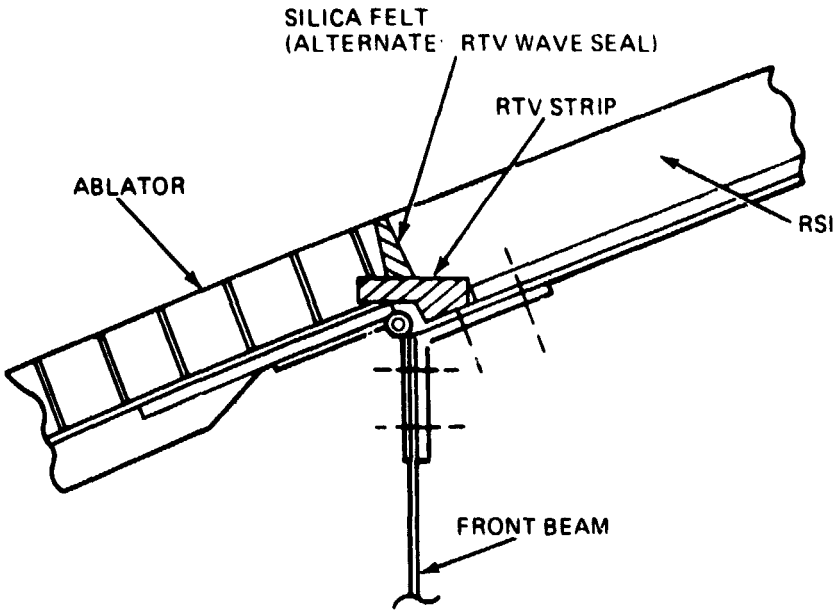

LEEWARD SURFACE
ABLATOR/RSI JOINT

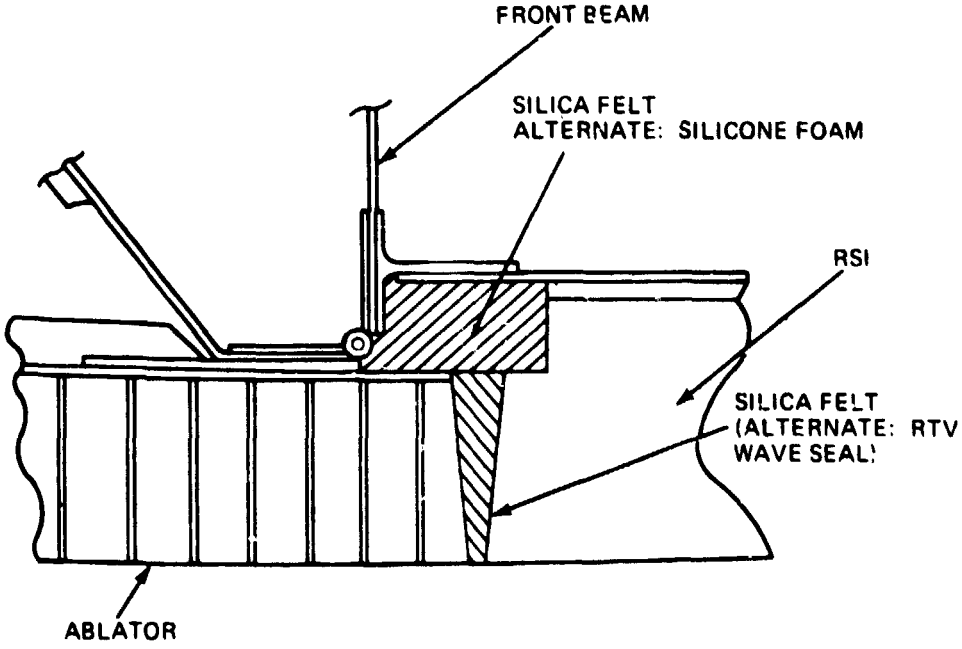

WINDWARD SURFACE
ABLATOR/RSI JOINT

Figure 121 Ablator/RSI Joint Candidate Designs

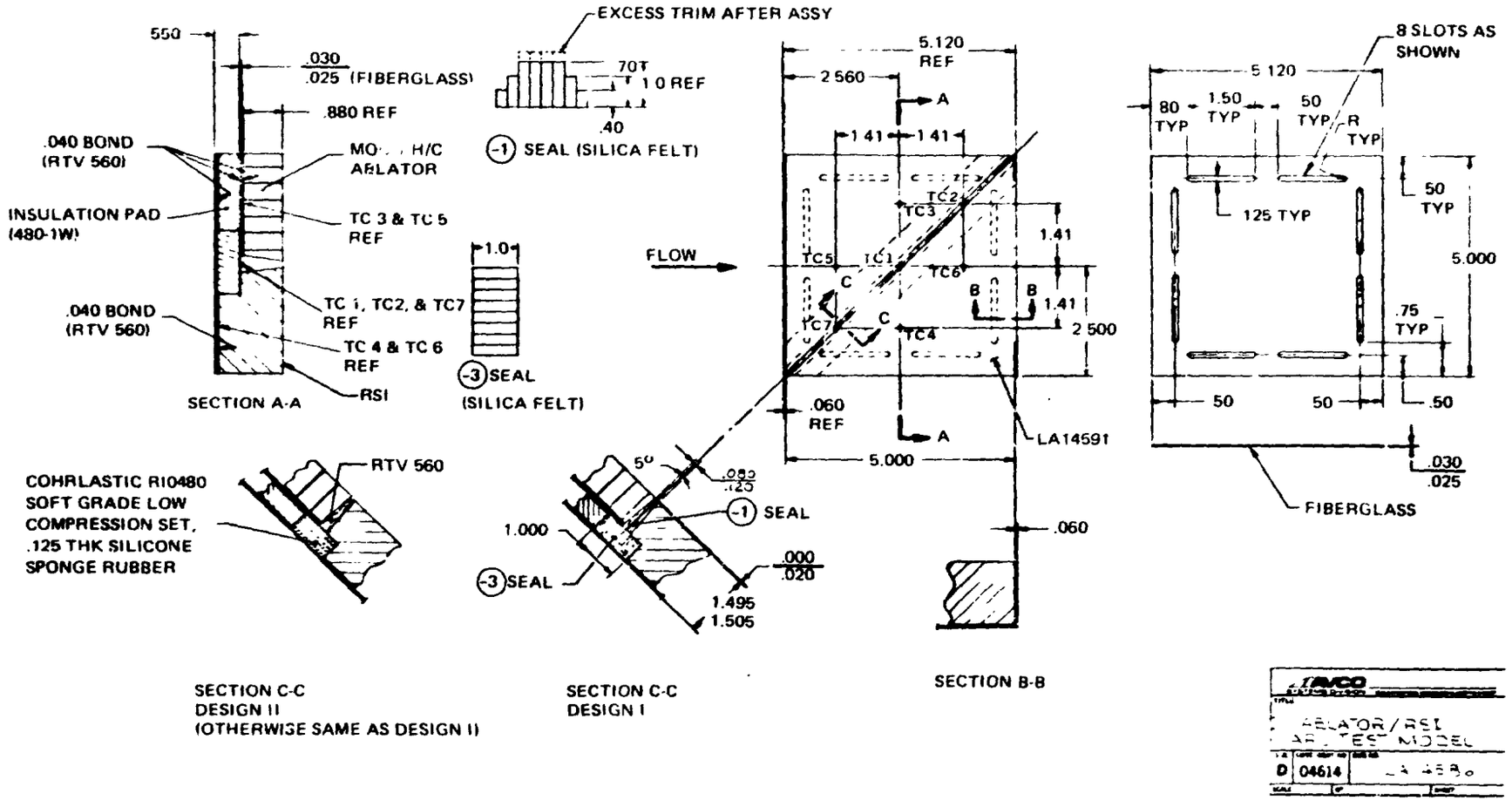

Figure 122 Ablator/RSI Arc Test Model

6.5.2.5 Selected Design for Ablator/RSI Joint

The selection of the design out of the two candidates had to be done without A/RSI test data. In view of the A/A test data and the overall design requirements at the ablator/RSI interface, although not substantiated by the sub-scale tests, the silica felt was by far the best candidate for the seal (see figure 121). It met all requirements enumerated earlier, of low compressibility, no contamination, no protrusion into the air stream and it could be easily installed.

The installation procedure will be taken up in Section 6.6.

6.6 Final Design

6.6.1 Drawing

A layout of the Leading-Edge Final Design for the midspan section of a typical Space Shuttle wing is shown in figure 123 (the drawing attached to this volume). The wing plan form chosen for this presentation is the Rockwell 7D orbiter and is typical of the current base-line design.

6.6.2 Characteristics of the Final Design

The main features of the design are summarized in table 40. In particular the design uses a single honeycomb reinforced ablator (Mod 7 Hc or 3560 HF) bonded to an integrally rib stiffened aluminum substructure. Each leading edge segment is approximately 31" long and is attached to the front beam using an easily removable piano hinge. Vehicle refurbishment is accomplished by completely removing the leading edge segments (22 per wing, 44 per vehicle) and replacing them with new segments. The entire segment, once flown, is discarded (i.e. the substructure is not reused).

Leading-edge removal is semisequential in that every sixth segment is a key segment which can be removed externally be removing bolts which fasten the

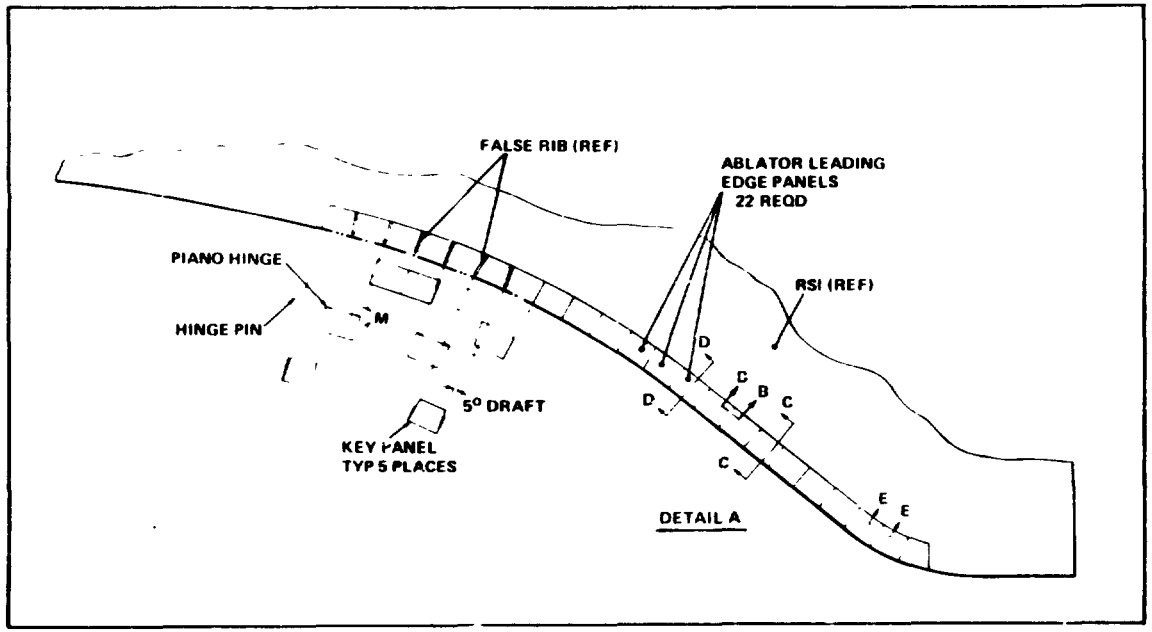

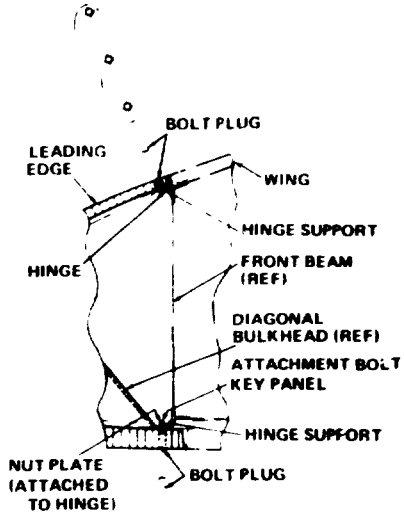

SECTION C-C

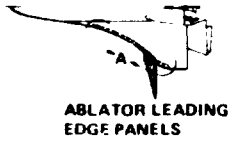

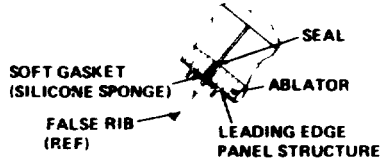

SECTION B-B
SECTION E-E (SIMILAR)

DETAIL M
(TYP BOTH ENDS OF PANEL)

FINAL DESIGN – ABLATOR LEADING EDGE

Figure 123 Sheet 1

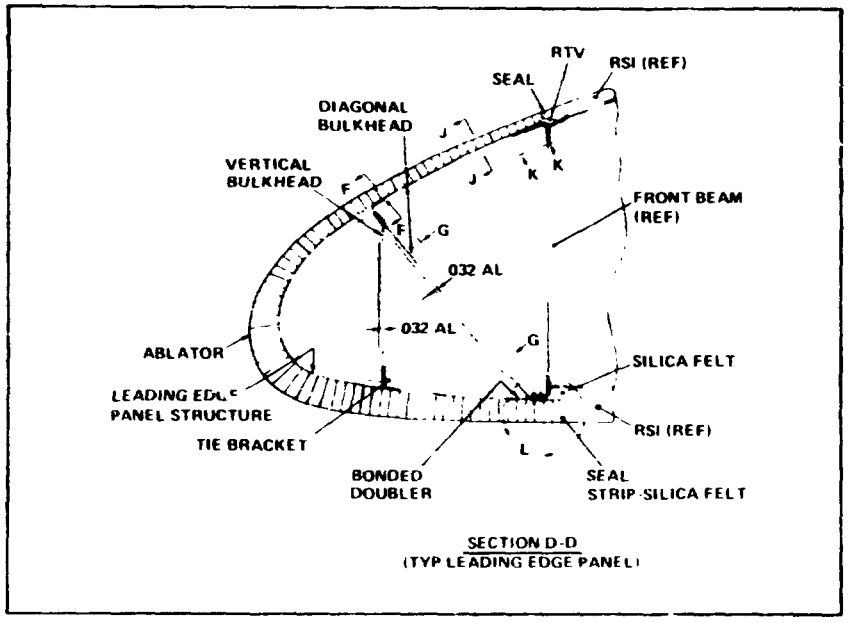

SECTION D-D
(TYP LEADING EDGE PANEL)

SECTION F-F

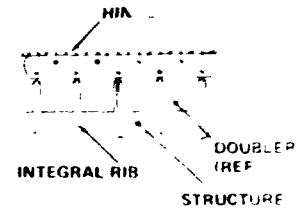

VIEW K-K

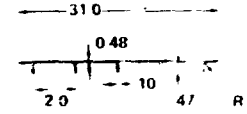

SECTION J J
(SHOWN WITH ABLATOR REMOVED)

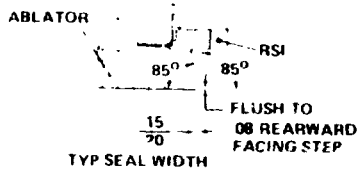

DETAIL "L"
(TYP UPPER & LOWER SURFACE)

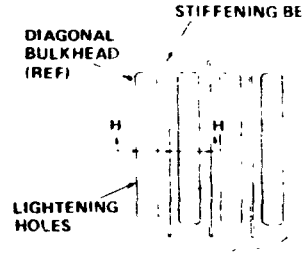

VIEW G G

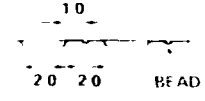

SECTION H H

FINAL DESIGN ABLATOR LEADING EDGE
Figure 123 Sheet 2

Table 40 Characteristics of Ablative L.E. Final Design (Data for MOD 7 H/C Ablator)

Item	Characteristic
L.E. Refurbishment	Detach L.E. Segments from front beam and replace
Turn Around Time	4 Days
Attachment of L.E. Segment to Vehicle	Piano Hinge – except bolt/plugs on key segments
Attachment of Ablator to Substructure	Direct bonding of H.C. core.
Substructure	Integrally stiffened aluminum/refurbished in shop
L.E. Area	600 sq. ft.
No. Segments	44 per vehicle, each 31" long
Operational Sequence	See Table 41

structure to the hinge connection. Access to the bolts is gained by removal of bolt plugs in the ablator. Having removed the key segments the adjacent segments can be detached simply by extraction of the upper and lower piano hinges. To facilitate removal the hinge pins have been designed such that they may be removed from either side. Consequently, in the limiting condition it would be necessary to remove only one key segment by external means and the remaining 21 segments could conceiveably be removed by simply removing the pins, since even the key segments retain the hinge connection. Table 41 presents a breakdown of the operational sequence required to refurbish the leading edge.

Gaps between abutting ablator segments are sealed with a compressible silicone foam (Cohrlastic R10470) to prevent hot gas entry. The seal is sufficiently compressible such that it can be installed with a precompression during installation of adjacent segments. Retention of the seal is accomplished by this precompression as well as the slight taper provided along the chordwise edges of the ablator. The seal is trapped by blocking off the joint at the substructure rear surface with a second sponge gasket (see Section BB). This gasket is supported on a 'false' rib ('false' because it has no primary structural function except to close off the back surface of the joints) that acts as a former during leading edge installation.

Spanwise joints at the ablator/RSI interface along the front beam attachment also employ a seal material, i.e. silica felt (Astro Quartz, Style 550). The small void beneath the seal (due to the difference in thicknesses between the RSI and the ablator at this joint) is filled with a preformed RTV strip on the leeward side and with silica felt on the thicker windward side. The silica felt strip can easily be inserted and removed after each flight.

Table 41 Refurbishment Operational Procedure

Step No	Operation
1	Locate and Remove Ablator Bolt Plugs (Top and Bottom Surfaces) on Key Panels exposing attachment bolts
2	Remove Attachment Bolts
3	Attach Removal Tool and Extract Key Panels
4	Remove hinge pins from adjacent segments using pin removal tool (top and bottom)
5	Lift off associated panels
6	Repeat steps 4 and 5 for newly exposed hinge pins for all subsequent panels
7	Remove silica felt seal strip at RSI interface (top and bottom)
8	Inspect hinge straps attached to front beams and exposed RSI edges (top and bottom)
9	Inspect soft gasket on false rib cap and replace or rebond as required
10	Identify two center segments between each pair of key panels
11	Install silica felt seals for two center segments, using contact cement to hold in place
12	Install one of the two center segments and insert hinge pins (top and bottom)
13	Install preformed chordwise seal adjacent to second center panel position
14	Position second center panel adjacent to previously installed segment
15	Attach segment installation tool in front beam
16	Align segment to be installed, ensuring clearance between hinge straps
17	Using installation jack segment in spanwise direction (compressing chordwise seal) until hinge segments are aligned
18	Jack panel normal to front beam using installation tool, into position and insert hinge pins (top and bottom)
19	Repeat steps, 11, 13 thru 19 for remaining segments except key panels
20	Install silica felt seals for key panel
21	Install two preformed chordwise seals to panels adjacent to key panel
22	Position key panel and insert slip strips between edges of key panel and previously installed chordwise seals
23	Jack key panel into position perpendicular to front beam
24	Install attachment bolts
25	Install ablator bolt plugs
26	Remove slip strips
27	Install remaining key segments repeating steps 21 thru 27
28	Inspect and trim where necessary all protruding seals and surface irregularities to conform to applicable drawings.

The substructure shown in Section C-C of the drawing consists of an integrally rib stiffened aluminum shell reinforced with two continuous stamped aluminum bulkheads. Its fabrication is planned as follows.

The aluminum shell is extruded in long sheets, cut to length, and then stretch formed to the leading edge shape. The two bulkheads are stamped to shape and subsequently riveted to the rib stiffened shell. For all but the key segments the piano hinge is riveted to the aluminum substructure using flush rivets. An aluminum doubler (View K-K) is bonded to the leading edge along the hinge connection line prior to riveting the hinge strap in place.

The completed substructure is used as the form for fabricating the heatshield where the honeycomb core is first bonded to the substructure and subsequently filled with the ablative material. Once the core is filled and the ablator is cured, the contour and edges are trimmed to shape and the surface is sealed to complete the assembly.

The thicknesses for both heatshield materials (Mod 7 Hc and 3560 HF) are given in figure 124 for the root, midspan and tip stations. Included in this figure is a normal cross section of the leading edge typical of the midspan location showing the relative thickness variation around the perimeter.

6.6.3 Final Design Weights

Tables 42 and 43 present a summary of the weight distribution for the midspan segment for the ablator l.e. final design shown in figure 123*. In

* The system weight per square foot of 7.24 lb/ft^2 is slightly greater than that predicted in the earlier trade-off studies which gave a value of 6.50 lb/ft^2 for reference Concepts 9 and 10. The major increase in this weight is due to the added weight of the substructure as a result of including the two bulkheads. These bulkheads were required solely to limit the leading edge deflections and would be required in all the designs examined in the trade-off studies. Consequently, all concepts in Section 6.1.1 should have the substructure weights increased by a constant amount resulting in no change in the relative ranking of the concepts.

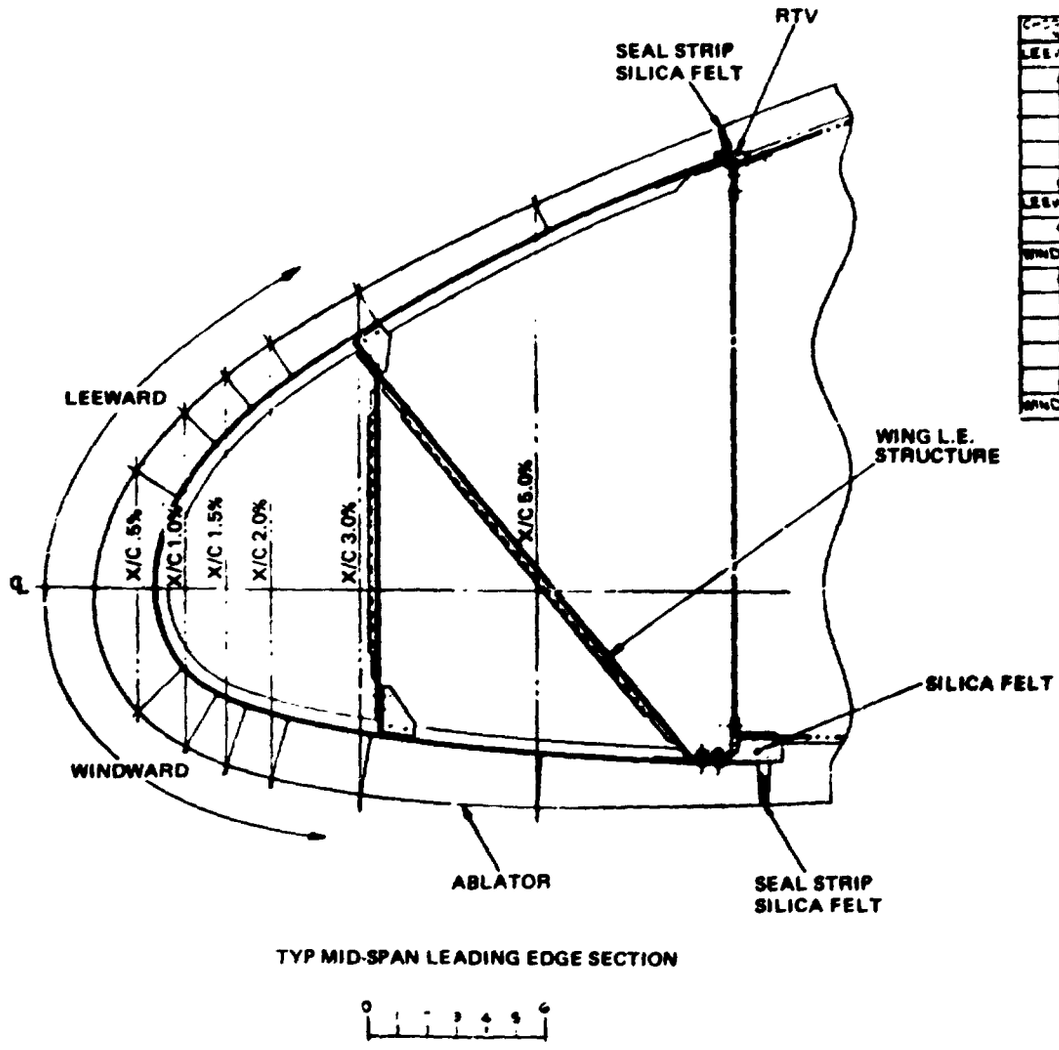

TYP MID-SPAN LEADING EDGE SECTION

LEEWARD							
	5.0						
	3.0						
	2.0						
	1.5						
	1.0						
LEEWARD	0.5						
	0.0						
WINDWARD	0.5						
	1.0						
	1.5						
	2.0						
	3.0						
	5.0						
WINDWARD							

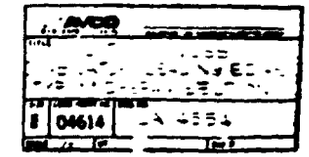

Figure 124 Leading Edge Heat Shield Thickness

Table 42 Weight Summary

Mid Span L.E. Segment

Length 31.0"

Surface Area 11.84 S.F.

Component	Item	Material	Weight (lb)	Totals (lb)
Substructure	Skin with Integral Ribs	Al.	13.4	
	Doublers	Al.	1.0	
	Hinge & Pin	Stl.	0.6	
	Vert. BHD	Al.	1.2	
	Diag. BHD	Al.	1.7	
	Tie Bkts.	Al.	0.4	
	Hdw. & Dblr. Bond	–	0.5	
		Total Substructure:		18.8
Heatshield	Ablator	Mod-7HC(ESA-3560HF)	63.5 (63.6)	
	Bond & Coating	HT-424	1.9 (~ 1.9)	
		Total Heatshield:		65.4 (65.5)
Gaskets & Seals	Abl/Abl Seal	Silicone Foam	1.7	
	Abl/RSI Seal	Silica Felt	0.0	
		Total Seals:		1.7
		Total Segment Wt (lbs)		85.9 (86.0)

table 42 the weights of the individual components are itemized to show the contribution of each item. These weights are subdivided into three major areas; namely, substructure, heatshield, and gaskets and seals. Since two ablators were considered, two weights are given, one for Mod 7 Hc and one for ESA 3560 HF, shown in parenthesis. Note that both ablator weights are essentially the same and that they constitute the bulk of the overall leading edge weight. This is illustrated in table 43 which presents the percent of the total weight and weight per square foot for each component. Here one can see that the heat shield contributes 76% of the total weight.

Although the total segment weight given applies to a midspan segment only, the weight per square foot calculated for this segment should represent a reasonable average value for estimating the total weight of the complete leading edge system. This follows from the fact that at the root the ablator weight per square foot would be somewhat less than at the midspan due to the combined effects of a slightly thinner ablator (see figure 124) and a larger surface area. At the tip the reverse is true where a thicker H/S and smaller surface area combine to bring about a slightly higher weight per square foot. Little change in the substructure unit weight is anticipated along the entire span since the applied loads tend to be lower at the deeper roof section and gradually increase toward the tip.

As a result, a reasonable estimate of the leading edge system weight can be obtained using an average unit weight of 7.24 lb/ft^2. Taking the base line area of 600 ft^2, the estimated weight of the ablator leading edge system per vehicle would be 4,344 lb.

7. COMMENTS ON WING SPECIAL AREAS AND FIN L.E.

The design of the leading edge presented in this report is that typical of a wing midspan location under nominal heating conditions. There are other regions, however, to which the results contained here can be extrapolated, namely; 1) areas of shock impingement heating (if the shock impingement is localized, as in the Grumman 473 orbiter), and 2) fin l.e.

The main problem that arises due to shock impingement is the ability of the selected ablators (Mod 7 Hc and ESA 3560 HF) to withstand the higher heating and pressure gradients without erosion. While negligible recession is predicted for the nominal leading edge condition for either of the ablators the increased heating due to the shock can produce significant recession in the stagnation line region. This effect will introduce undesirable gouging along the span. This problem can be solved by substitution of a higher density silica phenolic material (ρ = 100 lb/ft^3) for the reference ablators in these localized regions. The use of the silica phenolic appears attractive since negligible recession will occur and in addition the thickness requirements should be close enough to the adjacent ablator so that only minor local modifications to the design will be required.

In the fin region typical heating levels of $30{,}000 < Q_c < 40{,}000$ Btu/ft^2 are expected. This environment requires Mod 7 Hc or ESA 3560 HF thicknesses on the order of 2.0 inches (see figure 6-17). The radii (normal to the l.e.) of the root, midspan , and tip of the fin are 5.65, 3.96 and 2.0 inches respectively for the Rockwell orbiter 000089B. In view of these data it appears that a design similar to the leading edge can be used in the fin root and mid-span but an alternate approach must be used in the fin tip area if the 2.0 inch radius cannot be increased. One possible redesign would be to have the fin

tip fabricated out of a solid aluminum to which a relatively thin covering of Mod 7 Hc or ESA 3560 HF is bonded. The additional heat capacity offered by the solid aluminum would be large enough so that the ablator thickness could be reduced to a level in the order of 0.50 inch.

Table 43 Average Weight/Square Foot

Mid Span L E Segments (Mod 7HC)

Surface Area = 11 84 S.F.

Component	Weight (lb)	Per Cent Total Weight	Wt/Ft^2
Substructure	18 8	22.0	1.58
Heat Shield	65.4	76.0	5 52
Seals	1 7	2.0	.14
		Total.	7 24

8. WING ABLATOR LEADING EDGE COSTS

The expenditure requirements for the leading edge can be broken up into two major categories, i.e. the non-recurring (or DDT&E) and recurring (production) costs. Program costs can then be determined using these data together with any given traffic model. For the cost analysis presented below, this was done for the following three traffic models for the operational flights:

1. 15 flights (3 per year for 5 years, 2 operational orbiters)
2. 120 flights (24 per year for 5 years, 2 operational orbiters)
3. 445 flights (average production rate during the 1980's is 60 flights/year).

In all cases, there are in addition five test flights. All costs were based on 1973 dollars with no escalation factor. Unless otherwise noted all costs are based on a requirement of 600 ft^2/vehicle.

In general, the program envisioned is cost-conscious, thrifty and directed to essentials.

8.1 Non-Recurring (DDT&E) Costs

The elements contained in these costs and their estimated value is shown in table 44. This effort will essentially be completed before the major production effort is reached and does not presume committment to the production effort. Five flight tests are included in the DDT&E phase. The estimated total for this DDT&E phase is eight million dollars.

8.2 Recurring Costs

Figure 125 shows the total costs of the ablator for the various traffic models as a function of unit ablator cost (this included fabrication of the ablator and seals, bolt plugs, insulation, etc). Also indicated on the figure are the

Table 44 Non-Recurring DDT&E Costs

Elements	Estimated Cost
1. L/E Design (entire L/E, develop test excluded)	$2,000,000
2. Material Development	800,000
3. Design Development Tests	700,000
4. Production Development (entire L/E, ablator + rest)	1,000,000
5. Qualification, Acceptance and Certification (entire L/E)	500,000
6. Tooling and Special Equipment (entire L/E, ablator + rest)	2,000,000
7. Five Flight Tests	1,000,000
Total	$8,000,000

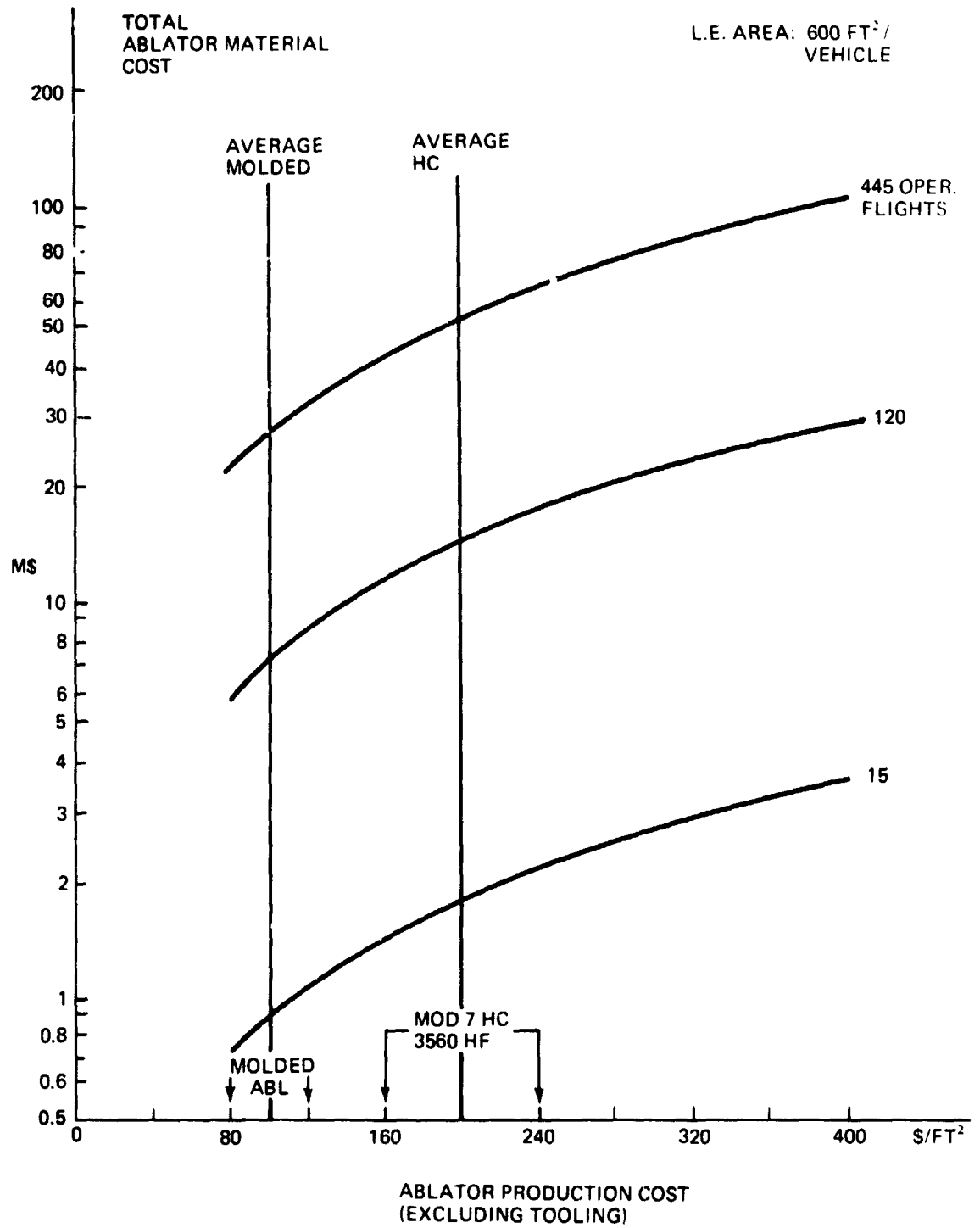

Figure 125 Total Ablator Cost For Wing L.E.

estimated ranges of cost for the molded and honeycomb reinforced elastomeric materials. These total ablator costs include all expenditures required for ablation materials, fabrication, machining, bonding, and inspection, and also allowances for seals, bolt plugs, etc.

The aluminum structure cost is estimated to range from $150/ft^2$ for the 15 flights traffic model to a 445-traffic model level of $40/ft^2$. Similarly operational (refurbishment) costs are expected to range between $80/ft^2$ in the 15 flights to $45/ft^2$ for the 445 traffic model.

8.3 Program Costs

Figure 126 presents the total program costs for the ablative leading edge. These data include all DDT&E, ablator, structure, and operational costs associated with the effort. As expected, the cost of a small traffic model is controlled to a great extent by the DDT&E requirements. For materials in the Mod 7 Hc and ESA 3560 HF category the cost of the program varies between 12 and 90 million dollars for the traffic models considered. If a molded ablator could be used the cost would be reduced to 10 to 52 million.

While this study has as a ground rule that an ablator is used forward of the front beam with an associated area of 600 ft^2, the Shuttle program leading edge designs which currently utilize RSI in areas forward of the front beam, require only about 280 ft^2/vehicle of ablator. The effect of this latter design is shown in figure 127 and the dramatic influence is apparent. The ablator program costs are now reduced to 9 to 45 million dollars for the variances in traffic models assuming that either Mod 7 Hc or ESA 3560 HF is used.

The first unit cost is estimated to be $500,000 for ablator, substructure (including attachments), and installation for a vehicle with a wing leading edge area of 600 ft^2.

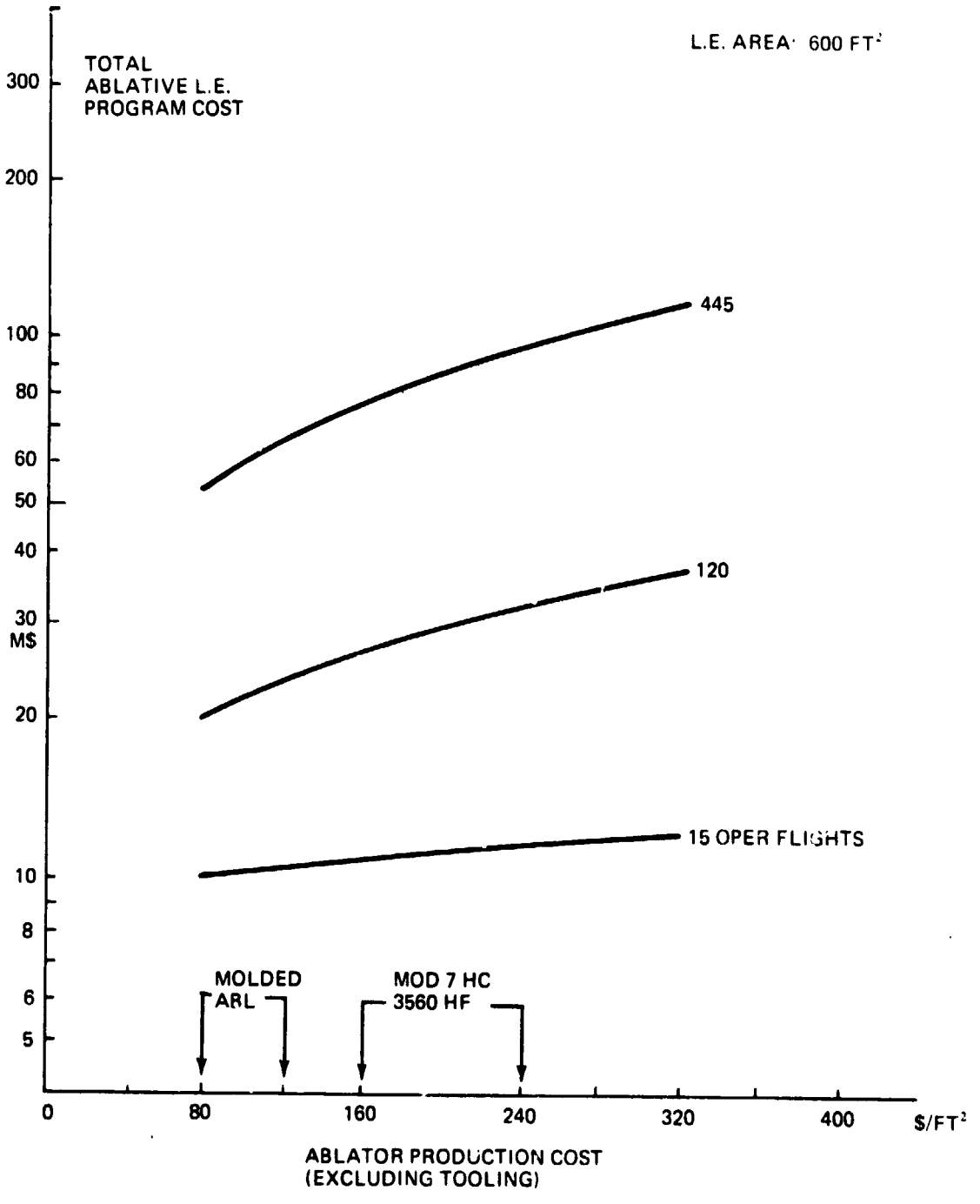

Figure 126 Total Program Cost For Wing L.E. Of 600 Ft²

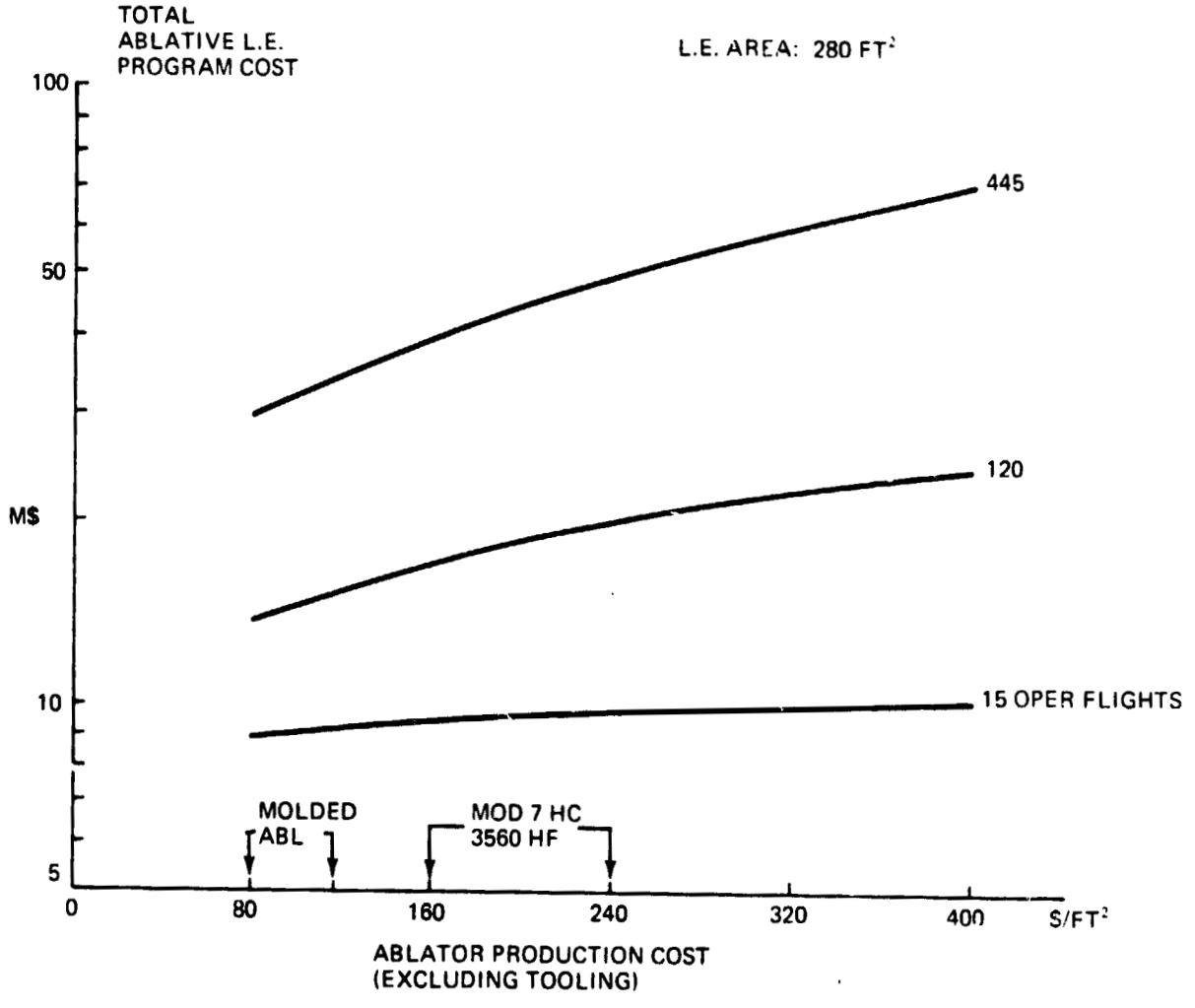

Figure 127 Total Program Cost For Wing L E. of 280 FT²

9. PROSPECTIVES FOR COST/WEIGHT IMPROVEMENTS

The results discussed in Section 8 clearly indicate that the ablator cost is the driving factor in determining the total program funding requirements. Therefore the search to reduce overall costs should concentrate on finding some way to modify the Mod 7 or ESA 3560 so that the unit ablator costs can be reduced from the $\$200/ft^2$ to $\$80/ft^2$ category. The following sections describe some alternatives along these lines that could reduce costs significantly.

9.1 Molded Ablators

While none of the three molded materials could be accepted for the design, there is some hope that by varying the fiber, resin, filler ratios of the constituents a satisfactory molded material could be realized. The primary problem with the molded elastomeric material is that a weak interface exists between the charred and virgin material. This "weak link" is of concern because of the basic requirement of clear integrity. By proper variation of the constituents it may be possible to produce a stronger char/virgin interface to relieve this problem.

In addition, one molded material, Mod 7 M, performed well during simulated ascent heating, cold soak and entry heating*, but developed char separation after entry cooldown. This would seem to indicate that thermal performance during entry heating may be acceptable, but of course char separation may be objectively unacceptable from other points of view such as impact damage to the RSI, contamination of the RSI, and low speed aerodynamic characteristics. It is also conceivable that tests that do not simulate the gradual increase/decrease of the heating pulse and surface temperatures as experienced in flight result

---

* In these steps of the test sequence, both the 5026/39 M and the ESA 3560 II A developed objectionable char or cracks features.

in poorer performance of Mod 7 M. And it may even turn out that this material is acceptable. This would lead to an ablative l.e. that is comparable in costs to the CC (see Section 9-5). Therefore, further evaluation of molded materials performing like Mod 7 M seems especially in order.**

9.2 Alternate Ablator Reinforcement Techniques

The major problem with both the Mod 7 Hc and ESA 3560 HF materials is in the honeycomb. Not only is the honeycomb material itself expensive but its use also introduces costly filling and inspection functions. Figure 128 shows an alternate reinforcement system (Ref. 75) which should reduce fabrication costs significantly. This concept consists of a loop pile construction of a backing material to anchor and stabilize the char. Tests conducted at Avco on an elastomeric material similar to the Mod 7 M (Ref. 75) showed that the char remained anchored to the fiberglass loops even when the char progressed completely back to the fiberglass base.

** Since in this application there are two 'cooldowns' in a flight, one after ascent and one after entry, one may wish to eliminate the first cooldown even though the char interface is very close to the surface. One approach is to coat the molded ablator with a low cost coating which will absorb most of the ascent heating and therefore provide a "non-charred" material for reentry. While this concept will not solve the post reentry interface problem, it will provide a predictable strong surface on the ablator prior to reentry and therefore reduce or eliminate the char erosion noted early in the LRC leading edge tests. The same idea could be applied to the Hc materials if an exactly predictable surface at the beginning of entry were required.

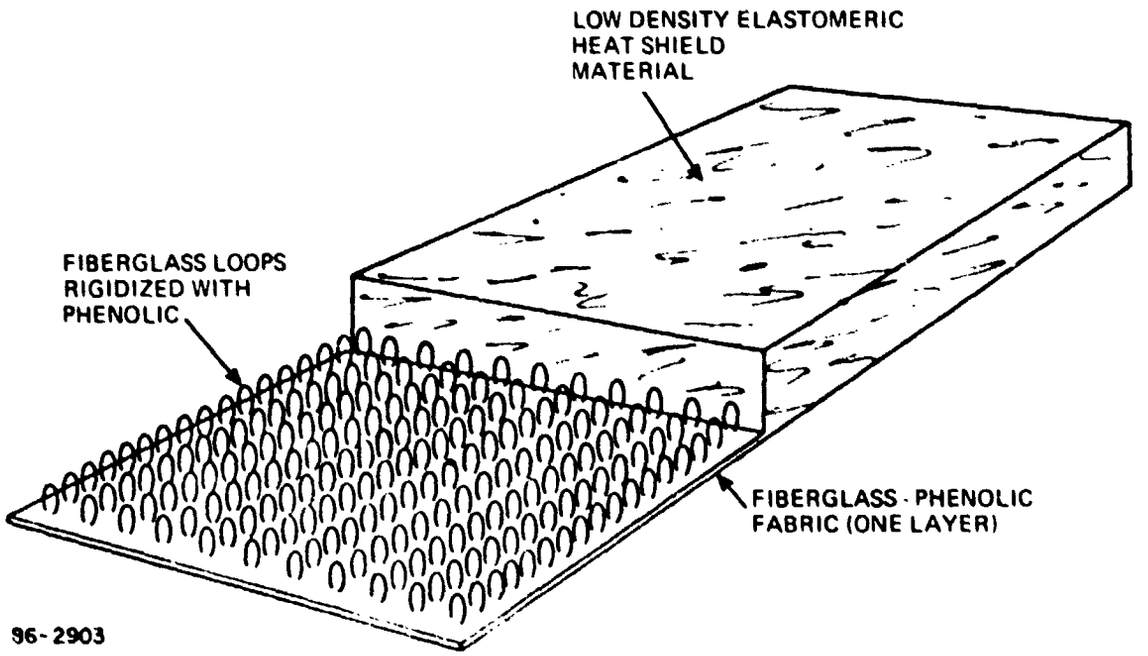

Figure 128 Loop Reinforcement Concept

9.3 Multiple Ablator Leading Edge

The need for honeycomb reinforcement in the stagnation region of the leading edge for all current ablator formulations has been amply demonstrated in the test program. Additionally it was shown that two molded (non-reinforced) materials (i.e. Mod 7 molded, 3560 II A) performed unsatisfactorily locally in the nose region, but the bulk of the ablative material both on the leeward and windward surfaces where the heating was lower showed no adverse effects after the tests.

Insofar as the current program is concerned, a single ablator leading design was a design decision that follows from the ground rule of selecting off-the-shelf ablators. Consequently, the honeycomb reinforcement was employed throughout. If, however, there were some effort directed at developing hybrids of off-the-shelf materials, a more cost effective design could be achieved by the use of multiple ablator materials. In the stagnation region a honeycomb reinforced heatshield would be used, and in areas downstream where the heating rates decreased a molded H/S could be employed. The Hc would taper off so that the ablator would form a single element eliminating a spanwise joint in a region of considerable heating. Moreover, to avoid the problem of trying to match materials and their attendant ablation and thermal properties it would be possible to use the identical material formulation throughout with honeycomb reinforcement placed only where needed. The Mod 7 would fulfill this need since it performed exceptionally well in the molded form and with Hc reinforcement it met all the mission requirements.

Further refinements of the multiple ablator concept could be achieved by changing material formulations entirely in an attempt to reduce the ablator weight through the use of a material in the 20 lb_f/ft^3 class. But as alluded to above this gives rise to problems of matching materials, differential ablation,

different thicknesses at the juncture, etc. Although not unfeasible, more study would be required to qualify this approach as opposed to concept where the only change involved is the inclusion of honeycomb. Also, as pointed out in Section 6.3.4 the desirability and cost effectiveness of a dual ablator leading edge system diminishes rapidly as the area forward of the front beam which is devoted to ablators rather than RSI is reduced.

9.4 Honeycomb Ablator Reuse

The appearance of two Hc materials (Mod 7 Hc and 3560 HF) after the tests of this program suggests that there may be a reuse capability, at least when these ablators are used twice on the windward side of the l.e. only (about half of the l.e. area in current carbon-carbon designs). It may be prudent - in the context of Shuttle program totally committed to minimum cost - to reexamine the following three questions of the reuse concept: a) thermal performance, b) trade-offs cost versus extra weight and, c) inspection after the first flight.

9.5 Estimates for Cost Savings

Figure 129(a) presents rough estimates for the costs savings for a few of the concepts proposed above, using as reference materials such as Mod 7 M and Hc in which there is a marked cost difference between the molded and Hc material. Figure 129(b) presents the corresponding savings if the l.e. area is comparable to the current carbon-carbon areas. It is clear that the molded materials costs are comparable to the CC costs for the 445 flights traffic.

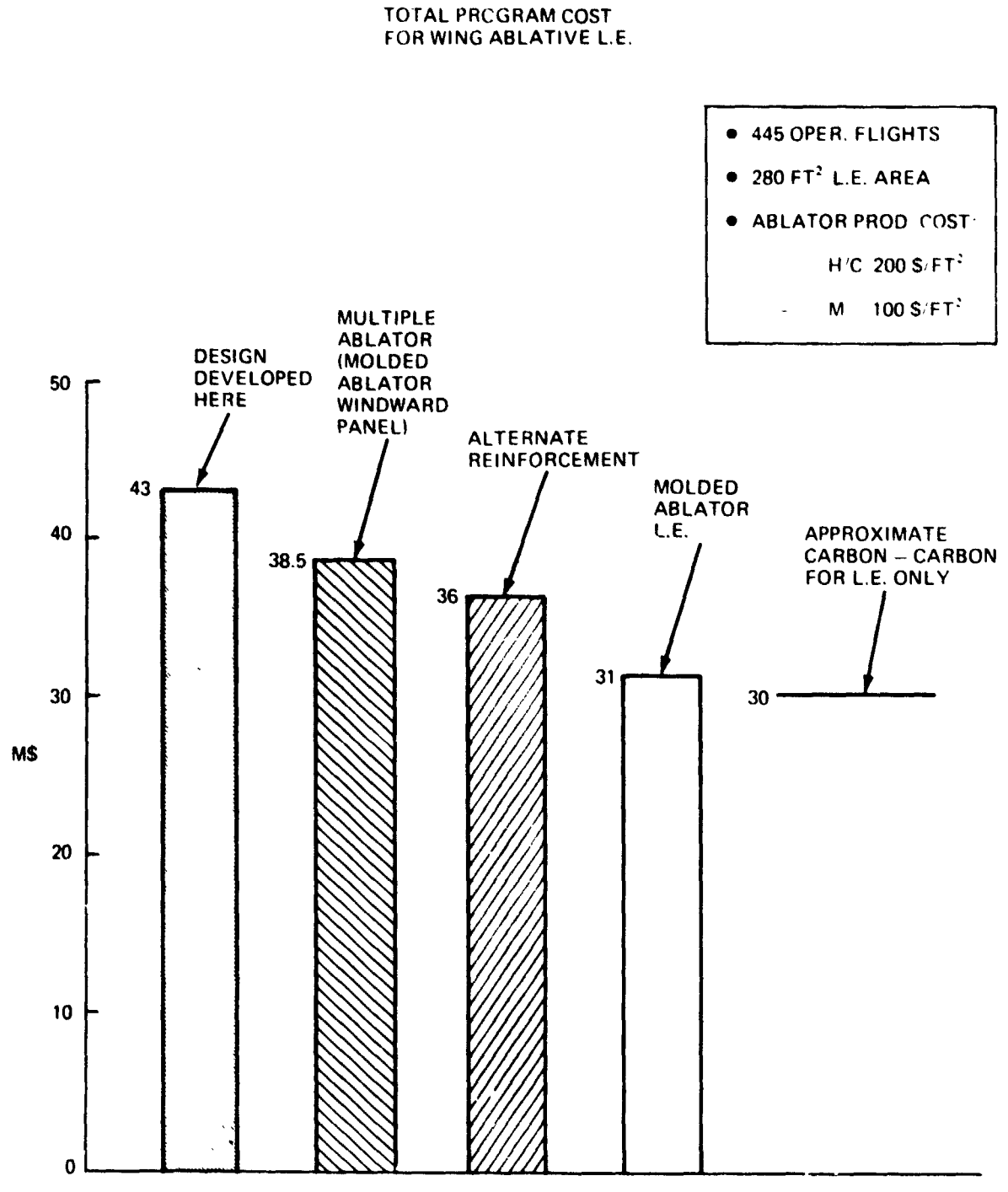

Figure 129 Total Program Cost Savings With Three Concepts Recommended For Development (a) Full Traffic Model

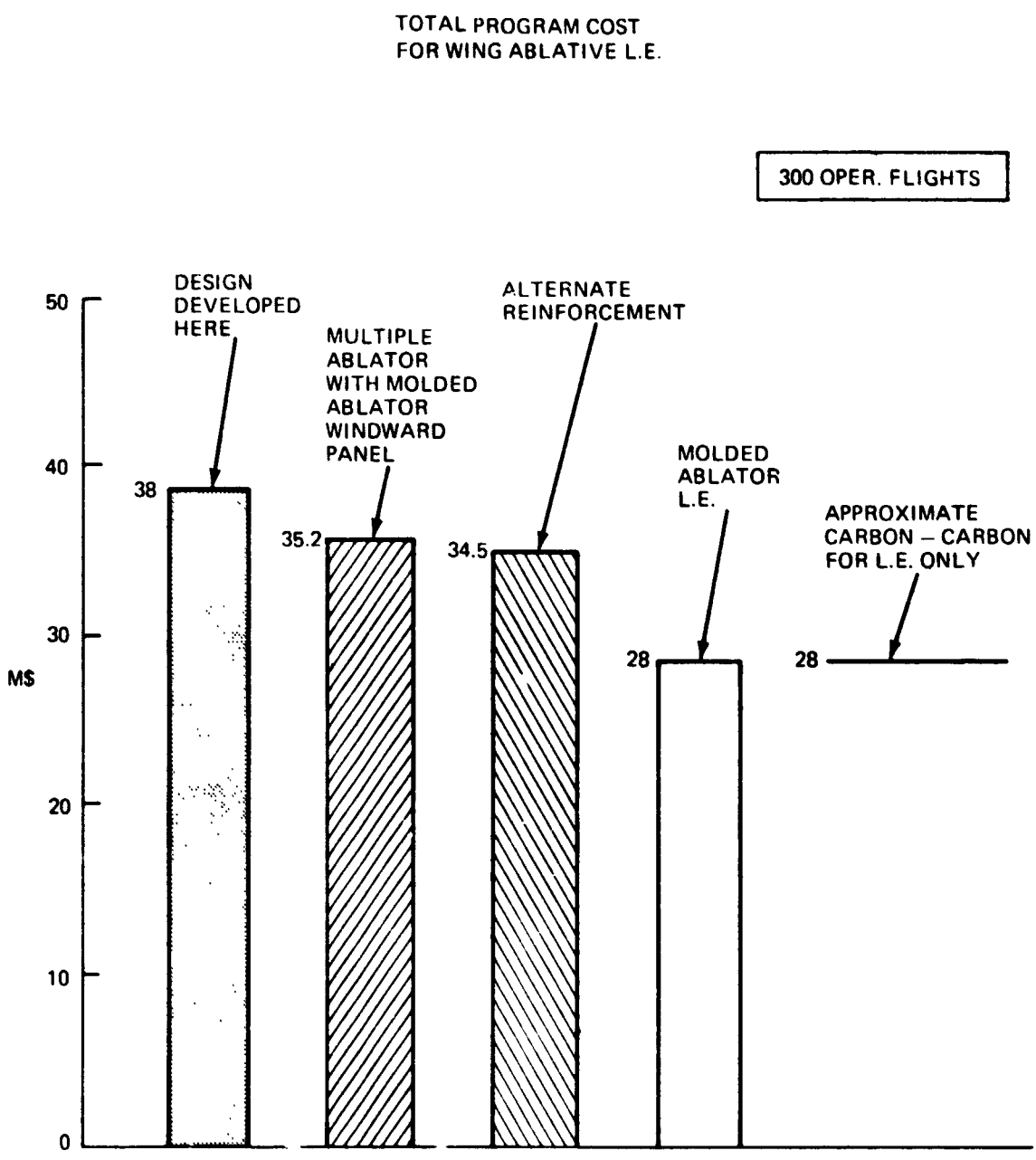

Figure 129 (cont'd) (b) Reduced Traffic Model

10. CONCLUSIONS

The main conclusions of this study are:

(On the ablator)

a) An ablative l.e. is feasible with four state-of-the-art ablators in the 30 to 60 lbs/ft^3 class (out of the eight candidate materials, see table 5-2);

b) Of the four materials, two proprietary elastomers, the Avco Mod 7 He and the MMC ESA 3560 HF, are best and equal within the data generated in this study;

c) In general, honeycomb reinforcement appears needed as none of the three molded materials tested (ESA 3560 IIA, 5026/39 M, Mod 7 M) is acceptable within the scope of this study;

d) Screening tests for the stagnation region must include in the test sequence ascent charring but the sequence can be simplified to three steps, ascent heating, cold soak and entry heating (of course there is no ascent charring in the windward or leeward joint area, so that there screening tests can be reduced to cold soak and entry heating). No attempt has been made to separate the two ascent heating effects, namely the production of some char and the preconditioning of the virgin material.

(On the degradation of low speed aerodynamic characteristics - preliminary conclusions)

e) The roughness of the two ablators selected produce small aerodynamic characteristics degradation; stability is unchanged and the $(L/D)_{max}$ decrease is about 0.1% and probably cost-free. These conclusions are configuration dependent, but appear typical of single-delta Phase-B orbiters with l.e. camber;

f) The recession measured for the two ablators selected, interpreted as indicated in this report, produces very small degradation of low speed aerodynamic characteristics; a concept for correcting recession effects is available but has not been found necessary;

(On the technical characteristics of the ablative l.e.)

g) Based on a study of 13 different l.e. refurbishment concepts, a design in which the l.e. is removed in a single piece from the wing front beam gives minimum weight and cost;

h) The piano-hinge pin attachment concept has been found the most attractive for attaching each l.e. segment to the wing front beam; no segment-to-segment attachment has been found necessary;

i) Both ablators, ESA 3560 HF and Mod 7 Hc, resulted in the same weight; ascent heating required an increase of 0.2 inches of material in the stagnation region;

l) An aluminum (350°F max) integrally rib-stiffened substructure turned out to give minimum weight and cost; it is discarded after each flight;

m) For the ablator-ablator joints between l.e. segments, a sealed gap, using as seal a compressible silicone foam was selected as the best design; however an alternate concept, i.e. a silica felt seal, was found promising and may turn out superior to the silicone foam seal in future tests; neither design could be tested on a l.e. model;

n) For the ablator-RSI joint, again a seal gap concept was found best, with the gap filled with (very compressible) silica felt;

o) The weight of an ablative l.e. for typical delta-wing orbiters turns out to be 7.24 psf (78% heatshield and 22% substructure);

p) An initial design incorporating the features above has been developed;

q) The ablative l.e. turned out to be made up of 44 segments per vehicle, each 31 inches long, 80 lbs heavy. The procedure recommended for removal and installation is semisequential. The refurbishment of the orbiter wing l.e. can be carried out in four days;

r) The weight of the ablative l.e. (600 ft^2 of l.e. area) turned out to be 4350 lbs;

(Estimated ablative l.e. costs)

s) The ablative l.e. costs are estimated around $8M for DDT&E. Total program cost for 445 flights is estimated $43M (for 600 ft^2 of l.e. area) and $38M (for 280 ft^2 area as in the current carbon-carbon wing l.e.);

(Prospectives for cost reduction)

t) Since one molded ablator performed well up to and including the entry heating, but developed char separation after entry cooldown, further evaluation and/or improvements may prove that this ablator or ablators performing in similar manner are acceptable. This would lead to ablative l.e. costs comparable to CC (280 ft^2 of l.e. area, 445 flights); and

u) Hybrid Hc-and-molded ablative l.e.'s also offer attractive cost savings.

11. RECOMMENDATIONS

11.1 Development of the Ablative L.E.

We recommend that a modest effort be continued with the aim of providing a backup for the carbon-carbon l.e., at a price that the Space Shuttle Program can live with.

The areas we recommend for investigation are:

a) Improved molded ablators (See Section 9-1)

b) Alternate reinforcement schemes (See Section 9-2)

c) Multiple ablators with a molded panel (See Section 9-3)

These concepts seem to imply costs (see figure 129) that the Shuttle Program could live with.

The evaluation of these concepts can take the form of a modest program for fabrication and test evaluation of l.e. models, summarily instrumented, subjected to ascent heating, cold soak and entry heating.

11.2 Tests with Models Fabricated under the Present Study

Under this study or in connection with this study, many models have been produced that have not yet been tested. The recommendation is that these models be tested and the results used to continue the ablative l.e. development. The models in questions are the following:

a) The 8 l.e. models, 4 of Mod 7 Hc and 4 of 3560 HF, that have been fabricated for future testing at JSC. These models will provide a good small-scale evaluation of the materials and the A/A joint in tests at high enthalpy. The description of these models is given in Appendix 6.

b) The 4 joint models, 2 l.e. for the A/A joints and 2 flat models for the A/RSI joint, that were fabricated. but not tested in the LaRc

Apparatus A and D. These four models will give a good evaluation of the joint designs, which are the two designs finally selected (A/A and A/RSI), a backup design for the A/RSI joint and a better (but as yet untested) design for the A/A joint. These models and the test procedures are presented in Appendix 5.

c) The three rain erosion samples of MMC ablators of this program (i.e. 3560 HF, 5500, 3560 II A). Initially tests were planned on these samples (after charring) in the Bell Whirling-arm facility. By NASA directions, these tests were cancelled. However, the interest for data on rain erosion still remains.

d) The eight strips (one for each candidate ablator of this study) used for the flexure tests of the virgin ablators were intact after the tests. If anything, they have been preconditioned with strains representative of the max $q\alpha$ condition during ascent. These models can be tested, in a representative sequence, to give more data on the performance of the two selected materials (or, for that matter, of all eight materials) in the windward region of the l.e. (Recall that the charred strips in this study have not been subjected to ascent heating and cold soak). A test condition, and a crude calorimeter are available for these tests in the Avco ROVERS facility (see Appendix 3).

e) Both Martin and Avco produced modification of their basic materials, especially adapted for the shuttle orbiter l.e.* Eight l.e. models exactly as those used in this program have been submitted to NASA (one

---

* There was also a modified 5026/39 Hc l.e. model that was produced for the special purpose of elimination of the flow in the LaRc Apparatus A. This model was summarily instrumented and tested under ascent testing (ROVERS facility) and entry heating (Apparatus A).

modified 480 M, three modified 3560 HF, two modified 5500 and two modified 3560 II A). Even though these modified formulations may not turn out successful, we recommend that the models be tested and something learned in the line of performance improvement potential (which may mean weight savings and, if a molded version works, cost savings).

f) A 480-1B M l.e. model is also available. It is the counterpart of the 480 1B Hc tested under this program. There is still some question as to why the 480 1B Hc performed so badly in the entry test. Therefore there may still be some ground for testing this molded material given that the model is available.

g) The reuse concept for the l.e. windward side can be tested with available models. The strips mentioned under(d) could be subjected to repeated heat pulses. Moreover the two A/RSI joint models can also be subjected to multiple heat pulses thereby providing even an evaluation of the joint and of the added RSI contamination due to reuse.

11.3 Plan for Detailed Study of Aerodynamic Characteristics Degradation

On the grounds of the preliminary assessment (Section 4), a detailed study should be directed at applying the procedure of Section 4.2, as carried out in Sections 4.3 and 4.5, to a typical double-delta orbiter for which considerable data, analyses, and numerous low-speed tunnel models are already available. It may be necessary to update the requirements on float time, landing speed and safety factors, together with the policy as to whether there is potential recovery through clean-ups.

We assume, consistent with Section 11.1, that this detailed study would be modest and would not attack fundamental questions such as understanding of the fluid mechanics of the l.e. separation on the orbiter wing, or Reynolds number effects at high α.

The study should comprise the tasks outlined below:

11.3.1 Study Criteria

The following should be done:

- Update, if necessary, the ground rules (float times, safety factors, etc) and establish limits of acceptable degradation of C_{n_β} C_{l_β} $(L/D)_{max}$, C_L.
- Estimate the expected roughness ranges for the 3560 HF and Mod 7 Hc, the predicted recession and also the estimated recession-uncertainties l.e. profile. The question of the roughness density should be examined more closely, so that the Hc roughness of the two ablators can be reasonably represented via grit density.
- Select baseline configuration.

11.3.2 Test Program

The objective of this program is to determine separately the effects of camber, i.e. roughness and shape changes.

The facility preferred is the NASA LaRc LTPT 3 x 7-1/2-ft tunnel which has a high Reynolds number capability along with a very precise force-measuring capability which is very useful in accurately determining the oftentimes small force increments. However, the key question is whether for the configuration selected there is a model available for this facility, especially a model that has been run, as was the case for the 1/67.5 scale H33 models, in the Langley 8-ft transonic and 4-ft unitary tunnels. Then all model support and compatibility problems have already been solved. The wing should be removable without removing the model from the sting. If not available on the model, a new wing with several interchangeable leading edges should be fabricated out of fiberglass.

As far as grit application one should take advantage of the technique used in the Grumman tests with total model refurbishment (cleaning and regritting) times of about 15 minutes. This technique simply involved sticking on precut strips of Monokote, and adhesive-backed Mylar used by amateur modelmakers, on the desired model surface regions. The strips are prepared prior to testing by gluing carborundum grit of the desired fineness on the roughened tape surface with a polyurethane spray and allowing 12 hours for drying. The technique should be able to cope with the dynamic pressure of the LTPT tunnel; however if it does not, one can fabricate two wings or just two leading edges, which can be pregritted and rapidly interchanged. This appears better than applying the grit to the model itself. It's important that grit density be maintained and the grit size varied.

Tentative test conditions include:

- Grit sizes Nos. 20, 24, 36, 46, 60 & 150
- M = 0.25; $Re/L = 14 \times 10^6$ ft^{-1}
- Some runs are repeated at $Re/L = 8 \times 10^6$ ft^{-1} to determine whether the data actually correlate with Re_k at low Re (say 1.5×10^6 ft^{-1}) and high Re (say $Re/L = 14 \times 10^6$ ft^{-1})
- Tunnel test conditions are compared with flight in figure 11-1. Re_{kmax} can be simulated even though k/r_n is too large (flight 0.1, tunnel 0.6)

Other points that will be incorporated include:

- Include runs without grit and with standard transition strips (for flight data estimation)
- Repeat runs with new roughness application
- While the bulk of the runs will have roughness on wing/tail/nose, in a few cases isolate the relative contributions of wing, tail and nose as in the Grumman and NASA test series.

Instrumentation will include standard six component force and moments. The accuracy of the LTPT balance is adequate. Flow visualization: tufts on video. It would be extremely useful to provide transition visualization.

11.3.3 Analysis and Comparisons with Data

It would be very useful to carry out, in parallel with the experiment, a study similar to that of Ref. 25, using single infinite-cylinder boundary layer theory together with the pressure distribution predicted from Ref. 76.

11.3.4 Analysis of Experimental Data and Extrapolation to Flight

To overcome the characteristic mismatch between tunnel and flight Reynolds number (see figure 130) we anticipate using the 'plateau' procedure. This

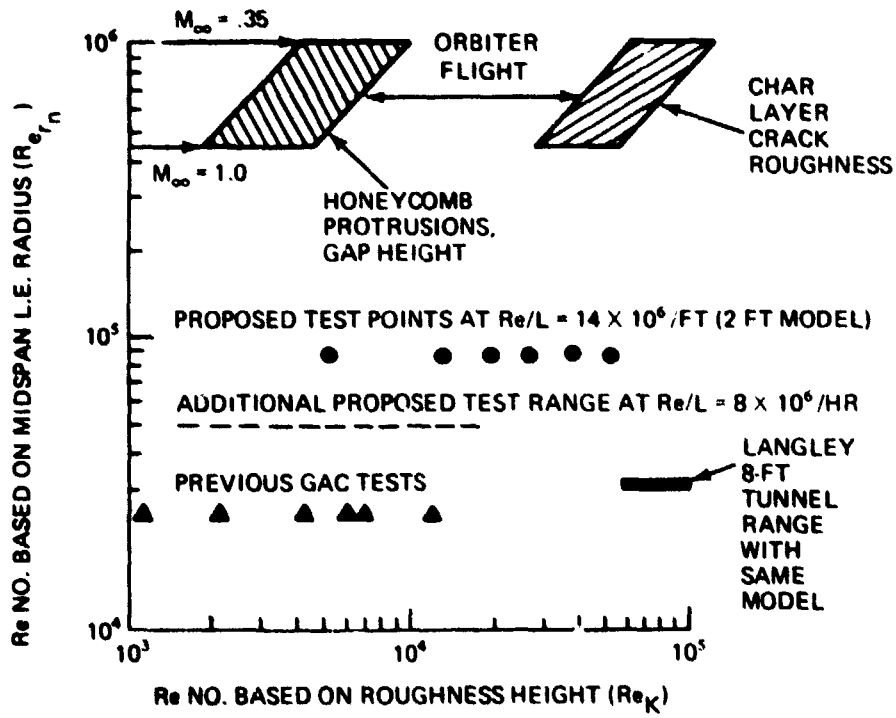

Figure 130 Proposed Tunnel Tests And Flight Conditons

procedure, or other possibilities, such as comparisons of aerodynamic characteristics at same Re_k but wrong k/r_n, should be at least partially checked with the data obtained. Effort should be devoted to this task, especially for the extrapolation of c_{Lmax}, but it is not easy to describe what should be tried.

11.3.5 Conclusions on Aerodynamic Performance Degradation and Recommendations for Ablative Leading-Edge Design

This is a repeat of the study of Sections 4.3 and 4.5 for $c_{l\beta}$ $c_{n\beta}$ (L/D) max and c_{Lmax}. In particular the results will be a new estimate of the $\Delta c_{l\beta}$ $\Delta c_{u\beta}$ ΔL/D max and Δc_{Lmax} for the roughness and reunion of the 3560 HF and Mod 7 Hc ablators.

12. REFERENCES

1 Tillian, D. J., and Roscoe, T. J., "Thermal Evaluation Tests of Ablator and Wood Models of the MSC 25K Shuttle Orbiter Wing Tip Leading Edge in the MSC 10 MW Arc-Heated Tunnel," NASA MSC Memorandum ES5/7-15(0) /171 (M), July 21, 1970.

2 Graham, J., et at., "Ablative Leading Edge Design Concepts for the Shuttle Orbiter," NASA Space Shuttle Technology Conference, Volume II, Structures and Materials, NASA TMX-2273 (1971), pp. 195-231.

3 Johannesen, B., "Post-Test Report of the Low Speed Force Test on the 1/25 Scale GAC H33 Orbiter Model in the Grumman 7 x 10 Low Speed Tunnel," GWTT 300, Nov. 1971.

4 Johannesen, B., "Post-Test Report of the Low Speed Force Test on the 1/25 Scale GAC H33 Orbiter Model in the Grumman 7 x 10 Low Speed Tunnel," GWTT 304, March 1972.

5 Niblock, G. A., Reeder, J. C. and Huneidi, F., "Four Space Shuttle Wing Leading Edge Concepts," American Institute of Aeronautics and Astronautics, Paper No. 73-738, 1973.

6 (Anon.) "Space Shuttle Program," NASA Manned Space Center, RFP No. 9-BC-421-67-2-40P, 1972, pp. 1-7 and 1-8.

7 Forcht, B. A., "Development of a Fail-Safe Design Oxidation-Resistant Reinforced Carbon System for the Wing L.E. of a Space Shuttle Vehicle," LTV Vought System Division, VSC Report T143-5R-30008, June 1973.

8 Moss, H., "Value of a Pound," Grumman Aerospace Corp., Shuttle Program Memorandum B35-18MC-86, Jan. 26, 1972.

9 Moss, H., "Parallel Burn SRM Value of a Pound," Grumman Aerospace Corp., Shuttle Program Memorandum B35-40M0-72005, March 23, 1972.

10 "Current (1973) Values Used in Space Tug Studies," private communication from B. Frumkin, Grumman Aerospace Corp.

11 (Anon.) "KSC Space Shuttle Processing Study, Preliminary Planning Baseline Operational Flow," NASA Document (unnumbered), March 1973.

12 DaForno, G. and Peinemann, M., "Some Effects of Ablative Leading Edge Roughness Upon Low Speed Aerodynamic Characteristics of Shuttle Orbiters," presented at LRC Ablation Technology Symposium, Nov. 1971.

13 Pyle, J. S. and Montoya, L.C., "Effect of Roughness of Simulated Ablated Material on Low-Speed Performance Characteristics of a Lifting Body Vehicle," NASA TMX-1810, 1969 (CONFIDENTIAL).

14 Decker, J. P., "Some Effects of Ablation Surface Roughness on the Aerodynamic Characteristics of a Reentry Vehicle at Low Subsonic Speeds," NASA TMX-2318, 1969 (CONFIDENTIAL).

15 Decker, J. P. and Abel, I., "Some Effects of Ablation Surface Roughness on the Aerodynamic Characteristics of a Reentry Vehicle at Mach Numbers from 0.30 to 1.00," NASA TMSX-2050, 1971 (CONFIDENTIAL).

16 Pyle, J. S., Ash, "Performance Characteristics of the Lifting Body Vehicle," NASA TMX-2101, 1970

17 Minutes of the NASA/DOD Space Shuttle Aerothermodynamic/Configureation Working Group Meeting, March 9 & 10, 1972.

18 Personal communication of J. Graham (Avco) to G. DaForno (Grumman), Nov. 1971.

19 Personal communication of H. Chandler to G. DaForno, Nov. 1971

20 Letter by J. Graham (Avco) to W. Wolter (Grumman), GACSS/JWG/3 dated Jan. 26, 1971.

21 McVey, D. F., Auerbach, I., and McBride, D. D., "Some Observations on the Influence of Graphite Microstructure on Ablation Performance," AIAA Paper No. 70-155, 1970.

22 Rogers, E. W. and Hall, I. M., "Investigation at Transonic Speeds of the Performance of Various Distributed Roughness Bands Used to Cause Boundary Layer Transition Near the Leading Edge of a Cropped Delta Half Wing," ARC CP 481, 1960.

23 Decker, J. P. and Ware, G. M., "Effects of Roughness on Aerodynamic Characteristics of Grumman H33 Orbiter at M = 0.25," DMS-DR-2139, NASA/LRC, April 1972.

24a Schlichting, H., "Boundary Layer Theory," Pergamon Press, 1955.

24b Droblenkov, V. F., "The Turbulent Boundary Layer on a Rough Curvilinear Surface," NASA TM 1440, 1958, (Translated from Izv. Akad. Nauk SSSR Otl. Tekhi. Nauk No. 8, 1955, p. 1721).

25 Tani, I., "Low-Speed Flows Involving Bubble Separation," in Kuechemann, D. and Stern, L., (eds), Progress in Aeronautical Sciences, Vol. 5, pp. 70-103, Pergamon, 1964.

26 Grumman video-tapes of tuft studies taken during GWTT 304.

27 Abbott, I.H., and Doenhoff, A. E., "Theory of Wing Sections," Dover, 1959.

28 Treon, S. T. and Steinle, F. W., Hofstetter, W. R., and Hagerman, J. R., "Data Correlation from Investigations of a High Subsonic Speed Transport Aircraft Model in Three Major Transonic Wind Tunnels," AIAA Paper No. 69-794, 1969.

29 Carlucci, F. T., "Data Report for Third Series of Tests on the 1/25-Scale GAC Orbiter Model H33 in the GAC Low Speed Wind Tunnel," GWTT 292, 1971.

30 Welsh, W. E., Starner, K. E., Leeds, D. H., and Slaughter, J. I., "Low Density Ablation Materials Survey," Grumman Aerospace Corp., TDR-669 (6240-10)-5, SSD-TR-66-35.

31 Welsh, W. E. and Slaughter, J., "Plasma Arc Tests of Carbon-Phenolic Materials for Lifting Reentry Vehicle Applications," Grumman Aerospace Corp. TDR-669 (5250-40)-1.

32 Meltzer, J., Rossof, J., and Slaughter, J., "Structure and Materials Aspects of the PRIME Flight Test Vehicle," AIAA/ASME 7th Structures and Materials Conference, Cocoa Beach, Fla., April 1966.

33 Bauer, P. E. and Kummer, D. L., "Developement and Performance of the Gemini Ablative Heatshield, "J. Spacecraft, Vol. 3, No. 10, Oct. 1966.

34 (Anon.) "Space Shuttle Materials Property Summary Report," AVSD-0478/70-CR, Oct. 1970, prepared for Grumman Aerospace Corp.

35 Grindle, S. L. and Todd, J. P., "Materials Evaluation for Lifting Reentry Applications," Plasmadyne Corp., TR AFML-TR-65-144, May 1965.

36 (Anon.) "Prime Lifting Body Spacecraft - A Collection of Papers," Air Force Report No. SAMSO-TR-68-111.

37 (Anon.) "Information About Space Material," Dow-Corning Co. Bulletin 61-051, June 1971.

38 Thomas, H. K. and Recesso. J. V., "Ablative Composites for Lifting Reentry Thermal Protection, "AVSSD-0081-68-RR, 1968.

39 Watman, H., "Criteria and Performance Charts for Assessing Reentry Glider Horizontal Landability," Grumman Aerospace Corp. AD Rept. No. ADR 01-07-64.1, Sept. 1964.

40 Chin, J., Moore, K. and Domas, D., "Results of a Preliminary Flying Qualities Analysis of the 040A Orbiter," Shuttle Program Memo B36-172MO-24, Jan. 1972.

41 Krepski, R. E., "Design 619 Orbiter - Estimated Aerodynamic Data," Grumman Aerospace Corp. IOM B36-156MO-72-016, May 26, 1972.

42 Jung, W. G. and Krepski, R. E., "Analysis of the First Series of Subsonic Wind Tunnel Tests of the Grumman Design 469 Delta Wing Orbiter at the Grumman Low Speed Wind Tunnel (GWTT 308)," Grumman Aerospace Corp. IOM B36-156MO-72-002, May 3, 1972.

43 Martorella, R. P. "Orbiter Design 619 Flying Qualities," Grumman Aerospace Corp. IOM B36-156MO-72-023, June 7, 1972.

44 Chin, J., Moore, K. and Domas, D., "Results of a Preliminary Flying Qualities Analysis of the 040A Orbiter," Shuttle Program Memo B36-172MO-24, Jan. 1972.

45 Tillian, D. J. and Roscoe, T. J., "Thermal Evaluation Tests of Ablator and Wood Models of the MSC 35K Shuttle Orbiter Wing Tip Leading Edge in the MSC 10 MW Arc-Heated Tunnel," Enclosure to Memorandum ES5/7-15(0)/171(M), NASA, MSC, 1970.

46 McDonnell-Douglas Corp.," Space Shuttle Phase B Study System Extension," Final Report, Part II, Vol. I, Technical Report, System and Orbiter, MDC E0 558, p. B.3-25, March 15, 1972.

47 Seiferth, R. W., "Ablative Heatshields Design for Space Shuttle," NASA CR-132,282 (1973).

48 Dolan, C. M., "Study for Development of Elastomeric Thermal Shield Materials," NASA CR-186.

49 Price, A. B., "Design Report: Thermal Protection System X-15A-2," NASA CR-82003, Jan. 1968.

50 Symly, E. D., and Pears, C. D., "Properties of Ablation and Insulation Materials" (3 volumes), NASA CR-111912, June 1971.

51 Thomas, H. K., and Recesso, J. V., "Ablative Composites for Lifting Reentry Thermal Protection," AFML-TR-67-270, July 1968 (Part II), April 1970 (Part III).

52 Weber, G. A., Rondthaler, T., and O'Connor, T. J., "Low-Density Heat-Shield Evaluation for the XRL Missile," AVMSD-0069-RR, Feb. 1969.

53 Welsh, W. E. and Starner, K. E., "Low Density Ablation Materials Survey," Grumman Aerospace Corp. Report TDR-669 (6240-10)-5, Jan. 1966.

54 Thomas, H. K., et al., "Processing and Properties of Low Density Silicone Ablator Mod 7," AVSSD-0380-67-RM, Oct. 1967.

55 Grumman Aerospace Corp., "Shuttle System Evaluation and Selection," Midterm Briefing, Vol. III, Orbiter Data, MSC-03802, p. 162, Dec. 15, 1971.

56 Private communication from S. Tompkins, Thermal Protection Branch, NASA Langley Research Center.

57 Meltzer, J., Slaughter, J., and Sallis, D., "PRIME Vehicle Heat Protection System Proceedings of Asset/Advanced Lifting Reentry Technology Symposium," Dec. 1965.

58 Lockheed Corp., "Alternate Space Shuttle Concepts Studies," LMSC A995887 ACS 186, Nov. 3, 1971.

59 McCown, J. W., Davis, R. M., "Radiative vs Ablative Heatshield Concepts for Manned Entry Vechicles,. J. Spacecraft Rockets, 4, 1967, pp. 725-731.

60 Moodie, D. M., "Apollo Heatshield Block II," Final Thermodynamics Report, Vol. I, Summary Doc. AVSSD - 0095-67-CR, April 15, 1967, Avco Systems Division.

61 Deriugin, V., et.al., "Thermal-Structural Combined Loads Design Criteria Study," NASA CR-2102, Oct. 1972.

62 (Anon.) "Structural Design Criteria Applicable to a Space Shuttle," NASA SP-8057, Jan. 1971.

63 Thomas, H. K., et al., "Processing and Properties of Low Density Silicone Ablator Mod 7, Avco Systems Div., Report AVSSD - 0380-67 - RM, Oct. 1967.

64 Thomas, H. K., et al., "Ablative Composites for Lifting Reentry Thermal Protection," Report AFML-TR-67-270, Part I, Sept. 1967.

65 Nagler, R. G., et al., "A Light-weight 6.5-ft Aeroshell for an Early Mars Probe Mission," JPL TR 32-1325, Sept. 1968.

66 Hess, T., et al., "Final Report for RSI TPS Development Program," Report GE-EYP-012, General Electric Co., Phila., Pa., May 1972.

67 Dietrich, R.W., "Design Tests: Load/Deflection Test for Candidate Seals Design," Avco Memo SS-RWD-40, Avco Systems Div., May 18, 1972.

68 Gasser, G., and Moodie, M., "Apollo Heatshield Block II, "Final Thermodynamics Report, Vol. VI, Ablator Analysis, AVSSD - 0095-67-CR, April 15, 1967, Avco Systems Div.

69 Herb. R. B., et al., "Apollo TPS Development," American Institute of Aeronautics and Astronautics, Paper 68-1142, 1968.

70 Mosher, D. A., "L. E. Seal Tests," Avco SD Memo F360-73-DAM-44, Avco Systems Div., Jan. 9,1973.

71 Hoercher, H. and Feeman, R., "Evaluation of Candidate L. E. Nose Region Seals," Avco TR-K500-73-HEH-RF-85, Avco Systems Division, April 2, 1973.

72 Movies of ROVERS Arc Run No. 623-1, 2, 2, and 624-1, 2, Avco Systems Div.

73 Private communication from D. Mosher (Avco) to P. Roy (Avco) Nov. 1972.

74 Buttram, R. D., "Space Shuttle TPS," Lockheed Corp., Vol. I, Final Report, LMSC-D152738, Jan. 1972.

75 Winkler, H. B. et al., "A Feasibility Study of an Experiment for Determining the Properties of the Mars Atmosphere," Final Report, Vol. III, Subsystem and Technical Analysis, Book II, Mechanics and Design, NASA CR-73,005, 1966, pp. 6-9.

76 Boppe, C., Unpublished Grumman - Neumann Wing-Body Computer Code, 1970.

77 Tillian, D. J. and Roscoe, T. J., "Thermal Evaluation Tests of Ablator and Wood Models of the MSC 25K Shuttle Orbiter Wing Tip Leading Edge in the MSC 10 MW Arc-Heated Tunnel"